“The Maladaptive Effects of HIV Protease Inhibitors (Lopinavir/Ritonavir) on the Rat Heart”

by

Kathleen Maria Simone Elise Reyskens

Dissertation presented for the degree of Doctor in Physiological Sciences in the

Faculty of Sciences at

Stellenbosch University

Supervisor: Professor M Faadiel Essop

December 2013

Declaration

By submitting this thesis electronically, I declare that the entirety of the work contained therein is my own, original work, that I am the sole author thereof (save to the extent explicitly otherwise stated), that reproduction and publication thereof by Stellenbosch University will not infringe any third party rights and that I have not previously in its entirety or in part submitted it for obtaining any qualification.

December 2013

Kathleen M S E Reyskens

Abstract (English)

Although antiretroviral treatment decreases HIV-AIDS morbidity/mortality, long-term effects include onset of insulin resistance and cardiovascular diseases. Increased oxidative stress and dysregulation of the ubiquitin-proteasome system (UPS) are implicated in protease-inhibitor (PI)-mediated cardio-metabolic pathophysiology. We hypothesized that PI treatment (Lopinavir/Ritonavir) elevates myocardial oxidative stress and concomitantly inhibits the UPS, thereby attenuating cardiac function. Lopinavir/Ritonavir was dissolved in 1% ethanol (vehicle) and injected into mini-osmotic pumps that were surgically implanted into Wistar rats for eight weeks vs. vehicle and sham controls. Subsequently, we evaluated metabolic parameters and heart function (*ex vivo* and *in vivo* methods) at baseline and following ischemia-reperfusion. PI-treated rats exhibited weight gain, increased serum LDL-cholesterol, higher tissue triglycerides (heart, liver), but no evidence of insulin resistance. It also upregulated hepatic gene expression of acetyl-CoA carboxylase β and 3-hydroxy-3-methylglutaryl-CoA-reductase, key regulators of fatty acid oxidation and cholesterol synthesis, respectively. Further, PI-treated hearts displayed impaired UPS, increased superoxide dismutase (SOD) activity and unaltered superoxide levels, and elevated peroxisome proliferator-activated receptor-γ coactivator 1-α (PGC-1α) peptide levels. Perfusion data revealed contractile dysfunction at baseline and following ischemia-reperfusion, while post-ischemic hearts exhibited decreased ATPase specific activity vs. matched controls. Early changes initiated by PI treatment resemble the metabolic syndrome and reflect a pre-atherogenic profile. Moreover, the effects of PIs on cardiac contractile function may in part be triggered by impaired UPS activity together with strain on the mitochondrial energetic system.

Our study alerts to cardio-metabolic side effects of PI treatment and raises the question of the most appropriate co-therapies for patients on chronic antiretroviral treatment.

Abstract (Afrikaans)

Alhoewel anti-retrovirale behandeling MIV-VIGS morbiditeit/mortaliteit verlaag, bestaan daar langtermyn effekte soos die aanvang van insulienweerstandigheid en kardiovaskulêre siektes. Verhoogde oksidatiewe stres en wanregulering van die ubikwitien-proteosoomsisteem (UPS) word geïmpliseer met protease-inhibeerder (PI) gemediëerde kardio-metaboliese patofisiologie. Ons hipotetiseer dat PI behandeling (Lopinavir/Ritonavir) miokardiale oksidatiewe stres verhoog, en gevolglik die UPS inhibeer waardeur dit kardiale funksie verander. Lopinavir/Ritonavir is in 1% etanol (draer) opgelos en in ‘n mini-osmotiese pomp ingespuit wat chirurgies in Wistar rottes ingeplant is vir agt weke vs. draer en valskontroles. Gevolglik het ons die metabolise parameters en hartfunksie (*ex vivo* en *in vivo* metodes) op basislyn en na afloop van ischemie-reperfusie ondersoek. PI-behandelde rotte het ‘n toename in massa getoon asook verhoogde serum LDL-cholesterol, hoër weefseltrigliseriede (hart, lewer), maar geen bewys van insulienweerstandigheid nie. Dit het ook hepatiese asetielko-ensiem A karboksilase β en 3-hidrokise-3-metielglutariel KoA reduktase geenuidrukking opwaarts gereguleer, wat sleutel reguleerders van vetsuuroksidasie en cholesterolsintese onderskeidelik is. Verder, het PI-behandelde harte ingeperkte UPS, verhoogde SOD aktiwiteit en onveranderde superoksiedvlakke vertoon, asook verhoogde peroksisoomproliferator-geaktiveerde reseptor-γ ko-aktiveerder 1-α (PGC-1α) peptiedvlakke. Perfusie data toon kontraktiele wanfunskionering gedurende basislyn en na afloop van ischemie-reperfussie, terwyl post-ischemiese harte verlaagde ATPase spesifieke aktiwiteit vs gepaarde kontrole vertoon. Vroeë veranderinge wat deur PI behandeling veroorsaak word, kom ooreen met die metabolise sindroom en reflekteer op ‘n pre-aterogeniese profiel. Bowendien kan die effekte van PIs op kardiale kontraktiele funksie deels

veroorsaak word deur die ingeperkte UPS aktiwiteit tesame met die las op die mitochondriale energie sisteem. Ons studie waarsku teen kardio-metaboliese newe effekte met PI behandeling en rig die vraag; wat die mees gepaste ko-behandeling vir pasiënte op chroniese anti-retrovirale behandeling is.

Acknowledgements

I would firstly like to thank my parents for their support, love and encouragement throughout the years, as well as their willingness to financially support my academic interests. Here it is also necessary to also thank the National Research Foundation and the Harry Crossley Foundation, who generously financially assisted my studies. A special thanks to my lovely sister Marina, for here odd sense of humour and being such a great sister to me. I am also grateful that two years ago I had to assist her with her Master's thesis, which gave me a tiny insight into the exhaustive and tedious preparation that is a thesis. Thank you Mina!

This thesis would not have been possible without the brilliant guidance and support of my supervisor, Professor M Faadiel Essop. Since the start of this work in 2008, he has taught me the value of inquisitive and independent thinking, while at the same time forging a strong a personal bond between us. Not only has he been very open and willing to support my ideas, which at times were not coherent, he has excelled in every facet in being a personal mentor. I am very grateful that Prof allowed me the time to visit the USA, and Europe on two occasions – my horizons have been exponentially expanded! Prof, you are an amazing individual, and I am very grateful to have you part of my life. No words can say how truly thankful I am.

I would also like to thank the Cardio-Metabolic Research Group (CMRG) for their amazing support and seriously fun time doing science! A special thanks to: Danzil Joseph, Dr. Rudo Mapanga, Dr. Uthra Rajamani, Taryn-Lee Fisher, Burger Symington, Kim Strauss, Carla Pool, Delita Otto, Clare

Springhorn, Kirsty Garson and all the members of CMRG over the years! You have all made me the scientist I am today, and I am very grateful for your support, especially went the science went wrong.

Many thanks to the Department of Physiological Science students and staff; who are too numerous to mention here but I appreciate each and every one. Thank you for such a wonderful and stimulating environment to work in, the support, and the epic social events! A special word of thanks to Dr. Theo Nell for translating my thesis abstract from English to Afrikaans.

I also owe much of my sanity to the gods of creativity, endowing me with artistic abilities such as painting, drawing, and crocheting. If not for these treasures, I would not have been able to make it through the tough times when research became overwhelming and I needed a distraction. Similarly, becoming a runner and completing the Old Mutual Two Oceans Half Marathon in March 2013 allowed me to discover another passion during my studies.

Last but not least, I would like to thank my partner Kevin, for his constant enthusiasm, support and absolute bewilderment that I would embark on such a strange and complicated study that is the Ph.D.

"Anyone who has never made a mistake has never tried anything new." - Albert Einstein

Kathleen Reyskens

September 2013

Table of Contents

List of Abbreviations 12

List of Figures 18

List of Tables 22

List of Publications 23

Chapter 1 24

Literature Review

References 67

Chapter 2 88

Establishment and characterization of a rodent model of chronic PI exposure

Introduction 89

Materials & Methods 91

Results 95

Discussion 102

Conclusion 106

References 107

Chapter 3 111

The effect of PIs on heart function in a rodent model

Introduction 112

Materials & Methods 115

A: Ex vivo Working Heart Perfusions 116

Results 120

Discussion 124

Conclusion 126

B: Ex vivo Langendorff Perfusions 127

Results 131

Discussion 138

Conclusion 141

C: In vivo Heart functional assessments 142

Results 145

Discussion 149

Conclusion 151

References 152

Chapter 4 158

The molecular mechanisms underlying cardio-metabolic dysfunction with HIV PI therapy

Introduction 159

Materials & Methods 161

Results 173

Discussion 190

Conclusion 197

References 198

List of Abbreviations

±*dP/dt*	Maximal/minimal contractile force
AAR	Area at risk
ACC/*acc*	Acetyl CoA carboxylase (protein/*gene*)
ACS	Acute coronary syndrome
ADD	Adipocyte differentiation determination factor
ADP	5'-adenosine diphosphate
AIDS	Acquired immune deficiency syndrome
AMP	5'-adenosine monophosphate
AMPK	AMP-activated protein kinase
ANOVA	Analysis of variance
ApoB	Apolipoprotein B
ART	Antiretroviral therapy
ARV	Antiretroviral
ATP	5'-adenosine triphosphate
ATPase	5'-adenosine-triphosphate synthase
bHLH-LZ	Basic helix-loop-helix zipper leucine
BMI	Body mass index
BSA	Bovine serum albumin
CaMKII	Calmodulin kinase II
cDNA	Copy Deoxyribonucleic acid

CICR	Calcium-induced calcium release
CO_2	Carbon dioxide
COX	Cyclo-oxygenase
Cu/Zn SOD	Copper/zinc superoxide dismutase
CVD	Cardiovascular disease
Cx43	Connexin 43
DAD	Data Collection for Adverse events of Anti-HIV Drugs
DNA	Deoxyribonucleic acid
DNP	Dinitrophenol
DNPH	2, 4-dinitrophenylhydrazine
ECC	Excitation-contraction coupling
ECG	Electrocardiogram
ECL	Enhanced chemiluminescence
ELISA	Enzyme-linked immunosorbent assay
eNOS	Endothelial nitric oxide synthase
ER	Endoplasmic reticulum
ERAD	ER-associated degradation
ETC	Electron transport chain
FA	Fatty acids
FAO	Fatty acid oxidation
FAS/*fas*	Fatty acid synthase
FFA	Free fatty acids

GPAM/*gpam*	Glycerol-3-phosphate acyltransferase (mitochondrial)
GPx	Glutathione peroxidase
H_2O	Water
H_2O_2	Hydrogen peroxide
HAART	Highly active antiretroviral therapy
HBP	Hexosamine biosynthetic pathway
HDL	High density lipoprotein
HE	Hemotoxilin and Eosin
HF	High fat
HIV	Human immunodeficiency syndrome
HMG-CoA	Hydroxyl-3-methyl-glutaryl-CoA
HMG-CR/*hmg-cr*	Hydroxyl-3-methyl-glutaryl-CoA reductase
HOMA-IR	Homeostatic model of assessment of insulin resistance
HRP	Horseradish peroxidase
IA	Infarcted area
IL-6	Interleukin 6
IMM	Inner mitochondrial membrane
iP	Inorganic phosphate
ipGTT	Intra-peritoneal glucose tolerance test
IR	Insulin resistance
JNK	c-Jun N-terminal kinase
kDa	Kilodalton

LDL	Low density lipoprotein
LDL-R/*ldl-r*	Low density lipoprotein receptor
LPL	Lipoprotein lipase
LVDP	Left ventricular developed pressure
MAD	Mitochondrial associated degradation
MAP	Mean arterial pressure
MAPK	Mitogen activated protein kinase
MEF2	Myocyte enhancing factor 2
MetS	Metabolic syndrome
MI	Myocardial infarction
MnSOD	Manganese superoxide dismutase
mRNA	Messenger ribonucleic acid
mtDNA	Mitochondrial deoxyribonucleic acid
mtTFA	Mitochondrial transcription factor A
NCX	Sodium-calcium exchanger
NFAT3	Nuclear factor of activated T-cells 3
NNRTI	Non-nucleoside reverse transcriptase inhibitor
NOX	NADPH oxidase
NRF-1	Nuclear respiratory factor 1
NRTI	Nucleoside reverse transcriptase inhibitor
O_2	Oxygen
$O_2^{\bullet -}$	Superoxide

$OH^{\bullet}$	Hydroxide radical
OMM	Outer mitochondrial membrane
$ONOO^{-}$	Peroxynitrite
PBS	Phosphate-buffered saline
PBS-T	Phosphate-buffered saline with Tween 20
PGC-1α	Peroxisome proliferator-activator receptor gamma coactivator 1 alpha
PI	Protease inhibitor
PKA	Protein kinase A
PKC	Protein kinase C
PLB	Phospholamban
PPARγ	Peroxisome proliferator-activator receptor gamma
PVDF	Polyvinylidene fluoride
qPCR	Quantitative polymerase chain reaction
REE	Resting energy expenditure
RFU	Relative fluorescence units
RNA	Ribonucleic acid
ROS	Reactive oxygen species
RPP	Rate-pressure product
RT	Reverse transcriptase
RTI	Reverse transcriptase inhibitor
RyR	Ryanodine receptor
S1P/S2P	Site 1/2 protease

SA	Sinal-atrial node
SCAP	SREBP cleavage activating protein
SCD2	stearoyl-CoA-destaurase 2
SDS	Sodium-dodecyl sulphate
SEM	Standard error of the mean
SERCA-2a	Sarcoplasmic/endoplasmic reticulum calcium ATPase
SH	Sulfyl-hydryl group
SOD	Superoxide dismutase
SR	Sarcoplasmic reticulum
SRE	Sterol response element
srebf	Sterol regulatory element binding factor
SREBP	Sterol regulatory element binding protein
T2DM	Type 2 diabetes mellitus
TBS-T	Tris-buffered saline with Tween 20
TG	Triglycerides
TMB	3, 3', 5, 5'-tetrametylbenzidine
TNFα	Tumor necrosis factor α
TTC	2, 3, 5-triphenyl tetrazolium chloride
UCP	Uncoupling protein
UPS	Ubiquitin-proteasome system
Vif	Viral infectivity factor
VLDL	Very low-density lipoprotein

List of Figures

Chapter 1

Fig. 1 HIV infection and HAART: detrimental side effects 27

Fig. 2 HIV lifecycle and antiretroviral drugs..... 30

Fig. 3 The SREBP pathway 38

Fig. 4 The effects of PIs on lipid metabolism 43

Fig. 5 The ubiquitin-proteasomal degradation system (UPS) 45

Fig. 6 The effect of PIs on the ubiquitin-proteasome system (UPS) 47

Fig. 7 Excitation-contraction coupling (ECC) and calcium homeostasis 49

Fig. 8 Connexin biology and alterations in expression 54

Fig. 9 The PGC-1α pathway 53

Fig. 10 Molecular hypothesis for PIs and their detrimental effects on heart function 59

Fig. 11 PIs and oxidative stress 63

Chapter 2

Fig. 1 Body weight changes in response to 8 weeks PI treatment 95

Fig. 2 Terminal weight and percentage change due to PI and high fat dietary intervention 96

Fig. 3 Total food consumed during 8 weeks of PI and high fat dietary intervention 97

Fig. 4 Intra-peritoneal glucose tolerance test (ipGTT) 98

Fig. 5 Weekly fasting glucose levels during 8 weeks of PI therapy 99

Fig. 6 HOMA-IR and other parameters of glucose metabolism 99

Fig. 7 Lipid profile in response to 8 weeks PI therapy 100

Fig. 8 Cytokine profile of TNFα and IL-6 in response to PI therapy 101

Chapter 3

Fig. 1 Working heart perfusion rig set-up 118

Fig. 2 Baseline function and ischemia-reperfusion protocol for working heart perfusions 119

Fig. 3 Baseline working heart function in response to PI and high fat treatment 121

Fig. 4 Rate-pressure product at baseline in response to PI treatment ± high fat diet 122

Fig. 5 Heart function in response to ischemia-reperfusion with PI treatment 123

Fig. 6 Retrograde Langendorff perfusion rig set-up 128

Fig. 7 Langendorff retrograde perfusion protocol 130

Fig. 8 Heart-to-body weight ratio in response to 8 weeks PI treatment 131

Fig. 9 Baseline heart functional parameters for 8 weeks PI treatment 132

Fig. 10 Additional baseline heart functional parameters in response to 8 weeks PI therapy 133

Fig. 11 Contractile parameters after ischemia-reperfusion in response to 8 weeks PI treatment 134

Fig. 12 Additional contractile parameters during ischemia-reperfusion 135

Fig. 13 Recovery of LVDP and survival rate after ischemia-reperfusion with PI treatment 136

Fig. 14 Infarct size in response to 8 weeks PI therapy 137

Fig. 15 The materials used for recording the rat blood pressure *in vivo* 143

Fig. 16 Cannulation of the carotid artery 144

Fig. 17 ECG recordings at baseline 146

Fig. 18 Baseline ECG parameters in response to PI treatment 147

Fig. 19 Post-ischemic ECG parameters in response to PI therapy 148

Chapter 4

Fig. 1 Different methods of normalizing nuclear extracts in heart tissue 167

Fig. 2 Histological analyses of 8 weeks PI therapy in multiple organs 174

Fig. 3 Heart and liver lipid profile in response to 8 weeks PI therapy 176

Fig. 4 Gene profile at baseline 177

Fig. 5 Expression of SREBP-1 at baseline in response to 8 weeks PI treatment 178

Fig. 6 ATP content and AMPKα expression in response to 8 weeks PI therapy 179

Fig. 7 Cardiac ATPase specific activity at baseline 180

Fig. 8 Proteasomal activity following 8 weeks PI treatment 181

Fig. 9 Global ubiquitination of cytosolic and nuclear proteins in response to PI therapy 182

Fig. 10 Protein expression of contractile regulators following PI treatment 183

Fig. 11 Calcium pathway protein expression in response to PI therapy 185

Fig. 12 PGC-1α pathway protein expression in response to 8 weeks PI treatment 186

Fig. 13 Baseline myocardial SOD activity and superoxide production in response to 8 weeks PI treatment 187

Fig. 14 Glutathione levels in response to PI treatment 188

Fig. 15 Carbonylation content and catalase activity in response to 8 weeks PI therapy 189

Fig. 16 Model demonstrating the influence of PI therapy on calcium handling and cardiovascular dysfunction 195

List of Tables

Chapter 1

Table I HIV ± HAART and the risk for MI and cardiovascular complications (clinical studies) 28

Table II PI treatment and the risk for MI and cardiovascular complications (clinical studies) 32

Table III Lipid changes associated with PI therapy (clinical studies) 34

Chapter 3

Table I Number of animals used for *in vivo* heart functional assessment and success with experiments 146

List of Publications

Parts of this thesis have been published in internationally acclaimed journals and the publications are listed below.

Original articles

1. KMSE Reyskens, MF Essop. **The maladaptive effects of HIV protease inhibitors (lopinavir/ritonavir) on the rat heart.** *Int J Cardiol* (2013) 168 (3): 3047-9.

   Accepted April 2013, Epub ahead of print May 11, impact factor: 7.078

2. KMSE Reyskens, T-L Fisher, JC Schisler, WG O'Connor, AB Rogers, MS Willis, C Planesse, P Rondeau, E Bourdon, MF Essop. **Cardio-metabolic effects of HIV protease inhibitors (Lopinavir/Ritonavir)**. *Plos One* (2013).

   Accepted October 2013, going to print, impact factor: 3.730

Review article

3. KMSE Reyskens, MF Essop. **HIV protease inhibitors and onset of cardiovascular diseases: a central role for oxidative stress and dysregulation of the ubiquitin-proteasome system**.

   Submitted October 2013 and undergoing review.

Chapter 1

Literature Review

Introduction

Human immunodeficiency virus (HIV) infection has increased dramatically in the last two decades, with more than 5 million of the 40 million globally infected individuals residing in sub-Saharan Africa [1,2]. The development of acquired immunodeficiency syndromes (AIDS) due to chronic inflammation decreases the quality of life amongst sufferers and places their long-term health in jeopardy. In parallel, the ever-increasing obesity epidemic developing alongside HIV infection with increased cardiovascular complications presents a dual burden of disease. With the advent of highly active antiretroviral therapy (HAART) life expectancy and quality has drastically improved for those infected [3,4], however, there are increased concerns regarding HAART-mediated metabolic derangements and its potential risk for cardiovascular diseases (CVD) in the long-term. Further, certain classes of antiretroviral (ARV) drugs e.g. protease inhibitors (PIs) are implicated in these perturbations, although mechanistic insight is lacking. This review will highlight the contributions of the HIV infection itself, HAART, and the specific HAART drug class the PIs to the onset of cardio-metabolic complications.

HIV infection and cardiovascular diseases

HIV infection is characterized by a compromised immune system and subsequent chronic, life-long inflammation and the development of AIDS. Cardiac abnormalities were noted as early as 1989 [5,6] (pre-HAART era) and included dilated cardiomyopathy, endo-, myo- and peri-carditis, and pulmonary hypertension [5–8]. Prevalence during this time period was between 28 and 73% [5,7,9]. HIV is able to directly infect cardiac tissue [10], though this may be attributed to the stage of HIV/AIDS, but nonetheless compounds future health outcomes and survival of an HIV-infected individuals. During the HAART era, it is important to understand the relative contributions of both antiretrovirals and HIV infection in the onset of CVD and related manifestations, especially since HIV infection is a potential risk factor for CVD (to be discussed later).

Co- and multi-morbidity patterns in HIV infection are alarming. For example, when comorbidities are stratified by HIV status, age and severity; not only was HIV infection a risk for future health concerns, but long-term HAART is also linked to detrimental cardiovascular consequences [11]. Further, disease advancement with HIV infection is associated with renal, vascular and pulmonary complications that are commonly found in ageing populations (**Fig. 1**). When morbidity patterns are stratified by obesity by employing the body mass index (BMI) [12], up to 65% of HIV-infected individuals have multi-morbidities with obesity exacerbating these effects. A long-term study investigated the expected survival and mortality rates of an HIV-infected population during 1995 to 2005 [13], where each case of HIV infection was matched with up to 99 individuals according to age, gender and seronegative status. From the age of 25 years, the HIV-infected cohort of 3, 990 individuals displayed lower survival rates than their healthy counterparts (19.9 years vs. 51.1 years). However, during the period 2000 – 2005, survival increased to 32.5 years and coincided with the availability of HAART.

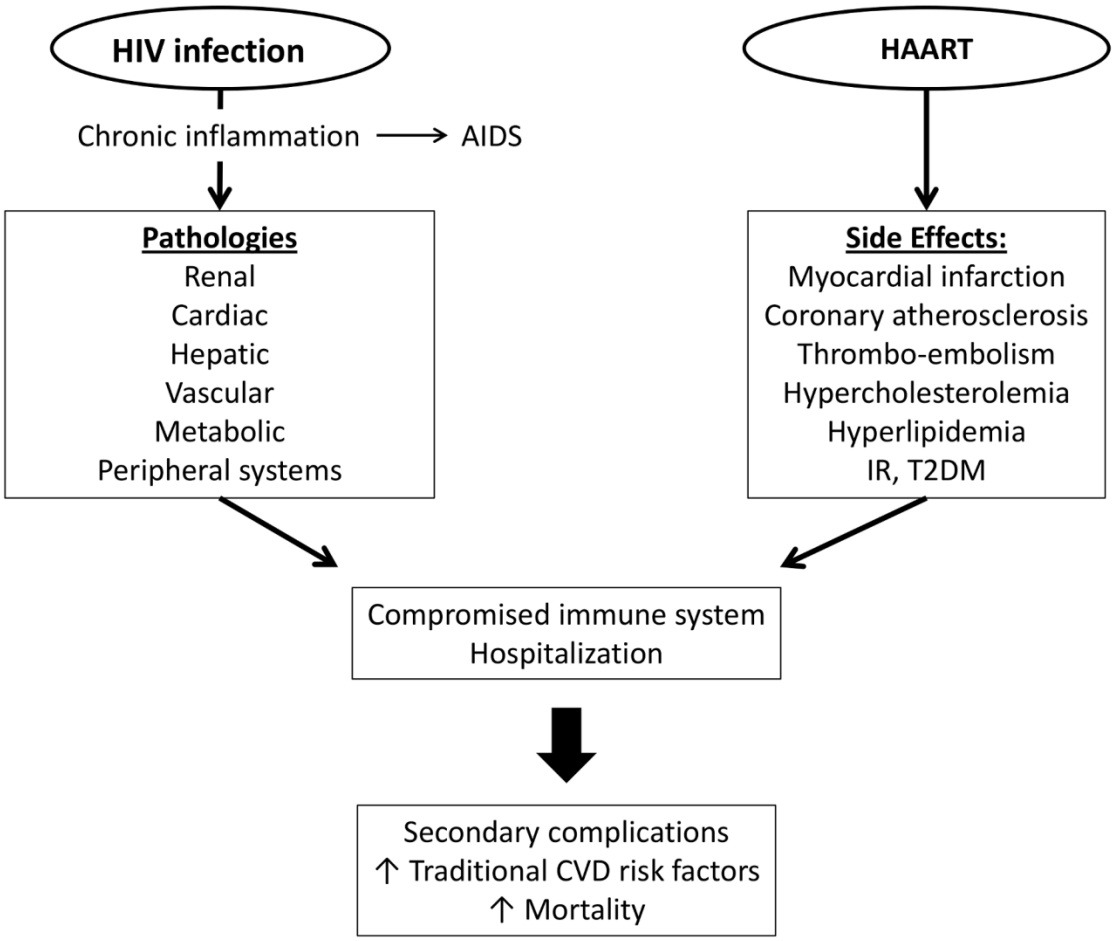

Figure 1. HIV infection and HAART: detrimental side effects. Multiple organ systems are adversely affected by infection with the HI virus, and treatment with HAART drugs (e.g. protease inhibitors) further exacerbate side-effects with their own unique pathologies. Ultimately the patient's quality of life (encompassing many facets) becomes compromised, leading to an increased risk for future cardiovascular and organ pathologies. *AIDS – acquired immunodeficiency syndrome, IR – insulin resistance, T2DM – type 2 diabetes mellitus, CVD – cardiovascular diseases.*

Chronic immune activation presents quite a challenge to the myocardium and key studies highlight the role of HIV in the cardiovascular disease burden. Firstly, Becker and colleagues (2010) [14] observed that HIV-infected HAART naïve patients with acute coronary syndrome (ACS) exhibited less traditional CVD risk factors than their HIV negative counterparts (with ACS), but a significantly higher thrombotic burden (43% vs. 17%) and different angiographic characteristics. Not only were these

results confirmed in similar studies [15,16], but data pointed towards a distinct pathogenesis of cardiovascular abnormalities in HIV-infected versus healthy individuals. Here HIV-positive individuals with ACS were compared to HIV negative and diabetic non-ACS counterparts, and although the extent of multi-vessel disease in all three groups was similar, HIV-positive individuals were much younger and had less complex lesions than their controls. Further, the degree of subclinical coronary atherosclerosis was elevated within the HIV-infected population [16]. These studies and others are presented in **Table I**. Therefore, the nature of HIV itself allows for viral-mediated activation of pathways that contribute to the development of thrombotic and atherosclerotic disease infection in addition to the traditional risk factor pathways. However, the focus has now shifted from opportunistic infections to metabolic and cardiovascular complications, especially within the context of HAART and extended lifespans. The focus of this review article is therefore on HAART-linked onset of cardio-metabolic complications, with particular emphasis on the damaging role of PIs.

Table I. HIV ± HAART and the risk for MI and cardiovascular complications (clinical studies).

Author	Outcome
Jericó C [17], de Saint Martin L [18], Lo J [16]	**Atherosclerosis, coronary-intima-media-thickness alterations, subclinical atherosclerosis**
Lijfering WM [19], Sullivan PS [20], Maggi P [21]	**Thrombosis, vascular lesions**
Majluf-Cruz A [22], Gazzaruso C [23], Lekakis J [24], Boccara F [25], Butt AA [26]	**ACS, heart failure, CAD, MI**

Abbreviations: *ACS – acute coronary syndrome, CAD – coronary artery disease, HAART – highly active antiretroviral therapy, HIV – human immunodeficiency virus, MI – myocardial infarction.*

PIs and cardiovascular consequences

ARVs increase life expectancy and quality of life of HIV-positive individuals and its usage is essential to combat HIV's detrimental effects. ARVs inhibit the viral lifecycle at key stages and the combination of different classes as HAART constitutes critical weaponry in the fight against HIV/AIDS (**Fig. 2**). For example, an extensive study comprising of 41, 213 HIV-infected patients exposed to HAART for ≥72 months revealed that ARVs significantly improved death rate versus HAART-naïve patients (20.9 deaths per 100 person-years observation vs. 5.2 deaths) [27].

PIs act by inhibiting HIV aspartyl protease leading to the production of immature and non-infectious viral particles [28]. More than 10 HIV PI-type drugs have been developed since the advent of HAART in 1995 [29], with Lopinavir/Ritonavir the latest, and the drug of choice for this study. Lopinavir and Ritonavir are heterocyclic compounds with the liver a major site for Lopinavir metabolism. Kumar *et al*. (2004) [30] investigated metabolism of Lopinavir in a number of species and established that after uptake and release into circulation, most of it binds to plasma proteins (>97%). Moreover, they found that Lopinavir was taken up, to varying degrees, by most tissues including the heart (in rats). However, it poorly penetrated the blood-brain barrier. Lopinavir is metabolized to a number of oxidative metabolites, although the parent compound is the major circulating drug with only a small percentage of metabolites present [30,31]. Such metabolites are also less potent inhibitors of HIV protease [32]. Since Lopinavir is metabolized by the hepatic enzymes CYP3A4 and CYP3A5 [31], its circulating concentrations are inadequate to suppress viral replication (if employed as monotherapy). However, Ritonavir potently inhibits CYP3A4 and CYP3A5, thereby ensuring higher Lopinavir plasma concentrations [33,34]. In light of this, Ritonavir was co-formulated with Lopinavir, i.e. Kaletra ™ and Aluvia ™ (the latter with improved heat stability) [33].

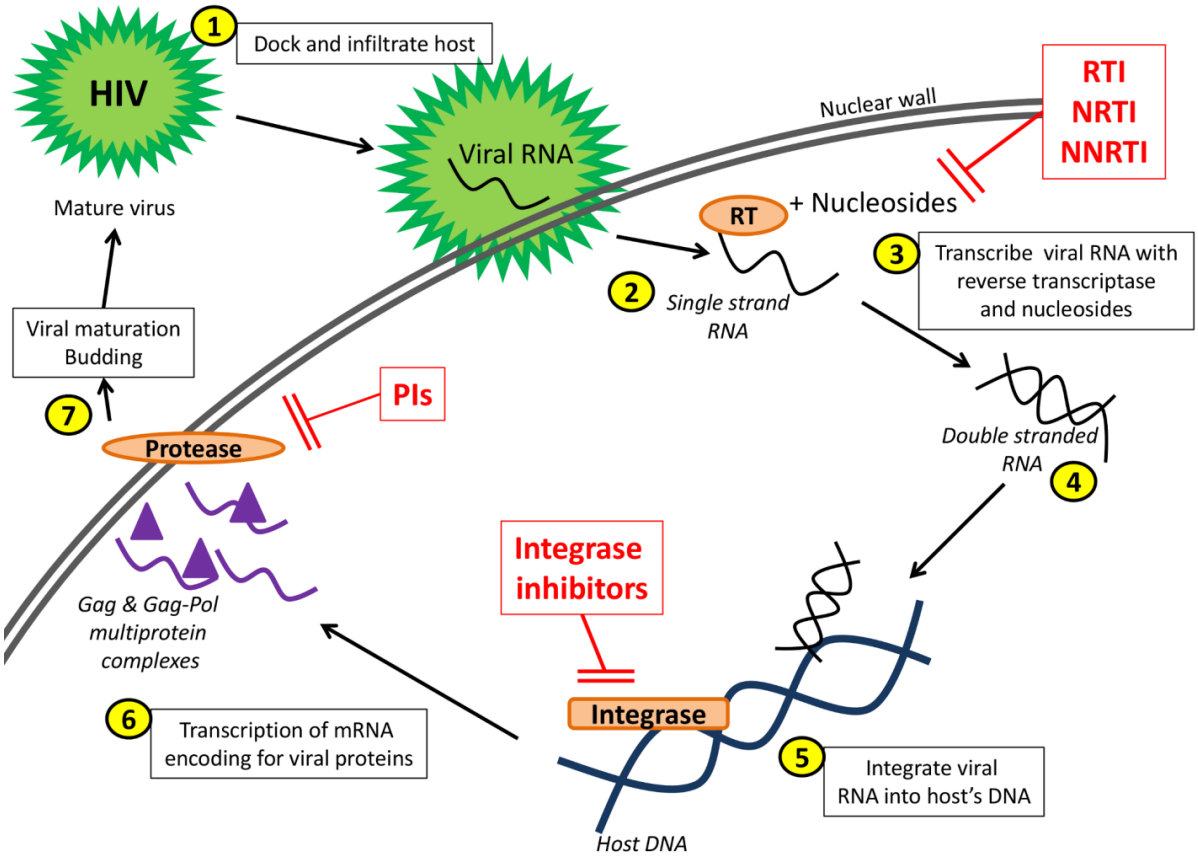

Figure 2. HIV lifecycle and antiretroviral drug targets. 1. The virus docks and infiltrates the cell membrane of the host cell. 2. Single-strand viral RNA enters the host nucleus where 3. Viral reverse transcriptase transcribes single-stranded RNA. 4. Production of double-stranded RNA. 5. RNA enters the nucleus and integrates itself within the host's DNA with integrase. 6. The host's transcription system allows viral mRNA production for viral proteins, 7. Gag and Gag-pol multi-protein complexes assemble and bud at the host's cell wall where proteases cleave proteins and mature viral particles. HAART can inhibit key viral enzymes at various stages of the viral life cycle – reverse transcriptase (RTI), nucleosides and non-nucleoside reverse transcriptase inhibitors (NRTI, NNRTI), integrase inhibitors and protease inhibitors (PI). *DNA – deoxyribonucleic acid, HIV – human immunodeficiency virus, mRNA – messenger RNA, RNA – ribonucleic acid.*

PIs are also implicated in the onset of cardiovascular complications with increased risk for myocardial infarction (MI) and coronary syndromes. In one of the largest clinical studies assessing the risk for MI with HAART, the Data Collection for Adverse events of Anti-HIV Drugs (DAD) Study Group recruited 23, 468 HIV-positive patients on HAART [35–37]. Here cumulative exposure to HAART was linked to a strong increase in the incidence of MI (26% relative change), with PIs contributing the most significant risk. Although the absolute risk for MI was low when adjusted for confounding parameters, HAART and PIs exacerbated traditional CVD risk factors such as cholesterol and lipid abnormalities, and type 2 diabetes mellitus (T2DM). Similar results were found in large cohort studies where the absolute rate of MI events remains low [38,39] and PIs are significantly associated with the occurrence of MI [20,35,36,38–40]. Further, cumulative time exposed to HAART regimens (including PI) can increase mortality [27,37,41]and hospitalization for cardiovascular complications [42] in the long-term.

Echocardiographic abnormalities are also associated with the use of Ritonavir. For example, baseline echocardiography revealed significant rates of left ventricular systolic and diastolic dysfunction, pulmonary hypertension and left atrial enlargement in an HIV-infected cohort [43]. Though some studies do not support a link between PIs and atherosclerosis [20,44] (due to minimal differences between PIs and other antiretrovirals (ARV) in HAART), many others do report a clear link with the development of subclinical atherosclerotic lesions [17,18,21,45] and thrombotic environments [19,22]. Studies linking cardiovascular and MI incidence are summarized in **Table II**.

Table II. PI treatment and the risk for MI and cardiovascular complications (clinical studies).

Author	Outcomes
Friis-Møller N [35,36], Smith C [37], Holmberg SD [38], Mary-Krause M [39], Durand M [40], Lang S [46], Coplan PM [47]	PIs ↑ AMI events, associated with MI risk, and ↑ risk for CVD
Triant VA [41], Klein D [42], Lifson AR [48]	PIs ↑ mortality and/or hospitalization due to cardiovascular complications
Mondy KE [43]	ECG abnormalities with PI use
Sullivan PS [20], Lyonne L [44]	Minimal link with PIs and atherosclerotic lesions
Maggi P [21], Bernal E [45], de Saint Martin L [18], Jerico C [17]	PIs associated with subclinical atherosclerotic lesions

Abbreviations: *AMI – acute myocardial infarction, CVD – cardiovascular disease, ECG – electro-cardiogram, MI – myocardial infarction, PI – protease inhibitor.*

PIs and changes to lipid metabolism

HIV PIs likely exert direct and indirect effects (e.g. altered metabolism – systemic and organ-related) on the cardiovascular system. Its' direct effects on the heart is less well understood compared to indirect changes elicited. In terms of the latter, PIs can trigger metabolic side-effects that resemble the metabolic syndrome (MetS), a combination of risk factors that predispose to future onset of T2DM and CVD [49]. Various definitions and cut-off parameters exist for the MetS but the main risk factors include abdominal obesity, atherogenic dyslipidemia, insulin resistance (IR) (with or without glucose intolerance), elevated blood pressure, pro-inflammatory status and a pro-thrombotic state [49–51]. In support, human- [52–58], animal- [59–61] and cell-based [62–65] studies demonstrate that increased plasma cholesterol and triglyceride (TG) levels, and the development of lipodystrophy and IR are the most common metabolic perturbations found with PI treatment. Together such metabolic derangements trigger inflammation, stress the myocardium [66,67], and may potentially predict the onset of IR and cardiac dysfunction [56,68] . **Table III** summarizes the main clinical findings relating to alterations in lipid metabolism with PIs.

Table III. Lipid changes associated with PI therapy (clinical studies).

Author	Outcomes
Behrens G [52], Bastard J [53], Carr A [54], Dong K [55], Gan S [56], Tsiodras S [57], Floris-Moore M [58]	↑ plasma cholesterol, ↑ TG, LD and IR development with PIs
Sekhar R [69]	LD, ↑ REE, ↑ FAO, ↑ FFA
Mulligan K [70], Bernal E [45], Carr A [66,71,72], Gazzaruso C [23], Biron A [73]	Anthropometric changes accompanied with development of dyslipidemia and MetS with PI treatment ≥ 12 months

Symbols: ↑ - *increase.* Abbreviations: *FAO – fatty acid oxidation, FFA – free fatty acid, IR – insulin resistance, LD – lipodystrophy, MetS – metabolic syndrome, PI – protease inhibitor, REE – resting energy expenditure, TG - triglycerides.*

With lipodystrophy an imbalance in fat partitioning occurs with lipoatrophy occurring at the extremities (e.g. lower legs, arms, face) and central accumulation of fatty tissue especially at subcutaneous sites (e.g. waist, hips, neck). The over-accumulation of subcutaneous fat elevates cholesterol and TG levels within the abdominal area and cause dyslipidemia. Further, the increased burden of lipodystrophy with HIV infection can alter fatty acid (FA) metabolism. For example, Sekhar and colleagues (2002) [69] found that HIV-positive men with lipodystrophy displayed higher resting energy expenditure rates, elevated free fatty acids (FFA) and fatty acid oxidation (FAO) versus healthy non-infected controls. Moreover, lipid parameters measured in these individuals were highly indicative of MetS.

Studies assessing anthropometric changes established that PI-mediated metabolic derangements may occur before the onset of overt body changes such as increased waist circumference and weight gain [70]. However, dyslipidemia and MetS can manifest simultaneously with anthropometric alterations, especially for PI therapy longer than 12 months [23,45,71–73]. Lastly, alterations to glucose metabolism are linked to PIs, e.g. it can impair glucose tolerance as well as whole-body glucose disposal, glucose uptake, transport and phosphorylation and cause IR at peripheral sites such as skeletal muscle [52,74,75]. These data indicate that HIV PIs have far-reaching consequences on metabolism that may impact on cardiovascular function. How does this occur? It is likely that PIs act early-on at the molecular level to activate key metabolic pathways, and initiate a cascade of detrimental alterations that progressively contribute to the development and presentation of dyslipidemia, lipodystrophy and weight gain. This then provides impetus for further downstream lipid- and glucose-mediated derangements and related pathophysiology such as oxidative stress, mitochondrial impairment, IR/T2DM and the onset of CVD.

Molecular mechanisms underlying PI perturbations

The molecular mechanisms underlying cholesterol and FA synthesis strongly implicate transcriptional (sterol-regulatory element binding protein [SREBP] and peroxisome proliferator-activator gamma coactivator one alpha [PGC-1α]) and the proteasomal degradation pathway in this process.

SREBPs

The SREBPs are master transcriptional regulators of enzymes required for the production of cholesterol, TG and FA synthesis [76]. SREBPs are basic helix-loop-helix-leucine-zipper (bHLH-LZ) transcription factors [77] and is bound to the endoplasmic reticulum (ER) and the nuclear membrane. This precursor SREBP consists of 3 connected parts spanning the sarcolemma: i.e. an NH_2-terminal domain, two hydrophobic trans-membrane-spanning domains, and a COOH-terminal domain. The SREBP gene is located on two chromosomes, namely 17p11.2 (generates SREBP-1a and -1c) [78] and 22q13 (generates SREBP-2) [79].

Tontonoz *et al.* (1993) earlier referred to the SREBP-1c isoform as adipocyte differentiation dependent factor 1 (ADD1) since it plays a role in adipogenesis [80]. SREBPs are ubiquitously expressed, i.e. SREBP-1a in cells with high proliferative capacity [81] while SREBP-1c is the dominant form in liver, white adipose, skeletal, cardiac, adrenal, and brain tissues.

The SREBP pathway is an example of end-product feedback regulation of gene transcription (**Fig. 3).** The depletion of sterol levels triggers the pathway where SREBP cleavage activating protein (SCAP) associates with the SREBP precursor protein on the ER. Site 1 and Site 2 proteases (S1P, S2P) proteolytically cleave the hydrophobic trans-membrane domain from the NH_2-terminal and SREBP is translocated into the nucleus [82,83]. Thereafter SREBP binds to sterol-response elements (SRE) (5'-TCACNCCAC-3') or E-boxes (5'-CANNTG-3') [84] within the promoter regions of the SREBP and target genes thereby initiating gene transcription. Isoforms of the SREBP-1, -2 and target gene proteins further activate FA and cholesterol biosynthesis genes [76,85–87] resulting in increased production of sterols. Negative feedback regulates the pathway once appropriate sterol levels are produced.

Intra-nuclear SREBP levels are also regulated by proteasomal degradation. Here the 26S and 20S proteasomes first ubiquitinate and then degrade active nSREBPs [88–90]. However, if proteasome inhibitors are administered, nSREBP levels stabilize leading to increased gene expression of target genes [88]. Furthermore, SREBP-1a and 2 contain small ubiquitin-related modifiers that are able to decrease their transcriptional activity by sumoylation [91]. As sterol levels are replenished, the SREBP transcriptional pathway described is blunted, while enzyme activity and sterol production declines in parallel.

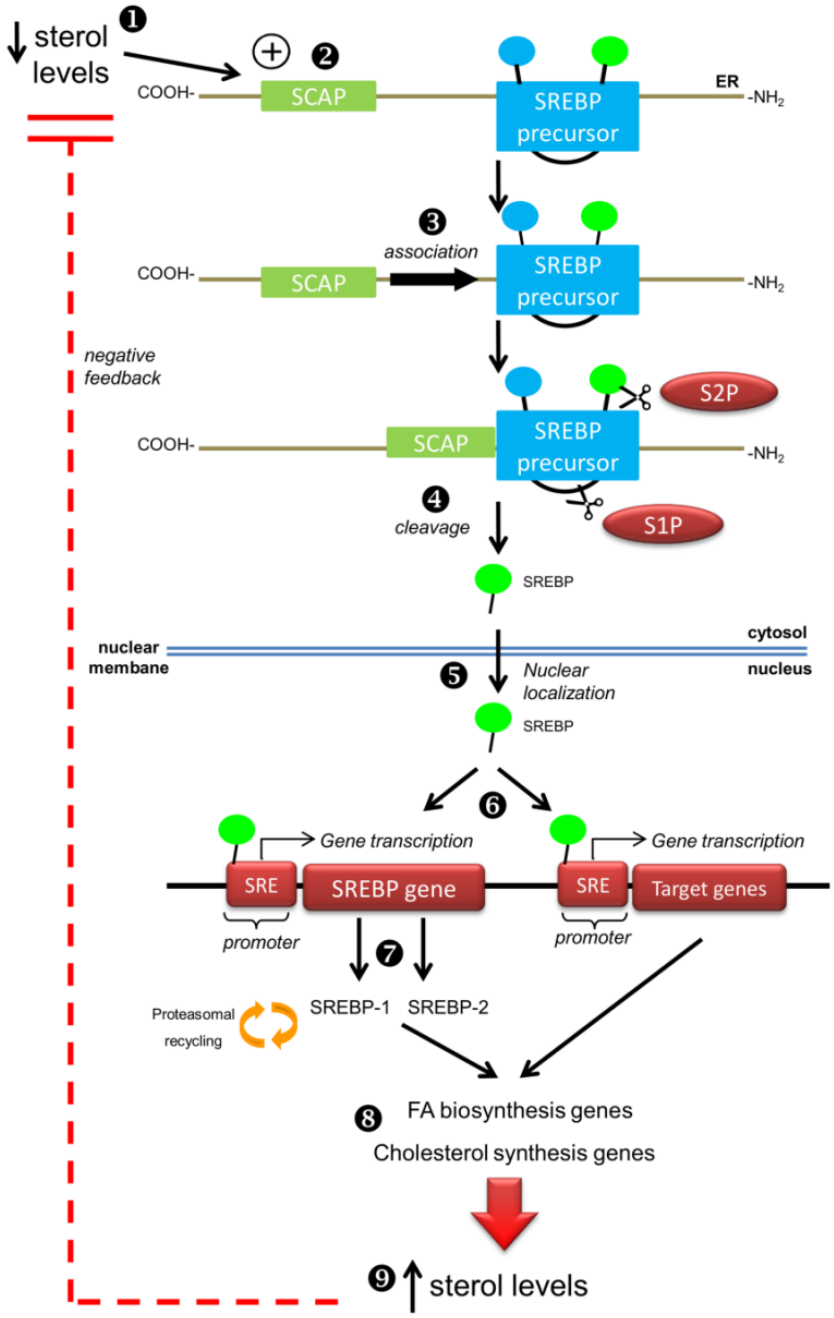

Figure 3. The SREBP pathway. 1) Depletion of sterol levels triggers pathway activation. 2) SREBP cleavage activating protein is stimulated (SCAP). 3) SCAP associates with the COOH-terminal of the SREBP precursor protein. 4) Site 1 and Site 2 proteases (S1P, S2P) proteolytically cleave the hydrophobic trans-membrane domain and release it into the cytosol. 5) Active SREBP is translocated into the nucleus via importin. 6) SREBP binds to sterol-response elements (SRE) or E-boxes within the promoter regions of the SREBP and target genes. 7) Isoforms of the SREBP gene (SREBP-1 and 2) are transcribed. 8) SREBP-1, -2 and target gene proteins further activate fatty acid (FA) and cholesterol biosynthesis genes [76,85–87] increasing sterol production. Negative feedback along with proteasomal recycling of SREBP-1 and -2 regulate the pathway.

The three SREBP isoforms allow for specific activation of target genes. Here SREBP-1 targets lipogenic genes for FA and TG biosynthesis [92] while SREBP-2 activates transcription of cholesterogenic genes [93]. Different organs also possess various lipogenic capacities, with liver and adipose tissue having a higher capacity [94] compared to muscle and heart tissue. This is to be expected since the latter are major sites for FAO [95]. The distinguishing mechanisms occur at the gene promoter level, i.e. lipogenic genes containing SRE/SRE-like elements are largely activated by SREBP-1a, while cholesterogenic genes are more likely be activated by SREBP-1c and 2 containing variations of the SRE/SRE-like elements within their promoters [96].

Acetyl-CoA is an important player in terms of actual SREBP gene targets. It is the precursor for the formation of lipid entities and diverges according to its end-product. Acetyl-CoA is converted to 3-hydroxy-3-methyl-glutaryl-coA (HMG-CoA) by HMG-CoA-synthase, and thereafter reduced to mevalonate via HMG-CoA-reductase. Mevalonate is thereafter further metabolized and ultimately produces cholesterol. The conversion of acetyl-CoA to malonyl-CoA is the first step of FA synthesis in lipogenic tissues such as the liver and fat cells. Fatty acid synthase (FAS) catalyzes the production of saturated FAs that are shunted to monosaturated FAs and fatty-acyl-CoA via stearoyl-CoA-destaurase 2 (SCD2). Ultimately, glycerol-3-posphate-acyltransferase-[mitochondrial] (GPAM) converts fatty-acyls to phospholipids (TGs) and FAs (extensively reviewed in [76,87]). Genes encoding for acetyl-CoA-carboxylase (ACC) [97,98], FAS [98,99], GPAM [100], HMG-CoA-reductase [101–104], HMG-CoA-synthase [105], SCD2

[106] and low-density lipoprotein receptor (LDL-R) [98,107] all contain SREBP binding sites and are thus directly regulated by SREBP and sterol levels within the cell.

A number of *in vitro* [108,109] and *in vivo* [109–112] studies show that PIs can exert lipid-related perturbations at the transcriptional level. For example, PIs inhibit adipocyte differentiation and transcription of FA-related genes in 3T3-L1 adipocytes when treated with therapeutic concentrations for ten days [108]. Furthermore, microarray analyses of 3T3-L1 adipocytes treated with PIs indicate robust transcriptional effects as genes involved in inflammatory cytokine production, oxidative stress, stress response, apoptosis and lipid metabolism were markedly altered with treatment [61,113,114]. Similar effects were found in cultured hepatocytes [109] and also when employing animal models [109–112], e.g. PIs elevated lipid production in mice (increased plasma TGs and cholesterol) while enhancing FAS protein levels in parallel [109]. Further, genes involved in FA synthesis and oxidation were up- and down-regulated, respectively, following seven days of PI administration to male Sprague-Dawley rats [110]. Interestingly, a Western-type diet administered together with Ritonavir (fourteen days) resulted in the exacerbation of the hyperlipidemic phenotype, hepatic steatosis and hepatomegaly [111]. However, animals co-administered a normal diet still showed marked levels of plasma lipids and activation of FA and cholesterol synthesis compared to PI-naïve controls. Here SREBP accumulated within the nucleus of hepatic and adipose tissues even though mRNA levels remained unaltered with PI therapy.

Apolipoprotein B (ApoB) levels are essential for the production of very-low density lipoprotein (VLDL) particles and contribute to the cholesterol pool. ApoB is hydrolyzed from TG-containing chylomicrons via lipoprotein lipase (LPL) and released from the liver into circulation as VLDL. Inhibition of the proteasomal degradation of ApoB leads to its accumulation; however, this does not translate directly in to elevated VLDL production as secretion of ApoB is also necessary in addition to its synthesis [115,116]. If *de novo* lipid and cholesterol synthesis are activated (e.g. via PI-mediated accumulation of SREBPs), this can contribute to an increase in the production of lipoproteins and ApoB [117]. Liang and colleagues (2001) [60] demonstrated that PIs can also inhibit LPL (in addition to proteasomal degradation of ApoB), with the subsequent accumulation of ApoB and activation of lipid synthesis. ApoB and lipoproteins are also significant factors in the development of atherosclerosis with HIV infection and antiretroviral therapy (ART) [118].

SREBPs are recycled via the ubiquitin-proteasome system (UPS) and this ensures lipid and cholesterol metabolism are optimally maintained. However, when the UPS is inhibited, levels of ubiquitinated SREBPs increase and subsequent activation of lipid genes [88]. Notably, ubiquitination of SREBP-1 occurs while it is bound to the promoter region of its target gene. Here the E3 ligase Fbw7 associates with the bound SREBP-1 to attach a ubiquitin moiety and the UPS can then remove and degrade SREBP, halting transcription of the target gene [119]. Thus SREBP levels are controlled by DNA binding, and UPS inhibition effectively means SREBPs remain bound to DNA promoters for longer. This in turn can increase target gene transcript levels without directly affecting SREBP levels.

Together this indicates that PIs can alter lipid metabolism by the SREBP transcriptional pathway and via its direct effect on key lipogenic and cholesterogenic enzymes that ultimately leads to an increased risk for future atherosclerotic and cardiovascular complications (**Fig. 4**).

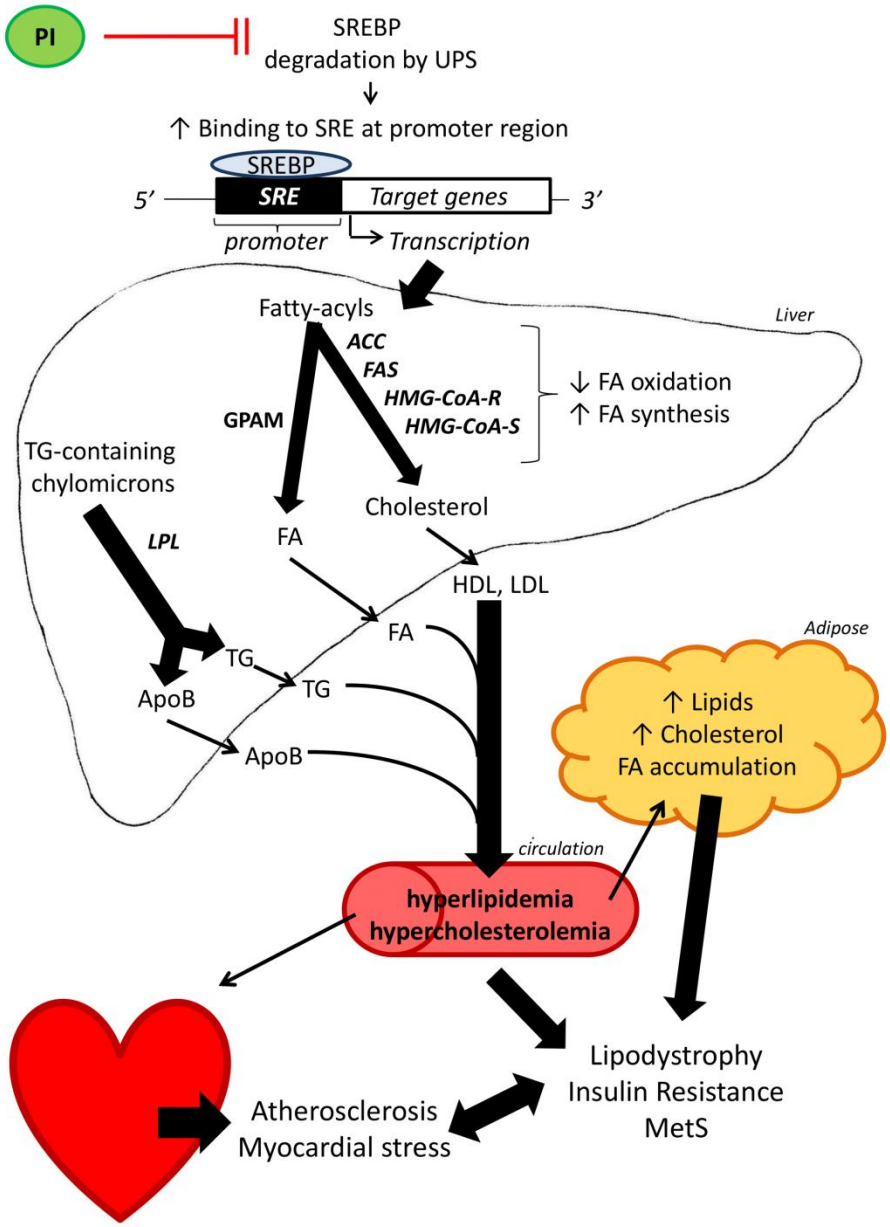

Figure 4. The effects of PIs on lipid metabolism. PIs inhibit proteasomal degradation of SREBP causing an accumulation of SREBP bound to the promoter region of target genes essential for the generation of metabolic enzymes catalyzing cholesterol and lipid synthesis pathways in liver and adipose tissues. Ultimately, the over-accumulation of fatty acids and cholesterol leads to hyperlipidemia and hypercholesterolemia – ensuring an atherogenic state within the myocardium and elevated risk for cardiovascular pathologies such as myocardial infarction and diabetes. *ACC – acetyl coenzyme A carboxylase, ApoB – Apolipoprotein B, FA – fatty acids, FAS – fatty acid synthase, GPAM –glycerol-3-phosphate-acyltransferase-[mitochondrial], HMG-CoA-R/S – 3-hydroxy-3-methyl-glutaryl-CoA-reductase/synthase, HDL/LDL – high/low-density lipoprotein, LPL – lipoprotein lipase, MetS – metabolic syndrome, PI – protease inhibitor, SREBP – sterol regulatory element binding protein, SRE – sterol-response element, UPS – ubiquitin proteasome system.*

HIV PIs and the ubiquitin-proteasome system

The UPS is an important regulatory system that exists to monitor protein turnover and removal of cellular debris, expired and/or damaged proteins. This pathway is especially important in cardiac cells where a high rate of protein turnover, energy requirement and physical stress occur and protein quality control is vital [120–122]. The UPS is a non-lysosomal degradation pathway involved in many cellular processes such as transcriptional regulation [123], mitochondrial protein turnover and function[124–128], cardiac ion channels and sarcomeric protein integrity [121,129]. The main steps of the UPS involve tagging a selected protein with a ubiquitin moiety and proteolysis via the proteasome complex (reviewed in [120]).

Ubiquitination occurs via 3 enzymes that require ubiquitin - E1, conjugation of ubiquitin - E2, and attachment via ligase - E3 (ATP dependent reactions). The 26S proteasome is a multicatalytic multi-unit complex consisting of a 20S proteolytic core capped at each end by 19S components (**Fig. 5**). The 20S catalytic subunit degrades proteins via its chymotrypsin-, trypsin- and caspase-like activities (ATP-independent process).

Mitochondrial proteins make up the bulk of ubiquitinated proteins (~38%) with those in the cytosol comprising approximately 27% [130]. The majority of mitochondrial electron transport chain (ETC) complexes and key contractile proteins possess ubiquitin binding sites and therefore act as ubiquitin substrates. These include F_1F_0-ATPase subunits, flavoproteins, NADH-ubiquinones, sarcoplasmic/endoplasmic reticulum ATPase 2 (SERCA2), desmin, contractile machinery and cardiac ion transporters [130]. Since the mitochondrion is a powerhouse of energy metabolism it is essential that it possesses in-house mechanisms for protein quality control.

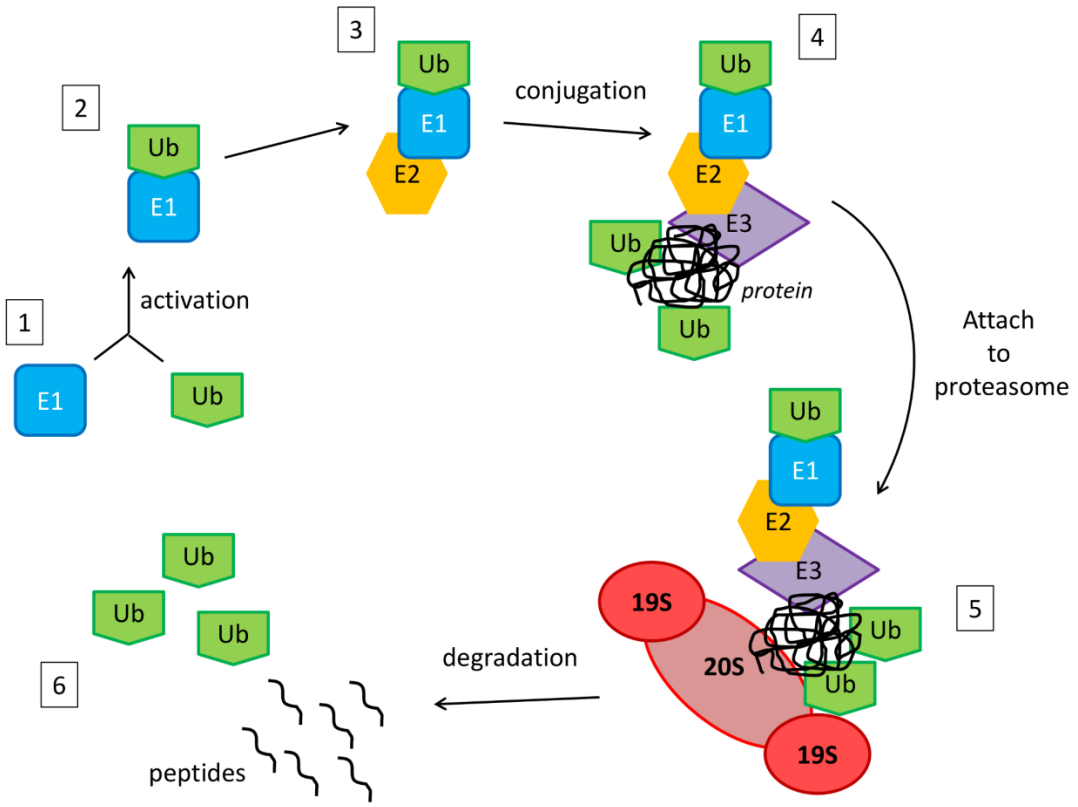

Figure 5. The ubiquitin-proteasomal degradation system (UPS). The UPS is sequentially activated with 3 key enzymes. 1) E1 activates and prepares ubiquitin. 2) E1 associates with ubiquitin to form a complex. 3) The conjugating enzyme E2 associates with the E1-Ub complex. 4) The conjugation of the Ub moiety and E3 on the target protein which then binds to the multicatalytic proteasome. 5) The proteasomal activities of the various subunits ensure that the target protein is degraded. 6) Ub dissociates from the complex and peptides are released into the cytosol for further processing. *Ub – ubiquitin.*

Mitochondria contain ubiquitin activating enzymes (E1) and E3 ligases found within the outer mitochondrial membrane (OMM) [131–133]. However, the proteasome is not present within mitochondria raising the question how mitochondrial proteins are actually ubiquitinated and degraded by the proteasome. Here mitochondrial-associated degradation (MAD) plays a role, i.e. mitochondrial E1 tags proteins for ubiquitination, with subsequent retro-translocation to the OMM. This is followed by further ubiquitination by the E3 ligases present on the OMM[124–128]. Emerging data

support this notion, e.g. Margineantu *et al.* (2007) [134] found that the F_1F_0-ATPase residing at the inner mitochondrial membrane (IMM) was retro-translocated to the OMM, ubiquitinated and subjected to proteolysis. The study also showed that proteasomal inhibitors caused mitochondrial protein accumulation, e.g. cyclo-oxygenase 1 (COXI). In support, others reported similar results for uncoupling protein 3 (UCP3) [135]. Indeed, proteasomal inhibition may leave "a path of destruction in its wake", e.g. certain conditions such as Parkinson's disease are associated with the accumulation of ubiquitinated proteins and defective degradation [136]. Moreover, accumulation of especially transcription factors and enzymes may incorrectly alter signaling pathways and thereby elicit detrimental consequences.

The intracellular redox status also has a significant impact on UPS function. The 26S proteasome is particularly sensitive to its oxidative environment, and lipid peroxidation can inhibit cardiac 20S proteasome activity [137,138]. Oxidatively modified proteins are known substrates for ubiquitination [139,140] and improper removal may increase the overall intracellular oxidant burden within the cell. Paradoxically, oxidative stress can also inhibit UPS activity and increase the generation of free radicals [136,140–142]. This ultimately places greater oxidative stress on the cell and anti-oxidant systems, and may create a vicious cycle of perpetual inhibition of proteolysis and accumulation of ubiquitin aggregates.

HIV PI-mediated alterations in the UPS could play havoc with metabolism and potentially predispose patients to lipid accumulation, and ultimately atherosclerotic phenotypes (**Fig. 6**). For example, previous work found that Ritonavir is a competitive inhibitor of some proteasome subunits [89], while microarray analyses revealed that rats acutely treated with Ritonavir displayed a marked increase in gene and protein content for proteasomal components [143]. Further evidence show that HIV-1 itself can directly interact with the proteasome and decrease the host's immune response

[144,145]. The viral infectivity factor (Vif) of HIV targets the cytidine deaminase APOBEC3 protein for ubiquitination and subsequent degradation, hindering C-to-U mutations within the viral DNA to inhibit viral replication [145]. This indicates that both the virus and PIs provide a double blow to the UPS and may therefore serve as a starting point for metabolic perturbations via SREBP-1 and mitochondrial metabolism. In light of the literature discussed, mitochondrial metabolism is implicated as a downstream effector since the PGC-1α, the SREBPs and the UPS pathways play a central role in this process.

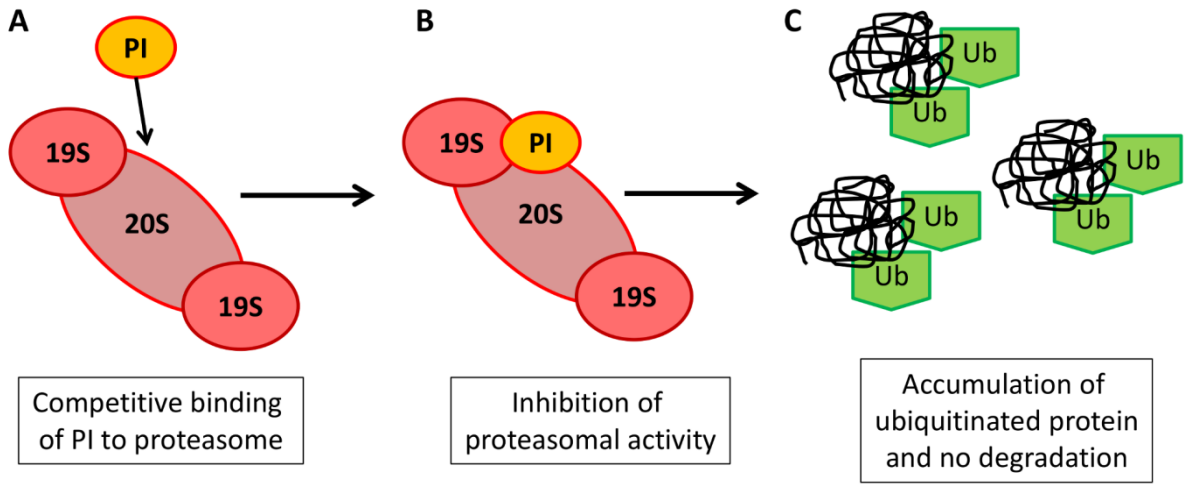

Figure 6. The effect of PIs on the ubiquitin-proteasome system (UPS).

PIs competitively bind to and inhibit proteasomal subunits, thereby decreasing its ability to degrade and recycle target proteins. This results in an accumulation of ubiquitinated proteins within the cell. *19S and 20S – proteasomal subunits, PI – protease inhibitor, Ub – ubiquitin*.

HIV PIs: calcium signaling and impulse propagation

Excitation-contraction coupling (ECC) refers to the mechanism whereby an electrical signal is propagated through nerve cells in the heart and transformed into a chemical message to induce cross-bridge formation and contraction of myofibers, known as the sliding filament theory. Stimulation occurs via autonomic signaling from the brain/cerebral vertebrae and travels down to the sinal-atrial (SA) node, more commonly known as the "pace-maker" of the heart.

Depolarization of the SA node occurs due to a difference in the relative charge across the neuron membrane and is propagated further as an action potential provided a great enough potential is reached. Action potentials eventually travel down the transverse T-tubules of individual cardiac muscle fibres and cause the opening of the voltage-dependent dihydropyridine-sensitive L-type calcium channel, which in turn allows the influx of relatively small amounts of calcium into the cytosolic compartment (known as "trigger calcium"). The binding of calcium ions to the ryanodine receptor (RyR) present on the sarcoplasmic reticulum (SR) results in its activation to allow an efflux of intra-sarcolemmal calcium into the cytosol. This is known as the calcium-induced calcium release (CICR) [146]. Calcium is now able to bind to the troponin-tropomyosin complex bound to the actin filament to expose its myosin binding site and thus allow for the attachment of myosin to actin. With the aid of 5'-adenosine triphosphate (ATP) a cross bridge is formed and the filaments slide past each other and cause the myofiber to contract. To release this bond, ATP must be hydrolyzed to ADP and inorganic phosphate (iP) and calcium removed via 5'-adenosine triphosphate synthase (ATPase) in the cytosol. Calcium is then sequestered and transported back into the SR lumen via another ATPase, SERCA. Calcium can also be taken up by the sodium-calcium exchanger (NCX) in a ratio of 3:1 (Na^{+}: Ca^{+2}). This represents one cycle of ECC under homeostatic conditions (**Fig. 7**).

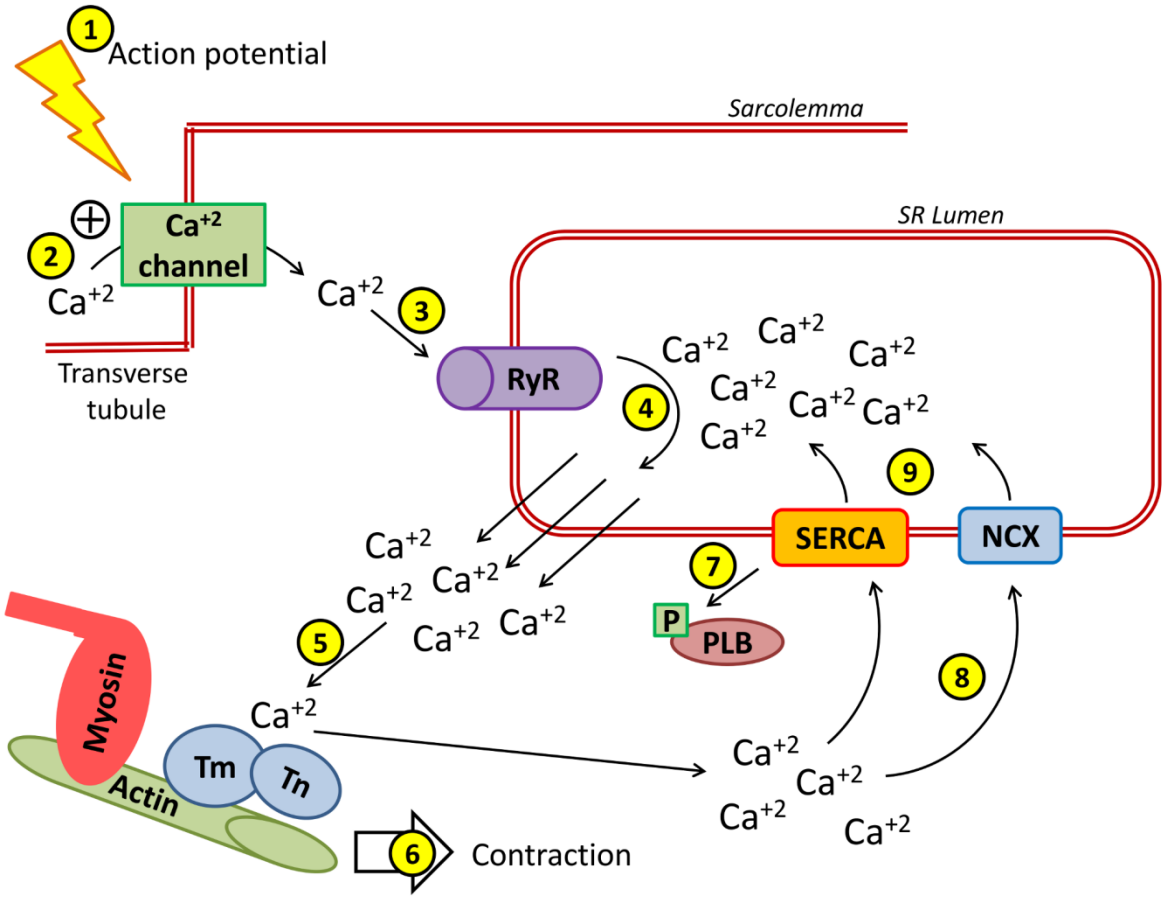

Figure 7. Excitation-contraction coupling (ECC) and calcium homeostasis. 1) Action potential (AP) received from a motor neuron travels down the transverse T-tubule of the muscle fiber and depolarizes the SR membrane. 2) The calcium channel present on the SR membrane opens and allows a small amount of calcium into the SR cytosol. 3) Calcium activates the ryanodine receptor (RyR). 4) A great efflux of calcium from the SR lumen into the cytosol occurs and is termed calcium-induced calcium release (CICR). 5) Calcium now binds to the troponin-tropomyosin complex exposing the myosin binding site on acting and allows for cross bridge formation. 6) Contraction takes place with the aid of ATP and calcium dissociates thereafter. 7) Phospholamban is phosphorylated to allow the SERCA channel to become activated. 8) Reuptake of calcium back into the SR lumen by SERCA and NCX channels.

AP – action potential, Ca^{+2} – calcium, NCX – sodium-calcium exchanger, RyR – ryanodine receptor, PLB – phospholamban, SERCA – sarcoplasmic-endoplasmic reticulum calcium ATPase, SR – sarcoplasmic reticulum, Tm – tropomyosin, Tn – troponin.

However, under oxidative conditions (e.g. HIV infection, chronic inflammation), ECC can become disrupted resulting in detrimental consequences for cardiac myofiber physiology. The RyR, SERCA and NCX all possess sulfhydryl (SH) groups of cysteine residues that can be modified by oxidation/reduction to alter channel sensitivity. For example, the RyR SH-groups are reduced to thiols thereby keeping the channel open [147–150], while the SERCA-2a [151–156] and NCX SH-groups [157–159] are oxidized rendering it inactive and unable to pump cytosolic calcium back into the SR. The consequence is calcium overload that leads to damaging downstream effects at both the mitochondrial and contractile levels; namely, a further exacerbation of ionic imbalance and toxicity, redox status of the myocardium, while excess reactive oxygen species (ROS) within the myocardium can inhibit calcium-ATP-hydrolysis coupling [151]. Thus cardiac calcium homeostasis is highly sensitive to ROS [160–162].

Calcium signaling itself is a major determinant of cardiac function and development of pathologies. Here it is SERCA, calcium/calcium-dependent pathways, phospholamban (PLB) and cardiac connexins that play a central role in the development, maintenance and propagation of cardiac contraction. Calcium transport for ECC is regulated by the RyR (on the SR membrane), SERCA-2a, and NCX, where SERCA-2a provides roughly 60% of the total calcium transport [163–165]. The action of SERCA pumping calcium into and from the SR ensures that a 1000-fold calcium gradient is maintained across the SR [166]. This is essential in providing the contractile machinery with the necessary calcium to initiate electrical propagation of the contractile stimulus and mechanical coupling, but to also reload the SR lumen with calcium for the next contraction.

SERCA isoforms are found in a variety of tissue types, where SERCA-1a is expressed in fast-twitch skeletal muscle, SERCA-1b during fetal development, SERCA-2a in slow-twitch skeletal muscle

and the myocardium, SERCA-2b in non-muscle and neuronal cells [167], and SERCA-3 in epithelial and endothelial cell types [168,169]. SERCA activity is mediated via β-adrenergic stimulation, phosphorylation [170,171], thyroid hormones [172] as well as insulin [172]. PLB is a key regulator of SERCA activity. Phosphorylation of PLB occurs at 3 different sites mediated by a variety of proteins: at Ser^{16} by protein kinase A (PKA), at Thr^{17} by calcium/calmodulin dependent protein kinase II (CaMKII) and at Ser^{10} by protein kinase C (PKC). Phosphorylation at these sites causes a conformational change in PLB, causing it to dissociate from SERCA and relieve its inhibitory effect [163,170,171,173–184]. Studies showed that PLB inhibition results in increased SERCA activity together with improved velocity of calcium uptake and heart function [185–189]. The SERCA:PLB ratio is also critical in determining cardiac contractility [177,182,183]. Further, modulation of PLB within the context of the failing heart is beneficial as genetic modification of PLB (knockout) results in an improvement in SERCA and contractile parameters [190–192].

Two major pathways regulate cardiac calcium homeostasis namely the calcium/calmodulin-calcineurin-NFAT and the calcium/calmodulin-dependent kinases-MEF2 pathways that involve calcineurin, calmodulin, nuclear factor of activated T-cells 3 (NFAT3) and myocyte enhancing factor 2 (MEF2) (reviewed in [163]). Calcium binds directly to calmodulin causing a conformational change to phosphorylated and activated CaMKII [193]. This in turn alters for the dephosphorylation of NFAT3 for transport into the nucleus, where it can activate cardiac genes associated with myocyte growth [194] and hypertrophy. MEF2 is also a downstream transcriptional regulator of NFAT3 and basal levels of expression help to maintain cardiomyocyte homeostasis. PGC-1α expression also works in conjunction with MEF2 [195] to promote mitochondrial biogenesis during cardiomyocyte growth.

Alterations in calcium metabolism with HIV PIs have been investigated in human [195,196] and cell-based studies [197]. For example, cultured HL-1 cardiomyocytes were treated with physiologically relevant doses of both Lopinavir and Ritonavir and assessed for electrical signal disturbances within ion channels[197]. PIs mediated the activation of the volume-sensitive chloride ion channel, important during the stress response (swelling) and mechanical force (stretching). Here the action potential duration was significantly shortened, together with altered mitochondrial membrane potential and increased mitochondrial ROS. These results indicate that PIs can have far reaching consequences on ionic and electrical homeostasis. Moreover, clinical data show that PI treatment prolonged the PR duration and QRS interval (ECG studies) of HIV-positive patients [195,196]. Here PIs emerged as independent predictors of increased PR durations and thus ECG abnormalities [196]. Similar studies have supported these findings [198–201], albeit inconsistently [202,203]. If ion channels are disrupted, action potential propagation does not occur correctly and can result in an ionic imbalance and also leakage of critical ions e.g. calcium, sodium and potassium into cellular compartments and upset the electrical gradient across membranes. This can further manifest as pathological signaling between the SA node within the atria and the ventricles with the Purkinje and His fibres. Prolonged portions of the ECG indicate a slowing of conductance velocity and do not allow the myocardium to maintain a steady rhythm during contraction. The depletion of endoplasmic calcium stores can also trigger ER stress that may result in the accumulation of unfolded proteins and ER-induced apoptosis (reviewed in [204]). In fact, ER stress is a common mechanism for PI-induced side-effects, e.g. Lopinavir is a potent inducer of ER stress that occurs downstream of ROS-dependent c-Jun N-terminal kinase (JNK) activation [205].

Impulse propagation between cardiomyocytes is another key factor that is tightly regulated. Here junctions are necessary to transfer electrical signals and chemical messengers between adjacent myocytes [206]. Such junctions are formed from two hemi-channels (connexons) and when two

neighboring gap junctions connect they become connexins. Connexins are named according to size and differentially distributed within the myocardium, e.g. connexin 43 (Cx43) is the most abundant [207–211]. Cx43 is also expressed in rat cardiac mitochondria, implicating mitochondrial biogenesis and ionic homeostasis in pathological alterations in Cx43 expression (**Fig. 8**).

When further elucidating connexin function, data revealed that the heart has a "conductance reserve". While gene knockout studies of either Cx40 or Cx43 do not always result in loss of function [208,212–217], transgenic *in vivo* models of connexin expression present with ventricular arrhythmias and atrial fibrillation [218–224]. Connexins have a relatively short half-life and undergo rapid turnover and recycling via the ER-associated degradation (ERAD) pathway with the assistance of proteasomal degradation [225–228]. Connexin phosphorylation results in activation and priming for ERAD [267], while connexins also regulate gating [268]. Studies found that when endocytosis of Cx43 for ERAD was inhibited this increased ubiquitinated Cx43 levels indicating that the proteasomal pathway is involved in Cx43 turnover and degradation [231–234]. To the best of our knowledge, no studies have been published regarding Cx43 biology and PI treatment.

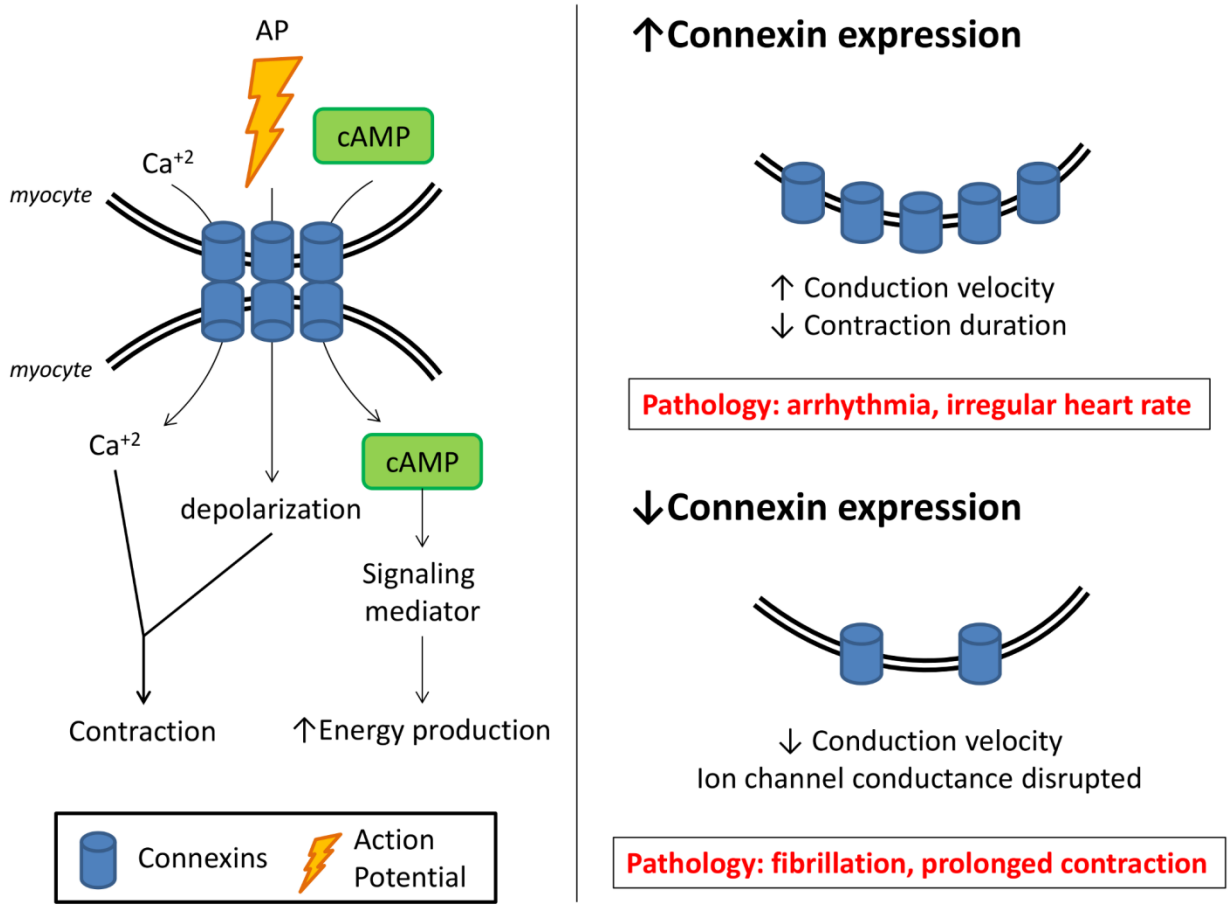

Figure 8. Connexin biology and alterations in expression. Left panel: ions and proteins such as calcium and cAMP and depolarizing stimuli in the form of action potentials are exchanged between neighboring myocytes through gap junctions. Calcium and depolarization can further ensure myocyte contraction and cAMP mediates energy producing pathways. Right: connexin expression for the formation of gap junctions is critical. Any alteration in connexin expression (genetically or via altered turnover through the proteasome) can create pathologies associated with ventricular fibrillation, arrhythmia and irregular heart rate. Further, ion channels and ionic gradients malfunction and lead to misfiring and incorrect propagation of electrical signals within the heart.

HIV PIs and energy homeostasis: role of PGC-1α

As previously mentioned, the dephosphorylation of NFAT3 and nuclear translocation promotes downstream gene transcription pathways involved in cardiomyocytes growth and mitochondrial biogenesis [194]. PGC-1α is a pivotal transcription modulator that regulates the transcription of mitochondrial and hypertrophic genes, and replication of mitochondrial DNA (mtDNA) and deserves further attention.

Regulators associated with PGC-1α include the mitogen-activated protein kinases (MAPK) [235–237], β-adrenergic/cyclic AMP [238], nitric oxide [239], AMP-activated protein kinase (AMPK) cascade [240], calcium/calmodulin/calcineurin pathway [241], peroxisome proliferator activator receptor gamma (PPARγ)[242,243] , thyroid hormones [244] and MEF2[245]. These regulators bind to the promoter region to activate transcription of PGC-1α, and may also bind to PGC-1α itself [246]. PGC-1α possesses an RNA processing domain and adaptor/scaffold ability to remodel chromatin as it is unable to bind directly to its DNA target [247–249]. Here the regulators directly interact with PGC-1α to activate downstream transcription factors such as nuclear respiratory actor 1 (NRF-1) [250] to promote the transcription of mitochondrial genes such as mitochondrial transcription factor A (mtTFA) [251]. mtTFA is transported to the mitochondrion from the nucleus and subsequently activates the transcription of ETC components such as the COX and ATPase subunits [252–254] . Thus NRFs together with PGC-1α ensure the activation of mitochondrial biogenesis [252,253,255,256] (**Fig. 9**).

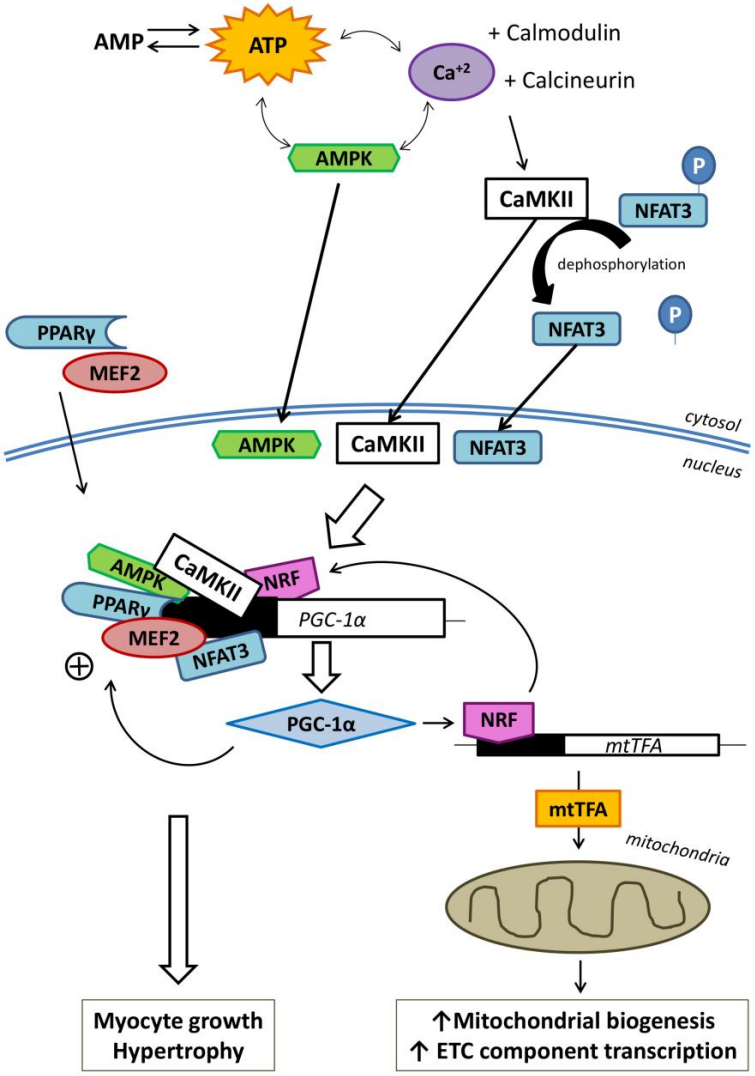

Figure 9. The PGC-1α pathway. Stressors such as exercise, hibernation or infection trigger a cascade of energy-sensing pathways. Here ATP levels, AMPK and calcium interlink and initiate the translocation of transcription factors to and within the nucleus, including dephosphorylated NFAT3. These transcription factors (PGC-1α, AMPK, NRF1, NFAT3, MEF2, PPARγ) bind to the promoter region of the PGC-1α gene to transcribe components essential for myocyte growth and hypertrophy. In parallel, NRF1 binds to the promoter region of the mtTFA gene to initiate the transcription and translocation of mtTFA to the mitochondrion – ensuring an increase in mitochondrial biogenesis, electron transport chain components and redox enzymes. These processes ensure that myocyte growth and energy capacity are elevated especially in the case of exercise and fiber-type switching. *AMP – adenosine monophosphate, ATP – adenosine triphosphate, AMPK – AMP kinase, CaMKII – calmodulin kinase II, ETC – electron transport chain, NFAT3 – nuclear factor of activated T-cells 3, NRF1 – nuclear respiratory factor 1, MEF2 – myocyte enhancing factor 2, mtTFA – mitochondrial transcription factor A, PPARγ – peroxisome proliferator-activator gamma, PGC-1α – PPARγ cofactor 1α.*

Mitochondrial biogenesis and energy metabolism are critical in meeting and maintaining intracellular energy requirements. Thus transcription of mitochondrial DNA and biogenesis needs to be tightly regulated to ensure optimal energetics. Studies overexpressing PGC-1α demonstrated increased mitochondrial number in cardiomyocytes [257], and enhanced mitochondrial biogenesis, respiratory rates, fuel substrate uptake and utilization [250,257,258]. Further, deletions of PGC-1α highlight its essential role in mitochondrial energetics [259]. In addition, decreased PGC-1α expression is a common feature of heart failure during pathological cardiac hypertrophy [260–262]. Current research involving PIs and the PGC-1α is sorely lacking, with a single study reporting that the PI Indinavir decreased mitochondrial respiration and ATP production together with attenuated expression of COX2 and COX4 [263]. Therefore further investigation is hastily required. Finally, prolonged PGC-1α overexpression caused mitochondrial biogenesis and cardiomyopathy that accompanies mitochondrial ultrastructural changes [257,264], implicating an elevated future risk for adaptive responses to become pathological. These results implicate PGC-1α in mitochondrial perturbations associated with PI treatment.

Oxidative stress plays a significant role in affecting the PGC-1α pathway. As noted by Richter *et al.* (1988) [265] and Ames *et al.* (1993) [266], human mtDNA is more susceptible to mutations and oxidative damage. Subsequently, mtDNA copy number increases with ageing but this does not alleviate the age-related decline in mitochondrial respiration [267]. However, PGC-1α combats this susceptibility in healthy individuals and early stages of ageing by regulating production of mitochondrial anti-oxidant enzymes such as superoxide dismutase (SOD), glutathione peroxidase (GPx), catalase and thioredoxin [259,266,268] . Thus the anti-oxidant role of PGC-1α is crucial to ensure cardiac mitochondrial and contractile functioning. Therefore, perturbations in the PGC-1 α pathway can have serious consequences on energy metabolism, mitochondrial health and cardiac contractility.

These data therefore shed light onto the potential mechanisms of PI-induced cardiac dysfunction and metabolic alterations, with the UPS playing a central role in the downstream effects. Our unifying hypothesis centres on the UPS and the detrimental downstream effects of PIs (**Fig. 10**). Here PIs competitively bind and decrease the UPS, thus attenuating degradation of key proteins such as the SREBPs, SERCA and the connexins. Subsequently, we propose that SREBPs remain bound to their target gene promoters and continue activating transcription of enzymes involved in lipid and cholesterol synthesis, thereby creating a hyperlipidemic and hypercholesterolemic environment within tissues and the blood. We further propose that SERCA activity will also be enhanced by the lowered UPS, and although it is tightly regulated by PLB, increased calcium transport back into the SR lumen may deprive the contractile machinery of the necessary calcium for contraction but also removal. Calcium supply is therefore disrupted and can have a knock-on effect on other calcium channels within the myocardium. Further, ionic imbalances may lead to a positive-feedback mechanism between calcium and the mitochondrial proton gradient, eventually contributing to an abnormal ionic status within the myocardium. Since connexins rely on frequent turnover, UPS inhibition may lead to over-accumulation of connexins thus disrupting normal electrical conductance. Here enhanced conduction velocity may develop into arrhythmias and irregular heart rate, ultimately resulting in contractile dysfunction and CVD in the long-term.

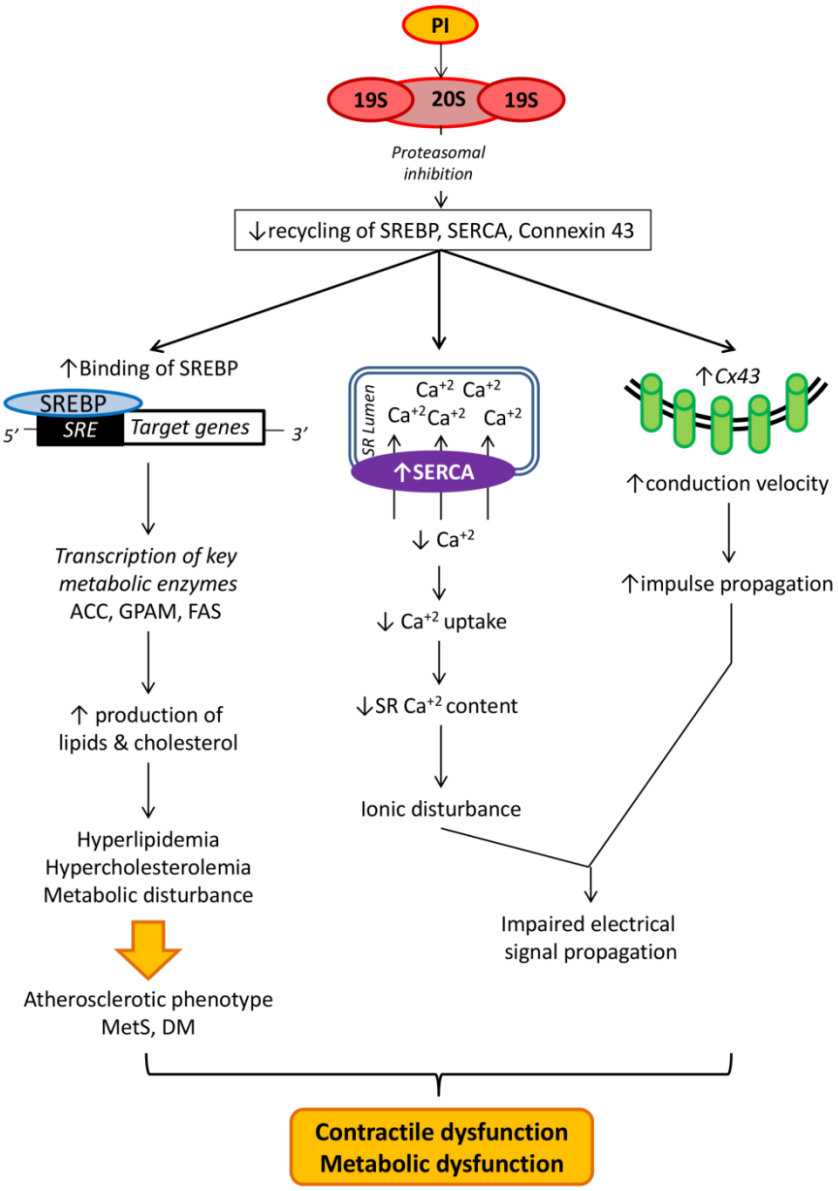

Figure 10. Molecular hypothesis for PIs and their detrimental effects on heart function. The unifying hypothesis encompasses the inhibition of the UPS as a central mechanism to PI-induced cardiac dysfunction. Over-accumulation of proteins that would otherwise be degraded, such as SREBP, SERCA and Cx43, have downstream consequences that impair the contractile machinery and metabolic processes. Ultimately, an atherosclerotic phenotype can develop and contractile dysfunction may occur. *19S/20S – proteasomal subunits, ACC – acetyl coa carboxylase, Ca^{+2} – calcium, Cx43 – connexin 43, DM – diabetes mellitus, ETC – electron transport chain, FAS – fatty acid synthase, GPAM – glycerol-3-phosphate-acyltransferase 1 [mitochondrial], MetS – metabolic syndrome, PGC-1α – peroxisome proliferator activator gamma coactivator 1 alpha, PI – protease inhibitor, SERCA – sarcoplasmic endoplasmic reticulum ATPase, SR – sarcoplasmic reticulum, SRE – sterol response element, SREBP – sterol regulatory element binding protein.*

PIs and cardiac dysfunction within the context of oxidative stress

Impaired redox status within the myocardium can be associated with negative outcomes in terms of functionality and contractility. As mentioned previously, mitochondria and related redox enzymes play a central role in the development of PI-related cardiomyopathies. However, the question still remains how and why PIs interfere with cardiac redox signaling ultimately manifesting in contractile pathologies.

The link between PI usage and increased ROS production is well established by several human [269], animal [270–273] and cell-based studies [274–278]. These include numerous cell and tissue types, i.e. macrophages [276], cardiomyocytes [197], endothelial cells [279,280], pancreatic β–cells [270,272], intestinal epithelial cells [281], pulmonary aortic endothelial cells [282], human skeletal muscle cells [273], adipocytes [274,283], hippocampal neurons [284], porcine arteries [277,285], and aortas in an atherogenic mouse model [277,279,285]. All these studies point towards an increase in the production of oxidant molecules and activation of pro-oxidant pathways that ultimately results in elevated oxidant stress within cells and surrounding tissue.

The main intracellular sources of ROS production include the mitochondrial ETC [286,287], NADPH oxidases (NOX) [288,289], xanthine oxidase [290,291], and cytochrome P450 [292,293]. However, the majority of ROS production originates from mitochondria, generated by respiratory chain complexes I and III located within the IMM [294]. Additional sources of mitochondrial ROS include matrix dehydrogenases and mono-amine oxidase in the OMM [reviewed in [295]]. Electrons leaking from mitochondrial respiratory complexes I and III are able to bind to molecular oxygen (O_2) to form superoxide ($O_2^{\bullet -}$). Intriguingly, these complexes generate two distinct $O_2^{\bullet -}$ pools. Complex I releases $O_2^{\bullet -}$ from the IMM (impermeable to superoxide) into the matrix [287,294]. Superoxide found within the mitochondrial

matrix can be converted to hydrogen peroxide (H_2O_2) by manganese superoxide dismutase (MnSOD), i.e. $2O_2^{\bullet -} + 2H^+ \rightarrow O_2 + H_2O_2$. However, complex III can release $O_2^{\bullet -}$ into both the mitochondrial matrix and the IMM space, and since the OMM is permeable to $O_2^{\bullet -}$ it can translocate into the cytosol. Here copper/zinc superoxide dismutase (Cu/Zn SOD) converts $O_2^{\bullet -}$ to H_2O_2 within the cytosol and the inter-mitochondrial membrane space. Thereafter H_2O_2 can be removed by catalase or GPx [296,297]. However, in the mitochondrial matrix GPx is the main regulator of H_2O_2 with catalase playing an insignificant role [298].

Physiologic ROS levels play a crucial role in regulating intracellular signaling pathways and gene expression, referred to as ''redox signaling'' [299,300]. Here NOXs are key modulators that generate highly regulated amounts of $O_2^{\bullet -}$ by electron transfer from NADPH to molecular oxygen [301–304]. However, excess and damaging reactive species may be generated by increased activation of reactive species-generating systems and/or decreased capacity of anti-oxidant defense systems. For example, if $O_2^{\bullet -}$ and H_2O_2 are not appropriately detoxified then H_2O_2 can be converted to the highly reactive hydroxyl anion ($OH^{\bullet}$) by non-enzymatic pathways, e.g. the Fenton reaction [305] while $O_2^{\bullet -}$ can react with nitric oxide to form peroxynitrite ($ONOO^-$) [305].

What are the origins of PI-induced ROS? The precise source(s) of ROS remain unclear although most studies suggest a mitochondrial origin [278]. However, Ritonavir treatment of porcine carotid arteries increased $O_2^{\bullet -}$ production by NOX indicating the presence of extra-mitochondrial ROS [277]. The exact mechanisms and sequence of events whereby PI treatment triggers intracellular ROS production are not well understood. Further, mitochondrial membrane biology is also affected by PI therapy. For example, PIs can increase mitochondrial membrane potential depolarization in HL-1 myocytes [197] that would be expected to impair mitochondrial respiration and ATP generating capacity.

In agreement, others found higher mitochondrial membrane depolarization together with an impairment of cellular oxygen consumption [306]. We are of the opinion that activation of UCPs may help mediate such effects, e.g. Nelfinavir treatment elevated UCP2 levels in pancreatic β–cells [272]. Impairment of mitochondrial function may also result due to mtDNA damage and fragmentation of the mitochondrial network [307,308].

In light of this we propose a unified model based on the current literature that features a wide variety of experimental models and cell types (**Fig. 11**). However, there is limited information of PI-mediated effects on the heart and further studies are required to ascertain whether this model applies to the mammalian heart. In the first instance we propose that PIs exert direct effects on enzymes that regulate the balance between ROS generation and detoxification. For example, Nelfinavir treatment of rat pancreatic cells decreased intracellular Cu/ZnSOD (but not MnSOD) activity, thereby elevating cytosolic ROS generation [272]. In agreement, glutathione levels were attenuated suggesting decreased GPx activity, although this was not determined. Diminished Cu/ZnSOD and GPx activities will be expected to increase ROS levels within the cytosol and the inter-mitochondrial membrane space. Cytosolic ROS levels may be further enhanced by leakage of reactive species across the porous OMM. We further propose that intracellular ROS thus generated (cytosolic and inter-membrane space) are able to inhibit respiratory chain complexes located within the IMM [reviewed in [309]].

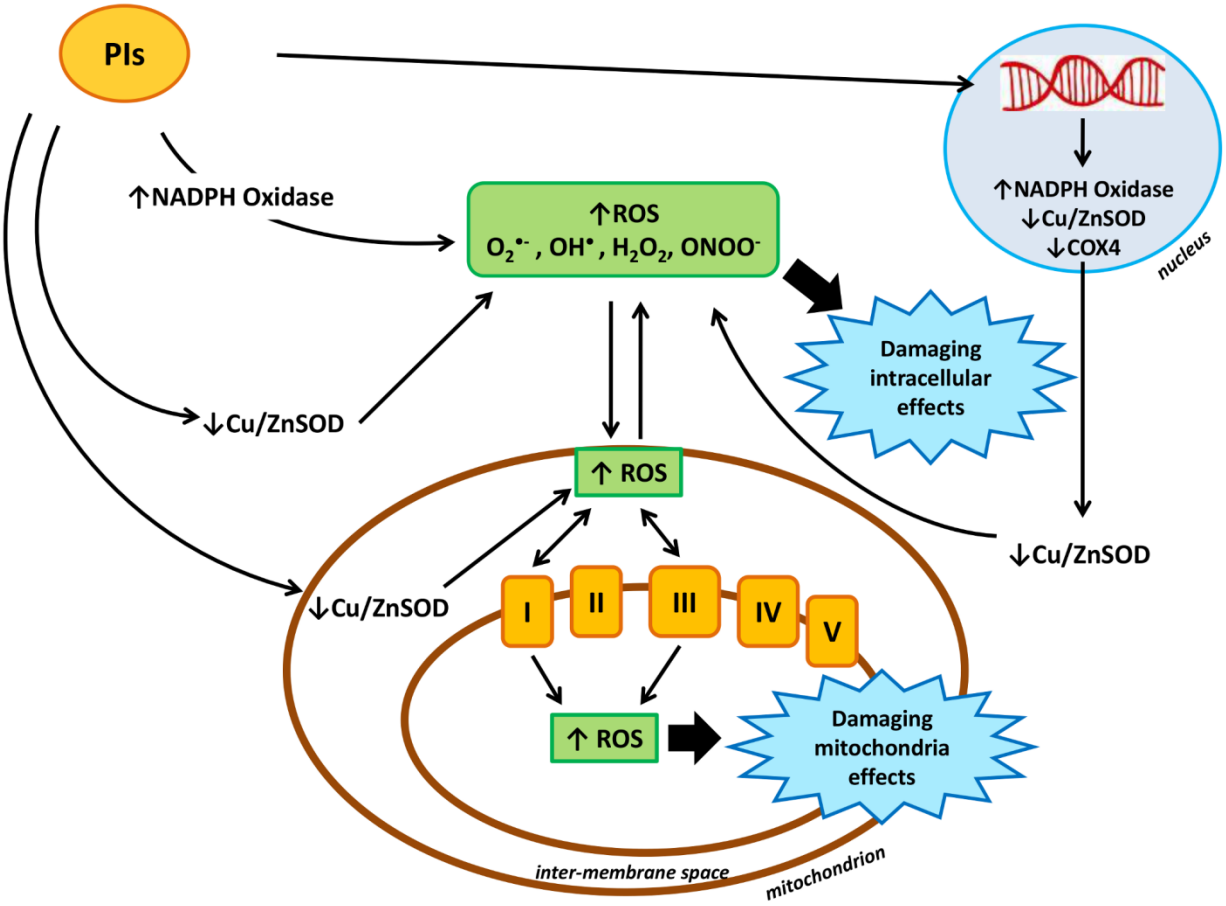

Figure 11. PIs and oxidative stress. HIV PIs elicit a variety of effects at the cellular level. For example, PIs increase NADPH oxidase, and decrease Cu/ZnSOD and COX4 gene expression. This would be expected to increase and decrease NADPH oxidase and Cu/ZnSOD activities, respectively. Moreover, lower COX4 levels may impair mitochondrial respiratory capacity. PIs can also directly affect enzyme activities of Cu/Zn SOD and NADPH oxidase in the cytosol, resulting in ROS generation with damaging intracellular effects. Mitochondrial Cu/ZnSOD activity is also downregulated and thus increases the generation of ROS within the intermembrane space. Higher ROS levels may inhibit complexes I and III of the ETC, thereby increasing matrix and cytosolic ROS levels. In this manner, mitochondria are also damaged. *$O_2^{\bullet-}$ superoxide free radical, $OH^{\bullet}$ - hydroxyl radical, H_2O_2 – hydrogen peroxide, $ONOO^-$ - peroxynitrite, Cu/Zn SOD – copper/zinc superoxide dismutase, COX4: cytochrome c oxidase 4, NADPH - nicotinamide adenine dinucleotide phosphate hydrogen, PI – protease inhibitor, ROS: reactive oxygen species.*

Thus a vicious cycle is created whereby decreased ETC activity will generate more reactive species thereby further elevating intracellular ROS levels, with damaging consequences. Moreover, greater superoxide production from complex I will elevate mitochondrial ROS levels (confined within the matrix) with detrimental effects. PI-induced increases in NOX activity will further exacerbate these effects by generating even higher $O_2^{\bullet -}$ levels. We believe that it is unlikely that PIs directly inhibit the respiratory chain complexes since there is no evidence, as far as we are aware, supporting PI localization within the mitochondrial matrix. In agreement, Vernochet *et al.* (2005) [310] tracked intracellular localization of PIs by fluorescent tagging and found no localization within the nucleus. They did not report on the mitochondrial localization of PIs, but its lack within the nucleus suggests it is unlikely that it entered the mitochondrial matrix. However, further studies are required to ascertain whether PIs are able to enter the matrix and exert direct effects on myocardial ETC complexes.

At another level, PIs may also exert transcriptional effects thereby altering expression of ROS generating/detoxifying enzymes and increasing intracellular reactive species levels. For example, Ritonavir-treated cells exhibited elevated mRNA levels of NOX subunits $p22^{phox}$, $p40^{phox}$, $p47^{phox}$, and $p67^{phox}$ [276]. NOX is a multi-subunit complex and its enzymatic activity depends on both catalytic and regulatory subunits (e.g. p22, p40, p47, and p67) [293]. Ritonavir treatment also increased $O_2^{\bullet -}$ levels, thus suggesting higher NOX activity.

Investigation of the NOX pathway further supports the role of PIs in oxidative stress. Chai and colleagues (2010) [311] investigated PI treatment in porcine coronary arteries and found decreased endothelial nitric oxide synthase (eNOS) expression with Ritonavir therapy, together with increased nitric oxide levels. Functional studies established decreased endothelium-dependent vasorelaxation thus confirming these findings [275,277,278,285,312]. Furthermore, HIV infection itself also plays a role in

altering intracellular oxidant status, i.e. a transgenic rodent model expressing HIV proteins Tat, gp120 and Nef revealed detrimental perturbations in the cysteine and glutathione pathways with additional changes to cardiac morphological parameters [313].

PI treatment can also attenuate expression of anti-oxidant modulators. For example, Nelfinavir decreased Cu/ZnSOD, but not MnSOD, peptide levels in rat pancreatic β–cells, associated with greater enzyme activity and higher ROS production [272]. These data suggest that PIs more likely exert transcriptional effects on nuclear-encoded compared to mitochondrial-encoded DNA. However, adipocytes exposed to PIs displayed reduced gene expression of both nuclear-encoded COX4, and mitochondrial-encoded COX2 [263]. Decreased COX levels may impair complex IV capacity (i.e. accepting electrons to reduce molecular oxygen to water), increase electron leakage within ETC complexes and thereby elevate $O_2^{\bullet -}$ production. Nonetheless, it remains uncertain whether PIs exert direct or indirect effect on the redox system, as the UPS and PGC-1α also play critical roles to play in regulating intracellular redox homeostasis. Together these studies suggest that PIs increase ROS by both direct (at enzyme activity level) and indirect means (altering gene expression, activating the PGC-1α pathway), thereby causing damaging effects within the cytosol and the mitochondrion. This in turn can result in damaging effects within the cytosol and the mitochondrion, i.e. decreased mitochondrial respiratory capacity, increased uncoupling of oxidative phosphorylation, lower mitochondrial ATP generation and greater activation of cell death pathways. Together this will increase the heart's susceptibility to stress, e.g. myocardial ischemia.

Conclusion

In conclusion, this review demonstrates that early changes triggered by PI treatment include increased body weight and lipid levels that resemble a pre-atherogenic profile and the MetS. Such changes are accompanied by an increased transcription (largely SREBP-mediated) of target genes for cholesterol and lipid metabolism. Furthermore, long-term PI usage can place the heart at a disadvantage from a metabolic and contractile point of view. Mitochondrial metabolism can be impaired and oxidant generation/removal systems together with the UPS may represent useful starting points for the molecular alterations associated with PIs that ultimately create a pro-oxidant status within the cell. Though this may represent an adaptive response initially, in the long-term it is unable to counteract strain on the mitochondrial energetic system and prevent contractile dysfunction. The UPS is also a downstream target of PIs and ROS, although there may be cross-talk between these systems. Moreover, HIV PIs may directly impair UPS in the heart. Dysfunctional UPS may also trigger alterations in ionic channels and interfere with electrical signaling in the myocardium. Thus while PIs substantially improve life expectancy and quality of life in HIV-positive patients, its long-term usage can initiate toxic side-effects that may lead to cardio-metabolic dysfunction. From a philosophical view point, it is therefore imperative that clinicians be mindful of the benefit-harm paradigm of ARVs within the clinical setting. Studies investigating the molecular mechanisms whereby HAART (and specifically PIs) can elicit such side-effects are therefore of the utmost importance.

References

1. UN AIDS. *2011 UNAIDS World AIDS Day report, Sub-saharan Africa*. 0–2 (2011).

2. Armstrong, W., Calabrese, L. & Taege, A. HIV update 2005: Origins, issues, prospects, and complications. *Clev Clin J Med* **72,** 73–78 (2005).

3. Melekhin, V. V *et al.* Antiretroviral therapy initiation before, during, or after pregnancy in HIV-1-infected women: maternal virologic, immunologic, and clinical response. *PloS One* **4,** e6961 (2009).

4. Palella, F. Human immunodeficiency virus infection. *N Engl J Med* **338,** 853–860 (1998).

5. Himelman, R. B., Chung, W. S., Chernoff, D. N., Schiller, N. B. & Hollander, H. Cardiac manifestations of human immunodeficiency virus infection: a two-dimensional echocardiographic study. *J Am Coll Cardiol* **13,** 1030–6 (1989).

6. Hecht, S., Berger, M., Van Tosh, A. & Croxson, S. Unsuspected cardiac abnormalities in the acquired immune deficiency syndrome. An echocardiographic study. *Chest* **96,** 805–8 (1989).

7. Kaul, S., Fishbein, M. & Siegel, R. Cardiac manifestations of acquired immune deficiency syndrome: a 1991 update. *Am Heart J* **122,** 535–44 (1991).

8. Rerkpattanapipat, P., Wongpraparut, N., Jacobs, L. E. & Kotler, M. N. Cardiac manifestations of acquired immunodeficiency syndrome. *Arch Int Med* **160,** 602–8 (2000).

9. De Castro, S. *et al.* Heart involvement in AIDS: a prospective study during various stages of the disease. *Eur Heart J* **13,** 1452–1459 (1992).

10. Grody, W. W., Cheng, L. & Lewis, W. Infection of the heart by the human immunodeficiency virus. *Am J Cardiol* **66,** 203–206 (1990).

11. Goulet, J. L. *et al.* Do patterns of comorbidity vary by HIV status, age, and HIV severity? *Clin Infect Dis* **45,** 1593–1601 (2007).

12. Kim, D. *et al.* Multimorbidity patterns in HIV-infected patients: the role of obesity in chronic disease clustering. *J AIDS* **61,** 600–5 (2012).

13. Lohse, N. *et al.* Survival of persons with and without HIV infection in Denmark, 1995-2005. *Ann Intern Med* **146,** 87–95 (2007).

14. Becker, A. *et al.* Acute coronary syndromes in treatment- naive black South Africans with human immunodeficiency virus infection. *J Interven Cardiol* **23,** 70–77 (2010).

15. Knudsen, A. *et al.* Angiographic features and cardiovascular risk factors in human immunodeficiency virus-infected patients with first-time acute coronary syndrome. *Am J Cardiol* **111,** 63–7 (2013).

16. Lo, J. *et al.* Increased prevalence of subclinical coronary atherosclerosis detected by coronary computed tomography agiography in HIV-infected men. *AIDS* **24,** 243–253 (2010).

17. Jerico, C. *et al.* Subclinical carotid atherosclerosis in HIV-infected patients: a role of combination antirtroviral therapy. *Stroke* **37,** 812–7 (2006).

18. De Saint Martin, L. *et al.* Premature atherosclerosis in HIV positive patients and cumulated time of exposure to antiretroviral therapy (SHIVA study). *Atherosclerosis* **185,** 361–7 (2006).

19. Lijfering, W. M., Ten Kate, M. K., Sprenger, H. G. & van der Meer, J. Absolute risk of venous and arterial thrombosis in HIV-infected patients and effects of combination antiretroviral therapy. *J Thromb Haemost* **4,** 1928–30 (2006).

20. Sullivan, P. S., Dworkin, M. S., Jones, J. L. & Craig, W. Epidemiology of thrombosis in HIV-infected individuals. *AIDS* **14,** 321–324 (2000).

21. Maggi, P., Lillo, A., Perilli, F. & Maserati, R. Colour-doppler ultrasonography of carotid vessels in patients treated with antiretroviral therapy: a comparative study. *AIDS* **18,** 1023–1028 (2004).

22. Majluf-Cruz, A. *et al.* Venous thrombosis among patients with AIDS. *Clin Appl Thromb Hemostas* **10,** 19–25 (2004).

23. Gazzaruso, C. *et al.* Hypertension among HIV patients: prevalence and relationships to insulin resistance and metabolic syndrome. *J Hypert* **21,** 1377–82 (2003).

24. Lekakis, J. *et al.* HIV-positive patients treated with protease inhibitors have vascular changes resembling those observed in atherosclerotic cardiovascular disease. *Clin Science* **115,** 189–196 (2008).

25. Boccara, F. *et al.* Acute coronary syndrome in human immunodeficiency virus-infected patients: characteristics and 1 year prognosis. *Eur Heart J* **32,** 41–50 (2011).

26. Butt, A. *et al.* Risk of heart failure with hum an immunodeficiency virus in the absence of prior diagnosis of coronary heart disease. *Arch Intern Med* **171,** 737–743 (2011).

27. Bozzette, S. A. *et al.* Long-term survival and serious cardiovascular events in HIV-infected patients treated with highly active antiretroviral therapy. *J AIDS* **47,** 338–341 (2008).

28. Debouck, C. The HIV-1 protease as a therapeutic target for AIDS. *AIDS Res Hum Retrovir* **8,** 153–64 (1992).

29. Chandwani, A. & Shuter, J. Lopinavir/ritonavir in the treatment of HIV-1 infection: a review. *Therap Clin Risk Man* **4,** 1023–33 (2008).

30. Kumar, G. N. *et al.* Metabolism and disposition of the HIV-1 protease inhibitor lopinavir (ABT-378) given in combination with ritonavir in rats, dogs, and humans. *Pharmaceut Res* **21,** 1622–30 (2004).

31. Kumar, G. N. *et al.* Potent inhibition of the cytochrome P-450 3A-mediated human liver microsomal metabolism of a novel HIV protease inhibitor by ritonavir: a positive drug-drug interaction. *Pharmacology* **27,** 902–908 (1999).

32. Sham, H. L. *et al.* Synthesis and antiviral activities of the major metabolites of the HIV protease inhibitor ABT-378. *Biorgan Med Chem Lett* **11,** 1351–3 (2001).

33. Kaplan, S. S. & Hicks, C. B. Safety and antiviral activity of lopinavir/ritonavir-based therapy in human immunodeficiency virus type 1 (HIV-1) infection. *J Antimicrob Chemother* **56,** 273–6 (2005).

34. Hsu, A., Granneman, G. R. & Bertz, R. Ritonavir. Clinical pharmakinetics and interactions with other anti-HIV agents. *Clin Pharmok* **35,** 275–91 (1998).

35. Friis-Møller, N. *et al.* Cardiovascular disease risk factors in HIV patients--association with antiretroviral therapy. Results from the DAD study. *AIDS* **17,** 1179–1193 (2003).

36. Friis-Møller, N. *et al.* Class of antiretroviral drugs and the risk of myocardial infarction. *N Engl J Med* **356,** 1723–1735 (2007).

37. Smith, C. *et al.* Factors associated with specific causes of death amongst HIV-positive individuals in the DAD study. *AIDS* **24,** 1537–48 (2010).

38. Holmberg, S. D. *et al.* Protease inhibitors and cardiovascular outcomes in patients with HIV-1 For personal use. *Lancet* **360,** 1747–1748 (2002).

39. Mary-Krause, M., Cotte, L., Simon, A., Partisani, M. & Costagliola, D. Increased risk of myocardial infarction with duration of protease inhibitor therapy in HIV-infected men. *AIDS* **17,** 2479–86 (2003).

40. Durand, M., Sheehy, O., Baril, J.-G., Lelorier, J. & Tremblay, C. L. Association between HIV infection, antiretroviral therapy, and risk of acute myocardial infarction: a cohort and nested case-control study using Québec's public health insurance database. *J AIDS* **57,** 245–53 (2011).

41. Triant, V. A., Lee, H., Hadigan, C. & Grinspoon, S. K. Increased acute myocardial infarction rates and cardiovascular risk factors among patients with human immunodeficiency virus disease. *Clin Endocrinol* **92,** 2506–2512 (2009).

42. Klein, D., Hurley, L. B., Quesenberry, C. P. & Sidney, S. Do protease inhibitors increase the risk for coronary heart disease in patients with HIV-1 infection? *J AIDS* **30,** 471–7 (2002).

43. Mondy, K. E. *et al.* High prevalence of echocardiographic abnormalities among HIV-infected persons in the era of highly active antiretroviral therapy. *Clin Infec Dis* **52,** 378–386 (2011).

44. Lyonne, L. *et al.* Thromboembolic events at the time of highly active antiretroviral therapies against human immunodeficiency virus. *Rev Med Intern* **29,** 100–104 (2008).

45. Bernal, E. *et al.* Hypertriglyceridemic waist phenotype is a risk factor fo subclinical atherosclerosis in human immunodeficiency virus-infected patients. *Med Clin* **139,** 561–565 (2012).

46. Lang, S. *et al.* Impact of individual antiretroviral drugs on the risk of myocardial infarction in human immunodeficiency virus-infected patients: a case-control study nested within the French Hospital Database on HIV ANRS cohort CO4. *Arch Int Med* **170,** 1228–38 (2010).

47. Coplan, P. M. *et al.* Incidence of myocardial infarction in randomized clinical trials of protease inhibitor-based antiretroviral therapy: an analysis of four different protease inhibitors. *Aids Res Hum Retrovir* **19,** 449–55 (2003).

48. Lifson, A. R. *et al.* Clinical, demographic and laboratory parameters at HAART initiation associated with decreased post-HAART survival in a U.S. military prospective HIV cohort. *AIDS Res Ther* **9,** 4 (2012).

49. Grundy, S. M., Brewer, H. B., Cleeman, J. I., Smith, S. C. & Lenfant, C. Definition of metabolic syndrome: report of the National Heart, Lung, and Blood Institute/American Heart Association conference on scientific issues related to definition. *Circulation* **109,** 433–8 (2004).

50. Reaven, G. in *The metabolic syndrome* (Hansen, B. & Bray, G.) 11–36 (Humana Press, 2008).

51. Third report of the National Cholesterol Education Program (NCEP) expert panel on detection, evaluation, and treatment of high blood cholesterol in adults (Adult Treatment Panel III). Final report. *Circulation* **106,** 3143–421 (2002).

52. Behrens, G. *et al.* Impaired glucose tolerance, beta cell function and lipid metabolism in HIV patients under treatment with protease inhibitors. *AIDS* **13,** F63–F70 (1999).

53. Bastard, J. *et al.* Association between altered expression of adipogenic factor SREBP1 in lipoatrophic adipose tissue from HIV-1-infected patients and abnormal adipocyte differentiation and insulin resistance. *Lancet* **359,** 1026–1031 (2002).

54. Carr, A. *et al.* HIV protease inhibitor substitution in patients with lipodystrophy: a randomized, controlled, open-label, multicentre study. *AIDS* **15,** 1811–1822 (2001).

55. Dong, K. *et al.* Changes in body habitus and serum lipid abnormalities in HIV-positive women on highly active antiretroviral therapy (HAART). *J AIDS* **21,** 107–13 (1999).

56. Gan, S. *et al.* Altered myocellular and abdominal fat partitioning predict disturbance in insulin action in HIV protease inhibitor-related Lipodystrophy. *Diabetes* **51,** 3163–3169 (2002).

57. Tsiodras, S., Mantzoros, C., Hammer, S. & Samore, M. Effects of protease inhibitors on hyperglycemia, hyperlipidemia, and lipodystrophy: a 5-year cohort study. *Arch Intern Med* **160,** 2050–6 (2000).

58. Floris-Moore, M. *et al.* Increased serum lipids are associated with higher CD4 lymphocyte count in HIV-infected women. *HIV Med* **7,** 421–30 (2006).

59. Hertel, J., Struthers, H., Horj, C. & Hruw, P. A structural basis for the acute effects of HIV protease inhibitors on GLUT4 intrinsic activity. *J Biol Chem* **279,** 55147–52 (2004).

60. Liang, J.-S. *et al.* HIV protease inhibitors protect apolipoprotein B from degradation by the proteasome: A potential mechanism for protease inhibitor-induced hyperlipidemia. *Nat Med* **7,** 1327–1331 (2001).

61. Parker, R. A. *et al.* Endoplasmic reticulum stress links dyslipidemia to inhibition of proteasome activity and glucose transport by HIV protease inhibitors. *Mol Pharmacol* **67,** 1909–1919 (2005).

62. Murata, H., Hruz, P. W. & Mueckler, M. Indinavir inhibits the glucose transporter isoform Glut4 at physiologic concentrations. *AIDS* **16,** 859–63 (2002).

63. Hruz, P. W., Yan, Q., Struthers, H. & Jay, P. Y. HIV protease inhibitors that block GLUT4 precipitate acute, decompensated heart failure in a mouse model of dilated cardiomyopathy. *FASEB J* **22,** 2161–7 (2008).

64. Hruz, P. HIV protease inhibitors and insulin resistance: lessons from in vitro, rodent and healthy human volunteer models. *Diabetes* **3,** 660–665 (2009).

65. Germinario, R. J., Colby-Germinario, S. P., Cammalleri, C. & Wainberg, M. A. The long-term effects of anti-retroviral protease inhibitors on sugar transport in L6 cells. *J Endocrinol* **178,** 449–56 (2003).

66. Carr, A. *et al.* Diagnosis, prediction, and natural course of HIV-1 protease-inhibitor-associated lipodystrophy, hyperlipidaemia, and diabetes mellitus: a cohort study. *Lancet* **353,** 2093–2099 (1999).

67. Grinspoon, S. K. *et al.* State of the science conference: Initiative to decrease cardiovascular risk and increase quality of care for patients living with HIV/AIDS: executive summary. *Circulation* **118,** 198–210 (2008).

68. Rudich, A., Ben-Romano, R., Etzion, S. & Bashan, N. Cellular mechanisms of insulin resistance, lipodystrophy and atherosclerosis induced by HIV protease inhibitors. *Acta Physiol Scand* **183,** 75–88 (2005).

69. Sekhar, R. V *et al.* Metabolic basis of HIV-lipodystrophy syndrome. *Am J Physiol Endocrinol Metab* E332–E337 (2002).

70. Mulligan, K. *et al.* Hyperlipidemimia and insulin resistance are induced by protease inhibitors independent of changes in body composition in patients with HIV infection. *J AIDS* **23,** 35–43 (2000).

71. Carr, A., Samaras, K., Chisholm, D. J. & Cooper, D. A. Pathogenesis of HIV-1-protease inhibitor-associated peripheral lipodystrophy, hyperlipidaemia, and insulin resistance. *Lancet* **351,** 1881–1883 (1998).

72. Carr, A. *et al.* Effects of boosted tipranavir and lopinavir on body composition, insulin sensitivity and adipocytokines in antiretroviral-naive adults. *AIDS* **22,** 2313–2321 (2008).

73. Biron, A. *et al.* Metabolic syndrome in French HIV-infected patients : prevalence and predictive factors. *AIDS Res Hum Retrovir* **28,** 1–7 (2012).

74. Behrens, G. M. N. *et al.* Impaired glucose phosphorylation and transport in skeletal muscle cause insulin resistance in HIV-1 – infected patients with lipodystrophy. *J Clin Invest* **110,** 1319–1327 (2002).

75. Woerle, H. *et al.* Mechanisms for the deterioration in glucose tolerance associated with HIV protease inhibitor regimens. *Diabetes* **52,** 918–925 (2003).

76. Eberlé, D., Hegarty, B., Bossard, P., Ferré, P. & Foufelle, F. SREBP transcription factors: master regulators of lipid homeostasis. *Biochimie* **86,** 839–48 (2004).

77. Hua, X., Sakai, J., Ho, Y. K., Goldstein, J. L. & Brown, M. S. Hairpin orientation of sterol regulatory element-binding protein-2 in cell membranes as determined by protease protection. *J Biol Chem* **270,** 29422–7 (1995).

78. Hua, X., Wu, J., Goldstein, J. L., Brown, M. S. & Hobbs, H. H. Structure of the human gene encoding sterol regulatory element binding protein-1 (SREBF1) and localization of SREBF1 and SREBF2 to chromosomes 17p11.2 and 22q13. *Genomics* **25,** 667–73 (1995).

79. Miserez, a R., Cao, G., Probst, L. C. & Hobbs, H. H. Structure of the human gene encoding sterol regulatory element binding protein 2 (SREBF2). *Genomics* **40,** 31–40 (1997).

80. Tontonoz, P., Kim, J. B., Graves, R. a & Spiegelman, B. M. ADD1: a novel helix-loop-helix transcription factor associated with adipocyte determination and differentiation. *Mol Cell Biol* **13,** 4753–9 (1993).

81. Shimomura, I., Shimano, H., Horton, J. D., Goldstein, J. L. & Brown, M. S. Differential expression of exons 1a and 1c in mRNAs for sterol regulatory element binding protein-1 in human and mouse organs and cultured cells. *J Clin Invest* **99,** 838–45 (1997).

82. Lee, S. J. *et al.* The structure of importin-beta bound to SREBP-2: nuclear import of a transcription factor. *Science* **302,** 1571–5 (2003).

83. Nagoshi, E. M. I. & Yoneda, Y. Dimerization of sterol regulatory element-binding protein 2 via the helix-loop-helix-leucine zipper domain is a prerequisite for its nuclear localization mediated by importin-beta. *Mol Cell Biol* **21,** 2779–2789 (2001).

84. Kim, J. B. *et al.* Dual DNA binding specificity of ADD1/SREBP1 controlled by a single amino acid in the basic helix-loop-helix domain. *Mol Cell Biol* **15,** 2582–8 (1995).

85. Brown, M. S. & Goldstein, J. L. The SREBP pathway: regulation of cholesterol metabolism by proteolysis of a membrane-bound transcription factor. *Cell* **89,** 331–40 (1997).

86. Brown, M. S. & Goldstein, J. L. A proteolytic pathway that controls the cholesterol content of membranes, cells, and blood. *Proc Nat Acad Sci U S A* **96,** 11041–8 (1999).

87. Horton, J. D., Goldstein, J. L. & Brown, M. S. SREBPs : activators of the complete program of cholesterol and fatty acid synthesis in the liver. *J Clin Invest* **109,** 1125–1131 (2002).

88. Hirano, Y., Yoshida, M., Shimizu, M. & Sato, R. Direct demonstration of rapid degradation of nuclear sterol regulatory element-binding proteins by the ubiquitin-proteasome pathway. *J Biol Chem* **276,** 36431–36437 (2001).

89. Schmidtke, G. *et al.* How an inhibitor of the HIV-I protease modulates proteasome activity. *J Biol Chem* **274,** 35734–35740 (1999).

90. Hawkins, J. *et al.* Pharmacological inhibition of site 1 protease activity inhibits sterol regulatory element-binding protein processing and reduces lipogenic enzyme gene expression and lipid synthesis in cultured cells and experimental animals. *J Pharmacol Exp Ther* **326,** 801–8 (2008).

91. Hirano, Y. Solution structure of atypical protein kinase C PB1 domain and its mode of interaction with ZIP/p62 and MEK5. *J Biol Chem* **279,** 31883–31890 (2004).

92. Shimano, H. *et al.* Isoform 1c of sterol regulatory element binding protein is less active than isoform 1a in livers of transgenic mice and in cultured cells. *J Clin Invest* **99,** 846–54 (1997).

93. Horton, J. D. *et al.* Activation of cholesterol synthesis in preference to fatty acid synthesis in liver and adipose tissue of transgenic mice overproducing sterol regulatory element-binding protein-2. *J Clin Invest* **101,** 2331–9 (1998).

94. Rome, S. *et al.* Microarray analyses of SREBP-1a and SREBP-1c target genes identify new regulatory pathways in muscle. *Physiol Genom* **34,** 327–37 (2008).

95. Rasmussen, B. B. *et al.* Malonyl coenzyme A and the regulation of functional carnitine palmitoyl transferase-1 activity and fat oxidation in human skeletal muscle. *J Clin Invest* **110,** 1687–1693 (2002).

96. Amemiya-Kudo, M. *et al.* Transcriptional activities of nuclear SREBP-1a, -1c, and 2 to different target promoters of lipogenic and cholesterogenic genes. *J Lip Res* **43,** 1220–35 (2002).

97. Kim, K.-H. & H-J, T. Pattern and regulation of acetyl-CoA carboxylase gene expression. *J Nutr* **124,** 1273S–1283S (1994).

98. Magaña, M. M., Lin, S., Dooley, K. & Osborne, T. F. Sterol regulation of acetyl coenzyme A carboxylase promoter requires two interdependent binding sites for sterol regulatory element binding proteins. *J Lipid Res* **38,** 1630–8 (1997).

99. Magaña, M. M. & Osborne, T. F. Two tandem binding sites for sterol regulatory element binding proteins are required for sterol regulation of fatty-acid synthase promoter. *J Biol Chem* **271,** 32689–94 (1996).

100. Ericsson, J., Jackson, S. M., Bum, J., Spiegelman, B. M. & Edwards, P. A. Identification of glycerol-3-phosphate acyltransferase as an adipocyte determination and differentiation factor 1- and sterol regulatory element-binding protein-responsive gene. *J Biol Chem* **272,** 7298–7305 (1997).

101. Lagor, W. R., Heller, R., Groh, E. D. De & Ness, G. C. Functional analysis of the hepatic HMG-CoA reductase pomoter by in vivo electroporation. *Exper Biol Med* **232,** 353–361 (2007).

102. Osborne, T. F., Gil, G., Goldstein, J. & Brown, M. Operator constitutive mutation of 3-hydroxy-3-methylglutaryl coenzyme A reductase promoter abolishes protein binding to sterol regulatory element. *J Biol Chem* **263,** 3380–3387 (1988).

103. Osborne, T. F. Single nucleotide resolution of sterol regulatory region in promoter for 3-hydroxy-3-methylglutaryl coenzyme A reductase. *J Biol Chem* **266,** 13947–13951 (1991).

104. Sudhof, T., Russell, D., Brown, M. & Goldstein, J. 42 bp element from LDL receptor gene confers end-product repression by sterols when inserted into viral TK promoter. *Cell* **48,** 1061–1069 (1987).

105. Smith, J., Osborne, T., Brown, M., Goldstein, J. & Gil, G. Multiple sterol regulatory elements in promoter for hamster 3-hydroxy-3-methylglutaryl-coenzyme A synthase. *J Biol Chem* **263,** 18480–18487 (1988).

106. Tabor, D., Kim, J., Spiegelman, B. & Edwards, P. Transcriptional activation of the stearoyl-CoA desaturase 2 gene by sterol regulatory element-binding protein/adipocyte determination and differentiation factor 1. *J Biol Chem* **273,** 22052–8 (1998).

107. Yokoyama C, Wang X, Briggs MR, Admon A, Wu J, Hua X, Goldstein JL, B. M. SREBP-1, a basic-helix-loop-helix-leucine zipper protein that controls transcription of the low density lipoprotein receptor gene. *Cell* **75,** 187–197 (1993).

108. Pacenti, M. *et al.* Microarray analysis during adipogenesis identifies new genes altered by antiretroviral drugs. *AIDS* **20,** 1691–705 (2006).

109. Lenhard, J. M., Croom, D. K., Weiel, J. E. & Winegar, D. A. HIV protease inhibitors stimulate hepatic triglyceride synthesis. *Arterioscler Thromb Vasc Biol* **20,** 2625–2629 (2000).

110. Lum, P. Y. *et al.* Gene expression profiling of rat liver reveals a mechanistic basis for ritonavir-induced hyperlipidemia. *Genomics* **90,** 464–473 (2007).

111. Riddle, T. M., Kuhel, D. G., Woollett, L. A., Fichtenbaum, C. J. & Hui, D. Y. HIV protease inhibitor induces fatty acid and sterol biosynthesis in liver and adipose tissues due to the accumulation of activated sterol regulatory element-binding proteins in the nucleus. *J Biol Chem* **276,** 37514–37519 (2001).

112. Prot, M. *et al.* Long-term treatment with lopinavir-ritonavir induces a reduction in peripheral adipose depots in mice. *Antimicrob Agents Chemother* **50,** 3998–4004 (2006).

113. Adler-Wailes, D. C., Guiney, E. L., Koo, J. & Yanovski, J. A. Effects of ritonavir on adipocyte gene expression: evidence for a stress-related response. *Obesity* **16,** 2379–2387 (2008).

114. Caron, M. *et al.* The HIV protease inhibitor indinavir impairs sterol regulatory element binding protein-1 intranuclear localization, inhibits preadipocyte differentiation, and induces insulin resistance. *Diabetes* **50,** 1378–1388 (2001).

115. Dixon, J. L., Furukawa, S. & Ginsberg, H. N. Oleate stimulates secretion of apolipoprotein B-containing lipoproteins from Hep G2 cells by inhibiting early intracellular degradation of apolipoprotein B. *J Biol Chem* **266,** 5080–6 (1991).

116. Adeli, K. *et al.* Intracellular assembly and degradation of apolipoprotein B-100-containing lipoproteins in digitonin-permeabilized HEP G2 cells. *J Biol Chem* **272,** 5031–5039 (1997).

117. Hui, D. Y. Effects of HIV protease inhibitor therapy on lipid metabolism. *Prog Lipid Res* **42,** 81–92 (2003).

118. Piconi, S. *et al.* Atherosclerosis is associated with multiple pathogenic mechanisms in HIV-infected antiretroviral-naïve or -treated individuals. *AIDS* **27,** 381–9 (2013).

119. Punga, T., Bengoechea-Alonso, M. T. & Ericsson, J. Phosphorylation and ubiquitination of the transcription factor sterol regulatory element-binding protein-1 in response to DNA binding. *J Biol Chem* **281,** 25278–25286 (2006).

120. Wang, X. & Robbins, J. Heart failure and protein quality control. *Circ Res* **99,** 1315–1328 (2006).

121. Willis, M. & Patterson, C. Into the heart: the emerging role of the ubiquitin-proteasome system. *J Mol Cell Cardiol* **41,** 567–579 (2006).

122. Gomes, A., Zong, C. & Ping, P. Protein degradation by the 26S proteasome system in the normal and stressed myocardium. *Antioxid Redox Signal* **8,** 1677–1691 (2006).

123. DeSalle, L. & Pagano, M. Regulation of the G1 to S transition by the ubiquitin pathway. *FEBS Lett* **490,** 179–189 (2001).

124. Germain, D. Ubiquitin-dependent and -independent mitochondrial protein quality controls: implications in ageing and neurodegenerative diseases. *Mol Microbiol* **70,** 1334–1341 (2008).

125. Livnat-Levanon, N. & Glickman, M. Ubiquitin–proteasome system and mitochondria: reciprocity. *Biochim Biophys Acta* **1809,** 80–87 (2011).

126. Neutzner, A., Benard, G., Youle, R. & Karbowski, M. Role of the ubiquitin conjugation system in the maintenance of mitochondrial homeostasis. *Ann NY Acad Sci* **1147,** 242–253 (2008).

127. Chatenay-Lapointe, M. & Shadel, G. Stressed-out mitochondria get MAD. *Cell Metab* **12,** 559–560 (2010).

128. Heo, J. *et al.* A stress-responsive system for mitochondrial protein degradation. *Mol Cell* **40,** 465–480 (2010).

129. Fielitz, J. *et al.* Loss of muscle-specific RING-finger 3 predisposes the heart to cardiac rupture after myocardial infarction. *Proc Natl Acad Sci* **104,** 4377–4382 (2007).

130. Jeon, H. B. *et al.* A proteomics approach to identify the ubiquitinated proteins in mouse heart. *Biochem Biophys Res Commun* **357,** 731–6 (2007).

131. Schwartz, A., Trausch, J., Ciechanover, A., Slot, J. & Geuze, H. Immunoelectron microscopic localization of the ubiquitin-activating enzyme E1 in HepG2 cells. *Proc Nat Acad Sci U S A* **89,** 5542–5546 (1992).

132. Haas, A. & Bright, P. The immunochemical detection and quantitation of intracellular ubiquitin-protein conjugates. *J. Biol. Chem.* **260,** 12464–12473 (1985).

133. Yonashiro, R. *et al.* A novel mitochondrial ubiquitin ligase plays a critical role in mitochondrial dynamics. *EMBO J* **25,** 3618–3626 (2006).

134. Margineantu, D., Emerson, C., Diaz, D. & Hockenbery, D. Hsp90 inhibition decreases mitochondrial protein turnover. *PLoS One* **2,** e1066 (2007).

135. Azzu, V. & Brand, M. D. Degradation of an intramitochondrial protein by the cytosolic proteasome. *J Cell Sci* **123,** 3616–3616 (2010).

136. Jenner, P. Oxidative stress in Parkinson's disease. *Ann Neurol* **53,** S26–S38 (2003).

137. Ishii, T., Sakurai, T., Usami, H. & Uchida, K. Oxidative modification of proteasome: identification of an oxidation-sensitive subunit in 26 S proteasome. *Biochemistry* **44,** 13893–13901 (2005).

138. Farout, L., Mary, J., Vinh, J., Szweda, L. & Friguet, B. Inactivation of the proteasome by 4-hydroxy-2-nonenal is site specific and dependant on 20S proteasome subtypes. *Arch Biochem Biophys* **453,** 135–142 (2006).

139. Davies, K. Degradation of oxidized proteins by the 20S proteasome. *Biochimie* **83,** 301–310 (2001).

140. Grune, T., Merker, K., G, S. & Davies, K. Selective degradation of oxidatively modified protein substrates by the proteasome. *Biochem Biophys Res Commun* **305,** 709–718 (2003).

141. Shringarpure, R. & Davies, K. Protein turnover by the proteasome in ageing and disease. *Free Radic Biol Med* **32,** 1084–1089 (2002).

142. Halliwell, B. Hypothesis: proteasomal dysfunction: a primary event in neurogeneration that leads to nitrative and oxidative stress and subsequent cell death. *Ann N Y Acad Sci* **962,** 182–194 (2002).

143. Waring, J. F. *et al.* Identification of proteasome gene regulation in a rat model for HIV protease inhibitor-induced hyperlipidemia. *Arch Toxicol* **84,** 263–270 (2010).

144. Danielson, C., Cianci, G. & Hope, T. Recruitment and dynamics of proteasome association with rhTRIM5α cytoplasmic complexes during HIV-1 infection. *Traffic* **13,** 1206–17 (2012).

145. Zhou, X., Evans, S., Han, X., Liu, Y. & Yu, X.-F. Characterization of the interaction of full-length HIV-1 Vif protein with its key regulator CBFβ and CRL5 E3 ubiquitin ligase components. *PLoS One* **7,** e33495 (2012).

146. Fabiato, A. Calcium-induced release of calcium from the cardiac sarcoplasmic reticulum. *Am J Physiol* **245,** C1–C14 (1983).

147. Kawakami, M. & Okabe, E. Superoxide anion radical-triggered Ca2+ release from cardiac sarcoplasmic reticulum through ryanodine receptor Ca2+ channel. *Mol Pharmacol* **53,** 497–503 (1998).

148. Marengo, J., Hidalgo, C. & Bull, R. Sulfhydryl oxidation modifies the calcium dependence of ryanodine-sensitive calcium channels of excitable cells. *Biophys J* **74,** 1263–1277 (1998).

149. Anzai, K. *et al.* Effects of hydroxyl radical and sulfhydryl reagents on the open probability of the purified cardiac ryanodine receptor channel incorporated into planar lipid bilayers. *Biochem Biophys Res Commun* 938–942 (1998).

150. Holmberg, S. *et al.* Reactive oxygen species modify the structure and function of the cardiac sarcoplasmic reticulum calcium-release channel. *Cardioscience* **2,** 19–25 (1991).

151. Rowe, G. T., Manson, N. H., Caplan, M. & Hess, M. L. Hydrogen peroxide and hydroxyl radical mediation of activated leukocyte depression of cardiac sarcoplasmic reticulum. Participation of the cyclooxygenase pathway. *Circ Res* **53,** 584–591 (1983).

152. Boraso, A. & Williams, A. Modification of the gating of the cardiac sarcoplasmic reticulum Ca2+-release channel by H2O2 and dithiothreitol. *Am J Physiol* **267,** H1010–6 (1994).

153. Scherer, N. & Deamer, D. Oxidative stress impairs the function of sarcoplasmic reticulum by oxidation of sulfhydryl groups in the Ca2+-ATPase. *Arch Biochem Biophys* **246,** 589–601 (1986).

154. Morris, T. & Sulakhe, P. Sarcoplasmic reticulum Ca2+-pump dysfunction in rat cardiomyocytes briefly exposed to hydroxyl radicals. *Free Radic Biol Med* **22,** 37 –47 (1997).

155. Kaneko, M., Beamish, R. & Dhalla, N. Depression of heart sarcolemmal Ca2+-pump activity by oxygen free radicals. *Am J Physiol* **256,** (1989).

156. Kaneko, M., Elimban, V. & Dhalla, N. Mechanism for depression of heart sarcolemmal Ca2+ pump by oxygen free radicals. *Am J Physiol* **257,** H804–11 (1989).

157. Reeves, J. P., Bailey, C. a & Hale, C. C. Redox modification of sodium-calcium exchange activity in cardiac sarcolemmal vesicles. *J Biol Chem* **261,** 4948–55 (1986).

158. Kato, M. & Kako, K. Na+/Ca2+ exchange of isolated sarcolemmal membrane: effects of insulin, oxidants and insulin deficiency. *Mol Cell Biochem* **83,** 15 –25 (1988).

159. Goldhaber, J. Free radicals enhance Na+/Ca2+ exchange in ventricular myocytes. *Am J Physiol* **271,** H823–33 (1996).

160. Sharikabad, M., Ostbye, K., Lyberg, T. & Brors, O. Effect of extracellular Mg2+ on ROS and Ca2+ accumulation during reoxygenation of rat cardiomyocytes. *Am J Physiol* **280,** H344–H353 (2001).

161. Temsah, R. M., Netticadan, T., Kawabata, K.-I. & Dhalla, N. S. Lack of both oxygen and glucose contributes to I/R-induced changes in cardiac SR function. *Am J Physiol Cell Physiol* **283,** C1306–12 (2002).

162. Gen, W., Tani, M., Takeshita, J., Ebihara, Y. & Tamaki, K. Mechanisms of Ca2+ overload induced by extracellular H2O2 in quiescent isolated rat cardiomyocytes. *Basic Res Cardiol* **96,** 623–9 (2001).

163. Zarain-Herzberg, A., Fragoso-Medina, J. & Estrada-Avilés, R. Calcium-regulated transcriptional pathways in the normal and pathologic heart. *IUBMB Life* **63,** 847–55 (2011).

164. Bers, D. M. Cardiac excitation-contraction coupling. *Nature* **415,** 198–205 (2002).

165. Bers, D. M. Calcium cycling and signaling in cardiac myocytes. *Ann Rev Physiol* **70,** 23–49 (2008).

166. Brandl, C. J., Martin, D. R. & David, H. Adult forms of the Ca2 + ATPase of sarcoplasmic reticulum. *J Biol Chem* **262,** 3768–3774 (1987).

167. Wuytack, F. *et al.* Regulation of alternative splicing of the SERCA2 pre-mRNA in muscle. *Ann N Y Acad Sci* 372–375

168. Burk, S. E., Lytton, J., MacLennan, D. H. & Shull, G. E. cDNA cloning, functional expression, and mRNA tissue distribution of a third organellar Ca2+ pump. *J Biol Chem* **264,** 18561–8 (1989).

169. Frank, K. F., Bölck, B., Erdmann, E. & Schwinger, R. H. G. Sarcoplasmic reticulum Ca2+-ATPase modulates cardiac contraction and relaxation. *Cardiovasc Res* **57,** 20–7 (2003).

170. Toyofuku, T., Kurzydlowski, K., Narayanan, N. & Maclennan, D. Identification of Ser38 as the site in cardiac sarcoplasmic reticulum ca+2-ATPase that is phosphorylated by ca+2/calmodulin-dependent protein kinase. *J Biochem* **42,** 26492–26496 (1994).

171. Narayanan, N. & Xu, A. Phosphorylation and regulation of the Ca+2-pumping ATPase in cardiac sarcoplasmic reticulum by calcium/calmodulin-dependent protein kinase. *Basic Res Cardiol* **92,** 25–35 (1997).

172. Kiss, E., Jakab, G., Kranias, E. G. & Edes, I. Thyroid hormone-induced alterations in phospholamban protein expression. Regulatory effects on sarcoplasmic reticulum Ca2+ transport and myocardial relaxation. *Circ Res* **75,** 245–251 (1994).

173. Simmerman, H. K. B. & Jones, L. R. Phospholamban: protein structure, mechanism of action, and role in cardiac function. *Physiol Rev* **78,** 921–947 (1998).

174. MacLennan, D. H., Abu-abed, M. & Kang, C. Structure-function relationships in Ca+2 ‡ cycling proteins. *J Mol Cell Cardiol* **34,** 897–918 (2002).

175. MacLennan, D., Asahi, M. & Tupling, A. The regulation of SERCA-type pumps by phospholamban and sarcolipin. *Ann N Y Acad Sci* **986,** 472–480 (2003).

176. MacLennan, D. & Kranias, E. Phospholamban: a crucial regulator of cardiac contractility. *Nat Rev Mol Cell Biol* **4,** 566–577 (2003).

177. Brittsan, A. G. & Kranias, E. G. Phospholamban and cardiac contractile function. *J Mol Cell Cardiology* **32,** 2131–9 (2000).

178. Bhupathy, P., Babu, G. & Periasmy, M. Sarcolipin and phospholamban as regulators of cardiac sarcoplasmic reticulum ca+2 ATPase. *J Mol Cell Cardiol* **42,** 903–911 (2007).

179. Tada, M. Molecular structure and function of phospholamban in regulating the calcium pump from sarcoplasmic reticulum. *Ann N Y Acad Sci* **671,** 92–103 (1992).

180. Tada, M. & Inui, M. Regulation of calcium transport by the ATPase-phospholamban system. *J Mol Cell Cardiol* **15,** 565–575 (1983).

181. Tada, M., Ohmori, F., Kinoshita, A. & Abe, H. Cyclic AMP regulation of active calium transport across membranes of sarcoplasmic reticulum: role of the 22, 000-dalton protien phospholamban. *Adv Cyclic Nucleotide Res* **9,** 355–369 (1978).

182. Kadambi, V. J. *et al.* Cardiac-specific overexpression of phospholamban alters calcium kinetics and resultant cardiomyocyte mechanics in transgenic mice. *J Clin Invest* **97,** 533–9 (1996).

183. Koss, K. & Kranias, E. Phospholamban: a prominent regulator of myocardial contractility. *Circ Res* **79,** 1059–1063 (1996).

184. Hoshijima, M., Knöll, R., Pashmforoush, M. & Chien, K. R. Reversal of calcium cycling defects in advanced heart failure toward molecular therapy. *J Am Coll Cardiol* **48,** A15–23 (2006).

185. Arai, M., Alpert, N. R., MacLennan, D. H., Barton, P. & Periasamy, M. Alterations in sarcoplasmic reticulum gene expression in human heart failure. A possible mechanism for alterations in systolic and diastolic properties of the failing myocardium. *Circ Res* **72,** 463–469 (1993).

186. Arai, M., Otsu, K., MacLennan, D. H., Alpert, N. R. & Periasamy, M. Effect of thyroid hormone on the expression of mRNA encoding sarcoplasmic reticulum proteins. *Circ Res* **69,** 266–276 (1991).

187. Reed, T. D. *et al.* ATPase and the Na/Ca exchanger are antithetically regulated during mouse cardiac development and in hypo/hyperthyroidism. *J Mol Cell Cardiol* **464,** 453–464 (2002).

188. Carr, A. N. & Kranias, E. G. Thyroid hormone regulation of calcium cycling proteins. *Thyroid* **12,** 453–7 (2002).

189. Kimura, Y., Otsu, K., Nishida, K., Kuzuya, T. & Tada, M. Thyroid hormone enhances ca+2 pumping activity of the cardiac sarcoplasmic reticulum by increasing ca+2 ATPase and decreasing phospholamban expression. *J Mol Cell Cardiol* **26,** 1145–1154 (1994).

190. Minamisawa, S. *et al.* Chronic Phospholamban – Sarcoplasmic Reticulum Calcium ATPase Interaction Is the Critical Calcium Cycling Defect in Dilated Cardiomyopathy. **99,** 313–322 (1999).

191. Kaprielian, R., del Monte, F. & Hajjar, R. J. Targeting Ca2+ cycling proteins and the action potential in heart failure by gene transfer. *Basic Res Cardiol* **97 Suppl 1,** I136–45 (2002).

192. Chu, G. *et al.* Compensatory mechanisms associated with the hyperdynamic function of phospholamban-deficient mouse hearts. *Circ Res* **79,** 1064–1076 (1996).

193. Schulman, H. & Braun, A. in *Calcium as a cellular regulator.* (Carafoli, E. & Klee, C.) 311–343 (Oxford University Press, New York, 1999).

194. Diedrichs, H. *et al.* Activation of the calcineurin/NFAT signalling cascade starts early in human hypertrophic myocardium. *J Int Med Res* **35,** 803–18 (2007).

195. Lin, J. *et al.* Transcriptional co-activator PGC-1 alpha drives the formation of slow-twitch fibres. *Nature* **418,** 797–801 (2002).

196. Soliman, E. *et al.* Boosted protease inhibitors and the electrocardiographic measures of QT and PR durations. *AIDS* **25,** 367–377 (2011).

197. Charbit, B., Gayat, E., Voiriot, P., Boccara, F. & Girard, P. Effects of HIV protease inhibitors on cardiac conduction velocity in unselected HIV-infected patients. *Clin Pharmacol Therap* **90,** 442–448 (2009).

198. Deng, W., Baki, L., Yin, J., Zhou, H. & Baumgarten, C. M. HIV protease inhibitors elicit volume-sensitive Cl − current in cardiac myocytes via mitochondrial ROS. *J Mol Cell Cardiol* **49,** 746–52 (2010).

199. Anson, B. *et al.* Blockade of HERG channels by HIV protease inhibitors. *Lancet* **365,** 682–686 (2005).

200. Chinello, P. *et al.* Role of antiretroviral treatment in prolonging QTc interval in HIV-positive patients. *J Infect* **54,** 597–602 (2007).

201. Ly, T. & Ruiz, M. E. Prolonged QT interval and torsades de pointes associated with atazanavir therapy. *Clin Infect Dis* **44,** e67–68 (2007).

202. Rathbun, R. C. *et al.* Electrocardiogram abnormalities with Atazanavir and Lopinavir / Ritonavir. *HIV Clin Trials* **10,** 328–336 (2009).

203. Charbit, B. *et al.* Relationship between HIV protease inhibitors and QTc interval duration in HIV-infected patients: a cross-sectional study. *Brit J Clin Pharmacol* **67,** 76–82 (2009).

204. Busti, A. *et al.* A prospective evaluation of the effect of atazanavir on the QTc interval and QTc dispersion in HIV-positive patients. *HIV Med* **7,** 317–322 (2006).

205. Yoshida, H. ER stressand disease. *FEBS J* **274,** 630–58 (2007).

206. Taura, M. *et al.* Comparitive analysis of ER stress response into HIV protease inhibitors: Lopinavir but not Darunavir induces potent ER stress response via ROS/JNK pathway. *Free Radic Biol Med* **Aug 20,** [Epub ahead of print] (2013).

207. Saez, J., Berthoud, V., Branes, M., Martinez, A. & Beyer, E. Plasma membrane channels formed by connexins : their regulation and functions. *Physiol Rev* **83,** 1359–1400 (2003).

208. Van Kempen, M., Fromaget, C., Gros, D., Moorman, A. & Lamers, W. Spatial distribution of connexin 43, the major cardiac gap junction protein, in the developing and adult rat heart. *Circ Res* **68,** 1638–51 (1991).

209. Jansen, J. A., Veen, T. A. B. Van, Bakker, J. M. T. De & Rijen, H. V. M. Van. Cardiac connexins and impulse propagation. *J Mol Cell Cardiol* **48,** 76–82 (2010).

210. Delorme, B. *et al.* Expression pattern of connexin gene products at the early developmental stages of the mouse cardiovascular system. *Circ Res* **81,** 423–437 (1997).

211. Coppen, S. R. *et al.* Connexin 45, a major connexin of the rabbit sinoatrial node, is co-expressed with connexin 43 in a restricted zone at the nodal-crista terminalis border. *J Histochem Cytochem* **47,** 907–918 (1999).

212. Verheijck, E. E. *et al.* Electrophysiological features of the mouse sinoatrial node in relation to connexin distribution. *Cardiovasc Res* **52,** 40–50 (2001).

213. Van Rijen, H., van Veen, T., Gros, D., Wilders, R. & de Bakker, J. *Connexins and cardiac arrhythmias. Advanced Cardiology: Cardiovascular Gap Junctions.* vol 42, 150–160 (Basel, Karger, 2006).

214. Guerrero, P. a *et al.* Slow ventricular conduction in mice heterozygous for a connexin 43 null mutation. *J Clin Invest* **99,** 1991–8 (1997).

215. Gutstein, D. E. *et al.* Conduction slowing and Ssdden arrhythmic death in mice with cardiac-restricted inactivation of connexin 43. *Circ Res* **88,** 333–339 (2001).

216. Thomas, S. A. *et al.* Disparate effects of deficient expression of connexin 43 on atrial and ventricular conduction evidence for chamber-specific molecular determinants of conduction. *Circulation* **97,** 686–691 (1998).

217. Eckardt, D. Functional role of connexin 43 gap junction channels in adult mouse heart assessed by inducible gene deletion. *J Mol Cell Cardiol* **36,** 101–110 (2004).

218. Van Rijen, H. V. M. Van, Bakker, J. M. T. De & Veen, T. A. B. Van. Hypoxia , electrical uncoupling , and conduction slowing : role of conduction reserve. *Cardiovasc Res* **66,** 9–11 (2005).

219. Reaume, A. *et al.* Cardiac malformation in neonatal mice lacking connexin 43. *Science* **267,** 1831–1834 (1995).

220. Huang, G. Y. *et al.* Alteration in connexin 43 gap junction gene dosage impairs conotruncal heart development. *Develop Biol* **198,** 32–44 (1998).

221. Duffy, H. S. & Wit, A. L. Is there a role for remodeled connexins in AF? No simple answers. *J Mol Cell Cardiol* **44,** 4–13 (2008).

222. Nattel, S., Maguy, A., Le Bouter, S. & Yeh, Y. Arrythmogenic ion-channel remodeling in the heart: heart failure, myocardial infarction, and atrial fibrillation. *Physiol Rev* **87,** 425–456 (2007).

223. Nattel, S., Shiroshita-Takeshita, A., Brundel, B. & Rivard, L. Mechanism of atrial fibrillation: lessons from animal models. *Prog Cardiovasc Dis* **48,** 9–28 (2005).

224. Severs, N., Bruce, A., Dupont, E. & Rothery, S. Remodelling of gap junctions and connexin expression in diseased myocardium. *Cardiovasc Res* **80,** 9–19 (2008).

225. Ya, J. *et al.* Heart defects in connexin 43-deficient mice. *Circ Res* **82,** 360–366 (1998).

226. VanSlyke, J. K., Deschenes, S. M. & Musil, L. S. Intracellular transport , assembly , and degradation of wild-type and disease-linked mutant gap junction proteins. *Mol Biol Cell* **11,** 1933–1946 (2000).

227. VanSlyke, J. K. & Musil, L. S. Dislocation and degradation from the ER are regulated by cytosolic stress. *J Cell Biol* **157,** 381–394 (2002).

228. Meusser, B., Hirsch1, C., Jarosch, E. & Sommer, T. ERAD: the long road to destruction. *Nat Cell Biol* **7,** 766 – 772 (2005).

229. Bonifacino, J. S. & Traub, L. M. Signals for sorting of transmembrane proteins to endosomes and lysosomes. *Ann Rev Biochem* **72,** 395–447 (2003).

230. Lampe, P. & Lau, A. The effects of connexin phosphorylation on gap junction communication. *Int J Biochem Cell Biol* **36,** 1171–1186 (2004).

231. Laird, D. W. Connexin phosphorylation as a regulatory event linked to gap junction internalization and degradation. *Biochim Biophys Acta* **1711,** 172–82 (2005).

232. Laing, J. G., Tadros, P. N., Westphale, E. M. & Beyer, E. C. Degradation of connexin 43 gap junctions involves both the proteasome and the lysosome. *Exper Cell Res* **236,** 482–92 (1997).

233. Laing, J. G. & Beyer, E. C. The gap junction protein connexin 43 is degraded via the ubiquitin proteasome pathway. *J Biol Chem* **270,** 26399–403 (1995).

234. Leithe, E. & Rivedal, E. Epidermal growth factor regulates ubiquitination, internalization and proteasome-dependent degradation of connexin 43. *J Cell Sci* **117,** 1211–1220 (2004).

235. Musil, L. S., Le, A. N., VanSlyke, J. K. & Roberts, L. M. Regulation of Connexin Degradation as a Mechanism to Increase Gap Junction Assembly and Function. *J Biol Chem* **275,** 25207–25215 (2000).

236. Puigserver, P., Rhee, J., Lin, J. & Al., E. Cytokine stimulation of energy expenditure through p38 MAP kinase activation of PPARgamma coactivator-1. *Mol Cell* **8,** 971–982 (2001).

237. Knutti, D., Kressler, D. & Kralli, A. Regulation of the transcriptional coactivator PGC-1 via MAPK-sensitive interaction with a corepressor. *Proc Natl Acad Sci U S A* **98,** 9713–9718 (2001).

238. Fan, M. *et al.* Suppression of mitochondrial respiration through recruitment of p160 myb binding protein to PGC-1alpha: modulation by p38 MAPK. *Genes Dev* **18,** 278–289 (2004).

239. Boss, O. *et al.* Role of the beta 3-adrenergic receptor and/or putative beta-4-adrenergic receptor on the expression of uncoupling proteins and peroxisome proliferator-activated receptor-gamma coactivator-1. *Biochem Biophys Res Commun* **261,** 870–876 (1999).

240. Nisoli, E. *et al.* Mitochondrial biogenesis in mammals: The role of endogenous nitric oxide. *Science* **299,** 896–899 (2003).

241. Handschin, C., Rhee, J., Lin, J., Tam, P. & Spiegelman, B. An autoregulatory loop controls peroxisome proliferator-activated receptor gamma coactivator 1 alpha expression in muscle. *Proc Natl Acad Sci U S A* **100,** 7111–7116 (2003).

242. Wu, H. *et al.* Regulation of mitochondrial biogenesis in skeletal muscle by CaMK. *Science* **296,** 349– 352 (2002).

243. Vega, R., Huss, J. & Kelly, D. The coactivator PGC-1 cooperates with peroxisome proliferator-activated receptor alpha in transcriptional control of nuclear genes encoding mitochondrial fatty acid oxidation enzymes. *Mol Cell Biol* **20,** 1868–1876 (2000).

244. Wang, Y., Lee, C., Tiep, S. & Al., E. Peroxisome-proliferator-activated receptor delta activates fat metabolism to prevent obesity. *Cell* **113,** 159– 170 (2003).

245. Puigserver, P., Wu, Z., Park, C. & Al., E. A cold-inducible coactivator of nuclear receptors linked to adaptive thermogenesis. *Cell* **92,** 829–839 (1998).

246. Michael, L., Wu, Z., Cheatham, R. & Al., E. Restoration of insulin-sensitive glucose transporter (GLUT4) gene expression in muscle cells by the transcriptional coactivator PGC-1. *Proc Natl Acad Sci U S A* **98,** 3820– 3825

247. Jager, S., Handschin, C., St-Pierre, J. & Spiegelman, B. AMP-activated protein kinase (AMPK) action in skeletal muscle via direct phosphorylation of PGC- 1alpha. *Proc Natl Acad Sci U S A* **104,** 12017–12022 (2007).

248. Wallberg, A., Yamamura, S., Malik, S., Spiegelman, B. & Roeder, R. Coordination of p300-mediated chromatin remodeling and TRAP/mediator function through coactivator PGC-1alpha. *Mol Cell* **12,** 1137–1149 (2003).

249. Puigserver, P. *et al.* Activation of PPARgamma coactivator-1 through transcription factor docking. *Science* **286,** 1368 –1371 (1999).

250. Monsalve, M. *et al.* Direct coupling of transcription and mRNA processing through the thermogenic coactivator PGC-1. *Mol Cell* **6,** 307–316 (2000).

251. Wu, Z. *et al.* Mechanisms controlling mitochondrial biogenesis and respiration through the thermogenic coactivator PGC-1. *Cell* **98,** 115–124 (1999).

252. Scarpulla, R. Nuclear control of respiratory chain expression in mammalian cells. *Bioenerg Biomembr* **29,** 109–119 (1997).

253. Clayton, D. Transcription and replication of animal mitochondrial DNAs. *Int Rev Cytol* **141,** 217–232 (1992).

254. Shadel, G. & Clayton, D. Mitochondrial transcription initiation: variation and conservation. *J Biol Chem* **268,** 16083–16086 (1993).

255. Attardi, G. & Schatz, G. Biogenesis of mitochondria. *Annu Rev Cell Biol* **4,** 289–333 (1988).

256. Evans, M. & Scarpulla, R. NRF-1: a trans-activator of nuclear-encoded respiratory genes in animal cells. *Genes Dev* **4,** 1023–1034. (1990).

257. Virbasius, J. & Scarpulla, R. Activation of the human mitochondrial transcription factor A gene by nuclear respiratory factors: a potential regulatory link between nuclear and mitochondrial gene expression in organelle biogenesis. *Proc Natl Acad Sci U S A* **91,** 1309–1313 (1994).

258. Lehman, J., Barger, P., Kovacs, A. & Al., E. Peroxisome proliferator-activated receptor gamma coactivator-1 promotes cardiac mitochondrial biogenesis. *J Clin Invest* **106,** 847–856 (2000).

259. St-Pierre, J., Lin, J., Krauss, S. & Al., E. Bioenergetic analysis of peroxisome proliferator-activated receptor gamma coactivators 1alpha and 1beta (PGC-1alpha and PGC-1beta) in muscle cells. *J Biol Chem* **278,** 26597–26603 (2003).

260. Lu, Z., Hu, X. & Fassett, J. PGC-1a regulates expression of myocardial mitochondrial antioxidants and myocardial oxidative stress after chronic systolic overload. *Antiox Redox Sign* **13,** (2010).

261. Barger, P., Brandt, J., Leone, T., Weinheimer, C. & Kelly, D. Deactivation of peroxisome proliferator-activated receptor-alpha during cardiac hypertrophic growth. *J Clin Invest* **105,** 1723–1730 (2000).

262. Sano, M. *et al.* Activation of cardiac Cdk9 represses PGC-1 and confers a predisposition to heart failure. *EMBO J* **23,** 3559–3569 (2004).

263. Arany, Z. *et al.* Transverse aortic constriction leads to accelerated heart failure in mice lacking PPAR-gamma coactivator 1alpha. *Proc Natl Acad Sci U S A* **103,** 10086 –10091 (2006).

264. Viengchareun, S. *et al.* Mitochondrial toxicity of indinavir, stavudine and zidovudine invloves multiple cellular targets in white and brown adipocytes. *Antiviral Therapy* **12,** 919–929 (2007).

265. Russell, L. *et al.* Cardiacspecific induction of the transcriptional coactivator peroxisome proliferator-activated receptor gamma coactivator-1alpha promotes mitochondrial biogenesis and reversible cardiomyopathy in a developmental stage-dependent manner. *Circ Res* **94,** 525–533 (2004).

266. Richter, C., Park, J. & Ames, B. Normal oxidative damage to mitochondrial and nuclear DNA is extensive. *Proc Natl Acad Sci U S A* **85,** 6465–6467 (1988).

267. Ames, B., Shigenaga, M. & Hagen, T. Oxidants, antioxidants, and the degenerative diseases of aging. *Proc Natl Acad Sci U S A* **90,** 7915–7922 (1993).

268. Lee, H. & Wei, Y. Mitochondrial role in life and death of the cell. *J Biomed Sci* **7,** 2–15 (2000).

269. Chance, B., Sies, H. & Boveris, H. Hydroperoxide metabolism in mammalian organs. *Physiol Rev* **59,** 527–605 (1979).

270. Zaera, M. *et al.* Mitochondrial involvement in antiretroviral therapy- related lipodystrophy. *AIDS* **15,** 1643–1651 (2001).

271. Zhang, S. *et al.* Protease inhibitors used in the treatment of HIV+ induce beta-cell apoptosis via the mitochondrial pathway and compromise insulin secretion. *Am J Physiol Endocrinol Metab* **296,** E925–35 (2009).

272. Lagathu, C. *et al.* Some HIV antiretrovirals increase oxidative stress and alter chemokine, cytokine or adiponectin prodcution in human adipocytes and macrophages. *Antiviral Therapy* **12,** 489–500 (2007).

273. Chandra, S., Mondal, D. & Agrawal, K. C. HIV-1 protease inhibitor induced oxidative stress suppresses glucose stimulated insulin release: protection with thymoquinone. *Exp Biol Med* **234,** 442–53 (2009).

274. Touzet, O. & Philips, A. Resveratrol protects against protease inhibitor-induced reactive oxygen species production, reticulum stress and lipid raft perturbation. *AIDS* **24,** 1437–47 (2010).

275. Ben-Romano, R. *et al.* Nelfinavir induces adipocyte insulin resistance through the induction of oxidative stress: differential protective effect of antioxidant agents. *Antiviral Therapy* **11,** 1051–1060 (2006).

276. Wang, X., Chai, H., Lin, P. H., Yao, Q. & Chen, C. Roles and mechanisms of human immunodeficiency virus protease inhibitor ritonavir and other anti-human immunodeficiency virus drugs in endothelial dysfunction of porcine pulmonary arteries and human pulmonary artery endothelial cells. *Am J Pathol* **174,** 771–81 (2009).

277. Wang, X. *et al.* Human immunodeficiency virus protease inhibitor Ritonavir inhibits cholesterol efflux from human macrophage-derived foam cells. *Am J Pathol* **171,** 304–314 (2007).

278. Conklin, B. S. *et al.* HIV protease inhibitor ritonavir decreases endothelium-dependent vasorelaxation and increases superoxide in porcine arteries. *Cardiovasc Res* **63,** 168–75 (2004).

279. Chai, H. *et al.* Effects of 5 HIV protease inhibitors on vasomotor function and superoxide anion production in porcine coronary arteries. *J AIDS* **40,** 12–9 (2005).

280. Jiang, B. *et al.* HIV antiretroviral drug combination induces endothelial mitochondrial dysfunction and reactive oxygen species production, but not apoptosis. *Toxicol Appl Pharmacol* **224,** 60–71 (2007).

281. Mondal, D., Pradhan, L., Ali, M. & Agrawal, K. C. HAART drugs induce oxidative stress in human endothelial cells and increase endothelial recruitment of mononuclear cells: exacerbation by inflammatory cytokines and amelioration by antioxidants. *Cardiovasc Toxicol* **4,** 287–302 (2004).

282. Wu, Y. *et al.* Estimation of 10-year risk of fatal and nonfatal ischemic cardiovascular diseases in Chinese adults. *Circulation* **114,** 2217–25 (2006).

283. Wang, X. Z. *et al.* Cloning of mammalian Ire1 reveals diversity in the ER stress responses. *EMBO J* **17,** 5708–17 (1998).

284. Lagathu, C. *et al.* HIV antiretroviral treatment alters adipokine expression and insulin sensitivity of adipose tissue in vitro and in vivo. *Biochimie* **87,** 65–71 (2005).

285. Schinder, A., Olson, E., Spitzer, N. & Montal, M. Mitochondrial dysfunction is a primary event in glutamate neurotoxicity. *J Neurosci* **16,** 6125–33 (1996).

286. Chai, H., Yan, S., Lin, P. & Lumsden, A. B. Curcumin blocks HIV protease inhibitor ritonavir-induced vascular dysfunction in porcine coronary arteries. *J Am Coll Sur* **200,** 820–830 (2005).

287. Chen, Q., Vazquez, E., Moghaddas, S., Hoppel, C. & Lesnefsky, E. Production of reactive oxygen species by mitochondria. *J Biol Chem* **278,** 36027–31 (2003).

288. St-Pierre, J., Buckingham, J., Roebuck, S. & Brand, M. Topology of superoxide production from different sites in the mitochondrial electron transport chain. *J Biol Chem* **277,** 44784–90 (2002).

289. Gupte, R. S. *et al.* Upregulation of glucose-6-phosphate dehydrogenase and NAD(P)H oxidase ctivity increases oxidative stress in failing human heart. *J Cardiac Fail* **13,** 497–506 (2007).

290. Varela, D., Simon, F., Riveros, A., Jorgensen, F. & Stutzin, A. NAD(P)H oxidase-derived H2O2 signals chloride channel activation in cell volume regulation and cell proliferation. *J Biol Chem* **279,** 13301–4 (2004).

291. Zweier, J. & Talukder, M. The role of oxidants and free radicals in reperfusion injury. *Cardiovasc Res* **70,** 181–90 (2006).

292. Pacher, P., Nivorozhkin, A. & Szabo, C. Therapeutic effects of xanthine oxidase inhibitors: renaissance half a century after the discovery of allopurinol. *Pharmacol Rev* **58,** 87–114 (2006).

293. Van der Vusse, G. J., van Bilsen, M. & Glatz, J. F. Cardiac fatty acid uptake and transport in health and disease. *Cardiovasc Res* **45,** 279–93 (2000).

294. Akki, A., Zhang, M., Murdoch, C., Brewer, A. & Shah, A. M. Journal of Molecular and Cellular Cardiology Review article NADPH oxidase signaling and cardiac myocyte function. *J Mol Cell Cardiol* **47,** 15–22 (2009).

295. Muller, F., Yuhong, Z. & Van Remmen, H. Complex III releases superoxide to both sides of the inner mitochondrial membrane. *J Biol Chem* **279,** 49064–73 (2004).

296. Zorov, D. B., Juhaszova, M. & Sollott, S. J. Mitochondrial ROS-induced ROS release : an update and review. *Biochim Biophys Acta* **1757,** 509 – 517 (2006).

297. McCord, J. & Fridovich, I. An enzymatic function for erythrocuprein (hemocuprein). *J Biol Chem* **244,** 6049–55 (1969).

298. Buckley, B., Tanswell, A. & Freeman, B. Liposome-mediated augmentation of catalase in alveolar type II cells protects against H2O2 injury. *J Appl Physiol* **63,** 359–67 (1987).

299. Antunes, F., Han, D. & Cadenas, E. Relative contributions of heart mitochondria glutathione peroxidase and catalse to H2O2 detoxification in in vivo conditions. *Free Rad Biol Med* **33,** 1260–7 (2002).

300. Finkel, T. Oxidant signals and oxidative stress. *Curr Opin Cell Biol* **15,** 247–254 (2003).

301. Giordano, F. Oxygen, oxidative stress, hypoxia, and heart failure. *J Clin Invest* **115,** 500–508 (2005).

302. Kurosawa, K. *et al.* Kinetics of hydrogen peroxide degradation by NADP glutathione system in mitochondria. *J Biochem* **108,** 9–16 (1990).

303. Lambeth, J. NOX enzymes and the biology of reactive oxygen. *Nat Rev Immunol* **4,** 181–189 (2004).

304. Cave, A. *et al.* NADPH oxidases in cardiovascular health and disease. *Antioxid Redox Signal* **8,** 691–728 (2006).

305. Bedard, K. & Krause, K. The NOX family of ROS-generating NADPH oxidases: physiology and pathophysiology. *Physiol Rev* **87,** 245–313 (2007).

306. Gutteridge, J. Iron promoters of the Fenton reaction and lipid peroxidation can be released from haemoglobin by peroxides. *FEBS Letters* **201,** 291–295 (1986).

307. Jiang, B. *et al.* HIV antiretroviral drug combination induces endothelial mitochondrial dysfunction and reactive oxygen species production, but not apoptosis. *Toxicol Appl Pharmacol* **224,** 60–71 (2007).

308. Zhong, D. D. *et al.* HIV protease inhibitor ritonavir induces cytotoxicity of human endothelial cells. *Arterioscler Thromb Vasc Biol* **22,** 1560–1566 (2002).

309. Roumier, T. *et al.* HIV-1 protease inhibitors and cytomegalovirus vMIA induce mitochondrial fragmentation without triggering apoptosis. *Cell Death Differ* **13,** 348–51 (2006).

310. Sivitz, W. & Yorek, M. Mitochondrial dysfunction in diabetes: from molecular mechanisms to functional significance and therapeutic opportunities. *Antiox Redox Signal* **12,** 1–41 (2010).

311. Vernochet, C. *et al.* Human immunodeficiency virus protease inhibitors accumulate into cultured human adipocytes and alter expression of adipocytokines. *J Biol Chem* **280,** 2238–43 (2005).

312. Chai, H. *et al.* Ginsenosides block HIV protease inhibitor ritonavir-induced vascular dysfunction of porcine coronary arteries. *Vasc Surg* **288,** 2965–2971 (2010).

313. Fu, W., Chai, H., Yao, Q. & Chen, C. Effects of HIV protease inhibitor ritonavir on vasomotor function and endothelial nitric oxide synthase expression. *J AIDS* **39,** 152–8 (2005).

314. Otis, J. S., Ashikhmin, Y. I., Brown, L. A. S. & Guidot, D. M. Effect of HIV-1-related protein expression on cardiac and skeletal muscles from transgenic rats. *AIDS Res Ther* **5,** 8 (2008).

Chapter 2

Establishment and characterization of a rodent model of chronic PI exposure

Introduction

PIs form an integral part of HAART and side effects include the development of dyslipidemia, i.e. increased production of plasma TGs and lipids, together with an adverse cholesterol profile [1] as well as peripheral and central fat hypertrophy [2]. Together such metabolic derangements elicit inflammation, stress the myocardium [3,4], and may potentially predict the onset of IR and cardiac dysfunction [5,6] .

The most common side effects experienced with Lopinavir/Ritonavir usage are diarrhea, nausea, and lipid abnormalities (elevated cholesterol and TG) [7]. Moreover, metabolic changes associated with PI usage resemble the MetS, a combination of risk factors that predispose to future onset of T2DM and CVD [8]. In support, human [6,9–14], animal [15–17] and cell-based [18–21] studies demonstrate that increased plasma cholesterol and TG levels, and the development of lipodystrophy and IR are the most common metabolic perturbations found with PI treatment.

In the setting of lipodystrophy, an imbalance in fat partitioning occurs, with lipoatrophy occurring at the extremities and accumulation of fatty tissue more centrally especially at subcutaneous sites such as the waist, hips and neck. Such an accumulation of lipids may predispose an individual to dyslipidemia. Further, the increased burden of lipodystrophy with HIV infection can

alter FA metabolism and ensure that abnormal lipid levels become indicative of the MetS phenotype. Such alterations may or may not be accompanied by anthropometric changes, e.g. body weight, waist circumference and BMI [22]. However, dyslipidemia and MetS can co-manifest with anthropometric alterations, especially for PI administration regimens longer than 12 months [23–27]. Lastly, PI-mediated perturbations to glucose metabolism can also occur. For example, PIs can impair glucose tolerance as well as multiple facets of glucose metabolism, ultimately resulting in IR [9,28,29].

These data therefore indicate that PIs have far reaching consequences on metabolism. Moreover, PIs act early at the molecular level, e.g. activating key metabolic pathways (mitochondrial impairment, oxidative stress), thereby initiating a cascade of detrimental alterations contributing to the development and presentation of dyslipidemia, lipodystrophy and weight gain. However, the precise molecular mechanisms defining PI-mediated cardio-metabolic changes remain less well understood. In light of this, we set out to first establish a rat model of chronic PI utilization as a platform to further investigate this intriguing system. For this study we hypothesize that PIs pathologically alter lipid metabolism and glucose metabolism. Here an attempt was made to investigate this hypothesis in the context of varying dietary intake (normal versus high fat diets) to try and simulate realities faced by individuals receiving HAART.

Materials & Methods

Animal model

The use of animals and procedures were reviewed and approved by the Animal Research Ethics Committee of the Faculty of Natural Sciences of Stellenbosch University (application numbers 2006B02006, 11NF_REY01, SU_ACUM11_00006, and related amendments). This study adheres to the guidelines set out by the National Institutes of Health's *Guide for the Care and Use of Laboratory Animals* and performed with the approval of the Animal Ethics Committee of Stellenbosch University (South Africa). Male Wistar rats were housed (maximum 4 animals per cage) in the Faculty's animal facility and a standard light/dark cycle (12 h-12 h) maintained throughout the duration of the study. We ensured animals had access to food and water *ad libitum*; with body weight, food consumption and general health monitored on a daily basis. Rats were acclimatized for 14 days (starting at day -14) to their housing conditions and the investigator, after which experiments were initiated. Interventions commenced on the first day (Day 0) when rats exhibited weights of 160-220 grams (g). A total of 8 rats were used per experimental group and as follows: sham, vehicle, PI-treated, high fat (HF) and PI-treated animals on a high fat diet (PI+HF) (deviations explained for individual experiments further below).

Dietary intervention

Animals were fed either low fat chow (D12450B, Research Diets, New Brunswick, NJ) with 10% kilocalories as fat, or HF chow with 45% kilocalories fat (D12451, Research Diets). The dietary constituents were as follow (% kcal): Low fat chow – fat (10), protein (20), carbohydrates (70); and

high fat chow – fat (45), protein (20), and carbohydrates (35). All animals were provided with the low fat chow during the acclimatization period (Day -14 to Day 0) and thereafter received the low or HF diet, respectively, for a total of 8 weeks. This will be indicated in the results section of this chapter.

Drug administration

Lopinavir/Ritonavir (Kaletra™, Abbott Laboratories, Abbot Park IL) was crushed and dissolved in a 1% ethanol (vehicle) solution at human steady-state plasma concentration (7.1 ± 2.9 µg/mL), sterile filtered and injected into a mini-osmotic pump (Alzet, Cupertino CA). Male Wistar rats (160-220 g) received either: mock surgery (sham), vehicle-, or PI-containing pump for a total of 8 weeks (n=8 per group). Here we attempted to simulate a relatively early stage of PI treatment, i.e. if the average lifespan of 2-3 years is taken for Wistar rats then 8 weeks translates to ~ 6% of its total lifespan. This would correspond to ~ 2-3 years of PI treatment for a 30 year-old started on HAART treatment and with a life expectancy of ~ 60-70 years.

Briefly, rats were anesthetized with isofluorane in oxygen (5% for induction, 1.5-3% for maintenance) after a 4-hour (hr) fasting period with the incision site shaved and sterilized below the right shoulder blade. A 1-2 cm incision was made into the skin and a pocket created with a hemostat to place the pump subscapular. After the pump was inserted the wound was closed with 2-3 sutures, wiped with iodine and intra-muscular painkiller (buprenorphine, 0.05 mg/kg) administered before the rats awoke from anesthesia. Rats recovered in individual cages for the first 6 hours (hrs) with access to food and water *ad libitum* to monitor wound healing, and placed back with litter mates within 24 hrs of surgery upon complete wound closure.

Body weight and food consumption

Weight gain was measured at weekly intervals throughout the 8-week treatment period. Food consumption was assessed daily and total intake was then determined and averaged per rat per cage.

Blood lipid profile and HOMA-IR assessment

In separate experiments, serum and tissue metabolite levels were evaluated following PI treatment. Due to financial constraints we did not continue with the HF feeding regimen and only assessed blood lipid profile and homeostatic model of assessment of insulin resistance (HOMA-IR) in PI-treated animals and their controls for the remainder of the study. After 8 weeks (4-7 days before termination of treatment period) rats underwent a 12-18 hr overnight fast where after blood was collected from the jugular vein, serum isolated and analyzed for: total and low-density lipoprotein (LDL) cholesterol, FFA and TG levels (NHLS, Tygerberg Hospital, South Africa). Weekly fasting glucose measurements via tail prick were also determined using a glucometer (Accutrend™ glucometer, Roche Diagnostics, IN). We also evaluated the HOMA-IR – here serum insulin and glucose levels were also determined (PathCare Laboratory, Stellenbosch, South Africa). The HOMA-IR was calculated as follows: (glucose [mg/dL] x fasting insulin [µU/mL] / 2.43) and the equation used in accordance with the guidelines for HOMA-IR assessment in rodents [30].

Cytokine profile

Serum was further analyzed after 8 weeks of PI therapy (no dietary intervention, see "Blood Lipid Profile" above) for cytokines associated with inflammation such as tumor-necrosis factor alpha (TNFα) and interleukin 6 (IL-6). The enzyme-linked immunosorbent assay (ELISA) technique was employed for TNFα (TNFα ELISA Ready-SET-Go!, eBioscience, San Diego CA) and IL-6 (Legend Max™ Rat IL-6 ELISA, BioLegend, San Diego CA). Both cytokines were assessed according to the

manufacturer's instructions. Briefly, a clear 96-well microtiter plate was pre-coated with primary antibody raised against the rat-specific immunogen of TNFα or IL-6. Serum was prepared according to the manufacturer's instructions with the necessary buffers supplied in the kit and diluted accordingly. A standard curve of known concentrations of either cytokine was made and the serum samples aliquoted into the remaining wells as the unknowns. Through various steps of incubation and washing, cytokines present in the serum samples were immunocaptured in the wells, excess antibody and serum components washed off, non-specific binding sites blocked, and secondary antibody conjugated to Avidin-HRP to detect cytokines via a color-change reaction. A colorimetric plate reader (Cecil CE2021 spectrophotometer, Cecil Instruments, Cambridge, UK) measured absorbance for both cytokines at 450 nm, and concentrations extrapolated from the standard curve were expressed as pg/mL.

Statistical analyses

One-way analysis of variance (ANOVA) was utilized for all experiments with a Bonferroni *post-hoc* test to compare variation between all the groups. Body weight over the 8-week treatment period was analyzed via two-way ANOVA. Statistical significance was considered when $p<0.05$, and data expressed as mean ± standard error of the mean (SEM).

Results

Since PI therapy has negative side effects that resemble the MetS, the aim of this study was to establish and characterize a novel rodent model with chronic PI treatment and further understanding of the mechanisms underlying such changes. Our first aim included assessment of weight during the 8-week treatment period as an indication of possible lipodystrophy – body fat redistribution – which could present as weight gain. Indeed, PI-treated rats exhibited weight gain (467 ± 18.1 vs. sham 385 ± 17.2 g, p< 0.001; and vs. vehicle 400 ± 18.1 g, p<0.001 (**Fig. 1A**). As expected the HF diet group also experienced significant weight gain in comparison to the control groups. However, neither this group nor the combination of a HF diet and PI treatment displayed differences in weight gain when compared to PI treatment alone (p>0.05) (**Fig. 1B**). Nonetheless, all three treatment groups i.e. PI, HF and PI+HF displayed greater weights at 8 weeks than sham and vehicle (**Fig. 2A**), though the percentage change was only significant for the HF diet group.

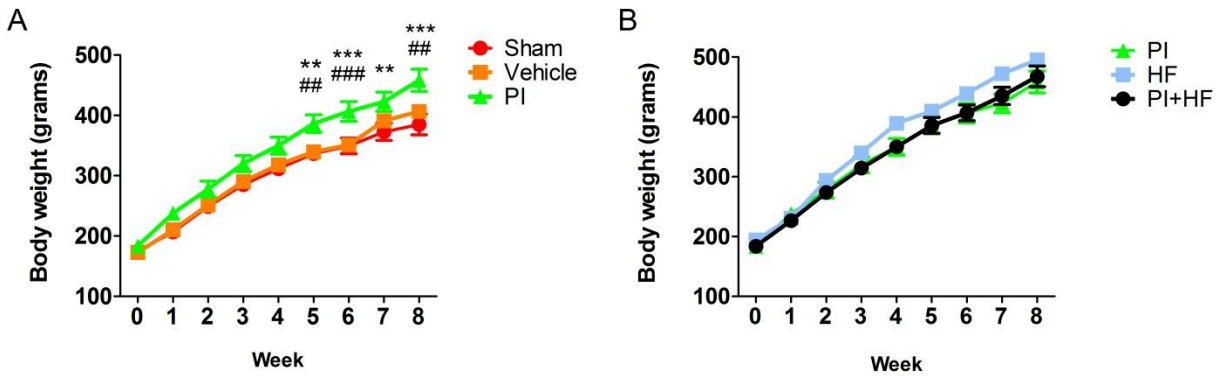

Figure 1. Body weight changes in response to 8 weeks PI treatment (n=16). A) PI-treated groups; and B) high fat treated groups. Data presented as mean ± SEM. **p<0.01 and ***p<0.001 vs. sham, ##p<0.01 and ###p<0.001 vs. vehicle. *HF – high fat, PI – protease inhibitor*.

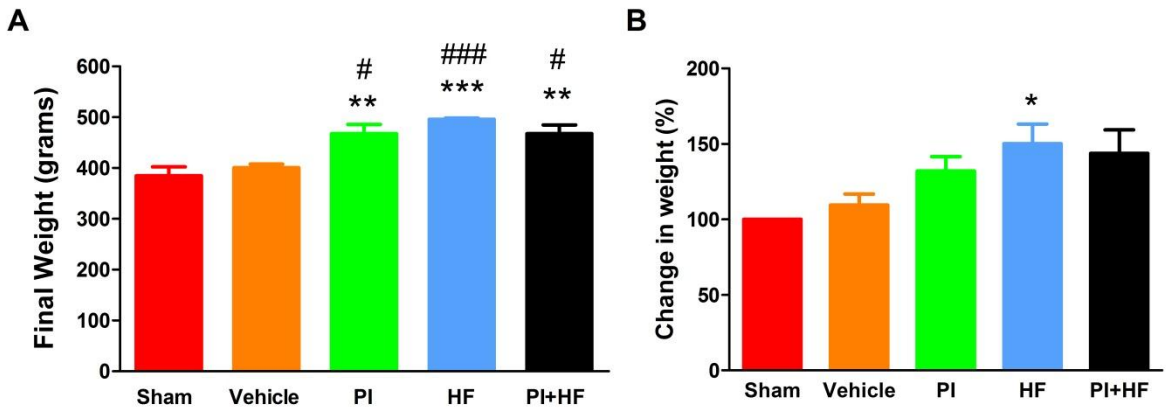

Figure 2. Terminal weight and percentage change due to PI and high fat dietary intervention (n=≥8). Final weights were measured on the day of killing after 8 weeks chronic PI treatment, and the change in weight is calculated as the percentage gain in weight normalized to the sham group. A) Final weight; and B) Percentage change in weight. Data presented as mean ± SEM. *p<0.05, **p<0.01, ***p<0.001 vs. sham; #p<0.05, ###p<0.001 vs. vehicle. *HF – high fat, PI – protease inhibitor.*

Food consumption reveals an interesting finding. PI-treated rats and the HF diet animals displayed higher food consumption (**Fig. 3**) versus controls (894 ± 17.8 g PI and 913 ± 64.4 g HF vs. sham and vehicle, p<0.05). Intriguingly, when PIs were co-administered with a HF diet, food consumption returned to baseline values (673 ± 35.2 vs. sham 707 ± 14.3 g, p>0.05; and vs. vehicle 717 ± 13.0 g, p>0.05).

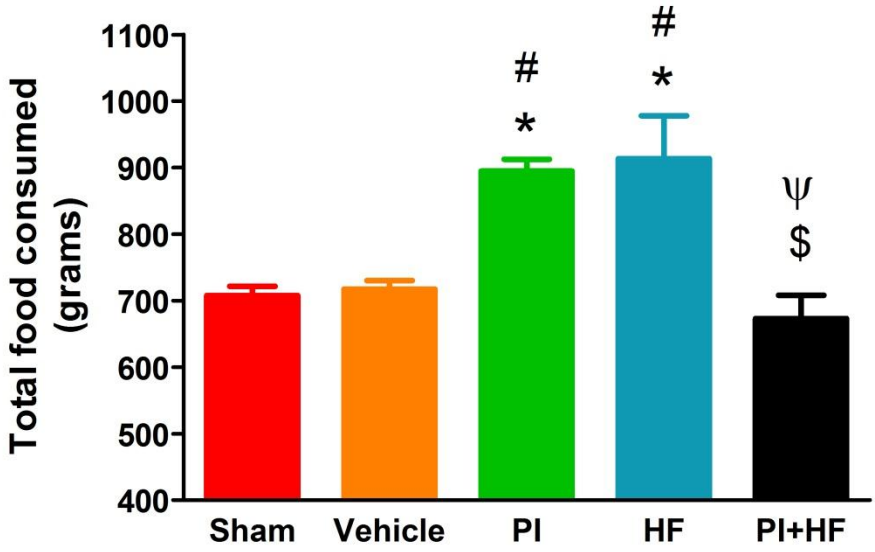

Figure 3. Total food consumed during 8 weeks of PI and high fat dietary intervention (n≥8). Food consumption was calculated as the average total amount of food consumed per rat for the duration of the intervention and averaged to the number of animals per cage. Data presented as mean ± SEM. *p<0.05 vs. sham, #p<0.05 vs. vehicle, $p<0.05 vs. PI, ψp<0.05 vs. HF. *HF – high fat, PI – protease inhibitor.*

Due to the nature of this study, the next set of experiments were carried out in a separate group of animals, and as previously mentioned, financial constraints led us to exclude the HF diet from subsequent analyses. Therefore, only sham, vehicle and PI-treated animals are utilized from this stage onwards. Since glucose abnormalities e.g. IR/T2DM are linked with PIs, we next assessed a) fasting glucose levels during 8 weeks of PI therapy with HOMA-IR, and b) an intra-peritoneal glucose tolerance test (ipGTT). However, due to technical difficulties the ipGTT was unsuccessful (**Fig. 4**). Weekly glucose measures revealed that none of the experimental groups experienced any significant changes to glucose levels that would indicate abnormalities ($p>0.05$ for all time points) (**Fig. 5**), and the HOMA-IR data confirmed this ($p>0.05$) (**Fig. 6**).

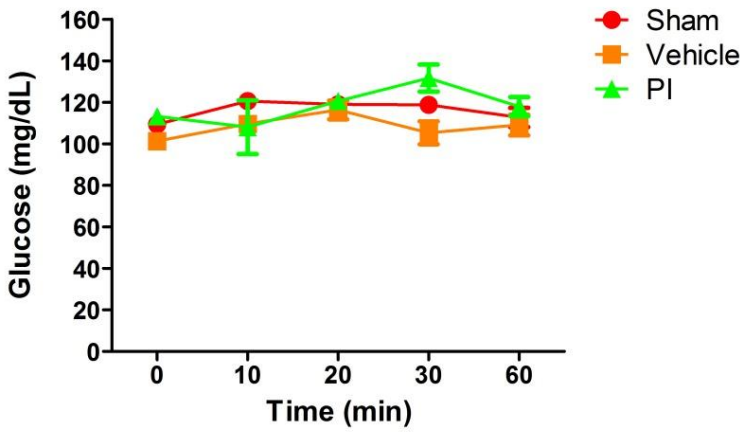

Figure 4. Intra-peritoneal glucose tolerance test (ipGTT) in response to chronic PI therapy (n=8). After an overnight fast, rats were injected i.p. with 2 mg/kg glucose and assessed for glucose response over 60 minutes. Data presented as mean ± SEM. *PI – protease inhibitor*.

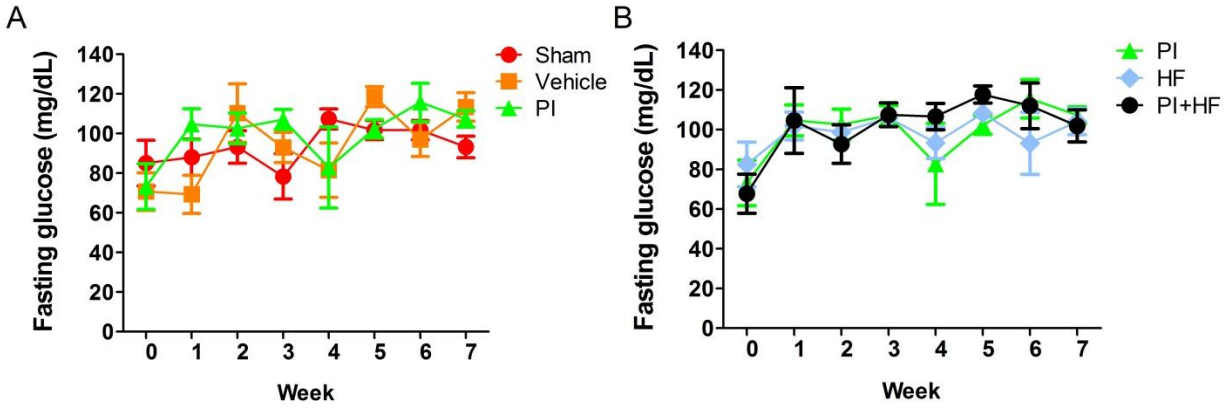

Figure 5. Weekly fasting glucose levels during 8 weeks of PI therapy (n=8). Weekly fasting glucose levels determined (commercial glucometer) for an 8-week period. A) PI-treatment; and B) HF diet. Data presented as mean ± SEM. *HF – high fat, PI – protease inhibitor.*

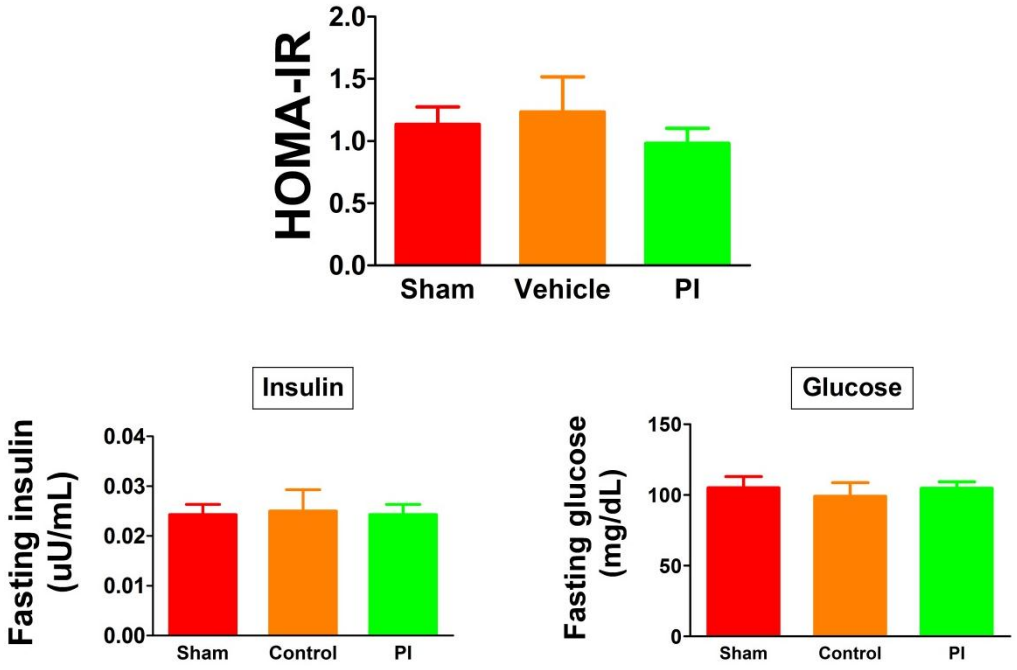

Figure 6. HOMA-IR and other parameters of glucose metabolism (n=8). PI treatment elicited no significant alterations in glucose metabolism parameters after 8 weeks of PI treatment versus controls. Data presented as mean ± SEM. *HOMA-IR – homeostatic model of assessment for insulin resistance, PI – protease inhibitor*.

Next, fasting serum levels for FFAs; TGs, total cholesterol, and LDL-cholesterol were assessed, but did not significantly differ with PI treatment (**Fig. 7**). However, PI treatment increased serum LDL-cholesterol levels to 0.433 ± 0.021 mM vs. sham 0.216 ± 0.005 mM, $p<0.05$; and vs. vehicle 0.216 ± 0.005 mM, $p<0.05$).

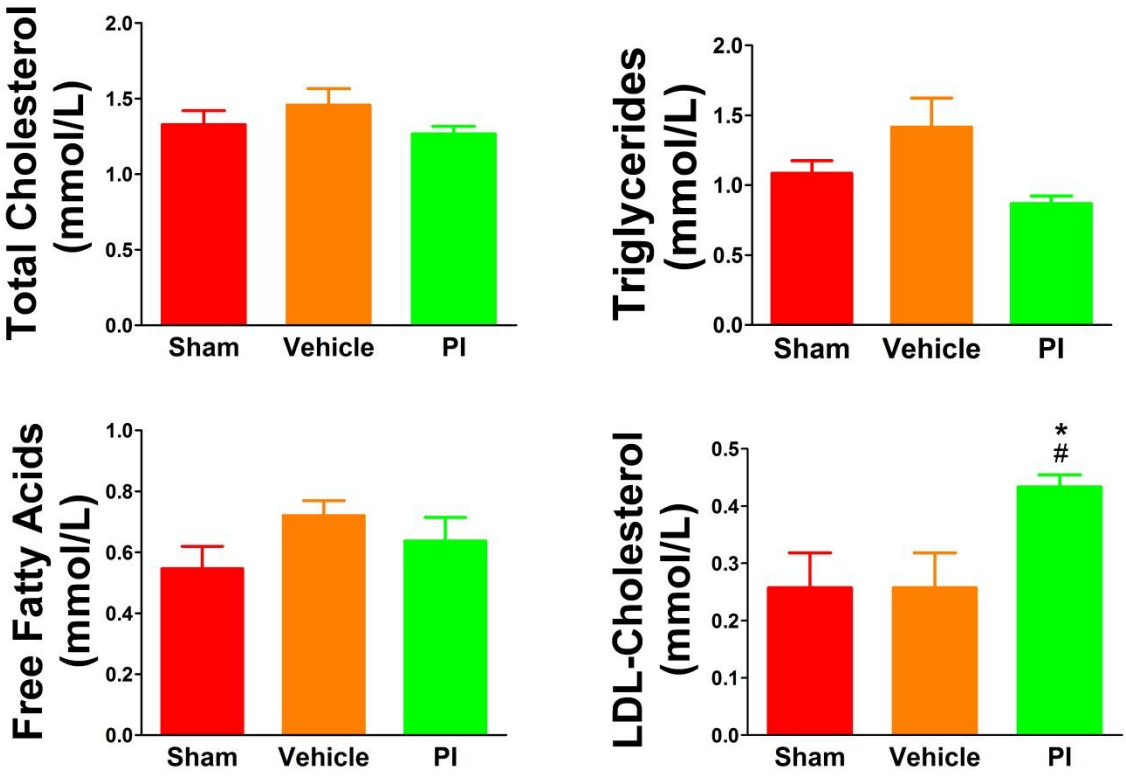

Figure 7. Lipid profile in response to 8 weeks PI treatment (n=8). Data presented as mean ± SEM. *$p<0.05$ vs. sham, #$p<0.05$ vs. vehicle. *LDL – low-density lipoprotein, PI – protease inhibitor*.

Cytokine profiles were also assessed in response to chronic PI treatment. However, since both serum TNFα and IL-6 levels fell below the detection limit of the ELISA kits (TNFα: 16 pg/mL and IL-6: 5.3 pg/mL) no conclusions could be drawn from this particular experiment (**Fig. 8**).

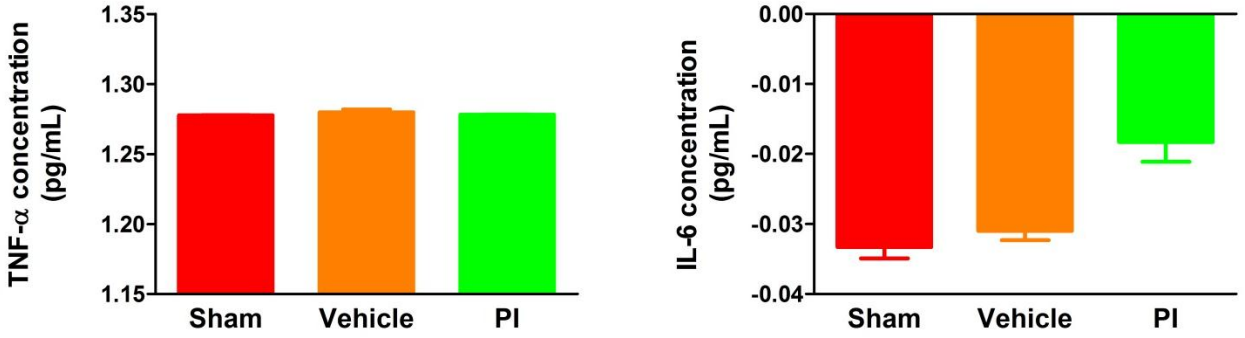

Figure 8. Cytokine profile of TNFα and IL-6 in response to PI therapy (n=8). Both cytokines were not detectable within physiologically relevant concentrations as determined by the ELISA method in response to PI treatment. *ELISA – enzyme-linked immune-sorbent assay, IL-6 – interleukin 6, PI – protease inhibitor, TNF – tumor necrosis factor alpha*.

Discussion

Although HAART markedly improves the quality of life and prognosis of HIV-infected individuals, it may elicit cardio-metabolic side effects in the long-term. Since molecular mechanisms underlying this process are poorly understood, early metabolic changes were evaluated in our unique rat model of PI treatment. The main findings of this study are 1) PI-treated rats exhibit increased weight gain; and 2) lipid abnormalities at this early time point were present.

PI-treated rats exhibit increased weight gain

The availability of a PI dose at a constant rate throughout the study, as opposed to fluctuating plasma drug concentrations due to daily administration, highlights a novel approach to this study. We believe this approach may be useful to elucidate molecular and functional effects of PI treatment, and may unlock innovative therapeutic interventions to better deal with the HIV/AIDS pandemic, especially within a chronic setting. The data reveal that both PI treatment and the HF diet increased weight gain in our model, but its combination did not result in an additive effect. We are of the opinion; however, that the moderate obese phenotype found in our experimental model with PI treatment may be representative of broader society as global obesity has risen in the last decades in parallel to the HIV pandemic.

The food consumption data yielded interesting results, i.e. increased with PI treatment and decreased with additional high fat feeding. It is unclear why this is the case. However, a relatively

crude measure to determine food intake was employed. It is possible that one or two animals may have consumed much more, or less food, thereby skewing the data. Alternatively, we speculate that differences in nutritional intake may be due to altered leptin and/or ghrelin levels that usually act as satiety signals. A variety of *in vitro* [31,32], *in vivo*[31,33,34] and human[24,35] studies have shown decreased leptin levels to be linked with the development of lipodystrophy [36], glucose intolerance (at central and peripheral adipose and skeletal depots), oxidative stress [31,33,34], lipid derangements and inversely correlated to chronic inflammation [10,31]. Leptin, neuropeptide Y and ghrelin are well-known regulators of dietary intake [37]. We propose that PI treatment in our model may perturb circulating leptin and/or ghrelin levels thereby interfering with dietary intake, and subsequently weight gain. These interesting possibilities require further investigation.

Previous studies demonstrated that a significant proportion of patients receiving HAART patients develop impaired glucose tolerance, IR and T2DM [5,6] but at a later stage in treatment duration. Here the data revealed that PI-treated rats displayed weight gain together with elevated serum LDL-cholesterol, identifying perturbed lipid metabolism as a relatively early occurrence. Although not focusing on initial PI-mediated changes, earlier research work also reported that lipid derangements are one of the commonest side-effects triggered by Lopinavir/Ritonavir usage [7]. Moreover, our study shows that the onset of IR follows at a later stage in the progression of cardio-metabolic dysfunction following PI treatment. How exactly does PI treatment induce the changes in lipid metabolism here observed? The mechanisms underlying higher food consumption with PI exposure are unclear and hence form part of our ongoing investigations.

Measurements of glucose and insulin metabolism

Fasting serum glucose levels did not significantly differ for the various experimental groups. We were not completely surprised since it is more likely to manifest after long-term PI therapy or HF intake, e.g. rats on a HF diet for 12 or more weeks [38] and in HIV-positive individuals receiving long-term HAART treatment [13]. Since rats were only moderately obese, it is likely that our 8-week experimental period is too short to induce profound hyperglycemia. The ipGTT unfortunately did not aid us in these investigations and the methods employed required further optimization. Such technical considerations are currently being assessed in our laboratory. This is unlike clinical [39] and *in vitro* [18] studies that previously reported the development of IR and the impairment of glucose uptake (via GLUT4) in response to PI treatment. However, these changes are very likely due to amount and duration of PI treatment. Additionally, the HOMA-IR and insulin levels confirmed our findings that our model is not insulin resistant nor in danger of developing a diabetic phenotype.

Chronic PI therapy elevated LDL-cholesterol

It is clear from the data that the elevation in LDL-cholesterol were not accompanied by similar changes in other lipid parameters and provide critical information as to how the PIs may elicit their metabolic response. The lipid profile was performed on serum samples, indicating that the increase in LDL-cholesterol very likely resulted from an increase in hepatic synthesis and release of cholesterol, even though total cholesterol levels remained unaltered. We also postulate that the increase in weight alongside lipid changes is indicative of the activation of key lipogenic and cholesterogenic genes within the liver and adipose tissues and may account for such an elevation. In addition, SREBPs play a central role by elevating gene transcription of key lipid synthesis genes such as *hmg-cr* [40,41] and

fas [42–46] and elevate the pool of cholesterol moieties. PIs have previously been shown to inhibit the UPS [47,48], a key modulator of SREBP metabolism, and thus it is a possibility that PIs may activate lipid synthesis and secretion via inhibition of the UPS and consequently exacerbate SREBP-induced gene transcription within the liver. Importantly, LDL-cholesterol may not necessarily translate into a pre-atherogenic profile on its own, but the involvement of increased availability of FAs and cholesterol may alter homeostatic FAO rates and mitochondrial oxidative capacity. Excess substrate supply does not bode well for mitochondria and we hypothesize that it is mitochondria that bear the brunt of PI-induced metabolic perturbations. This in turn may elicit downstream consequences e.g. oxidative stress, increased lipid peroxidation, insufficient mitochondrial energetics and ultimately cardiac inefficiency at multiple levels.

The fact that metabolic and phenotypic changes presented as early as 8 weeks requires attention. Many clinical models have reported lipid abnormalities with and without anthropometric changes in the context of PI treatment of more than one year [24–27,36,49]. Though our animal model attempts to complement chronic clinical PI administration of 2-3 years, human and *in vivo* models do not always correlate fully. More importantly, LDL-cholesterol is a critical pre-atherogenic marker and a well-known risk factor for cardiovascular disease [1,8,50] and its singular elevation by chronic PI treatment further support our hypothesis: lipid changes occur at the gene level through key lipogenic mediators and contribute to the pre-atherogenic profile as well as MetS commonly seen in PI-treated HIV-positive patients. It is therefore imperative that the key mediators of such pathways be investigated and the underlying molecular mechanisms elucidated.

Conclusions

Together this study shows that early changes induced by PI treatment resemble a pre-atherogenic state, a combination of risk factors that predispose to the future onset of IR, T2DM and CVD. Moreover, the higher serum LDL-cholesterol levels mirror the pre-atherogenic state that may eventually elicit the onset of various cardiac complications, e.g. acute MI. Altered metabolic pathways and mitochondrial regulation emerge as strong candidates that may play a role in this instance.

References

1. Riddle, T. M., Kuhel, D. G., Woollett, L. A., Fichtenbaum, C. J. & Hui, D. Y. HIV protease inhibitor induces fatty acid and sterol biosynthesis in liver and adipose tissues due to the accumulation of activated sterol regulatory element-binding proteins in the nucleus. *J Biol Chem* **276**, 37514–37519 (2001).

2. Hui, D. Y. Effects of HIV protease inhibitor therapy on lipid metabolism. *Prog Lipid Res* **42**, 81–92 (2003).

3. Carr, A. *et al.* Diagnosis, prediction, and natural course of HIV-1 protease-inhibitor-associated lipodystrophy, hyperlipidaemia, and diabetes mellitus: a cohort study. *Lancet* **353**, 2093–2099 (1999).

4. Grinspoon, S. K. *et al.* State of the science conference: Initiative to decrease cardiovascular risk and increase quality of care for patients living with HIV/AIDS: executive summary. *Circulation* **118**, 198–210 (2008).

5. Rudich, A., Ben-Romano, R., Etzion, S. & Bashan, N. Cellular mechanisms of insulin resistance, lipodystrophy and atherosclerosis induced by HIV protease inhibitors. *Acta Physiol Scand* **183**, 75–88 (2005).

6. Gan, S. *et al.* Altered myocellular and abdominal fat partitioning predict disturbance in insulin action in HIV protease inhibitor-related Lipodystrophy. *Diabetes* **51**, 3163–3169 (2002).

7. Walmsley, S. *et al.* Ritonavir versus nelfinavir for the initial treatment of HIV infection. *N Engl J Med* **346**, 2039–2046 (2002).

8. Grundy, S. M., Brewer, H. B., Cleeman, J. I., Smith, S. C. & Lenfant, C. Definition of metabolic syndrome: Report of the National Heart, Lung, and Blood Institute/American Heart Association conference on scientific issues related to definition. *Circulation* **109**, 433–8 (2004).

9. Behrens, G. *et al.* Impaired glucose tolerance, beta cell function and lipid metabolism in HIV patients under treatment with protease inhibitors. *AIDS* **13**, F63–F70 (1999).

10. Bastard, J. *et al.* Association between altered expression of adipogenic factor SREBP1 in lipoatrophic adipose tissue from HIV-1-infected patients and abnormal adipocyte differentiation and insulin resistance. *Lancet* **359**, 1026–1031 (2002).

11. Carr, A. *et al.* HIV protease inhibitor substitution in patients with lipodystrophy: a randomized, controlled, open-label, multicentre study. *AIDS* **15**, 1811–1822 (2001).

12. Dong, K. *et al.* Changes in body habitus and serum lipid abnormalities in HIV-positive women on highly active antiretroviral therapy (HAART). *J AIDS* **21**, 107–13 (1999).

13. Tsiodras, S., Mantzoros, C., Hammer, S. & Samore, M. Effects of protease inhibitors on hyperglycemia, hyperlipidemia, and lipodystrophy: a 5-year cohort study. *Arch Intern Med* **160**, 2050–6 (2000).

14. Floris-Moore, M. *et al.* Increased serum lipids are associated with higher CD4 lymphocyte count in HIV-infected women. *HIV Med* **7**, 421–30 (2006).

15. Hertel, J., Struthers, H., Horj, C. & Hruw, P. A structural basis for the acute effects of HIV protease inhibitors on GLUT4 intrinsic activity. *J Biol Chem* **279**, 55147–52 (2004).

16. Liang, J.-S. *et al.* HIV protease inhibitors protect apolipoprotein B from degradation by the proteasome: A potential mechanism for protease inhibitor-induced hyperlipidemia. *Nat Med* **7**, 1327–1331 (2001).

17. Parker, R. A. *et al.* Endoplasmic Reticulum Stress Links Dyslipidemia to Inhibition of Proteasome Activity and Glucose Transport by HIV Protease Inhibitors. *Mol Pharmacol* **67**, 1909–1919 (2005).

18. Murata, H., Hruz, P. W. & Mueckler, M. Indinavir inhibits the glucose transporter isoform Glut4 at physiologic concentrations. *AIDS* **16**, 859–63 (2002).

19. Hruz, P. W., Yan, Q., Struthers, H. & Jay, P. Y. HIV protease inhibitors that block GLUT4 precipitate acute, decompensated heart failure in a mouse model of dilated cardiomyopathy. *FASEB J* **22**, 2161–7 (2008).

20. Hruz, P. HIV protease inhibitors and insulin resistance: lessons from in vitro, rodent and healthy human volunteer models. *Diabetes* **3**, 660–665 (2009).

21. Germinario, R. J., Colby-Germinario, S. P., Cammalleri, C. & Wainberg, M. A. The long-term effects of anti-retroviral protease inhibitors on sugar transport in L6 cells. *J Endocrinol* **178**, 449–56 (2003).

22. Mulligan, K. *et al.* Hyperlipidemimia and insulin resistance are induced by protease inhibitors independent of changes in body composition in patients with HIV infection. *J AIDS* **23**, 35–43 (2000).

23. Carr, A., Samaras, K., Chisholm, D. J. & Cooper, D. A. Pathogenesis of HIV-1-protease inhibitor-associated peripheral lipodystrophy, hyperlipidaemia, and insulin resistance. *Lancet* **351**, 1881–1883 (1998).

24. Carr, A. *et al.* Effects of boosted tipranavir and lopinavir on body composition, insulin sensitivity and adipocytokines in antiretroviral-naive adults. *AIDS* **22**, 2313–2321 (2008).

25. Gazzaruso, C. *et al.* Hypertension among HIV patients: prevalence and relationships to insulin resistance and metabolic syndrome. *J Hypert* **21**, 1377–82 (2003).

26. Biron, A. *et al.* Metabolic syndrome in French HIV-infected patients : prevalence and predictive factors after 3 years of antiretroviral therapy. *AIDS Res Hum Retroviruses* **28**, 1672-8 (2012).

27. Bernal, E. *et al.* Hypertriglyceridemic waist phenotype is a risk factor fo subclinical atherosclerosis in human immunodeficiency virus-infected patients. *Med Clin* **139**, 561–565 (2012).

28. Behrens, G. M. N. *et al.* Impaired glucose phosphorylation and transport in skeletal muscle cause insulin resistance in HIV-1 – infected patients with lipodystrophy. *J Clin Invest* **110**, 1319–1327 (2002).

29. Woerle, H. *et al.* Mechanisms for the deterioration in glucose tolerance associated with HIV protease inhibitor regimens. *Diabetes* **52**, 918–925 (2003).

30. Cacho, J., Sevillano, J., De Castro, J., Herrera, E. & Ramos, M. P. Validation of simple indexes to assess insulin sensitivity during pregnancy in Wistar and Sprague-Dawley rats. *Am J Physiol Endocrinol Metab* **295**, E1269–E1276 (2008).

31. Lagathu, C. *et al.* Some HIV antiretrovirals increase oxidative stress and alter chemokine, cytokine or adiponectin prodcution in human adipocytes and macrophages. *Antiviral Therapy* **12**, 489–500 (2007).

32. Pacenti, M. *et al.* Microarray analysis during adipogenesis identifies new genes altered by antiretroviral drugs. *AIDS* **20**, 1691–705 (2006).

33. Sáinz, N. *et al.* Leptin administration downregulates the increased expression levels of genes related to oxidative stress and inflammation in the skeletal muscle of ob/ob mice. *Med Inflamm* **2010**, 784343 (2010).

34. Vyas, A. K., Koster, J. C., Tzekov, A. & Hruz, P. W. Effects of the HIV protease inhibitor ritonavir on GLUT4 knock-out mice. *J Biol Chem* **285**, 36395–36400 (2010).

35. Bastard, J. *et al.* Association between altered expression of adipogenic factor SREBP1 in lipoatrophic adipose tissue from HIV-1-infected patients and abnormal adipocyte differentiation and insulin resistance. *Lancet* **359**, 1026–1031 (2002).

36. Carr, A. *et al.* A syndrome of peripheral lipodystrophy, hyperlipidaemia and insulin resistance in patients receiving HIV protease inhibitors. *AIDS* **12**, F51–F58 (1998).

37. Lagathu, C. *et al.* HIV antiretroviral treatment alters adipokine expression and insulin sensitivity of adipose tissue in vitro and in vivo. *Biochimie* **87**, 65–71 (2005).

38. Wilson, C. R., Tran, M. K., Salazar, K. L., Young, M. E. & Taegtmeyer, H. Western diet, but not high fat diet, causes derangements of fatty acid metabolism and contractile dysfunction in the heart of Wistar rats. *Biochem J* **406**, 457–67 (2007).

39. Noor, M. A., Flint, O. P., Maa, J.-F. & Parker, R. A. Effects of atazanavir/ritonavir and lopinavir/ritonavir on glucose uptake and insulin sensitivity: demonstrable differences in vitro and clinically. *AIDS* **20**, 1813–21 (2006).

40. Magaña, M. M., Lin, S., Dooley, K. & Osborne, T. F. Sterol regulation of acetyl coenzyme A carboxylase promoter requires two interdependent binding sites for sterol regulatory element binding proteins. *J Lipid Res* **38**, 1630–8 (1997).

41. Magaña, M. M. & Osborne, T. F. Two tandem binding sites for sterol regulatory element binding proteins are required for sterol regulation of fatty-acid synthase promoter. *J Biol Chem* **271**, 32689–94 (1996).

42. Lagor, W. R., Heller, R., Groh, E. D. De & Ness, G. C. Functional analysis of the hepatic HMG-CoA reductase pomoter by in vivo electroporation. *Exp Biol Med* **232**, 353–361 (2007).

43. Osborne, T. F., Gil, G., Goldstein, J. & Brown, M. Operator constitutive mutation of 3-hydroxy-3-methylglutaryl coenzyme A reductase promoter abolishes protein binding to sterol regulatory element. *J Biol Chem* **263**, 3380–3387 (1988).

44. Osborne, T. F. Single nucleotide resolution of sterol regulatory region in promoter for 3-hydroxy-3-methylglutaryl coenzyme A reductase. *J Biol Chem* **266**, 13947–13951 (1991).

45. Sudhof, T., Russell, D., Brown, M. & Goldstein, J. 42 bp element from LDL receptor gene confers end-product repression by sterols when inserted into viral TK promoter. *Cell* **48**, 1061–1069 (1987).

46. Smith, J., Osborne, T., Brown, M., Goldstein, J. & Gil, G. Multiple sterol regulatory elements in promoter for hamster 3-hydroxy-3-methylglutaryl-coenzyme A synthase. *J Biol Chem* **263**, 18480–18487 (1988).

47. Schmidtke, G. *et al.* How an inhibitor of the HIV-I protease modulates proteasome activity. *J Biol Chem* **274**, 35734–35740 (1999).

48. Hirano, Y., Yoshida, M., Shimizu, M. & Sato, R. Direct demonstration of rapid degradation of nuclear sterol regulatory element-binding proteins by the ubiquitin-proteasome pathway. *J Biol Chem* **276**, 36431–36437 (2001).

49. Mulligan, K. *et al.* Hyperlipidemimia and insulin resistance are induced by protease inhibitors independent of changes in body composition in patients with HIV infection. *J AIDS* **23**, 35–43 (2000).

50. Piconi, S. *et al.* Atherosclerosis is associated with multiple pathogenic mechanisms in HIV-infected antiretroviral-naïve or -treated individuals. *AIDS* **27**, 381–9 (2013).

Chapter 3

The effect of PIs on rat heart function

Introduction

HIV infection is characterized by a compromised immune system and subsequent chronic, life-long inflammation and the development of AIDS. Cardiac abnormalities were noted as early as 1989 [1,2] in the pre-HAART and included dilated cardiomyopathy, endo-, myo- and peri-carditis and pulmonary hypertension [1–4]. Prevalence during this time period was between 28 - 73% [1,3,5]. Importantly, HIV is able to directly infect cardiac tissue [6], though this may be attributed to the stage of HIV/AIDS but nonetheless compounds the future health outcomes and survival of an HIV-infected individual.

In the era of HAART it is important to understand the relative contributions of ARVs and HIV infection to the onset of CVD and related manifestations, especially since HIV infection is a potential risk factor for CVD. In addition, HAART-associated cardiac complications are proposed to form distinct entities in terms of the development of CVD [7,8]. Thus the focus has now shifted from the opportunistic infections due to HIV and AIDS, to HAART-associated metabolic and cardiovascular complications. This is particularly relevant in the context of extended lifespans.

HIV PIs in particular, are strongly implicated in the onset of cardiovascular complications, with increased risk for MI and coronary syndromes. For example, in one of the largest clinical studies assessing the risk for myocardial infarction with HAART - the Data Collection for Adverse events of Anti-HIV drugs (DAD) Study Group recruited 23 468 HIV-positive patients on ART [9–11] - cumulative exposure to HAART saw a significant increase in the incidence of MI (26% relative change) with the most significant risk for MI due to PIs. Though the absolute risk for MI was low when adjusted for

confounding factors, cholesterol, lipid abnormalities and diabetes were highlighted as HAART and PIs exacerbate these traditional CVD risk factors. Similar results have been found in other large cohort studies [12,13] and PIs are significantly associated with the occurrence of MI [9,10,12–15]. Further, longer-term exposure to HAART regimens (including PIs) can increase mortality [11,16,17] and hospitalization for cardiovascular complications [18]. Echocardiographic abnormalities have also been associated with the use of the PI, Ritonavir [19], i.e. 656 HIV-infected cohort baseline echocardiography revealed significant rates of left ventricular systolic dysfunction, diastolic dysfunction, pulmonary hypertension and left atrial enlargement. Though some studies do not support a link between PIs and atherosclerosis [15,20] due to minimal differences between PIs and other ARVs in HAART, many other studies do report a clear connection with development of subclinical atherosclerotic lesions [21–24] and thrombotic environments [25,26]. Thus it is not only the overt presentation of cardiac maladies, but also the subclinical progression that impacts on the development of future cardiac disease risk.

In light of this there has been increased emphasis on delineating the underlying mechanisms driving HIV/HAART-mediated cardiovascular complications and thus oxidative stress is known to be an important factor within the context of cardiovascular pathology. For example, it is especially relevant during chronically activated immune activation with HIV infection. Moreover, under such conditions, ECC can become disrupted and have negative consequences in terms of cardiac myofiber physiology. For example, the RyR [27–30], SERCA [31–36] and NCX [37–39] channels are sensitive to oxidation that may result in altered functional effects, i.e. pathologically opened or closed. Calcium overload may then arise and this can lead to disastrous downstream effects, especially at the mitochondrial and

contractile level; namely, a further exacerbation of ionic imbalance and toxicity, and perturbed redox status of the myocardium. Here, excess ROS within the myocardium can inhibit calcium-ATP-hydrolysis coupling [31] since cardiac calcium homeostasis is highly sensitive to oxidative stress [40–42]. High intracellular calcium levels can also induce hyperactivation of electrical system leading to impaired cardiac contractile function. However, despite such progress not much is known regarding mechanisms driving contractile dysfunction with HIV/HAART. Moreover, it is often difficult to tease out the relative contributions of HIV and HAART, respectively, in this instance.

In light of this, we investigated *ex vivo* and *in vivo* heart function in a healthy rodent chronically treated with PIs, since as far as we are aware, this has not been performed previously. The aims were to characterize heart function of rats treated with HIV PIs for 8 weeks and to further elucidate the early molecular mechanisms underlying these processes. Here we made use of the Langendorff retrograde heart perfusion model (*ex vivo*) to study heart function for 60 min with an addition ischemia-reperfusion period. Further, the effect of a HF diet (refer to **Chapter 2**) co-administered with PIs was assessed to determine if any cumulative effect of treatment would occur. In addition, an *in vivo* model of ECG monitoring was also utilized. These data should provide significant insight regarding how these detrimental side effects can occur with PI usage.

Materials & Methods

Animal model

The use of animals and procedures were reviewed and approved by the Animal Research Ethics Committee of the Faculty of Natural Sciences of Stellenbosch University as discussed in **Chapter 2** (application numbers 2006B02006, 11NF_REY01, SU_ACUM11_00006, 012/005 AEC 012/005 and related amendments).

Drug administration

Lopinavir/Ritonavir (Kaletra™, Abbott Laboratories, Abbot Park IL) was crushed and dissolved in a 1% ethanol (vehicle) solution at human steady-state plasma concentration (7.1 ± 2.9 µg/mL), sterile filtered and injected into a mini-osmotic pump (Alzet, Cupertino CA) as previously described (**Chapter 2**).

A. *Ex vivo* Working Heart Perfusions

Working heart perfusion method

As previously described (**Chapter 2**) rats were administered PIs and a HF diet for 8 weeks, with 8 animals per experimental group. Assessment of heart function and recovery after an ischemic attack was investigated using the working heart perfusion technique [43]. Rats were euthanized with a single injection of pentobarbitone sodium (100 mg/kg) and hearts rapidly excised and placed in ice-cold Krebs-Henseleit buffer (in mmol/L: NaCl 118.0, KCl 4.7, $MgSO_4 7H_2O$ 1.2, $CaCl_2$ 1.25, $NaHCO_3$ 25.0, KH_2PO_4 1.2, and glucose 11). Hearts were cannulated to the perfusion apparatus within 50 sec and retrograde perfusion initiated with Krebs-Henseleit buffer at 37.0 ± 0.5^{o}C with a pressure of 80 cm H_2O, while the pulmonary vein was cannulated as well. Perfusion in the retrograde mode stabilized the heart for 20 min. The perfusion rig was set up as illustrated in **Fig. 1**. To evaluate baseline function, hearts were then perfused in the working mode with 15 cm H_2O preload and 80 cm H_2O afterload pressure for 50 min with a palmitate-containing Krebs-Henseleit buffer (**Fig. 2**). Palmitate (0.4 mM) was conjugated to bovine serum albumin (BSA) (BSA Fraction V, Roche Diagnostics, IN USA) and prepared as described previously [43]. The BSA contributed 0.3 mM FA towards the FA concentration, i.e. 0.7 mM total.

Functional recovery was assessed by inducing global ischemia for 10 min in the working mode after stabilization for 35 min (**Fig. 2**), with the heart submerged in buffer at 37.0 ± 0.5^{o}C to ensure correct simulation of the *in vivo* environment. Thereafter the buffer was drained and retrograde flow to the heart was once again initiated for 15 min with original Krebs buffer, followed by the working

mode for 20 min (with palmitate-containing Krebs buffer). Measurements of heart function and recovery (coronary and aortic flow, heart rate, aortic diastolic and systolic pressure, mean arterial pressure [MAP] and rate-pressure-product [RPP] [RPP = left ventricular developed pressure [LVDP] x heart rate]) were recorded throughout the perfusions and analyzed by employing ADInstuments™ LabChart Pro v.7 software (ADInstruments, NSW, Australia). At the end of the protocol hearts were quickly removed from the cannula and weighed and immediately snap frozen in liquid nitrogen and stored at -80°C. All perfusion buffers were maintained at a constant temperature of 37.0 ± 0.5°C via a water-jacketed apparatus.

Statistical analyses.

Two-way ANOVA was utilized for all experiments with a Bonferroni *post-hoc* test to compare variation between all the groups. Statistical significance was considered when $p<0.05$.

Only the mean + SEM is graphically represented for easy visualization, but the data have been analyzed as mean ± SEM.

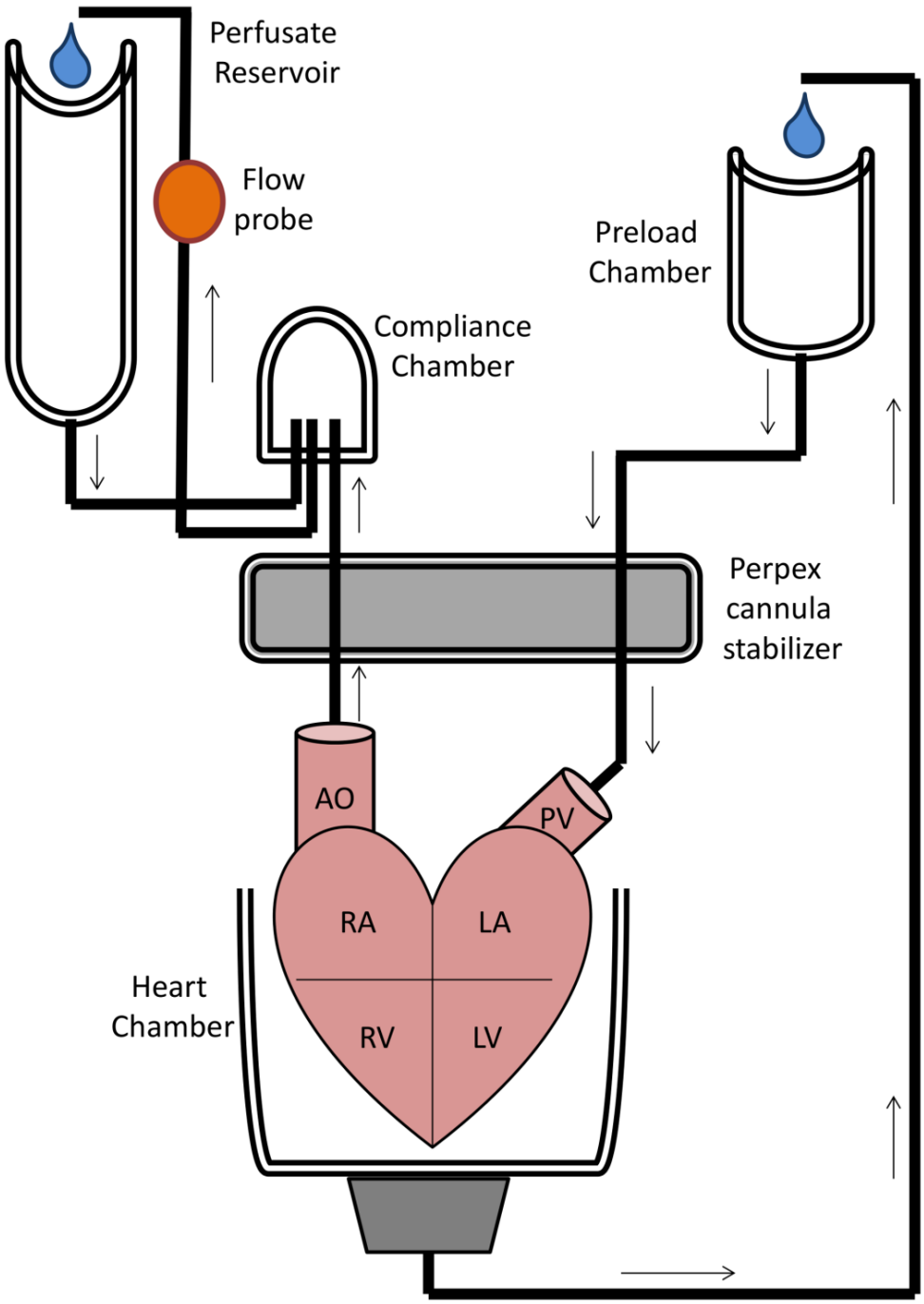

Figure 1. Working heart perfusion rig set-up. The heart is cannulated via the pulmonary vein (PV) and Krebs-Henseleit buffer flows through the left atrium (LA) into the left ventricle (LV) to create preload conditions. Perfusate is then pumped back through the right atrium (RA) and into the compliance chamber, where the overflow (aortic output) are measured via a flow probe. This mimics the *in vivo* pressure conditions and creates an aortic pressure that can be measured via a flow probe to indicate aortic flow rate amongst other measures of working heart function. Arrows indicate direction of flow of perfusate during working mode. *AO – aortic outlet, RV – right ventricle.*

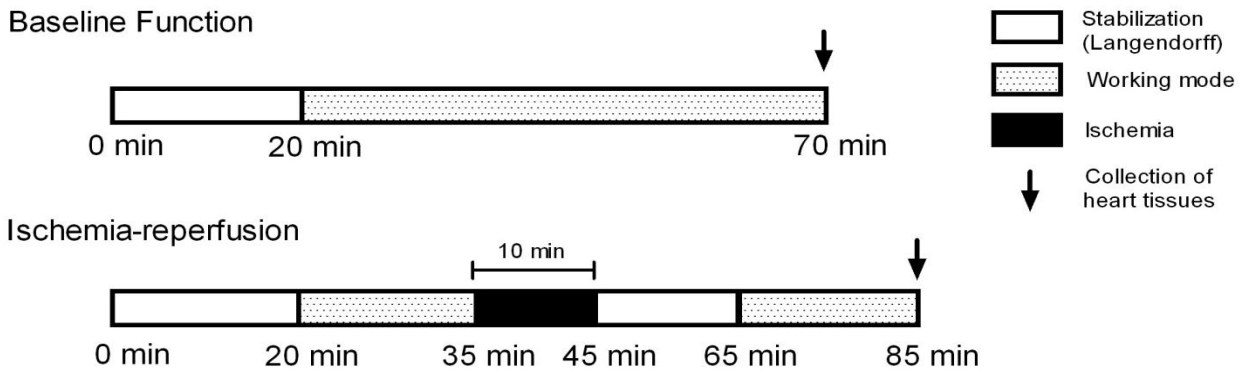

Figure 2. **Baseline function and ischemia-reperfusion protocol for working heart perfusions.** Hearts were perfused according to the above protocol with specified durations of stabilization, working heart perfusion, ischemia as well as reperfusion.

Results

To assess the effects of PI therapy as well as dietary intervention, heart functional analyses were performed using the working heart perfusion method. With the cannulation of the pulmonary vein, *ex vivo* pre- and after-load conditions were mimicked. During the stabilization phase, baseline MAP was not significantly different between any of the groups ($p>0.05$) (**Fig. 3A**), however, upon induction of the working mode it became apparent that the experimental set up might not be correct. MAP was non-existent for the vehicle group and declined significantly for all other treatment groups (PI – 31.7 ± 0.0 mmHg, HF – 27.9 ± 11.8 mmHg) to below the accepted cut-off for working heart perfusions. Heart rate during the stabilization period for both PI and HF groups were slightly below the range for Wistar rats (169-204 beats/minute) and did not alter significantly during the working phase (**Fig. 3B**). Coronary flow, however, proved the failed experiment further (**Fig. 3C**) as working heart perfusion flow rates were between 3.0-3.7 mL/min, well below the range expected during this type of perfusion. These alterations, or lack thereof where found in all treatment groups, and some groups refused to perform and had zero values. Further assessments such as RPP confirmed this (**Fig. 4**). In a separate but similar experiment excluding the sham and HF diet group (due to previous data), ischemia-reperfusion showed similar results. MAP, heart rate, coronary flow and RPP (**Fig. 5**) all significantly decreased below the accepted range and indicated that the hearts were not producing enough pressure and not functioning correctly.

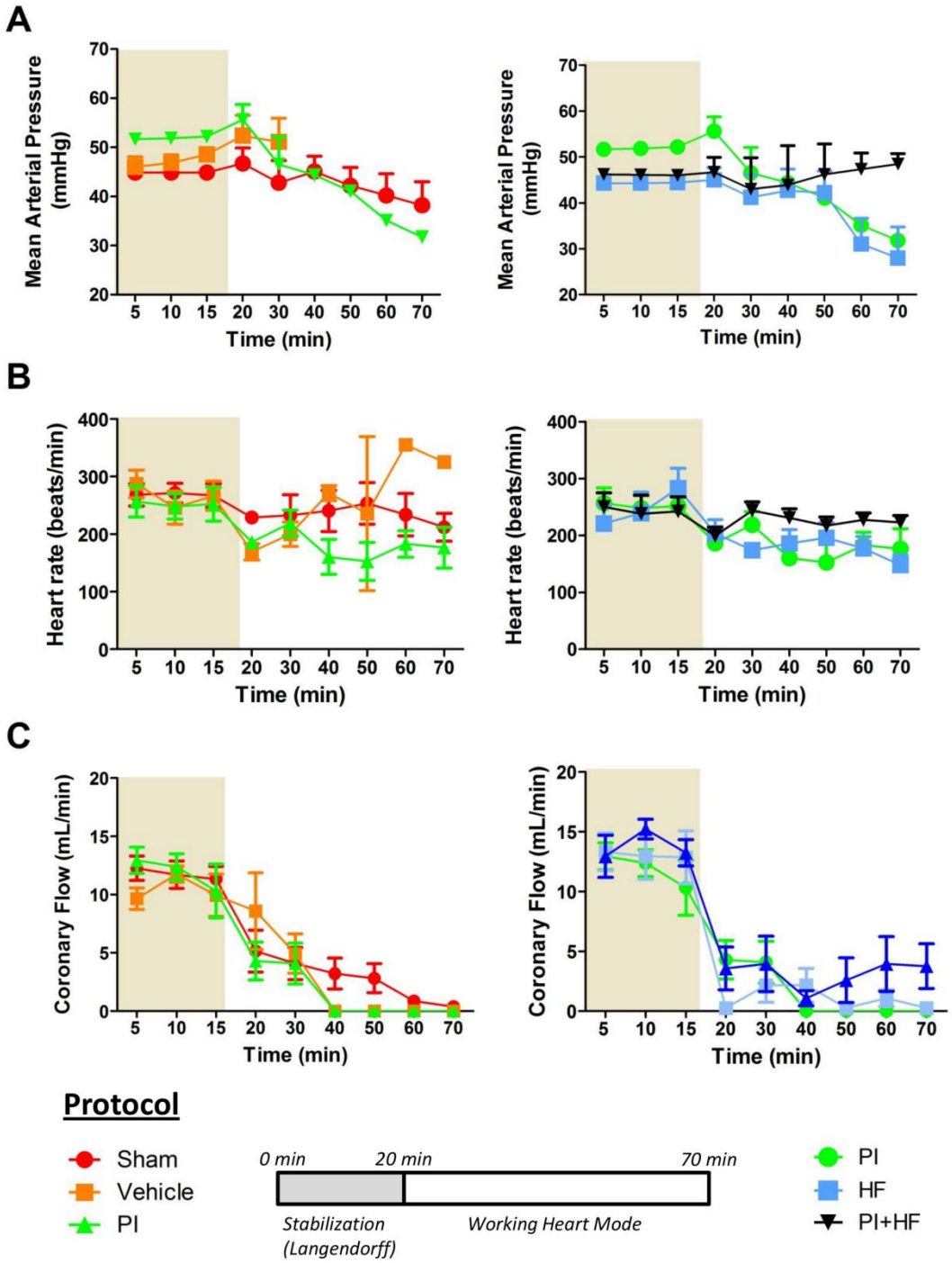

Figure 3. Baseline working heart function in response to PI and high fat treatment (n=8). Perfusion protocol indicated on graph. A) Mean arterial pressure; B) Heart rate; and C) Coronary flow separated per treatment group (PI treatment ± HF diet). Data presented as mean ± SEM. *HF – high fat, PI – protease inhibitor.*

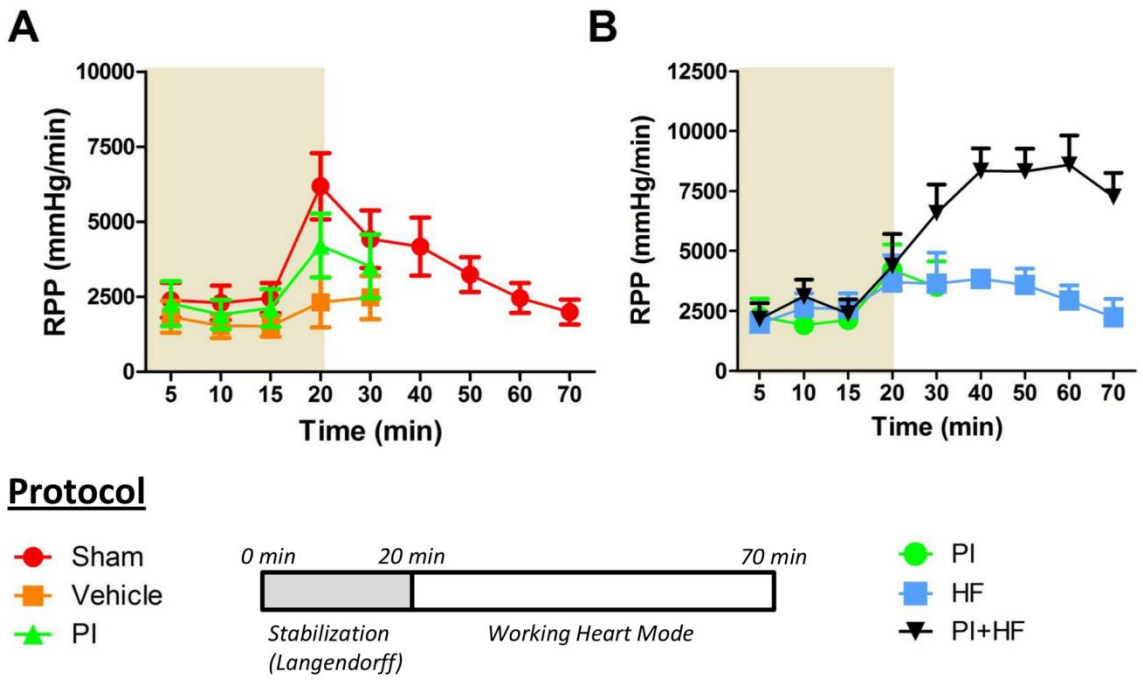

Figure 4. Rate-pressure product at baseline in response to PI treatment ± high fat diet (n=8). Perfusion protocol indicated on graph. A) RPP for PI treatment; and B) RPP for HF dietary intervention. Data presented as mean ± SEM. *HF – high fat, PI – protease inhibitor, RPP – rate-pressure product*.

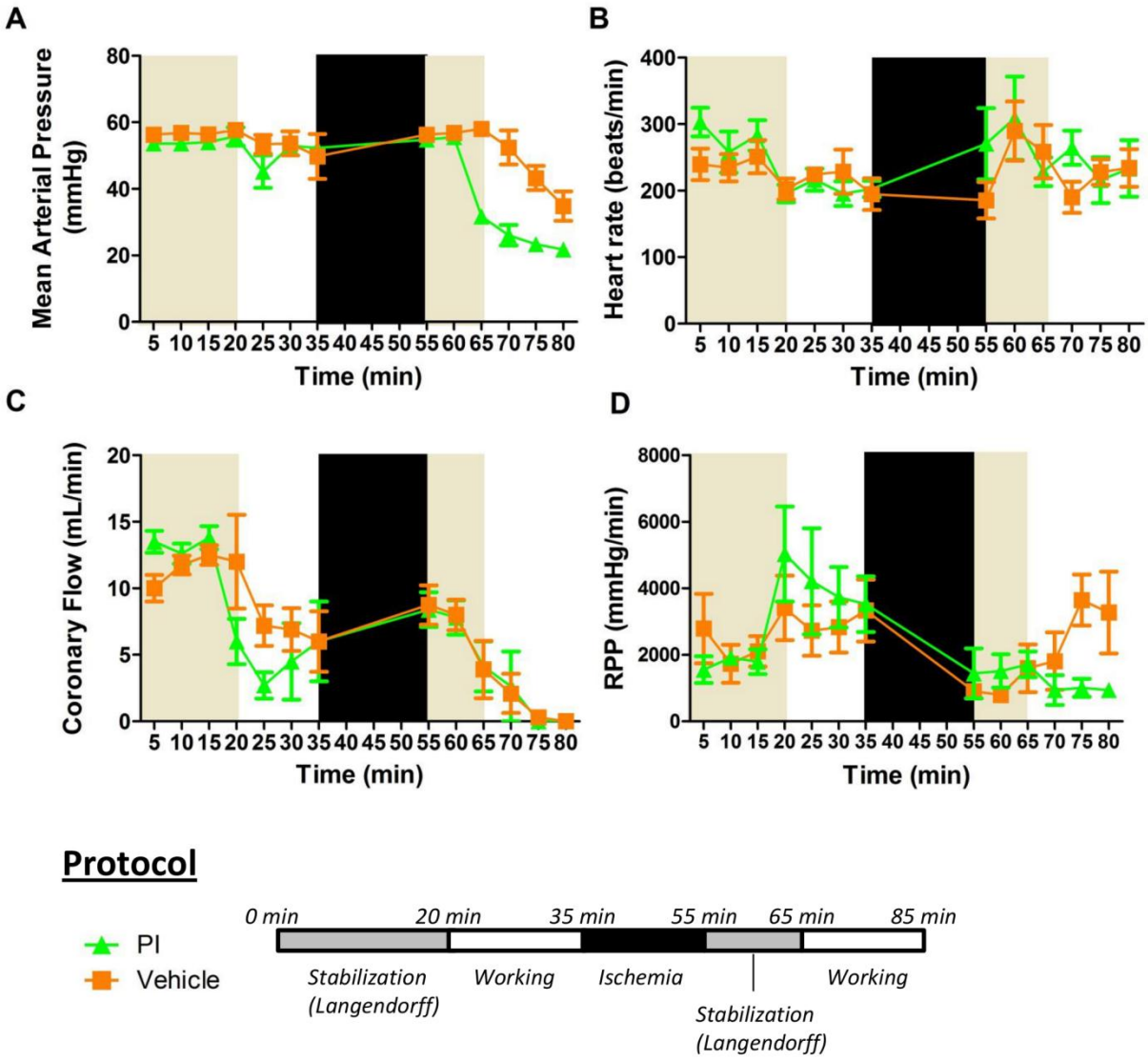

Figure 5. Heart function in response to ischemia-reperfusion with PI treatment (n=8). Perfusion protocol indicated on graph. A) Mean arterial pressure; B) Heart rate; C) Coronary flow; and D) RPP. Data presented as mean ± SEM. *RPP – rate-pressure product, PI – protease inhibitor*.

Discussion

Due to experimental complications, it was apparent that the working heart perfusion technique was not suited to assessing heart function with PI treatment and a HF diet. This was noted in all parameters during baseline and ischemia-reperfusion experiments. Although the stabilization phase appeared normal, the hearts failed to perform when put in the working mode.

Importantly, this technique was first discovered as a means to measure oxygen consumption and energy metabolism within an *ex vivo* setting. In 1967 Neely and colleagues [44] proposed a novel technique to investigate pressure development on oxygen consumption in an isolated rat heart, and this was further modified and improved upon by Taegtmeyer *et al.* (1980) [45]. Many other studies have since made use of this technique with success [46–48].

The technique is, however, not fool-proof and comes with a myriad of parameters that can and must be controlled correctly to ensure a working perfusion. Apart from mimicking *in vivo* pressure conditions by setting the preload on the heart to 11-15 cm H_2O and afterload at 80-100 cm H_2O, oxygenation of the buffer, flow rate, substrates present in the perfusate buffer and set-up of the compliance chamber all play a very big role in the success of the experiment [43]. In this experiment we made use of the conventional 15 cm preload and 80 cm afterload with 1 cm^3 airspace within the compliance chamber. This set of parameters was chosen with the advice of colleagues experienced in the technique. Further, Lopaschuk *et al.* (1997) [43] mention that the volume of air within the compliance chamber is traditionally suited to rats weighing 250-300 g. However, others [49] have

successfully employed it in rats weighing >500 g, which is more within the current study's body weight range and would therefore have been expected to be successful.

The use of FAs within the perfusate buffer was also carefully considered as the heart requires both carbohydrates and fats as energy sources, though relies on FAs *in vivo* for the majority of its energy requirements and carbohydrates during fetal development [50]. Further studies have made use of additional substrates such as oleate, insulin and pharmacological substances to manipulate experimental conditions depending on the hypothesis [46–48]. One could argue that our perfusate buffer did not contain insulin to mediate glucose uptake, but many research groups have/have not always included additional substrates and since 1965 it has remained controversial as to the provision and type of substrates (articles and reviews [51–60]).

The fact that the coronary flow and subsequently aortic output was zero indicates a more fundamental problem with the system's set-up, as aortic output is expected to be between 30-40 mL/min. It could very well be that the hearts were incorrectly cannulated at the pulmonary vein, leading towards incorrect pressure development and contractile dysfunction. This remains a possibility even though the investigator was thoroughly trained in performing the technique and had great success during practice runs.

Since our data yielded very promising results in terms of phenotypic characterization and insights into the molecular mechanisms of PIs (**Chapter 2**), an alternative but similar method was chosen: Langendorff retrograde heart perfusion. The Langendorff technique is relatively easy to master, requires minimal financial investment, and can render high-quality data within a relatively short period. We therefore pursued this type of analysis since no-one (as far as we are aware) has previously investigated *ex vivo* heart function in response to HIV PIs.

Conclusion

Although the experiment with the working heart perfusion technique was unsuccessful, it provided valuable practical experience for the investigator. Since our animal model has thus far provided valuable insights regarding the phenotypic and molecular changes induced by PI therapy, we next decided to use the Langendorff retrograde perfusion method to evaluate heart function parameters.

B. Ex vivo Langendorff Perfusions

Ex vivo Langendorff heart perfusion method

Due to financial constraints, rats did not receive any special dietary interventions for this set of experiments, and were thus placed on the traditional in-house animal diet. A pilot study assessing functional differences between the commercially obtained control diet and the traditional in-house animal house diet revealed no significant differences, indicating that it was appropriate to continue with the in-house diet. We analyzed 3 treatment groups: sham, vehicle- and PI-treated. Identical protocols as indicated in the beginning of this chapter were used in terms of housing and intervention duration.

Heart Function. At the end of the 8-week treatment period rats were anesthetized and hearts removed as previously described for *ex vivo* working heart perfusions with similar Krebs-Henseleit perfusate buffer (no FAs) and cannulated on a Langendorff perfusion rig (**Fig. 6**). We could not include FAs for the experiment due to cost of the BSA required for conjugation. To assess baseline function, hearts were retrogradely perfused [48] – 60 min perfusion period – via a water-filled latex balloon inserted into the left ventricle and diastolic pressure set between 5-15 mmHg. Hearts that did not produce a systolic pressure ≥ 70 mmHg and/or did not produce a coronary flow rate of 8-16 mL/min were excluded from analyses.

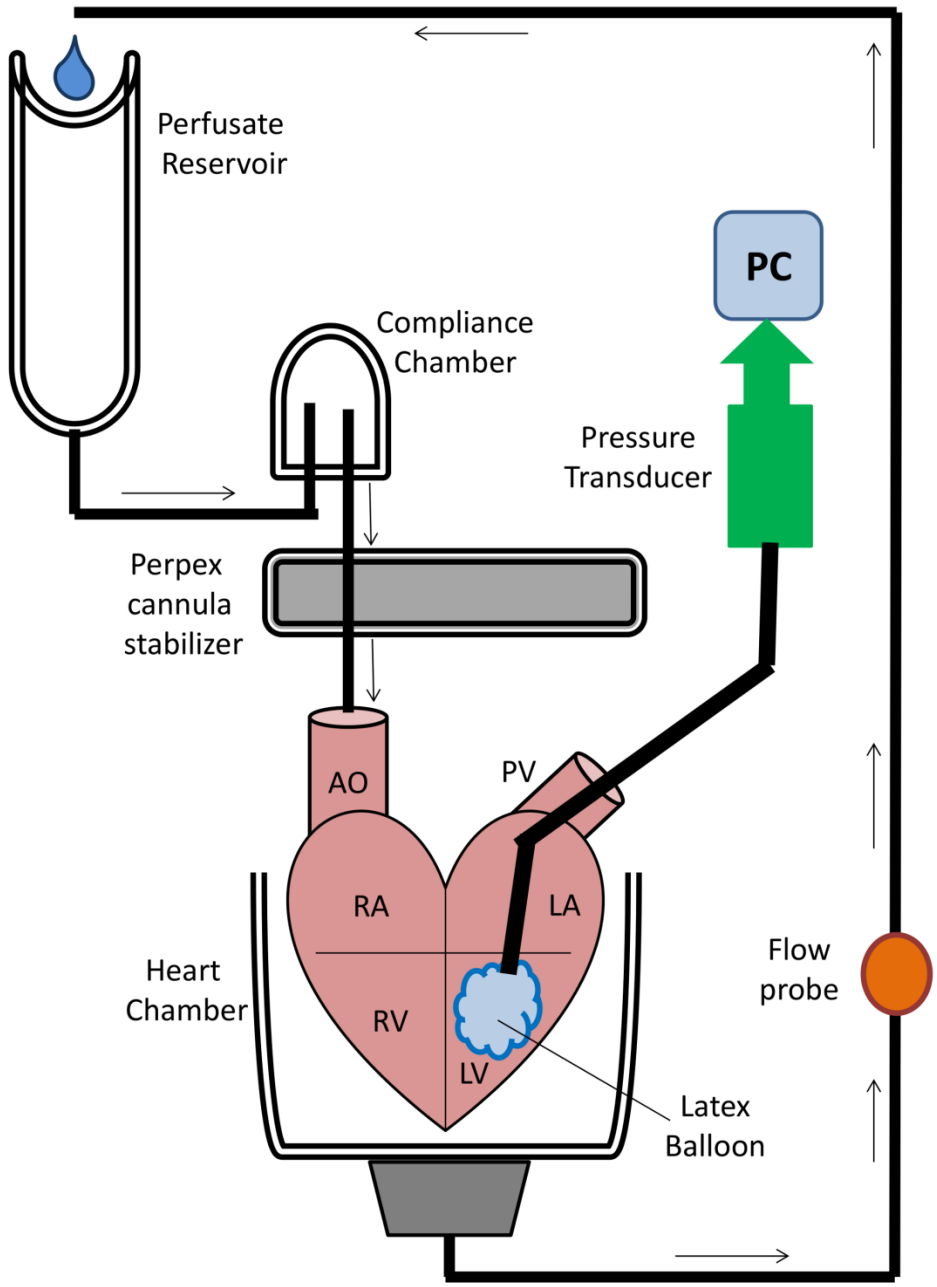

Figure 6. Retrograde Langendorff perfusion rig set-up. The heart is cannulated via the aortic branch (at AO) and through the flow of perfusate buffer at the osteoclasts situated just above the aortic valves, spontaneous firing of the S-A node is stimulated and contraction of the myocardium ensues. Through insertion of a latex balloon via the pulmonary vein (PV) into the left ventricle (LV), ventricular pressure and related measurements can be made and recorded with appropriate software on a PC. The coronary flow rate is measure via the amount of overflow perfusate from the heart into the heart chamber and measured via a flow probe. *AO– aortic outlet, PC – personal computer, RA – right atrium, RV – right ventricle.*

For the ischemia-reperfusion experiments, the 60 min stabilization period was followed by 30 min of global ischemia and 60 min of reperfusion. The experimental protocol is depicted in **Fig. 7**. Contractile parameters were assessed via pressure transducer (Stratham MLT 0380/D, ADInstruments Inc., NSW, Australia) included heart rate, LVDP, and RPP. Ventricular tissues were collected at the end of each experiment, freeze-clamped and stored at -80°C for further molecular and biochemical analyses.

Infarct Size. In a parallel but separate experiment (since ventricular tissue had already been collected), infarct sizes in response to regional ischemia were determined as previously described [48]. Briefly, after 60 min stabilization a period of 30 min of regional ischemia (cannulation of left anterior descending coronary artery via silk suture) was followed by 2 hrs reperfusion period (**Fig. 7**). The extended reperfusion period ensured flushing out of components that might interfere with the staining procedure. Thereafter, the suture was re-tightened and 2.5% Evans Blue dye (in Krebs-Henseleit buffer) perfused through the hearts. Hearts were subsequently removed from the Langendorff apparatus, blotted dry, suspended within 50 mL plastic tubes (using suture) and frozen at -20°C for 3 days. Frozen hearts were sliced into 2 mm transverse sections and incubated with 1% 2,3,5-triphenyl tetrazolium chloride (TTC) in phosphate-buffered saline (PBS) for 20 min at 37°C to identify non-infarcted (stained) from infarcted (non-stained) tissues. Slices were then fixed in 10% formalin for 24 hrs at room temperature before being placed between glass plates for scanning (both sides). The infarct area (IA) and the area at risk (AAR) size were calculated using Image J software (v1.46p, National Institutes of Health, USA). Values of tissue slices were added together in order to obtain the total IA and AAR for each heart analyzed. Infarct sizes in the sham group exceeding 60% were excluded due to the fact that this would represent a technical error (on the part of the

researcher) and should not be present in a control environment. We expressed the infarct size as the ratio of IA versus the AAR (% IA/AAR) for each heart analyzed (n=4-6).

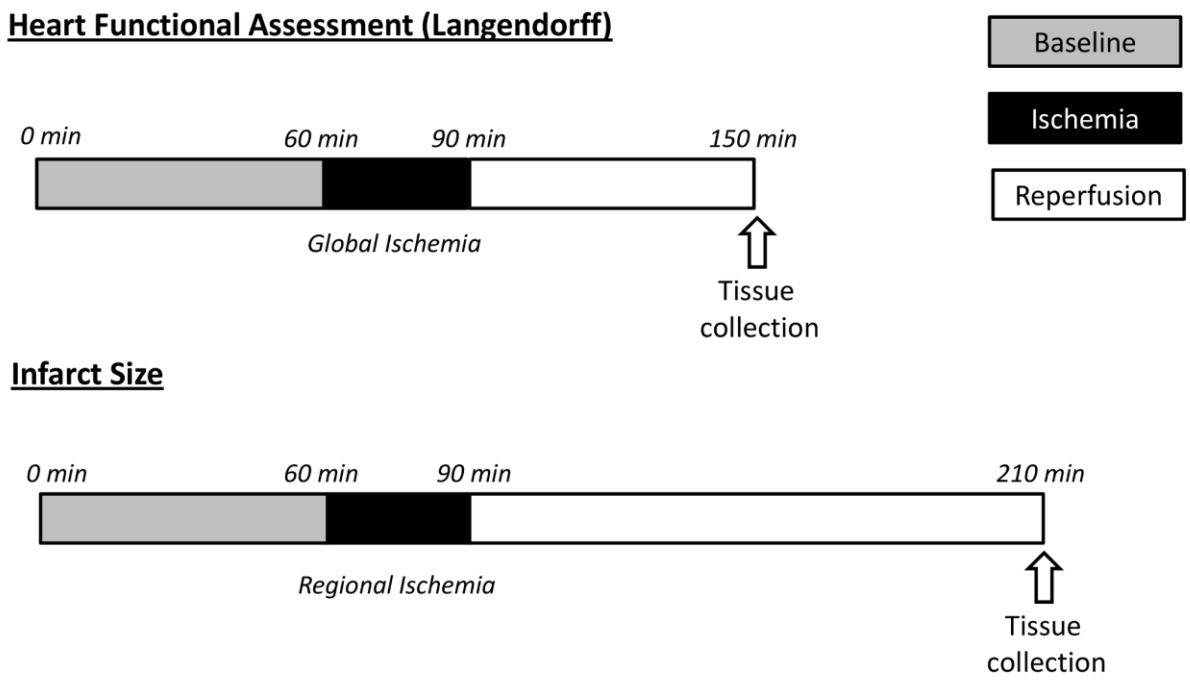

Figure 7. Langendorff retrograde perfusion protocol. Perfusion and ischemia durations are indicated for both heart functional assessment and infarct size analyses.

Statistical analyses

Two-way ANOVA was performed for all 3 groups for heart function, with a Bonferroni *post-hoc* test comparing all experimental groups to each other. One-way ANOVA was used to assess infarct size. Significance is indicted on graphs, and only the + SEM bar is represented for ease of visualization where necessary, though data was calculated as mean ± SEM. Significance is considered when $p<0.05$.

Results

Baseline heart function

Since PIs can negatively impact on heart function in HIV-positive patients, the aim of this study was to assess heart function in rats treated with PIs for 8 weeks. The heart weight to body weight ratio was calculated (as a marker of hypertrophy) and here experimental groups presented with similar ratios ($p>0.05$) (**Fig. 8**). This therefore indicates a lack of hypertrophic response at this early time point.

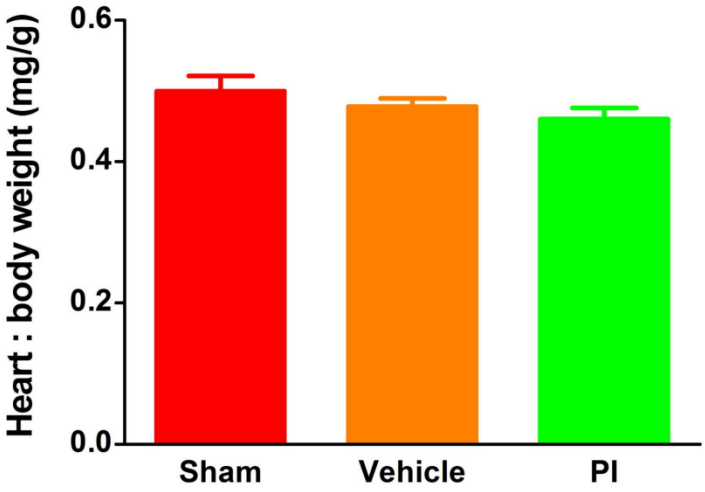

Figure 8. Heart-to-body weight ratio in response to 8 weeks PI treatment (n=8). After 8 weeks PI therapy heart weight was compared to body weight. Data presented as mean ± SEM. *PI – protease inhibitor.*

We next evaluated baseline heart function parameters. Both heart rate and coronary flow rate remained unaltered during the 60 min perfusion period in all experimental groups (p>0.05) (**Fig. 9**).

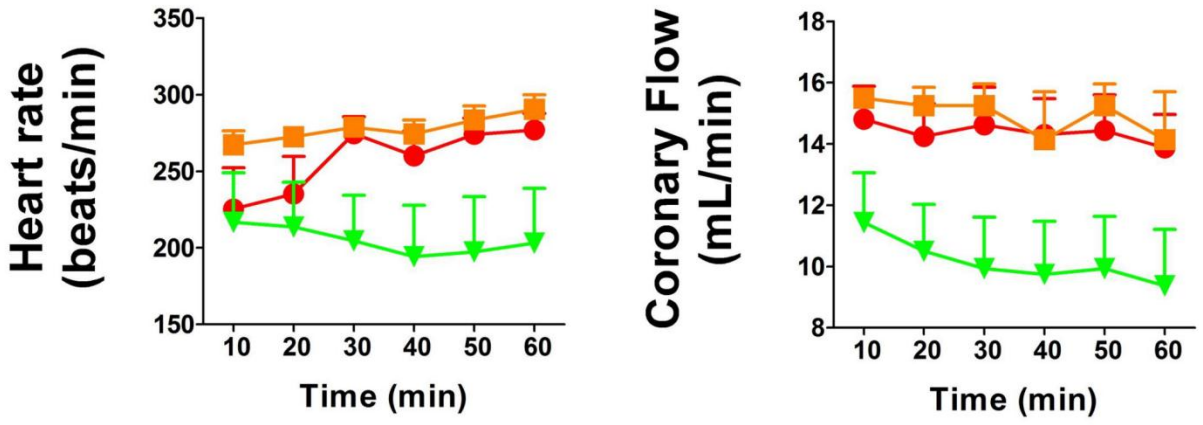

Figure 9. Baseline heart functional parameters for 8 weeks PI treatment (n=8). During *ex vivo* Langendorff perfusion heart rate and coronary flow of rats treated with PIs for a total of 8 weeks was measured. Data presented as mean ± SEM. *PI – protease inhibitor.*

Ex vivo perfusion data further revealed that PI treatment was detrimental to heart function (**Fig. 10**). PIs decreased LVDP to 35.50 ± 1.55 mmHg vs. 60.88 ± 2.4 mmHg (sham) ($p<0.01$) and vs. 53.14 ± 6.61 mmHg (vehicle) ($p<0.001$). Likewise, RPP was also attenuated in PI-treated hearts vs. matched controls. Further, maximal and minimal contractile force (±*dP/dt*) were significantly diminished at baseline throughout the baseline period (+*dP/dt* – PI 633.1 ± 57.7 vs. sham 1411.0 ± 126.9 mmHg/sec, $p<0.001$; vs. vehicle 1068.8 ± 70.9 mmHg/sec, $p<0.05$; - *dP/dt* – PI -338.4 ± 31.0 vs. sham -966.8 ± 71.9 mmHg/sec, $p<0.001$; vs. vehicle -782.1 ± 118.2 mmHg/sec, $p<0.01$).

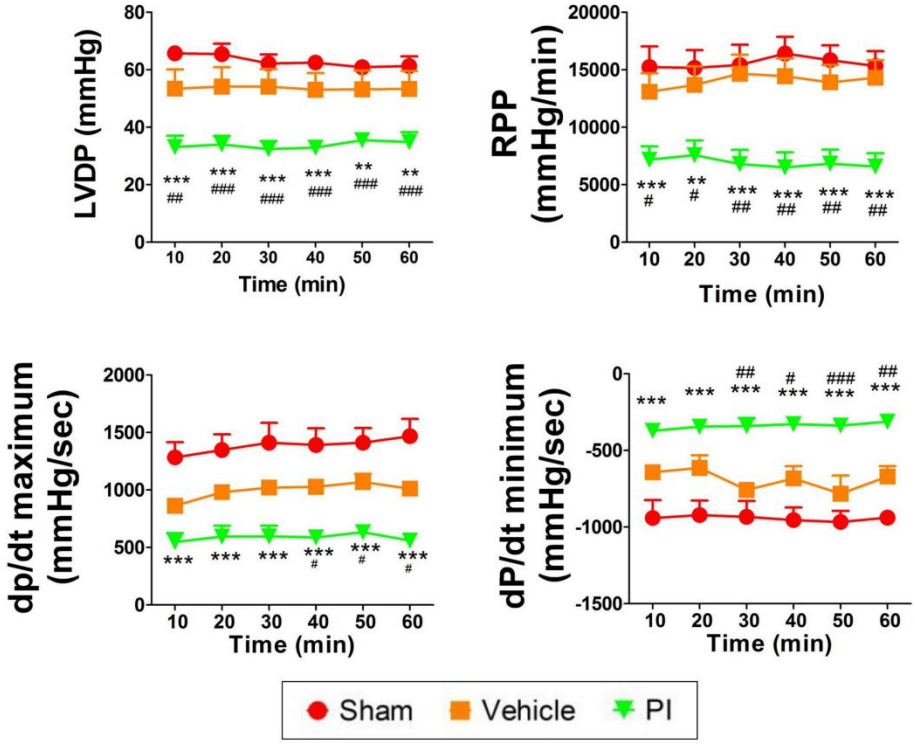

Figure 10. Additional baseline heart functional parameters in response to 8 weeks PI therapy (n=8). Baseline parameters were assessed for 60 min include LVDP, RPP, maximal and minimal contractile force. Data presented as mean ± SEM. **p<0.01, ***p<0.001 vs. sham; #p<0.05, ##p<0.01, ###p<0.001 vs. vehicle. *LVDP – left ventricular developed pressure, RPP – rate-pressure product, PI – protease inhibitor*.

Response to ischemia-reperfusion

We next evaluated how PI-treated hearts would respond to ischemia-reperfusion (**Fig. 11**). Coronary flow remained unchanged (p>0.05) during ischemia-reperfusion, however, heart rate was significantly diminished in PI-treated animals after 60 min of reperfusion, i.e. decrease in heart rate to 22.0 ± 22 beats/min compared to 203.9 ± 26 beats/min, p<0.001 (sham) and 180.0 ± 35 beats/min, p<0.01 (vehicle).

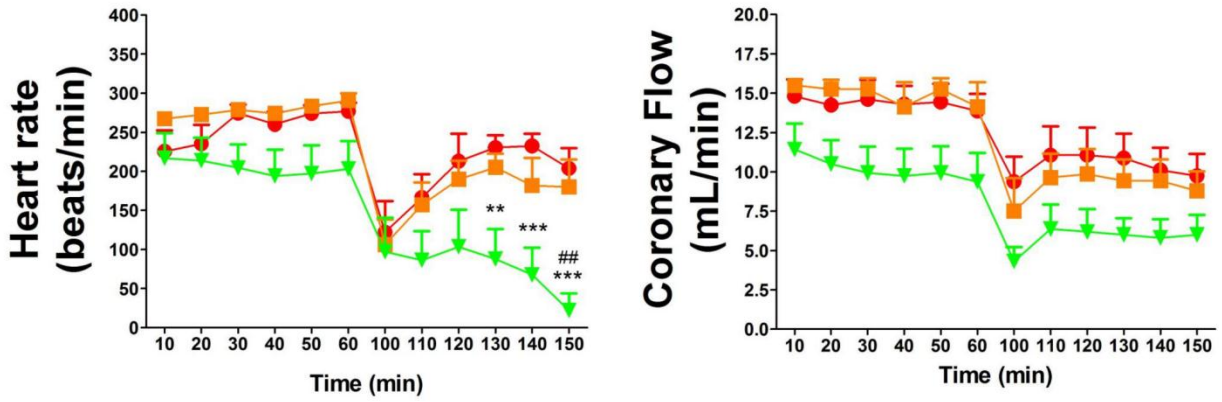

Figure 11. Contractile parameters after ischemia reperfusion in response to 8 weeks PI treatment (n=8). **p<0.01, ***p<0.001 vs. sham; ##p<0.01 vs. vehicle. *PI – protease inhibitor.*

Ischemia-reperfusion in the context of chronic PI treatment elicited similar detrimental effects on many other parameters. Here LVDP decreased in the PI-treated group in response to global ischemia, i.e. PI to 3.0 ± 2.36 mmHg vs. sham 35.38 ± 7.03 mmHg (p<0.001) and vs. vehicle 27.43 ± 5.07 mmHg (p<0.05) (**Fig. 12**). A similar pattern was found for RPP. Maximal and minimal contractile force was significantly decreased with PI treatment compared to sham animals (p<0.05) at many points during reperfusion, but no similar significance was obtained when compared to vehicle-treated rats (**Fig. 12**).

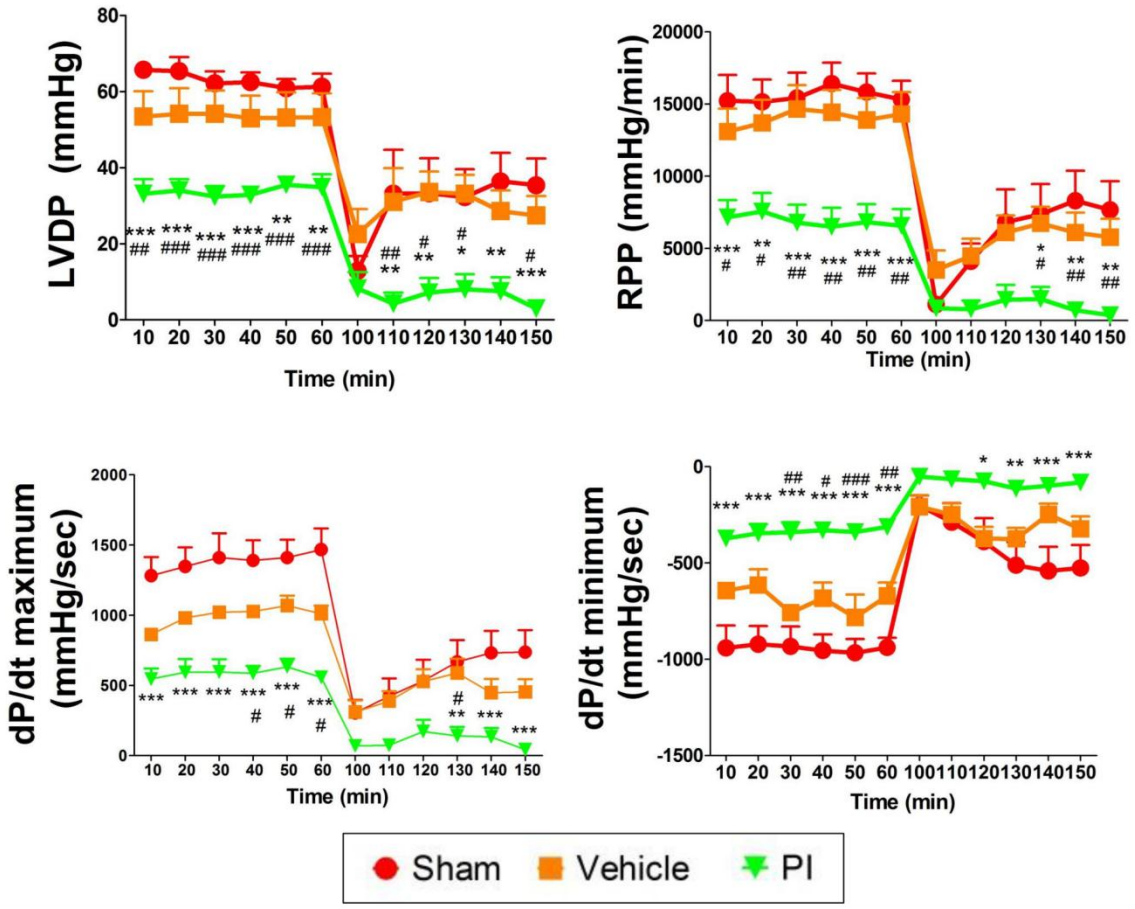

Figure 12. Additional contractile parameters during ischemia-reperfusion (n=8). Contractile parameters after ischemia-reperfusion in response to 8 weeks of PI therapy. *p<0.05, **p<0.01, ***p<0.001 vs. sham; #p<0.05, ##p<0.01, ###p<0.001 vs. vehicle. *LVDP – left ventricular developed pressure, PI – protease inhibitor, RPP – rate –pressure product.*

Interestingly, the percentage of LVDP recovery with global ischemia was not significantly different for PI treated groups vs. matched controls (p>0.05) (**Fig. 13**). Nonetheless, the survival rate dramatically decline after 30 min global ischemia where 50% of hearts treated with PIs did not perform adequately. Sham and vehicle-treated rats experienced up to a 20% decline in survival rate (**Fig. 13**).

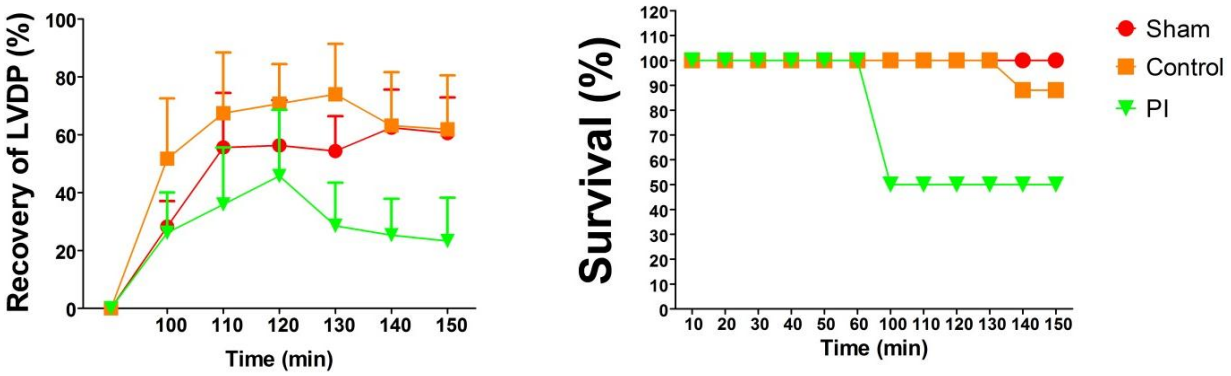

Figure 13. Recovery of LVDP and survival rate after ischemia-reperfusion with PI treatment (n=8). LVDP after ischemia-reperfusion was compared to baseline LVDP and expressed as a percentage, and number of hearts surviving the ischemia-reperfusion protocol expressed as percentage survival. *LVDP – left ventricular developed pressure, PI – protease inhibitor.*

Infarct size assessment

In separate experiments, PIs increased infarct size to 79.2 ± 40.7% vs. 46.3 ± 5.7% (sham) ($p<0.01$) and vs. 39.4 ± 8.4% (vehicle) ($p<0.01$) (**Fig. 14**). These data indicate that PIs are detrimental to heart function at many levels.

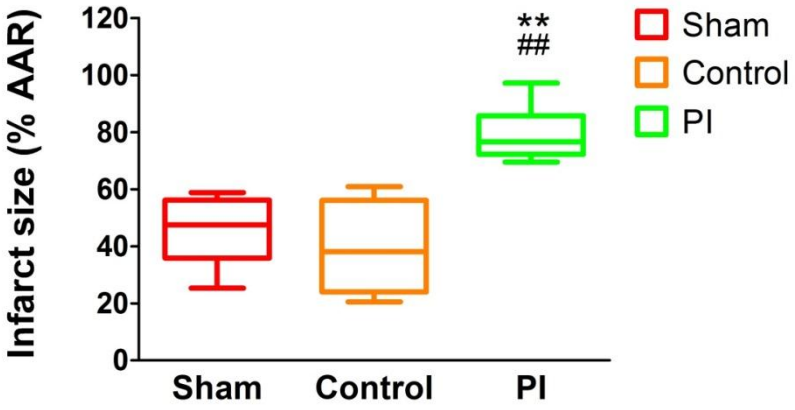

Figure 14. Infarct size in response to 8 weeks PI therapy (n=8). Infarct size was measured and expressed as a percentage of the area at risk in rats treated with PIs. Data presented as mean ± SEM. **$p<0.01$ vs. sham, ##$p<0.01$ vs. vehicle. *AAR – area at risk, PI – protease inhibitor.*

Discussion

Our baseline heart functional data show significant differences with PI treatment. Relaxation of the cardiac musculature was impaired at baseline and confirmed with additional parameters. Due to the fact that 50% of the PI group experienced failure with ischemia-reperfusion, this illuminates the possibility that electrical signaling within the heart and calcium homeostasis may be impaired.

Electrical conductance and calcium physiology must be taken in to consideration as our functional data point towards impairment of signal propagation and cross-bridge formation physiology. Alterations to calcium homeostasis can have a significant impact on heart function, as calcium enables ECC to take place [61]. In addition, maintenance of the calcium gradient by calcium pumps (e.g. SERCA) can influence calcium supply and removal from the myofiber. The rate of calcium removal determines the resting tension and resting calcium concentration within the myofiber [62], which in turn has a direct effect on the contractile force generated and also calcium available during the next contractile cycle. Importantly, heart rate was not significantly altered within our model with PI treatment and points toward a molecular and electrical pathology. Here, the depolarizing wave is still propagated at regular intervals but the translation into physical myofiber coupling and molecular interactions are impaired. Thus maximal contractile and relaxation force cannot be reached due to an imbalanced ionic and electrical homeostasis at various levels. Calcium contractile proteins such as calmodulin, calcineurin and CaMKII as well as SERCA and its regulator PLB need to be further investigated to elucidate this pathological mechanism.

These data therefore suggest that PI therapy decreases the heart's output and triggers a response within heart cells and mitochondria that could lead to disruption of electrical signaling. This may also be due to increased oxidative and energetic stress within cardiac mitochondria. We propose that PIs increase ROS production leading to mitochondrial damage and that the decline in heart function is mediated by an imbalance in calcium homeostasis and SR-related ion channels. Not only is calcium important during ECC, it is essential in maintaining calcium and ionic homeostasis within mitochondria. However, these concepts require further investigation.

It is important to note that these changes are present at a fairly early stage. Here we speculate that damaged mitochondria may trigger intracellular signaling cascades and gene transcription pathways to increase mitochondrial ATP production and antioxidant defense systems, for example SOD and catalase. Increased mitochondrial respiration would generate higher ATP levels leading to a greater amount of ROS produced by mitochondrial respiration complexes I and III, but also oxygen radicals such as $O_2^{\bullet -}$ and H_2O_2. These intriguing possibilities are currently being pursued in our laboratory.

Although we found significant differences in functional data at baseline, the PI-treatment group did not respond differently to the other groups in response to ischemia-reperfusion. Though heart rate declined significantly after 1 hr of reperfusion, LVDP recovery of the PI-treated hearts was not different to that of the controls. These data therefore indicate that although no significant phenotype is displayed after ischemia-reperfusion - PI treatment elicits molecular changes within the heart cell at baseline. Thus, even before an ischemic attack the heart is at a disadvantage but does not translate similarly thereafter. We propose that these changes are largely centred on PI-induced ionic imbalance, ROS generation and its possibly mitochondrial effects. This is in agreement with previous

studies that showed that Lopinavir treatment caused detrimental effects (via oxidative stress) on cardiac mitochondria [63]. Moreover, PIs are able to decrease the mitochondrial membrane potential causing a disruption in the electrochemical proton gradient essential for the production of ATP (reviewed in [64]). The activities of ETC complexes I and III can also be impaired by ROS, i.e. indirectly via activation of proteins and/or by impairment of electron flow through the ETC [65]. Thus a vicious cycle is established since more electrons leak into the mitochondrial matrix and the inter-mitochondrial membrane space, generating even more damaging ROS [66].

The consequences of PI administration on mitochondria and the myocardium are immense: mitochondrial toxicity from ROS; impaired respiratory capacity and energetics, impaired contractile functioning and disrupted metabolism, and are further exacerbated during ischemia-reperfusion.

Conclusion

These data reveal that PIs are detrimental to contractile function of the rat heart and we predict it creates a pathological environment of ionic imbalance and greater oxidative environment. Calcium signaling, ionic pumps, ROS and mitochondrial metabolism have been implicated as potential targets. These targets shall be further investigated to fully elucidate the mechanisms behind PI-associated heart dysfunction. *In vivo* heart function assessments in the form of an ECG will take place to corroborate our *ex vivo* findings and to fully investigate electrical conductance. Ultimately, these findings indicate that – when projected to the clinical setting – the patients' risk for cardiovascular and metabolic-related disease is increased in the long term with PI-containing HAART.

C. *In vivo* heart function assessments

In vivo heart function method

This functional assessment took place in collaboration with Dr. Roisin Kelly-Laubscher at the University of Cape Town, and complied with the necessary ethical procedures and housing requirements. Rats were handled as described previously (*ex vivo* Langendorff perfusions). At the end of the 8 week treatment period with PIs (no dietary interventions) rats were anesthetized with sodium pentobarbital (60 mg/kg i.p.), intubated, and thereafter ventilated with room air (2.5 mL/stroke) at a rate of 75 strokes/min via a rodent ventilator (Model 681, Harvard Apparatus, USA). Body temperature was monitored by a rectal temperature probe and a constant temperature was maintained throughout the surgical procedure by placing rats on a custom-made heating block. The depth of anesthesia was checked by assessing the pedal withdrawal reflex and by monitoring heart rate. Maintenance doses of anesthetic (6 mg/kg i.p.) were administered as required.

Lead II ECG was recorded via an Animal Bio Amplifier (ML136, ADInstruments, NSW, Australia). Carotid arterial blood pressure was recorded via a custom-made cannula attached to a pressure transducer (MLT0670, ADInstruments, NSW, Australia). Since formation of clots around intra-arterial cannulae poses a potential risk for arterial thrombosis, heparin (1000 IU/ kg i.p.) was injected concurrently with anesthetic [67,68]. A left thoracotomy was performed through the 4th intercostal space and the left lung collapsed using a damp swab. The left anterior descending coronary artery was thereafter ligated as previously described [69]. A 6–0 silk suture was placed around the left anterior descending coronary artery and its ends passed through a plastic tube. For induction of regional

ischemia the ends of the suture were used as a snare to occlude the artery by applying it gently onto the ventricular surface for 30 min. The efficacy of ischemia was confirmed by regional cyanosis and ECG changes. We employed S-T elevation (ECG) to confirm coronary artery ligation. The snare was released during reperfusion. Rat hearts were subjected to 30 min regional ischemia followed by 2 hrs of reperfusion. Upon termination of the experiment, rats were exsanguinated and hearts removed for *in vivo* infarct size assessment as previously described (*ex vivo* Langendorff perfusions). Equipment and procedure are depicted in **Fig. 15** and **Fig. 16.**

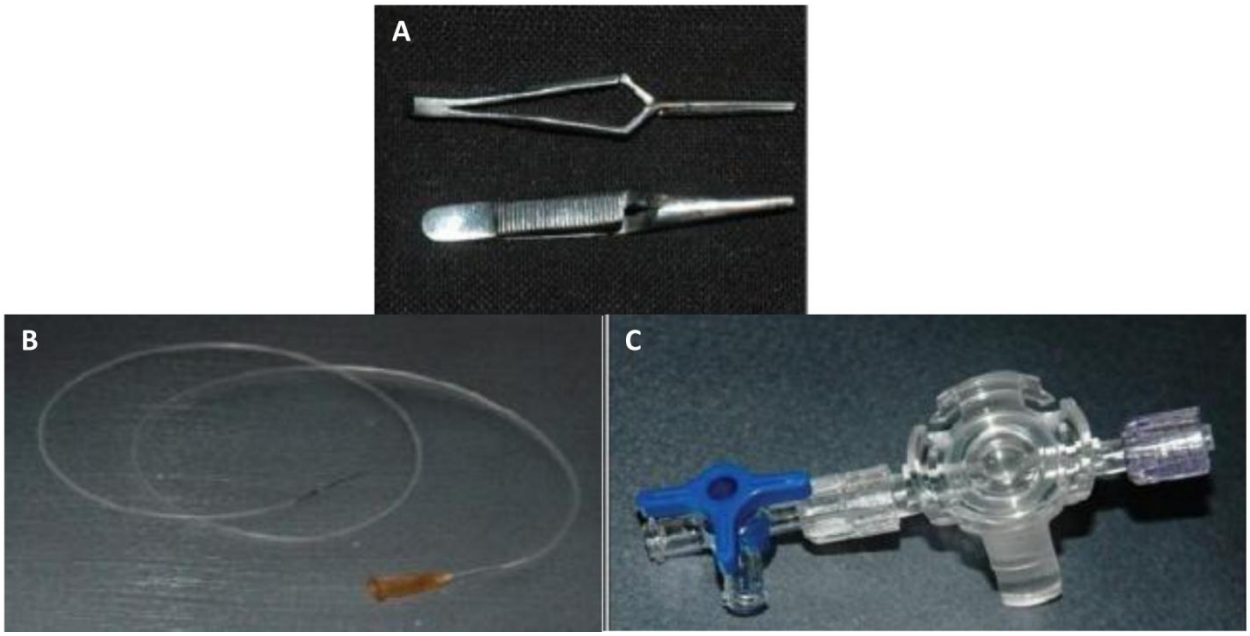

Figure 15. The materials used for recording the rat blood pressure *in vivo*. A) Bulldog clamp; B) Polyethylene tube [15-20 cm length] with a 26 G x ½" needle for carotid artery cannulation; and C) Disposable clip-on blood pressure transducer [70].

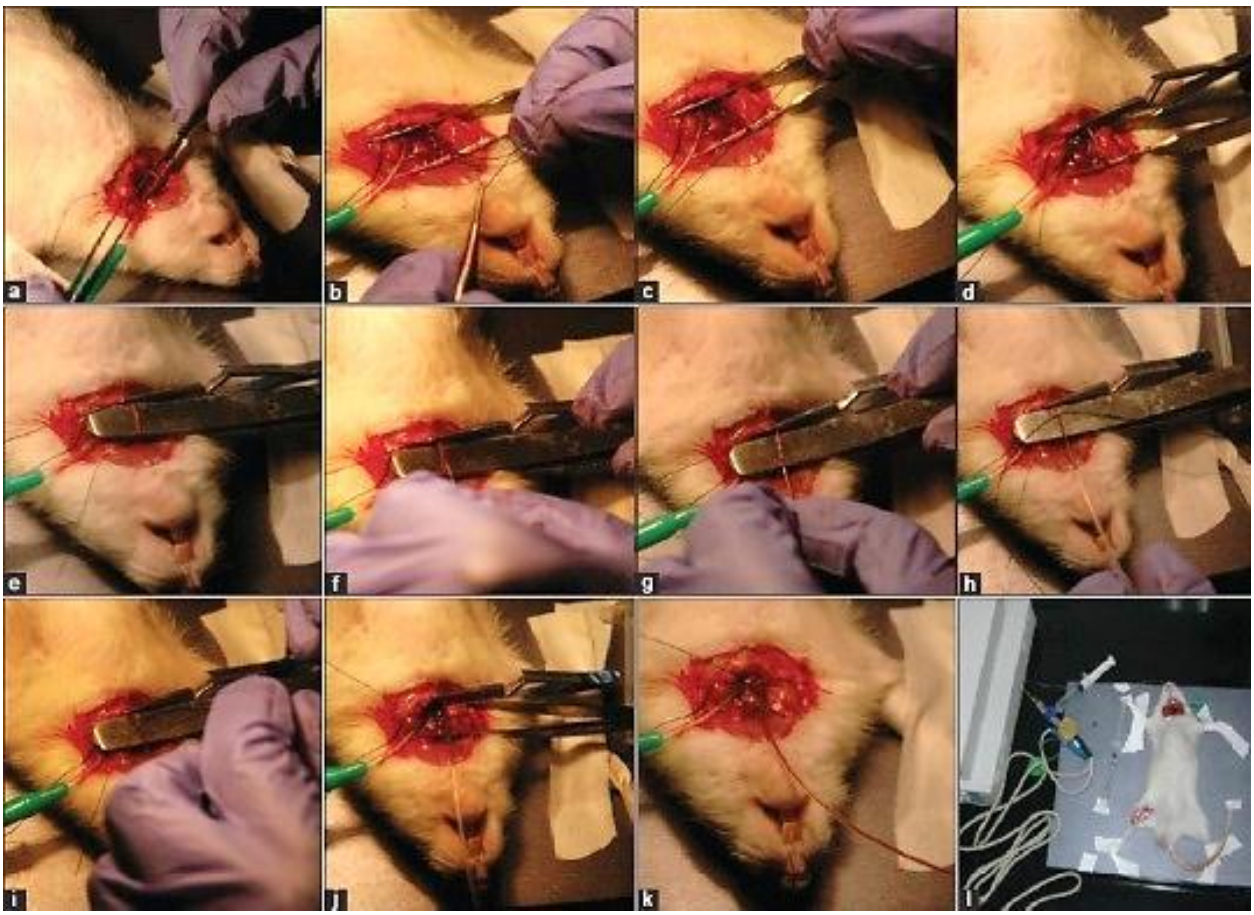

Figure 16. Cannulation of the carotid artery. A) Right side of the carotid artery is separated from the vagus nerve; B) and C) Cephalic end of the blood vessel is tied to avoid the bifurcation of blood pressure; D) Cardiac end of the blood vessel is clamped with a bulldog clamp for cannulation; E) Small platform is placed in the cannulation site; F - I) Carotid artery is cannulated and tied; J - K) The support platform and bulldog clamp are removed and ensure there is no leakage in the cannulation; and L) The carotid cannula is connected to the pressure transducer [70].

Results

The *ex vivo* heart function data indicated that PIs have a severe effect on heart function with a failure rate of 50% after ischemia-reperfusion, therefore the aim was to translate and compare these findings within an *in vivo* setting. Here a similar protocol was utilized; namely, 1) baseline heart function assessment and 2) regional ischemia followed by reperfusion and post-ischemic recovery assessment.

Each experimental group started out with 10 designated rats and subsequently anesthetized and intubated. However, the researchers experienced much difficulty with the handling of the rats throughout the protocol, with respiratory distress and anesthetic overload being potential (but not proven) factors. This led to a very small number of successful baseline recordings, far below what is statistically scientifically adequate for comparison. For both PI- and vehicle-treated groups, we could only complete 5 valid and useful ECG readings, while sham and control groups had a failure rate of 60 and 80%, respectively **(Table I)**. Comparison of ECG and pressure recordings reveal that rats that were unsuccessful had a markedly abnormal ECG – no clear electrical patterns with excess noise, while successful recording show the correct ECG wave pattern – namely a QRST wave (**Fig. 17**). Unfortunately, halfway during the experimental procedure the manometer refused to work, and although aortic blood pressure was then measured using a pressure transducer its accuracy was not trusted and therefore it was decided not to interpret the pressure recordings. These problems were present within all experimental groups during baseline as well as ischemia-reperfusion.

Table I. Number of animals used for *in vivo* heart functional assessment and success with experiments.

	Control	Sham	Vehicle	PI
Starting number	10	10	10	10
Succeful at Baseline	2	4	5	5
Failure rate (%)	80	60	50	50

PI – protease inhibitor

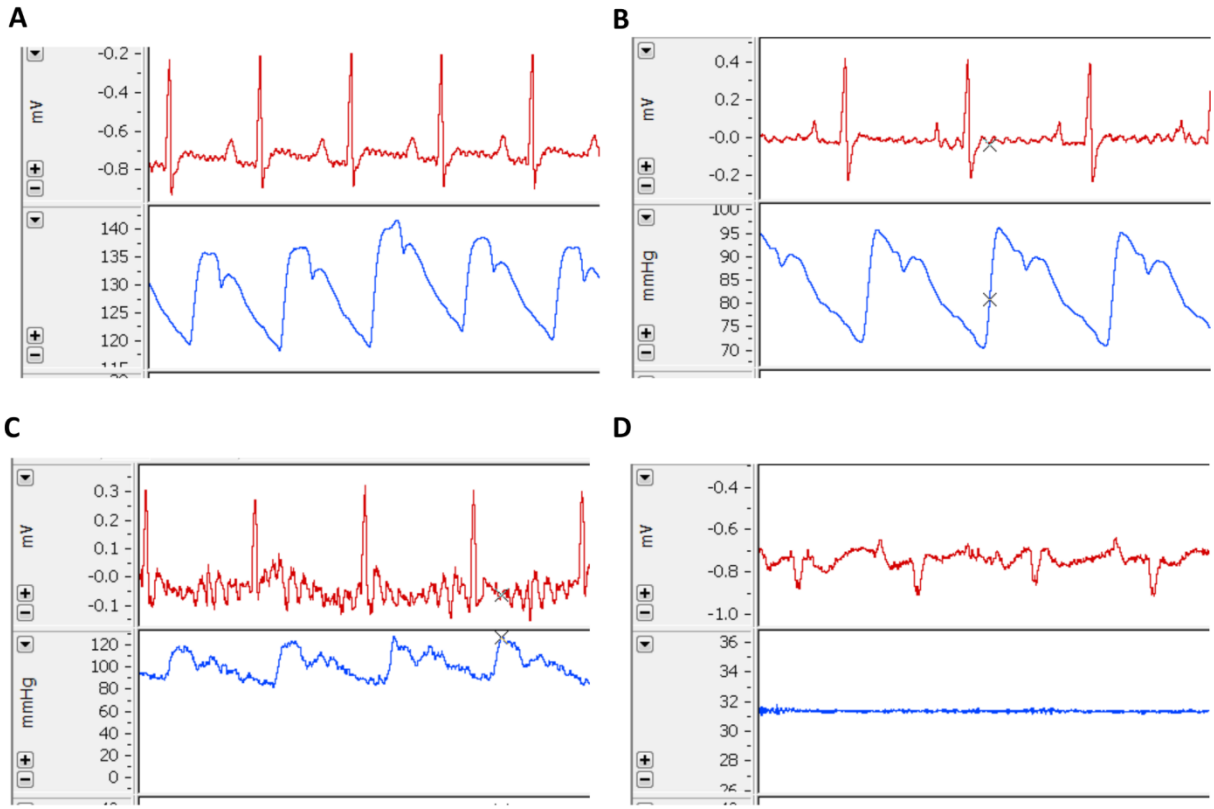

Figure 17. ECG recordings at baseline. ECG readings (in red, mV) as well as aortic blood pressure (in blue, mmHg) where recorded. Panel A and B indicate correct ECG recordings while panel C and D show incorrect ECG recordings. Panel D also indicates at the blue line that the manometer refused to work and could not generate pressure recordings. *ECG – electro-cardiogram*.

ECG parameters were further assessed in rats that survived the intubation as well as the ischemia-reperfusion. Significant differences were found between the experimental groups at baseline (**Fig. 18**) where P-wave amplitude was significantly elevated in comparison only to sham (0.109 ± 0.007 mV vs. 0.055 ± 0.02 mV, $p<0.05$), and ST-wave height significantly decreased (-0.014 ± 0.03 vs. sham -0.120 mV ± 0.02, $p<0.05$; vs. vehicle -0.14 mV ± 0.03, $p<0.05$). Parameters for post-ischemic function remained unaltered ($p>0.05$) (**Fig. 19**). However, due to the low number analyzed per group, especially the control groups, no definite conclusion can be drawn from these experiments as *all* experimental groups require at least n=4-5 to be statistically relevant.

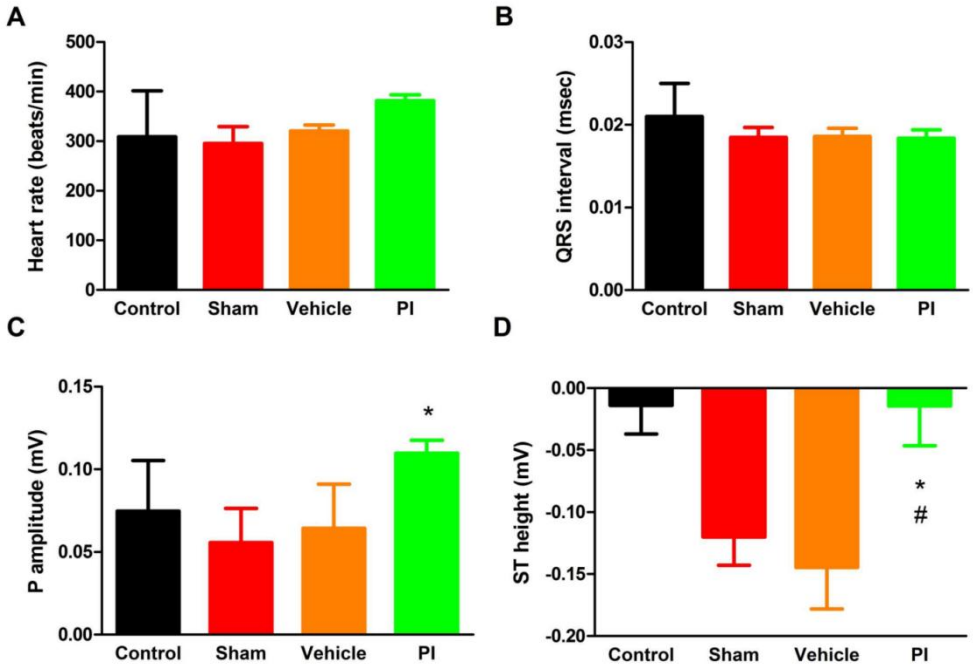

Figure 18. Baseline ECG parameters in response to PI treatment (n=2-5). A) Heart rate; B) QRS interval; C) P wave amplitude; and D) ST height. Data represented as mean ± SEM. *$p<0.05$ vs. sham, #$p<0.05$ vs. vehicle. *ECG – electro-cardiogram, PI – protease inhibitor.*

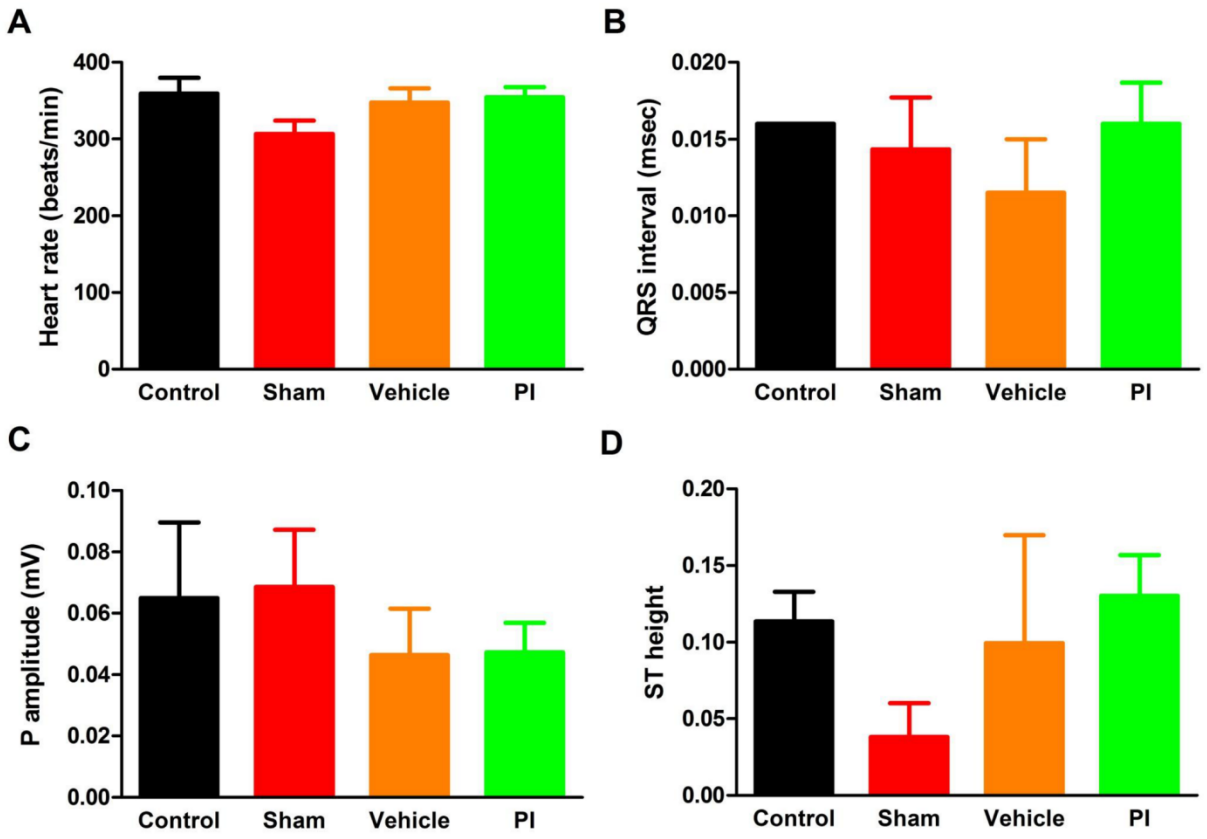

Figure 19. Post-ischemic ECG parameters in response to PI therapy (n=2-5). Hearts were subjected to 30 min regional ischemia and thereafter 2 hr of reperfusion *in vivo*. A) Heart rate; B) QRS interval; C) P wave amplitude; and D) ST height. Data represented as mean ± SEM. *ECG – electro-cardiogram, PI – protease inhibitor.*

Discussion

The aim of the *in vivo* heart function determination was not only to corroborate the *ex vivo* findings but to generate novel data to improve our understanding of the detrimental effects of PIs on heart function. An ECG can shed light in to the inner workings and ionic physiology behind a contraction and would thus aid our interpretation of ionic and calcium homeostasis.

The advantage of an *in vivo* rat model is that ECG analysis is standardized, relatively cheap and straightforward to perform, easy to manipulate with drugs and has less confounding pre-existing diseases [71]. The ECG was pioneered in the 19th century [72] and Farraj *et al.* (2011) [73] describe it as *"…the spatio-temporal changes in the distribution of the extracellular voltage field present at the body surface and is directly related to the local voltage field generated by its source, the heart*". Although the ECG is not a direct functional measurement, it can detect rhythm disturbances and abnormal conductance as well as ischemic injury [74]. The ECG is routinely used in health care but rats and humans differ in terms of heart rate and ECG pattern. The heart rate of a rat is typically between 300-500 beats/min [75–77] while that of a human is around 60-100 beats/min. This can also be attributed to the fact that the human action potential duration is 5 times longer than that of a rat [71]. Therefore, the ECG can impart important information about electrical conductance in the rat heart.

Due to unforeseen circumstances this experiment did not go as planned and with the aid of our collaborator, Dr. Kelly-Laubscher, her expertise was sought as to the reason. It was noted that many of the animals had respiratory difficulty from the time of intubation and during the procedure, even though intubation was successful and the correct volume of air circulated at the correct tempo.

The animal housing facility conducted routine tests and did not indicate danger for respiratory infections. At times it seemed that the larger rats would accumulate anesthetic within their fat pads, even though the anesthetic was correctly injected (i.p.). It has been noted before that PI-treated animals exhibit greater weight gain than their control counterparts and this was visually confirmed by the presence of excess abdominal adipose tissue while dissecting the animals in a separate study. Dr. Kelly-Laubscher also indicated that the rats might have been too old for this type of procedure, as her experience points towards younger (2 months or less) rats being successful with this technique. However, it is difficult to pinpoint the exact nature or causes why the ECG experiments failed. Due to the low number of successful ECG readings generated, we decided not to conclude anything from these data and instead focus on our *ex vivo* findings.

Conclusion

Due to unforeseen circumstances, data generated from *in vivo* heart functional assessments could not be fully utilized to help elucidate the molecular and ionic pathology of PI-induced heart dysfunction. No definitive conclusion is therefore derived from these experiments. Tissue samples and functional data from *ex vivo* assessments were therefore utilized and studied in subsequent experiments.

References

1. Himelman, R. B., Chung, W. S., Chernoff, D. N., Schiller, N. B. & Hollander, H. Cardiac manifestations of human immunodeficiency virus infection: a two-dimensional echocardiographic study. *J Am Coll Cardiol* **13,** 1030–6 (1989).

2. Hecht, S., Berger, M., Van Tosh, A. & Croxson, S. Unsuspected cardiac abnormalities in the acquired immune deficiency syndrome. An echocardiographic study. *Chest* **96,** 805–8 (1989).

3. Kaul, S., Fishbein, M. & Siegel, R. Cardiac manifestations of acquired immune deficiency syndrome: a 1991 update. *Am Heart J* **122,** 535–44 (1991).

4. Rerkpattanapipat, P., Wongpraparut, N., Jacobs, L. E. & Kotler, M. N. Cardiac manifestations of acquired immunodeficiency syndrome. *Arch Int Med* **160,** 602–8 (2000).

5. De Castro, S. *et al.* Heart involvement in AIDS: a prospective study during various stages of the disease. *Eur Heart J* **13,** 1452–1459 (1992).

6. Grody, W. W., Cheng, L. & Lewis, W. Infection of the heart by the human immunodeficiency virus. *Am J Cardiol* **66,** 203–206 (1990).

7. Knudsen, A. *et al.* Angiographic features and cardiovascular risk factors in human immunodeficiency virus-infected patients with first-time acute coronary syndrome. *Am J Cardiol* **111,** 63–7 (2013).

8. Lo, J. *et al.* Increased prevalence of subclinical coronary atherosclerosis detected by coronary computed tomography agiography in HIV-infected men. *AIDS* **24,** 243–253 (2010).

9. Friis-Møller, N. *et al.* Cardiovascular disease risk factors in HIV patients--association with antiretroviral therapy. Results from the DAD study. *AIDS* **17,** 1179–1193 (2003).

10. Friis-Møller, N. *et al.* Class of antiretroviral drugs and the risk of myocardial infarction. *N Engl J Med* **356,** 1723–1735 (2007).

11. Smith, C. *et al.* Factors associated with specific causes of death amongst HIV-positive individuals in the DAD study. *AIDS* **24,** 1537–48 (2010).

12. Holmberg, S. D. *et al.* Protease inhibitors and cardiovascular outcomes in patients with HIV-1 For personal use. *Lancet* **360,** 1747–1748 (2002).

13. Mary-Krause, M., Cotte, L., Simon, A., Partisani, M. & Costagliola, D. Increased risk of myocardial infarction with duration of protease inhibitor therapy in HIV-infected men. *AIDS* **17,** 2479–86 (2003).

14. Durand, M., Sheehy, O., Baril, J.-G., Lelorier, J. & Tremblay, C. L. Association between HIV infection, antiretroviral therapy, and risk of acute myocardial infarction: a cohort and nested case-control study using Québec's public health insurance database. *J AIDS* **57,** 245–53 (2011).

15. Sullivan, P. S., Dworkin, M. S., Jones, J. L. & Craig, W. Epidemiology of thrombosis in HIV-infected individuals. *AIDS* **14,** 321–324 (2000).

16. Triant, V. A., Lee, H., Hadigan, C. & Grinspoon, S. K. Increased acute myocardial infarction rates and cardiovascular risk factors among patients with human immunodeficiency virus disease. *Clin Endocrinol* **92,** 2506–2512 (2009).

17. Bozzette, S. A. *et al.* Long-term survival and serious cardiovascular events in HIV-infected patients treated with highly active antiretroviral therapy. *J AIDS* **47,** 338–341 (2008).

18. Klein, D., Hurley, L. B., Quesenberry, C. P. & Sidney, S. Do protease inhibitors increase the risk for coronary heart disease in patients with HIV-1 infection? *J AIDS* **30,** 471–7 (2002).

19. Mondy, K. E. *et al.* High prevalence of echocardiographic abnormalities among HIV-infected persons in the era of highly active antiretroviral therapy. *Clin Infec Dis* **52,** 378–386 (2011).

20. Lyonne, L. *et al.* Thromboembolic events at the time of highly active antiretroviral therapies against human immunodeficiency virus. *Rev Med Intern* **29,** 100–104 (2008).

21. Maggi, P., Lillo, A., Perilli, F. & Maserati, R. Colour-doppler ultrasonography of carotid vessels in patients treated with antiretroviral therapy: a comparative study. *AIDS* **18,** 1023–1028 (2004).

22. Bernal, E. *et al.* Hypertriglyceridemic waist phenotype is a risk factor fo subclinical atherosclerosis in human immunodeficiency virus-infected patients. *Med Clin* **139,** 561–565 (2012).

23. De Saint Martin, L. *et al.* Premature atherosclerosis in HIV positive patients and cumulated time of exposure to antiretroviral therapy (SHIVA study). *Atherosclerosis* **185,** 361–7 (2006).

24. Jerico, C. *et al.* Subclinical carotid atherosclerosis in HIV-infected patients: a role of combination antirtroviral therapy. *Stroke* **37,** 812–7 (2006).

25. Majluf-Cruz, A. *et al.* Venous thrombosis among patients with AIDS. *Clin Appl Thromb Hemostas* **10,** 19–25 (2004).

26. Lijfering, W. M., Ten Kate, M. K., Sprenger, H. G. & van der Meer, J. Absolute risk of venous and arterial thrombosis in HIV-infected patients and effects of combination antiretroviral therapy. *J Thromb Haemost* **4,** 1928–30 (2006).

27. Kawakami, M. & Okabe, E. Superoxide anion radical-triggered Ca2+ release from cardiac sarcoplasmic reticulum through ryanodine receptor Ca2+ channel. *Mol Pharmacol* **53,** 497–503 (1998).

28. Marengo, J., Hidalgo, C. & Bull, R. Sulfhydryl oxidation modifies the calcium dependence of ryanodine-sensitive calcium channels of excitable cells. *Biophys J* **74,** 1263–1277 (1998).

29. Anzai, K. *et al.* Effects of hydroxyl radical and sulfhydryl reagents on the open probability of the purified cardiac ryanodine receptor channel incorporated into planar lipid bilayers. *Biochem Biophys Res Commun* 938–942 (1998).

30. Holmberg, S. *et al.* Reactive oxygen species modify the structure and function of the cardiac sarcoplasmic reticulum calcium-release channel. *Cardioscience* **2,** 19–25 (1991).

31. Rowe, G. T., Manson, N. H., Caplan, M. & Hess, M. L. Hydrogen peroxide and hydroxyl radical mediation of activated leukocyte depression of cardiac sarcoplasmic reticulum. Participation of the cyclooxygenase pathway. *Circ Res* **53,** 584–591 (1983).

32. Boraso, A. & Williams, A. Modification of the gating of the cardiac sarcoplasmic reticulum Ca2+-release channel by H2O2 and dithiothreitol. *Am J Physiol* **267,** H1010–6 (1994).

33. Scherer, N. & Deamer, D. Oxidative stress impairs the function of sarcoplasmic reticulum by oxidation of sulfhydryl groups in the Ca2+-ATPase. *Arch Biochem Biophys* **246,** 589–601 (1986).

34. Morris, T. & Sulakhe, P. Sarcoplasmic reticulum Ca2+-pump dysfunction in rat cardiomyocytes briefly exposed to hydroxyl radicals. *Free Radic Biol Med* **22,** 37 –47 (1997).

35. Kaneko, M., Beamish, R. & Dhalla, N. Depression of heart sarcolemmal Ca2+-pump activity by oxygen free radicals. *Am J Physiol* **256,** (1989).

36. Kaneko, M., Elimban, V. & Dhalla, N. Mechanism for depression of heart sarcolemmal Ca2+ pump by oxygen free radicals. *Am J Physiol* **257,** H804–11 (1989).

37. Reeves, J. P., Bailey, C. a & Hale, C. C. Redox modification of sodium-calcium exchange activity in cardiac sarcolemmal vesicles. *J Biol Chem* **261,** 4948–55 (1986).

38. Kato, M. & Kako, K. Na+/Ca2+ exchange of isolated sarcolemmal membrane: effects of insulin, oxidants and insulin deficiency. *Mol Cell Biochem* **83,** 15 –25 (1988).

39. Goldhaber, J. Free radicals enhance Na+/Ca2+ exchange in ventricular myocytes. *Am J Physiol* **271,** H823–33 (1996).

40. Sharikabad, M., Ostbye, K., Lyberg, T. & Brors, O. Effect of extracellular Mg2+ on ROS and Ca2+ accumulation during reoxygenation of rat cardiomyocytes. *Am J Physiol* **280,** H344–H353 (2001).

41. Temsah, R. M., Netticadan, T., Kawabata, K.-I. & Dhalla, N. S. Lack of both oxygen and glucose contributes to I/R-induced changes in cardiac SR function. *Am J Physiol Cell Physiol* **283,** C1306–12 (2002).

42. Gen, W., Tani, M., Takeshita, J., Ebihara, Y. & Tamaki, K. Mechanisms of Ca2+ overload induced by extracellular H2O2 in quiescent isolated rat cardiomyocytes. *Basic Res Cardiol* **96,** 623–9 (2001).

43. Barr, R. L. & Lopaschuk, G. D. Direct measurement of energy metabolism rat heart in the isolated working. *J Pharmacol Toxicol Methods* **38,** 11–17 (1997).

44. Neely, J., Liebermeister, H., Battersby, E. & Morgan, H. Effect of pressure development on oxygen consumption by isolated rat heart. *Am J Physiol* **212,** 804–14 (1967).

45. Taegtmeyer, H., Hems, R. & Krebs, H. Utilization of energy-providing substrates in the isolated working rat heart. *Biochem J* **186,** 701–11 (1980).

46. Boudina, S. *et al.* Reduced mitochondrial oxidative capacity and increased mitochondrial uncoupling impair myocardial energetics in obesity. *Circulation* **112,** 2686–2695 (2005).

47. Kelly, R. F., Lamont, K. T. & Somers, S. Ethanolamine is a novel STAT-3 dependent cardioprotective agent. *Basic Res Cardiol* **105,** 763–770 (2010).

48. Mapanga, R. *et al.* Oleanolic acid: a novel cardioprotective agent that blunts hyperglycemia-induced contractile dysfunction. *PloS One* **7,** e47322 (2012).

49. Du Toit, E. F., Nabben, M. & Lochner, A. A potential role for angiotensin II in obesity induced cardiac hypertrophy and ischaemic/reperfusion injury. *Basic Res Cardiol* **100,** 346–54 (2005).

50. Lopaschuk, G. D., Ussher, J. R., Folmes, C. D. L., Jaswal, J. S. & Stanley, W. C. Myocardial fatty acid metabolism in health and disease. *Physiol Rev* **90,** 207–58 (2010).

51. Jeffrey, F., Diczku, V., Sherry, A. & Malloy, C. Substrate selection in the isolated working rat heart: effects of reperfusion, afterload, and concentration. *Basic Res Cardiol* **90,** 388–96 (1995).

52. Zierler, K. Fatty acids as substrates for heart and skeletal muscle. *Circ Res* **38,** 459–63 (1976).

53. Van der Vusse, G., Glatz, J., Stam, H. & Reneman, R. Fatty acid homeostasis in the normoxic and ischemic heart. *Physiol Rev* **72,** 881–940 (1992).

54. Spitzer, J. Effect of lactate infusion on canine myocardial free fatty acid metabolism in vivo. *Am J Physiol* **226,** 213–7 (1974).

55. Neely, J. & Morgan, H. Relationship between carbohydrate and lipid metabolism and the energy balance of heart muscle. *Annu Rev Physiol* **36,** 413–59 (1974).

56. Issekutz, B. J., Miller, H. & Paul P, Podahl, K. Effect of lactic acid on free fatty acids and glucose oxidation in dogs. *Am J Physiol* **209,** 1137–44 (1965).

57. Drake, A., Haines, J. & Noble, M. Preferential uptake of lactate by the normal myocardium in dogs. *J Physiol (Lond)* **339,** 1–15 (1983).

58. Drake, A. Substrate utilization in the myocardium. *Basic Res Cardiol* **77,** 76 (1982).

59. Bing, R. *et al.* Metabolic studies on the human heart in vivo. I. Studies on carbohydrate metabolism of the human heart. *Am J Med* **15,** 284–296 (1953).

60. Bing, R. Cardiac metabolism. *Physiol Rev* **45,** 171–213 (1965).

61. Fabiato, A. Calcium-induced release of calcium from the cardiac sarcoplasmic reticulum. *Am J Physiol* **245,** C1–C14 (1983).

62. Louch, W., Stokke, M., Sjaastad, I., Christensen, G. & Sejersted, O. No rest for the weary: diastolic calcium homeostasis in the normal and failing myocardium. *Physiology* **27,** 208–323 (2012).

63. Deng, W., Baki, L., Yin, J., Zhou, H. & Baumgarten, C. M. HIV protease inhibitors elicit volume-sensitive Cl − current in cardiac myocytes via mitochondrial ROS. *J Mol Cell Cardiol* **49,** 746–52 (2010).

64. Kadenbach, B. Intrinsic and extrinsic uncoupling of oxidative phosphorylation. *Biochim Biophys Acta* **1604,** 77–94 (2003).

65. Korge, P., Ping, P. & Weiss, J. Reactive oxygen species production in energized cardiac mitochondria during hypoxia/reoxygenation: modulation by nitric oxide. *Circ Res* **103,** 873–80 (2008).

66. Muller, F., Yuhong, Z. & Van Remmen, H. Complex III releases superoxide to both sides of the inner mitochondrial membrane. *J Biol Chem* **279,** 49064–73 (2004).

67. Walker, W. *et al.* Systemic heparinization for femoral percutaneous coronary arteriography. *New Eng J Med* **288,** 826–828 (1973).

68. Eyer, K. Complications of transfemoral coronary arteriography and their prevention using heparin. *Am Heart J* **86,** 428 (1973).

69. Deuchar, G., Opie, L. & Lecour, S. TNFalpha is required to confer protection in an in vivo model of classical ischemic preconditioning. *Life Sci* **80,** 1686–1691. (2007).

70. Parasuraman, S. & Raveendran, R. Measurement of invasive blood pressure in rats. *J Pharmacol Pharmacother* **3,** 172–7 (2012).

71. Curtis, M., Macleod, B. & Walker, M. Models for the study of arrythmias in myocardial ischaemia and infarction: the use of the rat. *J Mol Cell Cardiol* **19,** 399–419 (1987).

72. Waller, A. A demonstration on man of electromotive changes accompanying the heart's beat. *J Physiol* **8,** 229–234. (1887).

73. Farraj, A. K., Hazari, M. S. & Cascio, W. E. The utility of the small rodent electrocardiogram in toxicology. *Toxicol Sci* **121,** 11–30 (2011).

74. Berne, R. & Levy, M. *Cardiovascular Physiology: The heart generates its own pacemaker activity.* 28–38 (Mosby, Inc, 2001).

75. Farraj, A. K. *et al.* Increased non-conducted P-wave arrhythmias after a single oil fly ash inhalation exposure in hypertensive rats. *Environ Health Perspect* **117,** 709–15 (2009).

76. Hofstetter, J., Suckow, M. & Hickman, D. *The Laboratory Rat: Morphophysiology*. 93–126 (Elsevier, 2006).

77. Tontodonati, M., Fasdelli, N. & Dorigatti, R. An improved method of electrode placement in configuration Lead II for the reliable ECG recording by telemetry in the conscious rat. *J Pharmacol Toxicol Methods* **63,** 1–6 (2010).

Permission for use of images and text

Figure 15 and **Figure 16** including text are from " Parasuraman S, Raveendran R. Measurement of invasive blood pressure in rats. *J Pharmacol Pharmacother* (2012) 3:172-7 " [70].

Permission was requested on 15 March 2013 per email by KMSE Reyskens, and successfully granted on 16 March 2013. The images and accompanying texts are the sole and original works of Parasurman and Raveendran, thus all originality and copyright remains with the authors.

Chapter 4

Investigation of molecular mechanisms underlying cardio-metabolic dysfunction with HIV PI therapy.

Introduction

PIs form an integral part of HAART and side-effects include development of dyslipidemia, i.e. greater production of plasma triglycerides and lipids together with an adverse cholesterol profile [6–8]. Together such derangements elicit inflammation, stress the myocardium [9], and may potentially predict the onset of IR [10,11] and cardiac dysfunction [10]. PIs are also linked to increased risk for myocardial infarction [12] and cardiovascular abnormalities [13,14], with many changes resembling coronary artery disease [15]. Therefore, an emerging focus is to identify key metabolic and transcriptional pathways that mediate PI-induced cardio-metabolic pathophysiology. For example, our data show that rats exposed to 8 weeks of PI treatment displayed cardiac dysfunction (**Chapter 3**) [16]. Moreover, PI-treated HIV-infected individuals exhibit elevated ROS production [17–19] that may trigger the activation of detrimental signaling and cell death pathways [20].

HIV-PIs may also exert unfavorable effects at the gene transcriptional level, e.g. activating SREBP[21], a key lipid transcriptional modulator expressed in major metabolic tissues [22]. Upon activation, SREBP binds to SRE-containing promoter sequences in lipogenic and cholesterogenic genes (e.g. *hmgcr*) that ultimately results in the production of cholesterol (high-density lipoprotein [HDL] and LDL) and sterol components [23]. The UPS – responsible for removal of misfolded or damaged proteins - is also implicated in the onset of such metabolic side effects. For example, the PI Ritonavir attenuates chymotrypsin- and trypsin-like activities of the 20S UPS subunit in hepatocytes [24]. As a result, degradation of ApoB (major determinant of plasma lipid levels) was diminished thus providing a potential mechanism for PI-induced hyperlipidemia [25]. Furthermore, SREBPs are ubiquitinated and

degraded by the UPS [26,27] raising the possibility that an inhibition of this system may also contribute to development of dyslipidemia in HIV-infected individuals treated with PIs. Together this may establish a pro-atherogenic profile and increase the risk for the onset of CVD.

Despite such progress the underlying molecular mechanisms responsible for HAART-induced cardio-metabolic side effects are poorly understood and little is known about the earliest events driving this process. For the current study, we therefore hypothesized that HIV PI treatment enhances myocardial oxidative stress and concomitantly inhibits the UPS, thereby attenuating cardiac contractile function at baseline. Since our previous *ex vivo* rat heart work (**Chapter 3**) [16] implicated altered calcium homeostasis in PI-mediated cardiac dysfunction, we further investigated calcium signaling and mitochondrial energetic regulators in our established rat model of chronic PI drug delivery.

Materials & Methods

Animal model

An additional but separate set of male Wistar rats, treated in an identical fashion to those in **Chapter 3** were used. At the end of the 8-week treatment period rats were killed and a variety of analyses described below carried out on tissue collected immediately after sacrifice. All animals were treated in accordance with the Guide for the Care and Use of Laboratory Animals of the National Academy of Sciences (NIH publication No. 85-23, revised 1996) and performed with the approval of the Animal Ethics Committee of Stellenbosch University (South Africa).

Drug administration

Drug administration occurred as described in **Chapter 2.**

Histology

After 8 weeks, harvested tissues (heart, liver, adipose, pancreas and skeletal muscle) were fixed, processed and embedded in paraffin wax whereafter sections (4-5 µm) were stained with a) hematoxylin and eosin (HE) for general morphologic evaluation and b) Sirius red for detection of collagen deposits (fibrosis).

Tissue lipid profile

Isolated heart and liver tissues were also assessed for: total cholesterol, HDL, LDL/VLDL cholesterol and TG content according to the manufacturer's instructions. Briefly, tissue cholesterol content was assessed in heart and liver homogenates (BioVision, Milpitas CA). HDL-cholesterol and LDL/VLDL-cholesterol were separated via differential centrifugation and precipitation buffer supplied

with the kit and a non-separated sample denoted for total cholesterol determination. Thereafter, a cholesterol master mix including cholesterol esterase was added to each sample in a 96-well microtiter plate in reaction buffer in addition to the standards supplied. The enzyme was not included in the reaction mixture for total cholesterol measurement. Incubation of samples with the reaction mixture for 1 hr at 37°C generated a color reaction and absorbance was measured in a colorimetric plate reader at 570 nm (Cecil CE2021 spectrophotometer, Cecil Instruments, Cambridge, UK). Cholesterol concentrations were determined from a standard curve and expressed as mmol/L.

TGs in heart and liver tissue were also assessed by using a commercial kit (Abcam, Cambridge MA). Briefly, heart and liver tissue were homogenized in 5% NP-40 solution, heated to boiling point (100°C) to solubilize the TGs and subsequently centrifuged to remove insoluble material. Lipase was then added to convert TGs to glycerol and FA. Glycerol was then oxidized by the addition of a TG reaction mixture and the product generated reacted with a probe to generate color which was measured at 570 nm with a colorimetric plate reader (Cecil CE2021 spectrophotometer, Cecil Instruments, Cambridge, UK). Concentrations were extrapolated from the standard curve and expressed as mmol/L.

Genetic profile

Real-time quantitative polymerase chain reaction (qPCR) analysis for gene expression was assessed in heart, liver and adipose tissue collected after 8 weeks of PI therapy. These experiments were performed in collaboration with Professor Monte Willis (McAllister Heart Institute, Department of Pathology and Laboratory Medicine, University of North Carolina, Chapel Hill NC). Total RNA was isolated from homogenized tissues (n=8) using the RNeasy® Mini Kit (Qiagen, Germantown MD) according to the manufacturer's protocols as previously described [28,29]. First strand copy

deoxyribonucleic acid (cDNA) was made using the iScript™ cDNA synthesis kit (BioRad, Hercules CA) using 200 and 250 ng of RNA from liver, heart and adipose tissue, respectively, and included the Solaris synthetic RNA Spike Control (Thermo Scientific, Waltham MA) to test for reverse transcription and PCR inhibition. Samples that did not show significant inhibition ($\Delta C_q < 3$ compared to synthetic target alone, 69 of 72 samples) were diluted 20-fold in water and used for gene expression analysis. A total of three samples exhibited inhibition and were not used for qPCR analysis.

We evaluated expression of the following genes: Acetyl-CoA carboxylase isoforms (*accα*: marker of FA synthesis; *accβ*: marker of FA oxidation); Fatty acid synthase (*fas*: marker of FA synthesis); Glycerol-3-phosphate acyltransferase (mitochondrial) (*gpam*: marker of glycero-lipid synthesis); Hydroxyl-3-methyl-glutaryl-CoA reductase (*hmgcr*: marker of cholesterol synthesis); LDL receptor (*ldlr*: marker of LDL metabolism); SREBP isoforms (*srebpf1/2*: evaluate role of SREBPs); and glutamine fructose-6-phosphate amidotransferase (*gfat1*: Hexosamine biosynthetic pathway [HBP] marker). For all qPCR reactions, 2 µL of diluted cDNA (range ~ 2 – 5 ng of cDNA) was used in technical triplicate reactions using LightCycler® 480 Probes Master mix (Roche, Indianapolis IN) for 5´ exonuclease chemistry with primers and probes per manufacturer specifications (Primers [forward/reverse]: *actb* – cccgcgagtacaaccttct/cgtcatccatggcgaact; *hprt1* – gaccggttctgtcatgtcg/acctggttcatcatcactaatcac; *pgk1* – ccagataacgaataaccaaagga/gacttggctccattgtcca; *gapdh* – agctggtcatcaatgggaaa/ atttgatgttagcgggatcg; *g6pdh* – ttatcatcatgggtgcatcg/aaggtgtcttcgggtagaagg; *gusb* – ctctggtggccttacctgat/cagactcaggtgttgtcatcg; *tbp* – cccaccagcagttcagtagc/ cccaccagcagttcagtagc; RNA - tgcaagccaattcccgaag/ ccattgtagtgaacagtaggac and Probes: *18S* - Hs99999907_s1; *acaca* – Rn00573474_m1; *acacb* - Rn00588290_m1; *fasn* - Rn00569117_m1; *gfpt1* - Rn01765492_m1; *gpam* - Rn00568620_m1, *hmgcr* - Rn00565598_m1, *ldlr* -

Rn00598442_m1, *srebf1* - Rn01495769_m1; *srebf2* - Rn01502638_m1) (Life Technologies, Grand Island NY; Roche, Indianapolis IN; Thermo Scientific, Waltham MA).

Reactions were run on the LightCycler ® 480 qPCR instrument (Roche, Indianapolis IN). Relative quantification was calculated using the ΔC_q method corrected for amplicon efficiencies (range = 1.9 – 2.1). Reference gene fitness was determined by measuring a panel of genes: *18s*, *Actb*, *G6pdh*, *Gapdh*, *Hprt1*, *Pgk1*, and *Tbp*. The most stable genes across the three conditions for each tissue was determined using the NormFinder algorithm [30,31]; subsequently, the GeNorm algorithm [30,31] was used to calculate the number of reference genes needed to maximize stability. For liver tissue, three reference genes were utilized (*G6pdh*, *Hprt*, *Pgk1*- variation (V) = 0.3; and *18s*, *Tbp*, *Gapdh* - V = 0.1, respectively). For heart tissue, four reference genes were used (*18s*, *G6pdh*, *Hprt1*, *Tbp* - V = 0.4). Relative target gene expression levels were determined using the ΔC_q method followed by reference gene normalization as described [31].

Western blotting

Total protein was extracted from heart and liver tissue samples as described previously [32], while nuclear protein extraction was performed using the high-salt extraction method [33]. Protein concentrations for total and nuclear lysates were determined by the Lowry method. Target proteins included: cytosolic and nuclear SREBP-1, AMP-activated protein kinase (AMPK) and phosphorylated AMPK, peroxisome proliferator-activator gamma, coactivator 1 alpha (PGC-1α), sarcoplasmic/endoplasmic calcium ATPase (SERCA-2a), phospholamban (PLB) and phosphorylated PLB, calmodulin, calcineurin, calmodulin kinase II (CaMKII), nuclear factor of activated T-cells 3 (NFAT3), nuclear respiratory factor 1 (NRF1), mitochondrial transcription factor A (mtTFA), and connexin 43 (Cx43).

Briefly, 20 µg protein was loaded onto a pre-cast gel (BioRad Laboratories, Hercules CA) and run at 250 mV until adequate separation of proteins occurred with the aid of a pre-stained marker. Protein was then transferred using a semi-dry turbo transfer system (BioRad Laboratories, Hercules CA) at 25 mV, 2.5 amps for 7 min and polyvinylidene fluoride (PVDF) membrane. The membrane was subsequently blocked with 1% milk in Tris-buffered saline with Tween 20 (TBS-T), washed in TBS-T and incubated in primary antibody overnight for the following proteins:

- SREBP-1 (anti-rabbit SREBP-1 at 1:1,000, Santa Cruz Biotechnologies CA)
- AMPKα (anti-rabbit AMPKα at 1:1,000; Cell Signaling, Danvers MA), phosphorylated AMPKα (anti-rabbit pAMPKα at 1:1,000; Cell Signaling, Danvers MA)
- PGC-1α (anti-rabbit PGC-1α at 1:1,000, Cell Signaling, Danvers MA)
- SERCA-2a (anti-sheep SERCA-2a at 1:1,000, Abcam, Cambridge MA)
- PLB (anti-rabbit PLB at 1:1,000, Santa Cruz Biotechnologies, CA), phosphorylated PLB (anti-rabbit pPLB at 1:1,000, Santa Cruz Biotechnologies, CA)
- Calmodulin (anti-rabbit calmodulin at 1:1,000, Cell Signaling, Danvers MA)
- Calcineurin (anti-rabbit calcineurin at 1:1,000, Cell Signaling, Danvers MA)
- Phosphorylated CaMKII (anti-rabbit pCaMKII at 1:1,000, Cell Signaling, Danvers MA)
- NFAT3 (anti-mouse NFAT-c4 at 1:1,000, Santa Cruz Biotechnologies, CA)
- NRF1 (anti-rabbit NRF-1 at 1:1,000, Santa Cruz Biotechnologies, CA)
- mtTFA (anti-mouse mtTFA at 1:1,000, Santa Cruz Biotechnologies, CA)
- Cx43 (anti-mouse Connexin 43 at 1:1,000, Santa Cruz Biotechnologies, CA)

Appropriate secondary antibody (anti-rabbit/mouse/sheep) was used between 1:2,000 and 1:4,000 dilution for all blots. Visualization and detection of protein expression were performed with enhanced

chemiluminescence (ECL). Briefly, the horseradish peroxidase (HRP) linked to the secondary antibody catalyzes the conversion of luminol to 3-aminophthalae which is detected via emission of light at 428 nm. This signal is then detected via a digital camera after exposing the membrane to luminol and converted into a digital image on a computer. Protein detection was performed using standard methods [32] where expression was determined by the adjusted percentage volume (intensity units of pixels of band x mm^2) after background subtraction and normalized to β–actin (anti-rabbit β-actin at 1:1,000; Cell Signaling, Danvers MA) or Ponceau stain (Ponceau S Red stain, Sigma Aldrich, St. Louis MO) to correct for variations in loading (Quantity One Software v.4.6.9, BioRad Laboratories, Hercules CA). Thereafter, the average adjusted percentage volume of the sham group was calculated by the software and subsequently represented as 100% separately (sham values were represented as a percentage of the average). Values obtained for vehicle and PI were also expressed as a percentage of the average of the sham. This was done for each gel (separately) before all values were combined in the statistical program and presented as percentage of the control. Histone H3 was initially utilized for nuclear protein loading control, but yielded too much variation (though not significant, $p>0.05$) to be used effectively and indicated that this protein might be post-translationally modified via the PI treatment as it is monitored via the UPS [34]. Since Ponceau stain yielded similar results for cytosolic and nuclear (in terms of low variability), all subsequent membranes for the different cellular fractions were stained with Ponceau Red (**Fig. 1**). Initial data accumulation utilized β–actin normalization, whereas later on Ponceau Red stain was used. Both normalizations are indicated for the specific gels in the Results section.

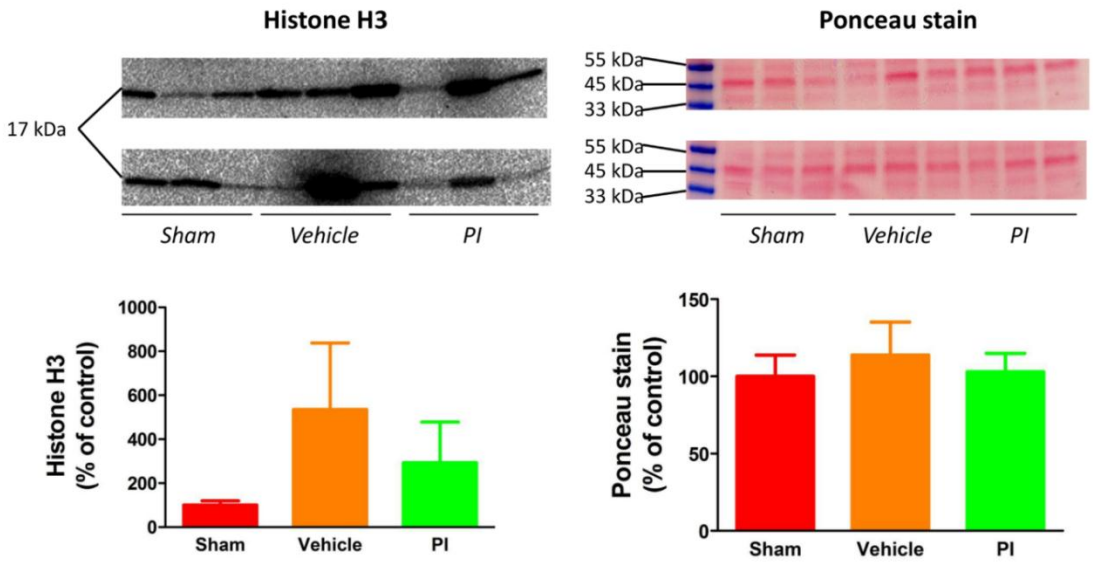

Figure 1. Different methods of normalizing nuclear extracts in heart tissue (n=6). Both Histone H3 antibody and Ponceau Red stain were used to provide a normalizing control for nuclear extracts. Histone H3 blots reveal more variation between groups than with the Ponceau stain, though neither attains significance. Data presented as mean ± SEM. *PI – protease inhibitor.*

Proteasome activity

Cardiac chymotrypsin-like, trypsin-like, and caspase-like activities of the proteasome were assayed in collaboration with Professor Emmanuel Bourdon (University of La Reunion, France) using fluorogenic peptides (Sigma-Aldrich, St Louis MO): Suc-Leu-Leu-Val-Tyr-7-amido-4-methylcoumarin (LLVY-MCA at 25 µM), N-t-Boc-Leu-Ser-Thr-Arg-7-amido-4-methylcoumarin (LSTR-MCA at 40 µM) and N-Cbz-Leu-Leu-Glu-b-naphthylamide (LLE-NA at 150 µM), respectively, as described before by us [35].

Specific activity of ATPase

ATP synthase specific activity (Abcam, Cambridge MA) in heart tissue was determined according to the manufacturer's instructions. Briefly, ATP synthase was immunocaptured via monoclonal antibody precoated ELISA plates and activity measured as decreased NADH absorbance (oxidation to NAD^+) at 340 nm. The quantity was measured via coupling of a Complex V antibody

conjugated to alkaline phosphatase and measured as increased color development at 405 nm. ATP content was determined as the amount of luciferase produced in proportion to the amount of ATP at 560 nm (FL_x800 Fluorometer, Bio-tek Instruments Inc, Winooski VT) and expressed as relative fluorescent units (RFU).

ATP content

ATP content in heart samples were measured using a commercial kit (Enlighten® ATP Assay System Bioluminescence Detection Kit, Promega, Madison WI). Briefly, the quantity of ATP was measured via the following reaction:

$$\text{ATP} + \text{D-Luciferin} + O_2 \rightarrow \text{Oxyluciferin} + \text{AMP} + \text{PPi} + CO_2 + \text{Light}$$

This light-emitting reaction is measured at 560 nm spectrophotometrically (Cecil CE2021 spectrophotometer, Cecil Instruments, Cambridge, UK) with light emitted proportional to the ATP concentration within the sample. ATP concentration was expressed as percentage change versus the sham.

Calcium content

The calcium content of the myocardium was determined colorimetrically (Calcium Detection kit, Abcam, Cambridge MA). Briefly, heart lysate up to 50 µL was added to a 96-well microplate and the chromogenic agent 0-cresolphthalein added to the wells with gentle mixing. A chromogenic complex is then formed with the calcium ions present within the samples. Assay buffer was the added and samples allowed to incubate briefly and subsequently analyzed spectrophotometrically at 575 nm (Cecil CE2021 spectrophotometer, Cecil Instruments, Cambridge, UK). Concentrations were

extrapolated from a standard curve and normalized to the volume of lysate added and expressed as mg/dL. The physiologically acceptable range of calcium is 0.4-100 mg/dL (0.1-25 mM).

Superoxide concentration

Superoxide levels were evaluated by homogenizing cardiac tissue in 10 volumes of 10% perchloric acid and centrifuged at 3000 x *g* for 20 min (Spectrofuge 24D microcentrifuge, Labnet International Inc., Edison NJ). Subsequently 100 µL of protein-free supernatant was incubated with 50 µL of 0.25 mM lucigenin in a white-walled 96-well plate for 5 min at room temperature. Chemiluminescence was detected at 430 nm / 452 nm and expressed as RFU x10^6 per mg tissue with a fluorometer (FL_x800 Fluorometer, Bio-tek Instruments Inc, Winooski VT).

SOD determination

SOD (Enzo Life Sciences, Farmingdale NY) activity was measured in total myocardial protein lysates and mitochondrial preparations (prepared according to Boudina *et al* [36]) as detailed in the manufacturer's instructions. Briefly, xanthine and oxygen are converted to uric acid and H_2O_2 by the addition of xanthine oxidase XO. The superoxide anion produced converts WST-1 to WST-1 formazan, which may be detected colorimetrically at 450 nm (Cecil CE2021 spectrophotometer, Cecil Instruments, Cambridge, UK). The addition of SOD will reduce the superoxide anion concentration and decrease the rate of WST-1 formazan formation, thereby indicating the activity of SOD. SOD activity is calculated as the amount of present in the extract that incurs 50% inhibition of the reaction as units/µL.

Glutathione determination

Total, free and oxidized glutathione levels were determined colorimetrically at 405 nm (Cecil CE2021 spectrophotometer, Cecil Instruments, Cambridge, UK) with a probe that reacts with the free

thiol group on glutathione (GSH) (Arbor Assays, Ann Arbor MI). Samples were treated with 2-vinylpyridine blocked free glutathione to allow for the measurement of oxidized and total glutathione. Concentration was extrapolated from a standard curve and expressed as percentage of control (sham).

Carbonylation content

Protein carbonyls are formed by a variety of oxidative mechanisms and are sensitive indices of oxidative injury. Protein carbonylation in heart tissue was determined by the carbonyl ELISA assay developed in the GEICO laboratory (Université de La Réunion, Saint Denis de La Réunion, France) based on recognition of protein-bound dinitrophenolhydrazine (DNPH) in carbonylated proteins with an anti-DNP antibody [37].

Here 5 µL of protein from heart tissue lysates (0.2-0.6 µg) was denatured by adding 10 µL 12% sodium dodecyl sulphate (SDS) solution. Subsequently, proteins were derivatized to DNP hydrazone with 10 µL of DNPH solution (10 mM in 6 M guanidine hydrochloride, 0.5 M potassium phosphate buffer, pH 2.5). DNPH is a chemical compound that specifically reacts and binds to carbonylated proteins. Samples were incubated at room temperature for 30 min and the reaction was neutralized and diluted in coating buffer (10 mM sodium carbonate buffer, pH 9.6) to yield a final protein concentration of 0.2 - 0.6 ng/µL.

Diluted samples were added to wells of a Nunc Immuno Plate Maxisorp (Dutscher, Brumath, France) and incubated at 37°C for 3 hrs, and thereafter washed 5x with phosphate-buffered saline with Twee-20 (PBS-T, 0.1%) between each of the following steps: blocking the wells with 1% BSA in PBS-T overnight at 4°C; incubation with anti-DNP antibody (Sigma-Aldrich, St Louis MO) (1:2,000 dilution in PBS-T [0.1%]/BSA [1%]) at 37°C for 3 hrs; incubation with HRP-conjugated polyclonal anti-

rabbit immunoglobulin (GE Healthcare, Mannheim, Germany) (1:4,000 dilution in PBS-T [0.1%]/BSA [1%]) for 1 hr at 37°C; addition of 100 µL of 3,3',5,5'-Tetramethylbenzidine (TMB) substrate solution and incubation for 10 min before stopping the coloration with 100 µL of 2 M sulphuric acid. Absorbances were read at 490 nm against the blank (DNP reagent in coating buffer without protein) with a Fluostar microplate reader (BMG Labtech, Ortenberg, Germany). Results are expressed as percentage of absorbance compared to sham values after normalization with protein concentrations.

Catalase activity

The catalase activity assay is based on the properties of catalase enzyme to reduce H_2O_2 into O_2 and water H_2O [38]. Assays were carried on about 80 µg of heart protein lysate in 25 mM Tris–HCl (pH 7.5). Blanks were measured at 240 nm just before adding 80 µL of H_2O_2 (10 mM final) to start the reaction. Catalase activity was determined by measuring the absorbance decrease of H_2O_2 at 240 nm (Cecil CE2021 spectrophotometer, Cecil Instruments, Cambridge, UK). The decomposition of H_2O_2 is a first order reaction type following H_2O_2 concentration and the rate constant K for the overall reaction is given by:

$$K = \frac{2.3}{\Delta t} * \log(\frac{DO_{zero}}{DO_t})$$

Each measurement was considered with 4 replicates and data are expressed as catalytic unit (U) per mg of total protein.

Statistical analyses

One-way ANOVA was performed for all experimental groups with a Bonferroni *post-hoc* test to compare differences between groups. Significance is indicated on graphs when $p<0.05$ and results are expressed as mean ± SEM. Where applicable, if significance was only obtained versus sham in relation

to PI treatment, but not to vehicle; data were then re-analyzed and the vehicle chosen to represent 100%. This ensured that all statistical data reported here are correct.

Results

Ex vivo heart function revealed that PI treatment detrimentally affects cardiac contractility at baseline (**Chapter 3**). Therefore, the aim of this study was to investigate metabolic, contractile and calcium-related markers to investigate underlying molecular mechanisms.

Histological analyses of a variety of tissues, including cardiac tissues, indicated no evidence of abnormal growth or ultrastructure (**Fig. 2**) between the treatment groups. Fibrosis was not found in any of the tissues when assessed via Sirius red staining (data not shown).

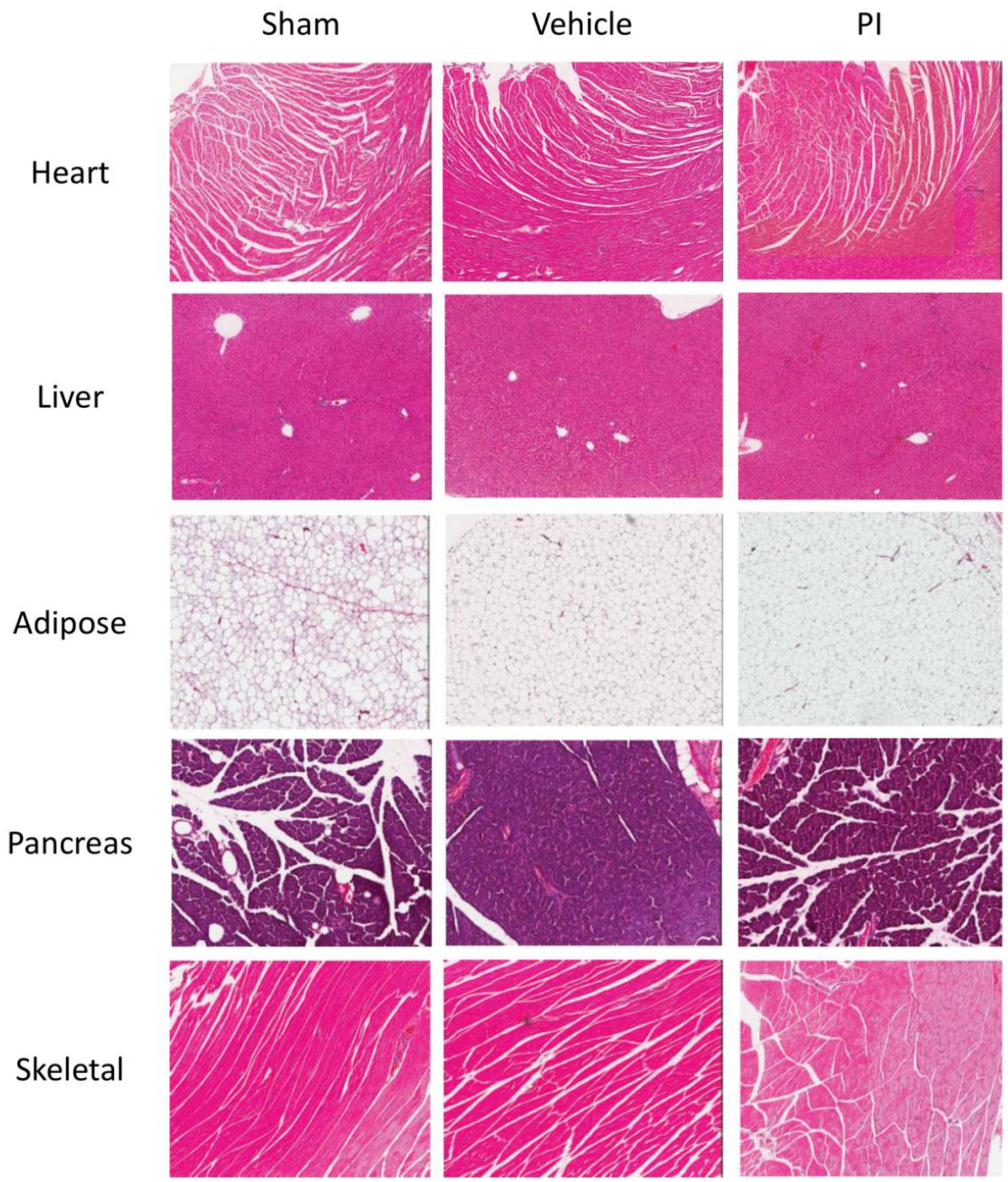

Figure 2. Histological analyses of 8 weeks PI therapy in multiple organs (n=3). Sections are 4-5µm (x100 magnification) and each image is representative of the group. *PI – protease inhibitor.*

Next, cholesterol content in two highly metabolically active tissues, i.e. heart and liver, was assessed. No significant alterations to total cholesterol and LDL/VLDL cholesterol content was found in cardiac tissues ($p>0.05$ vs. matched controls) (**Fig. 3, top panel**). Interestingly, myocardial HDL-cholesterol was significantly elevated with 8 weeks of chronic PI therapy (0.316 ± 0.025 vs. sham 0.240 mmol/L ± 0.008, $p<0.01$; vs. vehicle 0.242 mmol/L ± 0.004, $p<0.01$). Hepatic tissue displayed a notable increase in the TG content (0.618 ± 0.036 vs. sham 0.478 mmol/L ± 0.024, $p<0.05$; vs. vehicle 0.431 mmol/L ± 0.026, $p<0.01$) (**Fig. 3, lower panel**).

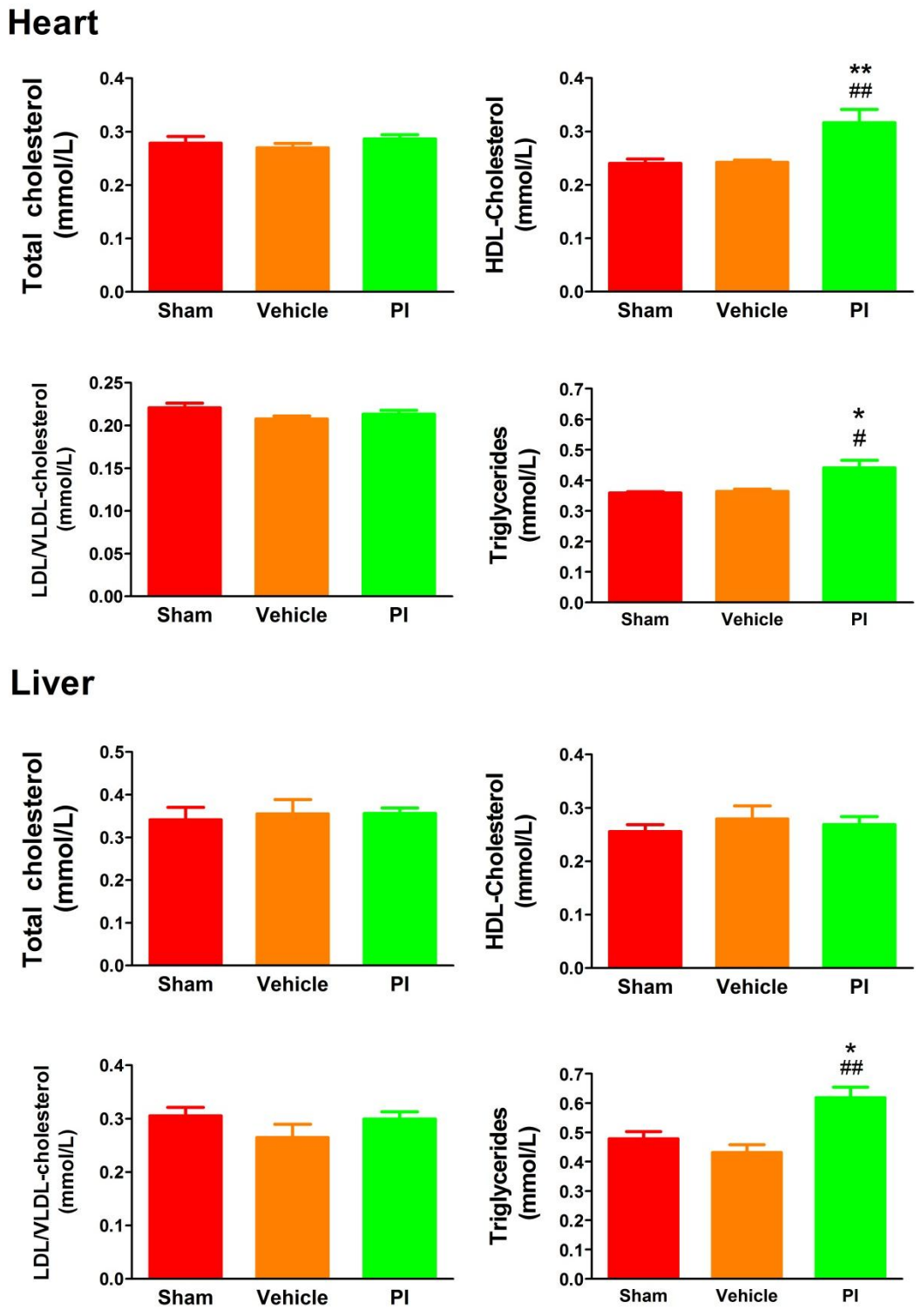

Figure 3. Heart and liver lipid profile in response to 8 weeks PI treatment (n=8). Data are presented as mean ± SEM. *p<0.05, **p<0.01 vs. sham; #p<0.05, ##p<0.01 vs. vehicle. *HDL – high-density lipoprotein, LDL/VLDL – low-density/very low-density lipoprotein, PI – protease inhibitor.*

To determine mechanisms responsible for early metabolic changes, we evaluated lipid and cholesterogenic genes in heart and liver tissues. Here PI treatment enhanced cardiac *gpam* expression (p<0.001 vs. sham), although this was not significant vs. vehicle-treated rats. However, hepatic *accβ* and *hmgcr* gene mRNA expression were upregulated in the PI group (p<0.05) (**Fig. 4**).

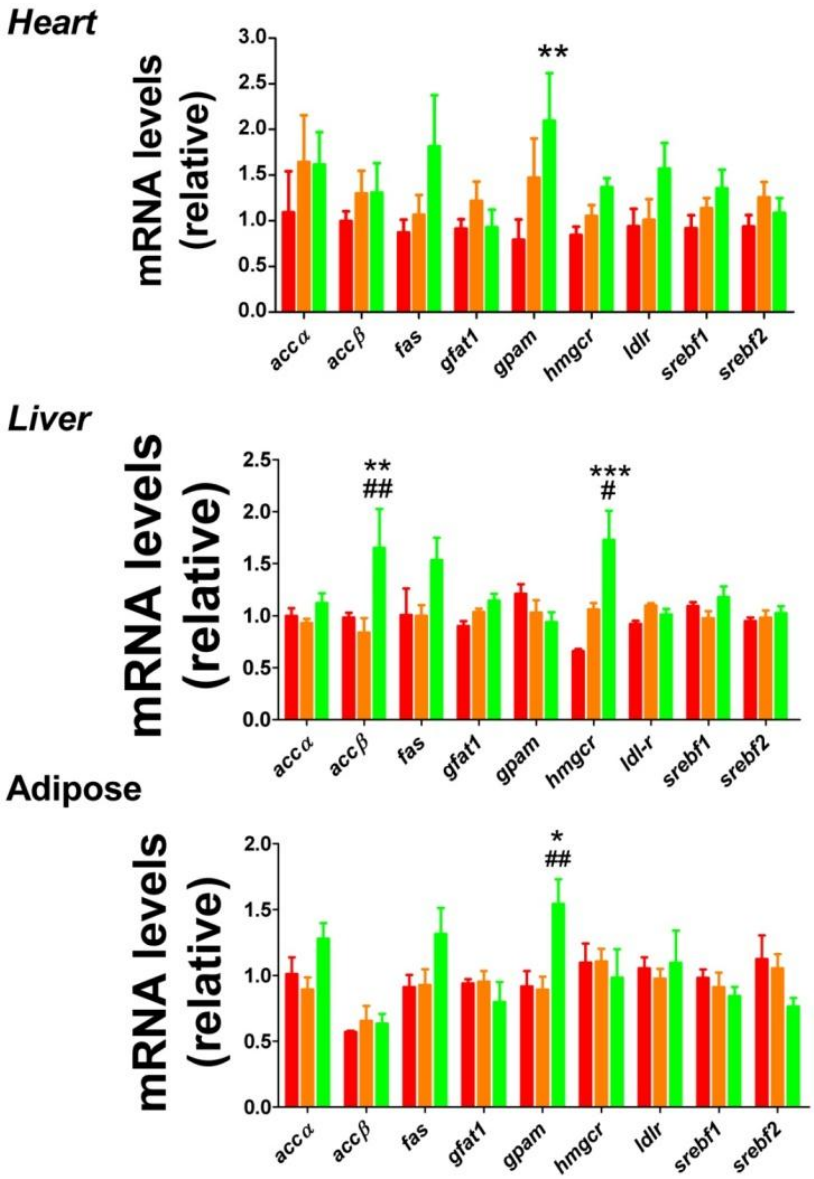

Figure 4. Gene profile at baseline (n=8). Metabolic genes assessed via RT-PCR in response to 8 weeks PI treatment. Data presented as mean ± SEM. *p<0.05, **p<0.01, ***p<0.001 vs. sham; #p<0.05, ##p<0.01 vs. vehicle. *acc – acetyl coA carboxylase, fas – fatty acid synthase, gfat – glutamine fructose-6-phosphate amidotransferase, gpam - glycerol-3-phosphate acyltransferase (mitochondrial), hmgcr – hydroxyl-3-methyl-glutaryl-coA reductase, ldlr – low-density lipoprotein receptor, PI – protease inhibitor, srebf – sterol regulatory element binding factor.*

Since our gene data point towards a molecular effect of PIs, we assessed protein levels of the sterol sensor, SREBP-1. Here the data showed no significant alterations within neither cytosolic nor nuclear compartments in terms of peptide expression (p>0.05 vs. sham and vehicle) (**Fig. 5**). Due to time differences in analysis of blots, cSREBP-1 was normalized to β-actin, while nSREBP-1 (completed at a later stage) was normalized to Ponceau S Red stain.

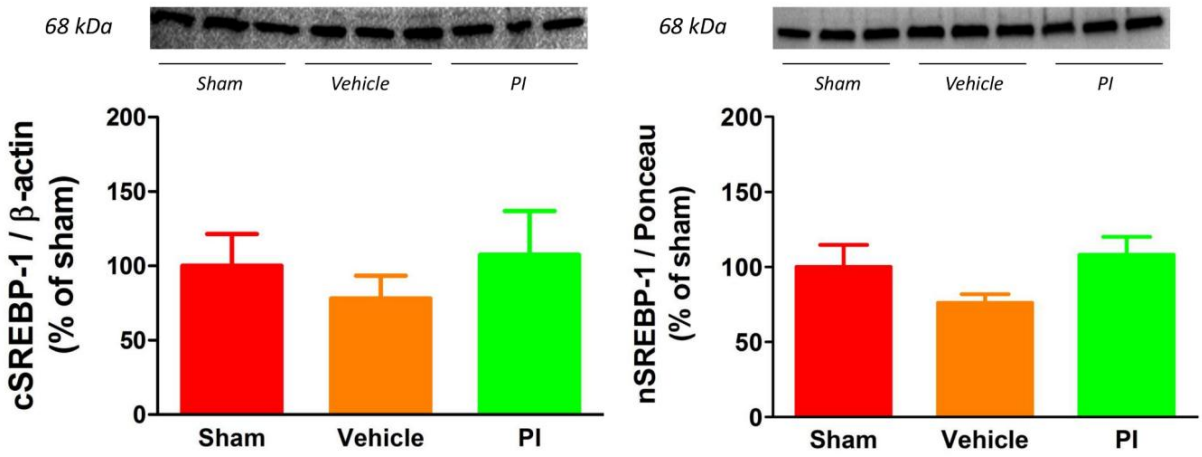

Figure 5. Expression of SREBP-1 at baseline in response to 8 weeks PI treatment (n=6-8). The activated form of SREBP-1 occurs at 68kDa. Data presented as mean ± SEM, and blot images are representative of the group. cSREBP was normalized to β-actin and nSREBP-1 to Ponceau S Red stain (refer to text for explanation). *cSREBP-1 – cytosolic, nSREBP-1 – nuclear, PI – protease inhibitor, SREBP – sterol regulatory element binding protein.*

Since energy homeostasis plays a critical role in heart function, we also evaluated myocardial ATP levels, AMPK expression and ATPase activity. Myocardial ATP content remained unchanged in response to 8 weeks PI therapy as did the expression of AMPK and phosphorylated AMPK (p>0.05 vs. matched controls) (**Fig. 6**).

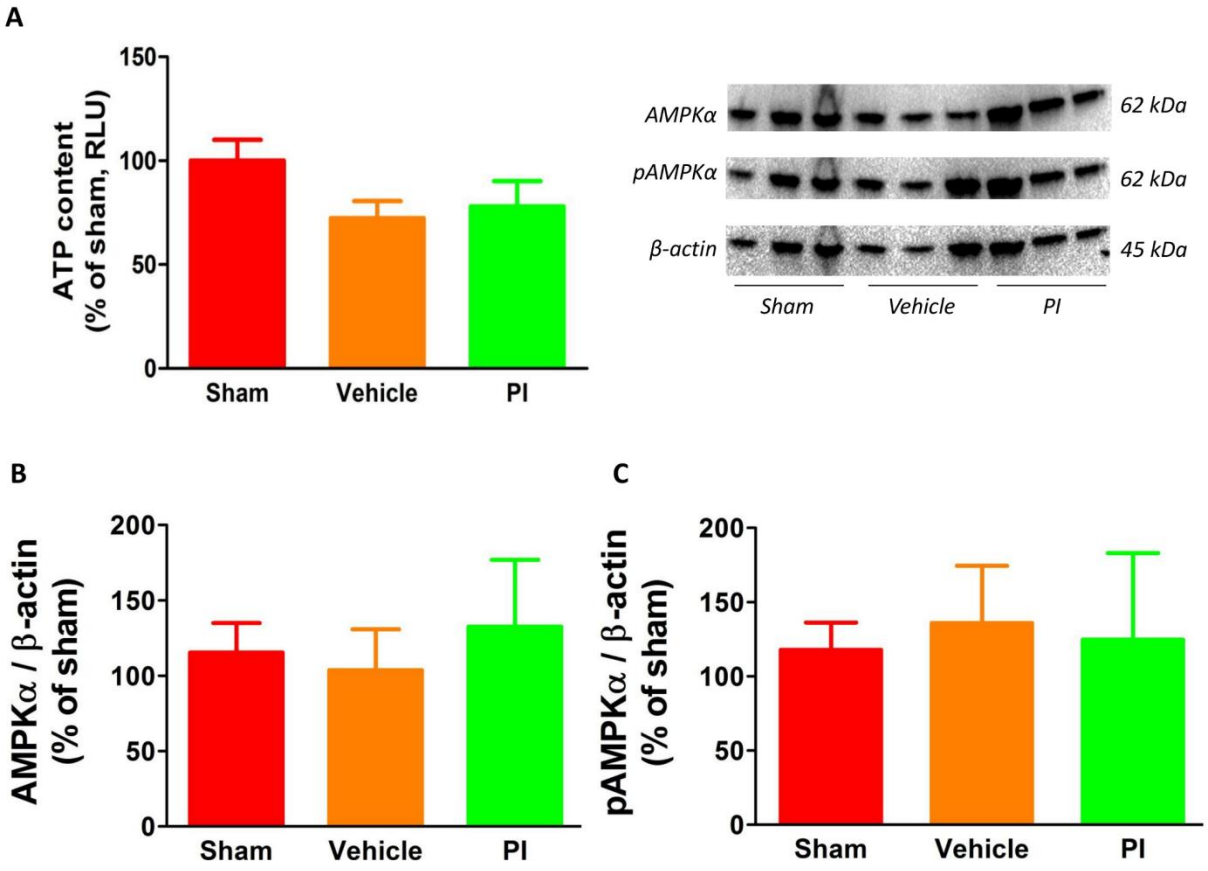

Figure 6. ATP content and AMPKα expression in response to 8 weeks PI therapy (n=6-8). A) Cardiac ATP content; B) AMPKα; and C) Phosphorylated AMPKα expression. Representative blots are shown in the top right corner. Data presented as mean ± SEM, and blot images are representative of the group and all blots are normalized to β-actin. *AMPK – AMP-activated protein kinase, ATP – 5'-adenosine triphosphate , PI – protease inhibitor.*

ATPase activity, expressed as the ratio of activity versus quantity, was not significantly altered in PI-treated hearts (**Fig. 7**).

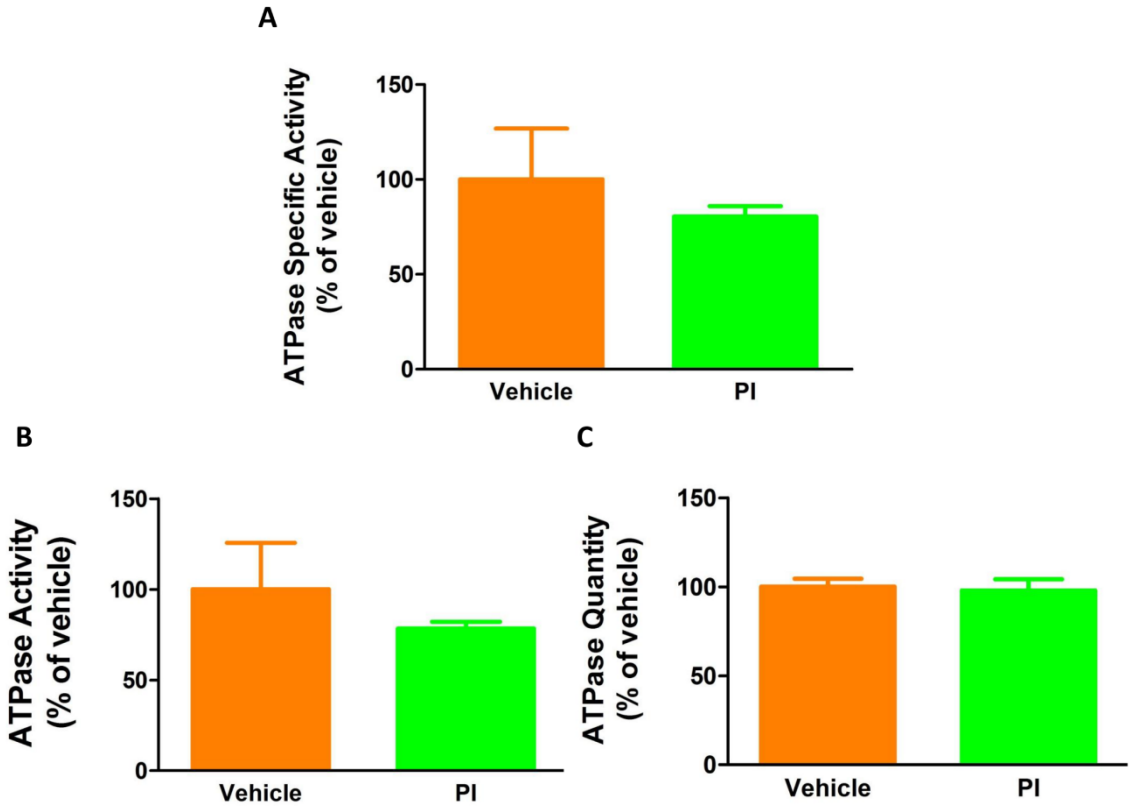

Figure 7. Cardiac ATPase specific activity at baseline (n=8). A) ATPase specific activity (a ratio of the activity versus quantity); B) ATPase activity; and C) ATPase quantity. Data presented as mean ± SEM. Vehicle is considered 100% (*see Methods and text for explanation*). *ATPase – 5'-adenosine triphosphate synthase, PI – protease inhibitor.*

We next evaluated the effects of PI treatment on the cardiac UPS system and our data demonstrate lowered chymotrypsin-like and caspase-like, but not trypsin-like proteasomal activities ($p<0.05$) (**Fig. 8**). In parallel, global ubiquitination of cytosolic proteins increased more than 2-fold with PI administration ($p<0.05$ vs. sham and vehicle) (**Fig. 9**).

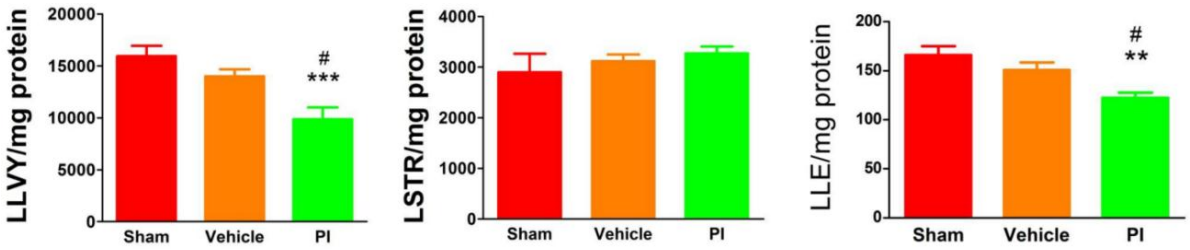

Fig 8. Proteasomal activity following 8 weeks PI treatment (n=8). LLVY (chymotrypsin-like activity), LSTR (trypsin-like activity), and LLE (caspase-like activity) of the proteasome. Data presented as mean ± SEM. **$p<0.01$, ***$p<0.001$ vs. sham; #$p<0.05$ vs. vehicle. *PI – protease inhibitor.*

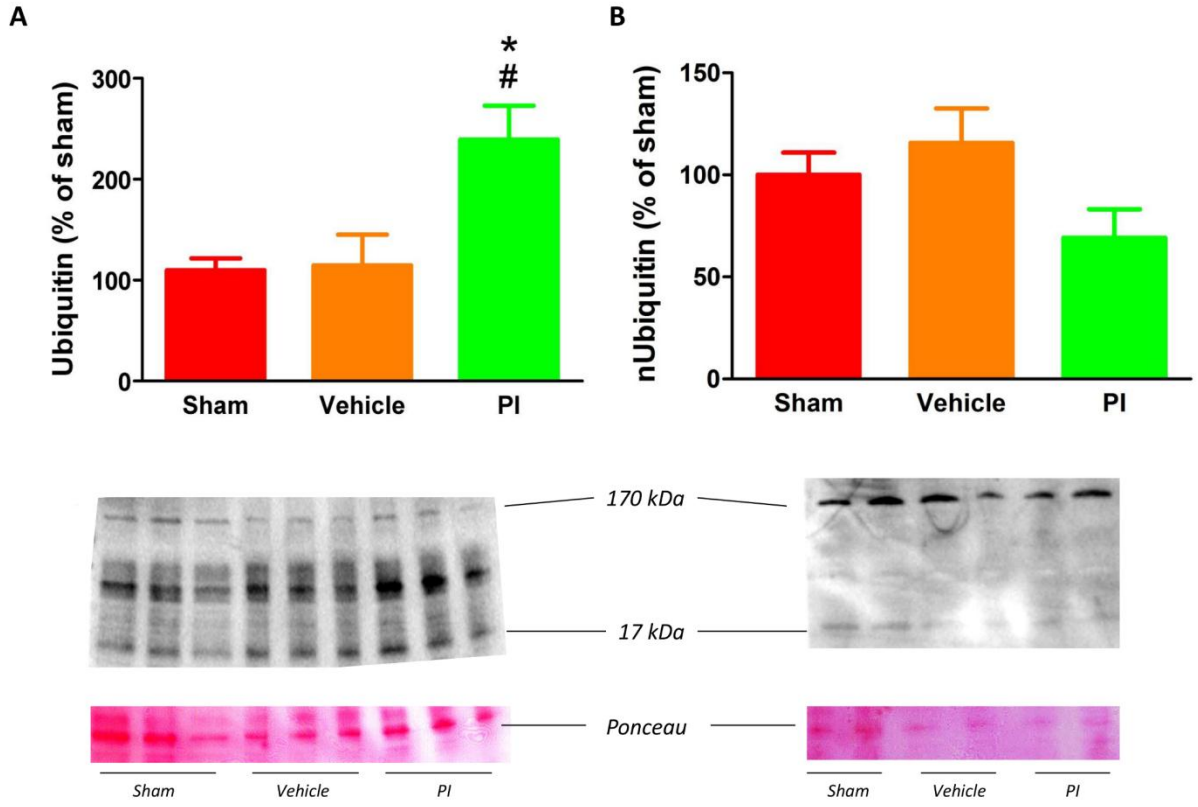

Fig 9. Global ubiquitination of cytosolic and nuclear proteins in response to PI therapy (n=5-8). Ubiquitination determined per lane (between 17 and 170 kDa) and expressed as global ubiquitination. Data presented as mean ± SEM, and blot images are representative of the group. All blots are normalized to Ponceau S stain. *p<0.05 vs. sham; #p<0.05 vs. vehicle. *nUbiquitin – nuclear ubiquitination*, *PI – protease inhibitor.*

To gain additional insight regarding PI-mediated contractile dysfunction, markers regulating ion channel homeostasis, electrical conductance and protein degradation were investigated. Here myocardial expression of the gap junction protein Cx43 (marker for electrical conductance), SERCA-2a (cardiac calcium transporter) and pPLB (SERCA-2a regulator) increased with PI treatment ($p<0.05$) (**Fig. 10**).

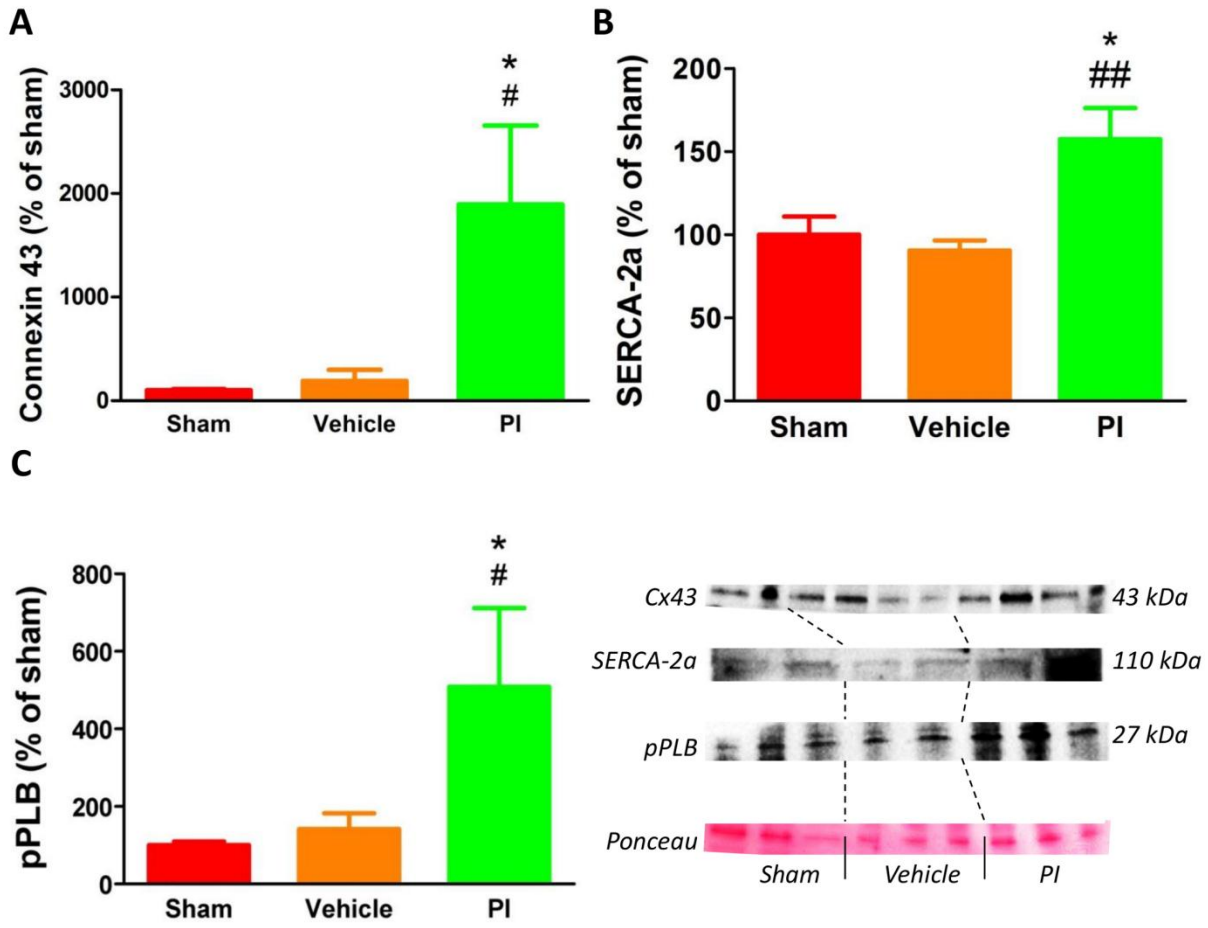

Fig 10. Protein expression of contractile regulators following PI treatment (n=6-8). A) Connexin 43; B) SERCA-2a; and C) Phosphorylated PLB. *$p<0.05$ vs. sham; #$p<0.05$, ##$p<0.01$ vs. vehicle. Data presented as mean ± SEM, and blot images are representative of the group. Blots normalized to Ponceau S stain. *pPLB – phosphorylated phospholamban, PI – protease inhibitor, SERCA – sarcoplasmic/endoplasmic reticulum calcium ATPase.*

We next assessed calcium and mitochondrial energetic signaling markers and found that myocardial calcium content was below the homeostatic range of 0.4 mg/dL with chronic PI therapy (0.165 ± 0.026 vs. sham 0.599 mg/dL ± 0.150, $p>0.05$; vs. vehicle 0.456 mg/dL ± 0.190, $p>0.05$) (**Fig. 11A**). PIs also significantly downregulated the expression of the calcium-binding protein calmodulin (**Fig. 11B**), while calcineurin within the cytosolic - but not nuclear - compartment was upregulated (**Fig. 11C, D**). However, pCaMKII levels remained unchanged while dephosphorylated nuclear NFAT3 expression (140 kilodaltons [kDa]) increased versus controls ($p<0.05$ vs. sham and vehicle) (**Fig. 11E, F**). The hyperphosphorylated form of NFAT3 (160 kDa) was undetectable in nuclear samples.

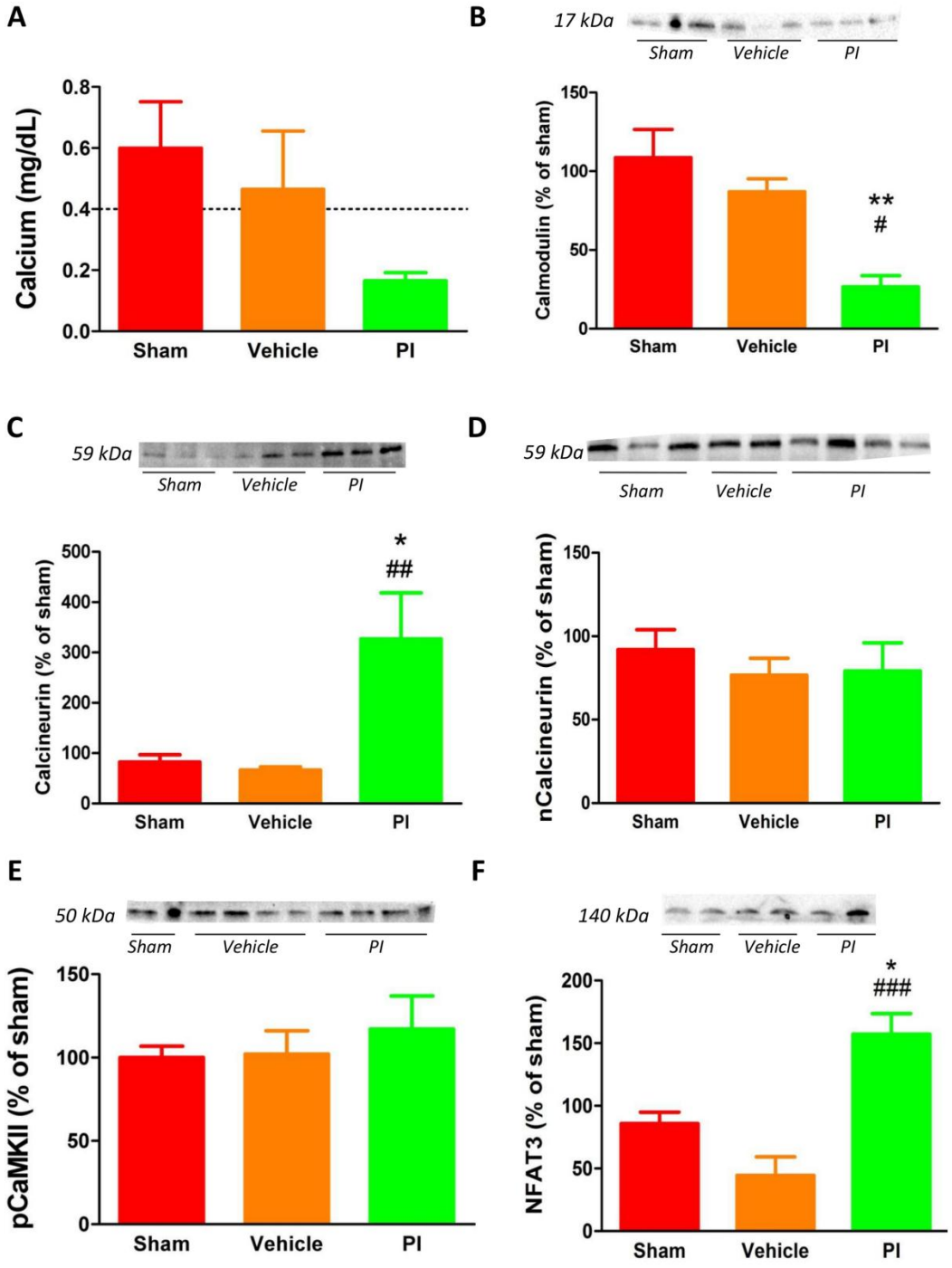

Fig 11. Calcium pathway protein expression in response to PI therapy (n=6-8). A) Calcium content; B) Calmodulin; C) Cytosolic calcineurin; D) Nuclear calcineurin; E) pCaMKII; and F) Dephosphorylated nuclear NFAT3. Data presented as mean ± SEM, and blot images are representative of the group. Blots are normalized to Ponceau S stain (not shown). *p<0.05, **p<0.01 vs. sham; #p<0.05, ##p<0.01 vs. vehicle. *NFAT3 – nuclear factor of activated T-cells 3, pCaMKII – phosphorylated CaMKII, PI – protease inhibitor.*

The expression of PGC-1α was significantly upregulated in PI-treated heart tissue (**Fig. 12A**) while no changes were found for mitochondrial biogenesis markers (mtTFA, NRF-1) (**Fig. 12B, C**).

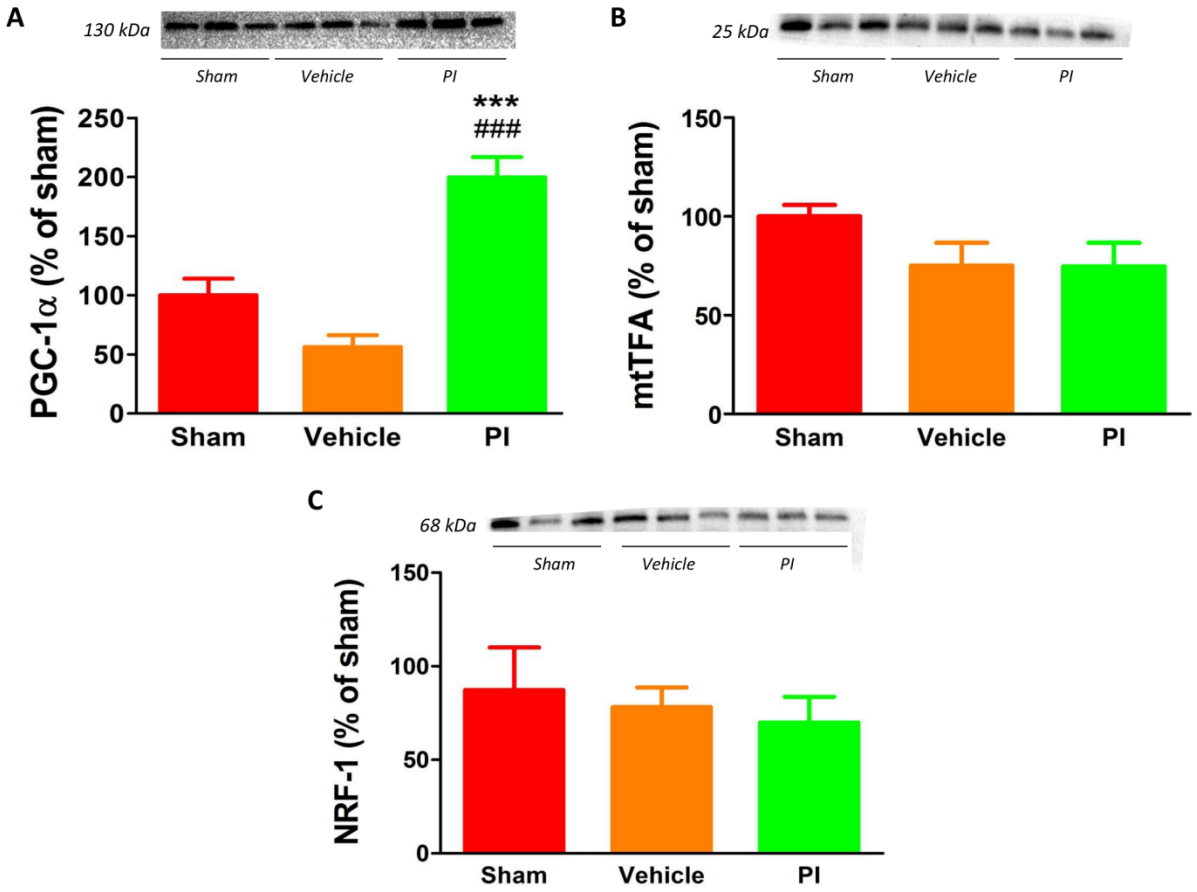

Figure 12. PGC-1α pathway protein expression in response to 8 weeks PI treatment (n=6-8). A) PGC-1α; B) mtTFA; and C) NRF-1. Data presented as mean ± SEM, and blot images are representative of the group. Blots are normalized to Ponceau S stain (not shown). ***p<0.001 vs. sham, ###p<0.001 vs. vehicle. *mtTFA – mitochondrial transcription factor A, NRF – nuclear respiratory factor, PGC-1α – peroxisome proliferator-activator receptor gamma, coactivator 1 alpha, PI – protease inhibitor.*

Markers of the redox system were next evaluated as we hypothesized that PI therapy can detrimentally alter the redox status within the heart. Myocardial SOD activity measured in both cytosolic and mitochondrial fractions were robustly increased with PI treatment versus matched controls ($p<0.001$) (**Fig. 13A, B**). Superoxide production, however, did not follow the same relationship and was not significantly altered with PI therapy ($p>0.05$ vs. sham and vehicle) (**Fig. 13C**). Myocardial superoxide production was unaltered after 8 weeks of PI therapy.

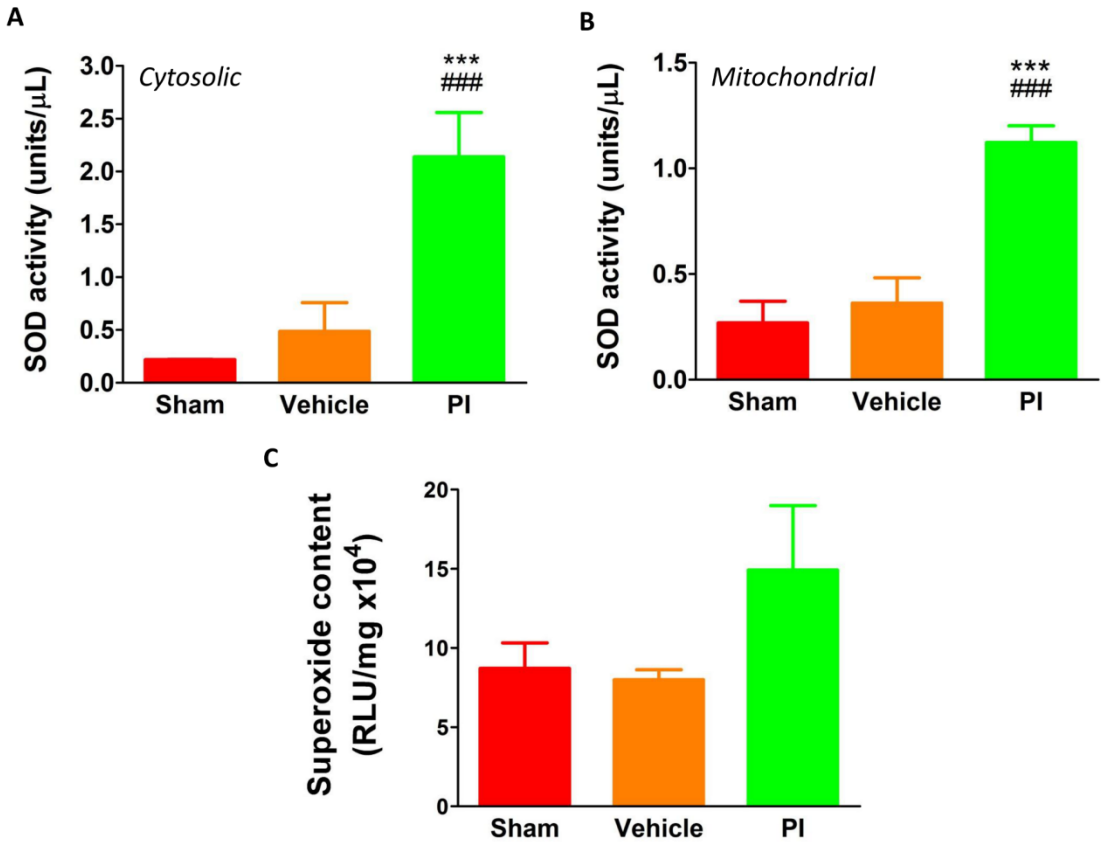

Figure 13. Baseline myocardial SOD activity and superoxide production in response to 8 weeks PI treatment (n=8). A) Cytosolic; and B) Mitochondrial SOD activity; C) Superoxide content. Data presented as mean ± SEM. ***$p<0.001$ vs. sham, ###$p<0.001$ vs. vehicle. *PI – protease inhibitor, SOD – superoxide dismutase.*

Further investigation into redox pathways such as glutathione revealed a similar relationship in that no alterations were apparent after 8 weeks of PI therapy. Here, oxidized glutathione (GSSG), total reduced and free glutathione (GSH) as well as the ratio (GSH/GSSG) were not significantly different in PI-treated hearts versus matched controls (p>0.05) (**Fig. 14**). The carbonylation content of myocardial proteins as well as catalase activity did not differ for any of the experimental groups (p>0.05) (**Fig. 15**).

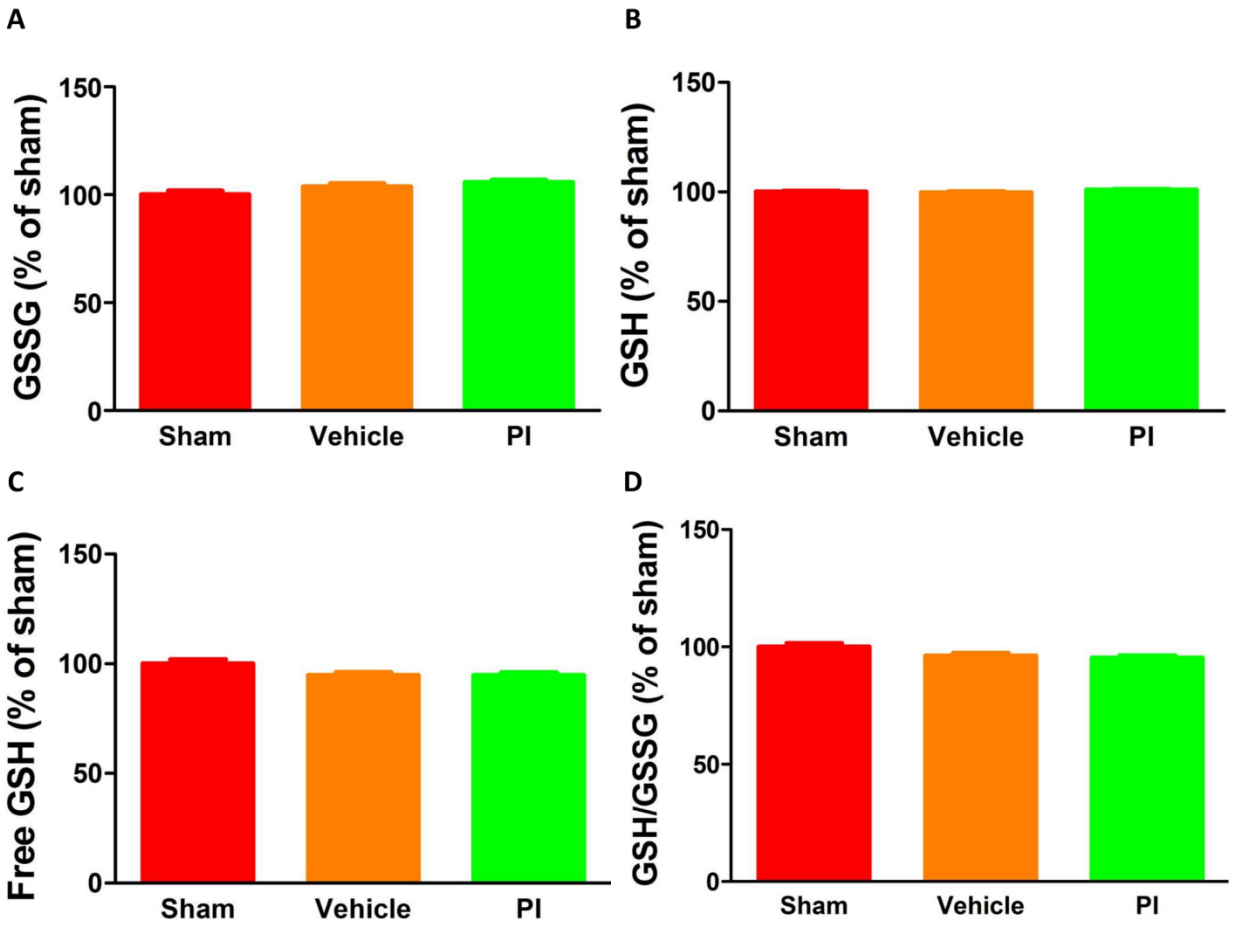

Figure 14. Glutathione levels in response to PI treatment (n=8). A) Oxidized glutathione (GSSG); B) Reduced total glutathione (GSH); C) Free glutathione (GSH); and D) GSH/GSSG ratio. Data presented as mean ± SEM. *PI – Protease inhibitor.*

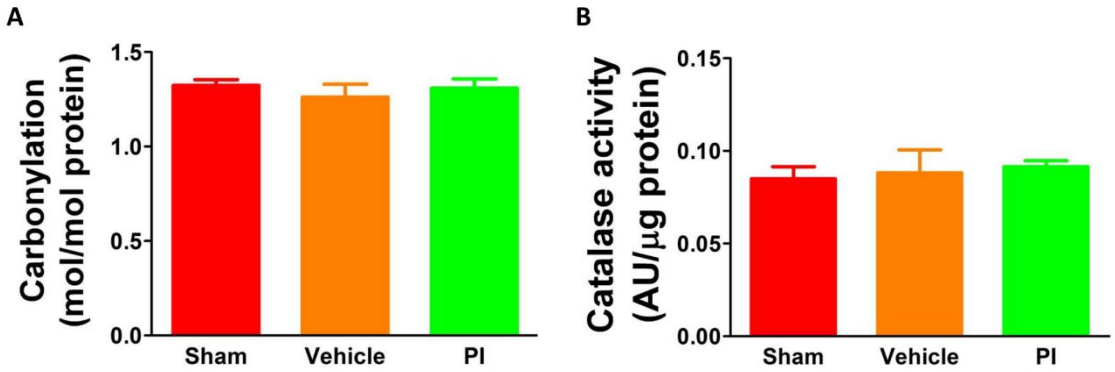

Figure 15. Carbonylation content and catalase activity in response to 8 weeks PI therapy (n=8). A) Myocardial protein carbonylation content; and B) Catalase activity. Data presented as mean ± SEM. *PI – protease inhibitor*.

Discussion

Although HAART markedly improves the quality of life and prognosis of HIV-infected individuals, it also elicits cardio-metabolic side–effects in the long-term. Since molecular mechanisms underlying this process are poorly understood, we evaluated the early cardio-metabolic changes in a novel rat model of PI treatment. The main findings of this study are: 1) PI-treated rats exhibit lipid abnormalities; and 2) Rats exposed to PIs display altered myocardial ubiquitin proteasome and calcium-handling pathways.

PI-treated rats exhibit lipid abnormalities.

Previous studies demonstrated that a significant proportion of HAART patients develop impaired glucose tolerance, IR and T2DM [10,39]. Here our data revealed that PI-treated rats displayed weight gain together with elevated serum LDL-cholesterol (**Chapter 2**) and cardiac/hepatic tissue TG levels, identifying perturbed lipid metabolism as a relatively early occurrence. Although not focusing on initial PI-mediated changes, previous work also reported that lipid derangements are one of the commonest side-effects triggered by Lopinavir/Ritonavir usage [40]. Moreover, clinical studies indicate that altered fat partitioning (i.e. lipodystrophy) is common with PI treatment [7,41,42] compared to overt increases in weight gain, and that this occurs within the first year of therapy. Our data show that the onset of IR likely follows at a later stage in the progression of cardio-metabolic dysfunction following PI treatment. In support, the HOMA-IR assessment that is usually strongly linked to IR and T2DM, was not activated in our model (**Chapter 2**).

How exactly does PI treatment induce the changes in lipid metabolism here observed? PI treatment induced gene expression of *accβ* and *hmgcr* in the liver that would be expected to enhance FAO and cholesterol synthesis, respectively. There were also early signs of elevated cardiac *gpam* expression (although not statistically significant versus all matched controls), while it was robustly upregulated in adipose tissue. The gene expression results therefore indicate that the higher serum LDL-cholesterol levels may result from greater adipose TG synthesis and subsequent export to the liver and heart. Here increased hepatic *hmgcr* expression may enhance VLDL production and with a corresponding elevation in the availability of circulating LDL-cholesterol. Interestingly, the serum total cholesterol remained unchanged, indicating that it is unlikely at this early time point that circulating LDL-cholesterol is affected and that the changes reside at the genetic level within our model.

Since PIs may also have direct transcriptional effects that trigger gene expression, we also assessed whether SREBPs – well-known transcriptional regulators of several lipid and cholesterol synthesis genes [22] - are implicated in the observed gene induction. We found no significant differences when analyzing SREBP expression (gene and protein levels) in liver and heart tissues, and suggest that other transcriptional modulators that regulate lipid and cholesterol genes may be involved [26]. An alternate explanation may relate to the fact that that Ritonavir is a reversible and competitive inhibitor of specific 20S proteasome subunits [24]. Since the UPS also plays a key role to regulate SREBP-1 binding to target gene promoters (mediating its degradation) [26,27], lower UPS activity may lead to more SREBP-1 remaining bound to gene promoter(s). This in turn could result in greater induction of target genes, even though total SREBP expression levels were unaltered. These possibilities are currently being pursued in our laboratory.

Together our study shows that early changes induced by PI treatment resembles the MetS, a combination of risk factors that predispose to the future onset of IR, T2DM and CVD. Moreover, the higher serum LDL-cholesterol levels mirror a pre-atherogenic state that may eventually trigger the onset of various cardiac complications, e.g. acute MI.

Rats exposed to PIs display altered myocardial ubiquitin proteasome and calcium-handling pathways with decreased contractile function.

What are the underlying mechanisms whereby PI administration impairs contractile function? Our results show no significant remodeling of hearts exposed to PIs, i.e. lack of ultrastructural changes, fibrosis and cardiac hypertrophic response. We also evaluated markers for myocardial oxidative stress since others found a link between PI exposure and elevated ROS production [17–19], but found no evidence of damaging effects of myocardial oxidative stress at baseline (no changes in degree of protein carbonylation). However, PI-treated hearts exhibited augmented myocardial SOD activity suggesting that increased oxidative stress is blunted by intracellular defense systems. Thus these data indicate that harmful effects of previously reported PI-induced ROS likely occur at a later stage during the HAART regimen. In agreement, our colleague (*Ms Tarryn-Lee Fischer, MSc student at the Department of Physiological Sciences, Stellenbosch University*) established that there was no ROS-mediated induction of several non-oxidative glucose metabolic pathways in PI-treated rats [43]. Importantly, we did not differentiate between the three SOD species/isoforms that are found within the cytosol and mitochondria. Total SOD content was measured and it is assumed that the cytosolic compartment contains a greater amount of the copper/zinc SOD (Cu/Zn SOD) isoform, while the mitochondrial compartment is richer in manganese SOD (MnSOD). Thus we interpret our data

cautiously as to the relative contributions of the SOD isoforms to total SOD content and subsequent detoxification capacities.

The heart functional data (**Chapter 3**) revealed attenuated contractile function without significant alterations to heart rate. Here the ±*dP/dt* findings implicate the myocardial calcium handling pathway, as diastolic calcium is a key determinant of contractile function and calcium signaling [44]. Since PI treatment decreased and increased myocardial UPS activity and ubiquitination, respectively, this may lead to an accumulation of contractile protein aggregates and impaired cardiac contractility and signaling pathways. For example, protein turnover of Cx43, PLB and SERCA-2a are all regulated by the UPS [45–49] and may explain the higher expression levels found here and before by us [16]. This in turn may result in detrimental effects on contractile function, e.g. others established that altered Cx43 expression can precede arrhythmias, ventricular fibrillation and incorrect signal propagation in the long-term [50–55].

This data reveal that PI treatment lowers myocardial calcium levels and elevates SERCA-2a protein expression, and further attenuates and increases calmodulin and pPLB expression levels, respectively. In parallel, we found increased myocardial calcineurin and NFAT3 expression levels. Together these findings indicate that perturbed calcium handling may contribute to the PI-mediated contractile dysfunction found in our experimental model. Of note, others found that cardiac-specific calcineurin overexpression resulted in enhanced pPLB and SERCA-2a expression and diminished phosphorylation and redistribution of Cx43 [56]. This was associated with depressed contractility and cardiac hypertrophy. Here the authors proposed that Cx43 may be a downstream target of calcineurin and that attenuated Cx43 levels may be linked to perturbed gap junction assembly and arrythmogenesis [56]. We propose that a similar scenario exists in our model and that greater

calcineurin activation may be linked to elevated Cx43 expression that could compromise gap junction function and ultimately decrease cardiac output. Increased SERCA-2a and pPLB expression may occur as a result of lower myocardial UPS and have also been implicated as downstream transcriptional targets of calcineurin [56]. Thus elevated SERCA-2a and pPLB expression may represent an adaptive response by PI-treated hearts to improve calcium handling and cardiac function under these conditions (refer model proposed in **Fig. 16**). Higher calcineurin activation also leads to increased dephosphorylation and translocation of NFAT3 to the nucleus for activation of downstream targets, e.g. PGC-1α and pro-hypertrophic genes [57,58]. However, since the calcineurin-NFAT3 pathway did not result in cardiac hypertrophy in our model, we are of the opinion that longer-term activation may eventually result in a hypertrophic response.

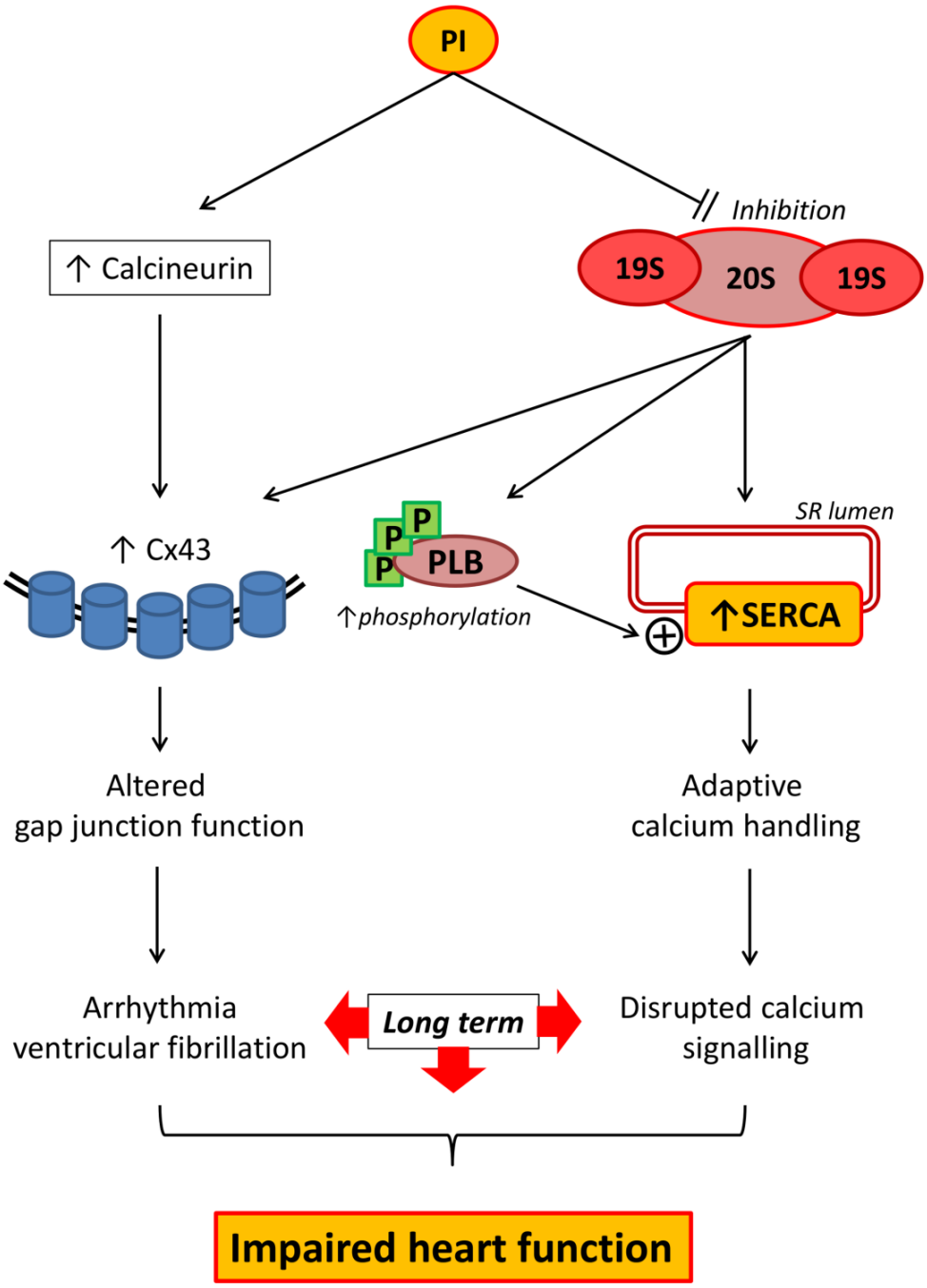

Figure 16. Model demonstrating the influence of PI therapy on calcium handling and cardiovascular dysfunction. The data show that 8 weeks of PI treatment increases calcineurin expression and inhibits proteasomal activity. Downstream targets include Cx43, PLB and SERCA-2a. Alterations to these pathways can lead to disrupted calcium signaling and impaired electrical signal propagation. Ultimately, calcium homeostasis and heart function are impaired in the long term. *Cx43 – connexin 43, P - phosphate, PLB - phospholamban, PI – protease inhibitor, SERCA – sarcoplasmic/endoplasmic reticulum calcium ATPase*.

Since myocardial PGC-1α was upregulated this implies that PIs exert initial effects at the mitochondrial level. PGC-1α is a well-described transcriptional regulator of mitochondrial biogenesis [59,60] (refer to **Fig. 7, Chapter 1)** and we propose that higher expression levels may represent an early compensatory response to energetic stress. In agreement with this notion, NRF-1 and mtTFA expression remained unaltered while we previously found no changes for myocardial ATP levels and AMPKα expression following 8 weeks of PI administration [16]. It is likely that reduced UPS activity in PI-treated hearts may contribute to the increased PGC-1α levels here observed. In support, others established that lower UPS-mediated protein turnover in fibroblasts resulted in PGC-1α stabilization and mitochondrial biogenesis [61], while it can also be rapidly degraded in the nucleus [62].

Conclusions

In conclusion, our study demonstrates that early changes triggered by PI treatment include increased body weight and serum LDL-cholesterol levels, together with decreased cardiac function. Furthermore, PI exposure inhibits the myocardial UPS and leads to elevated calcineurin and Cx43 expression that may contribute to cardiac contractile dysfunction. Thus our study alerts to cardio-metabolic side-effects of PI treatment and we propose that further clinical studies are needed to evaluate these pathways in HIV+ patients on chronic HAART.

References

1. World Health Organization *Global HIV/AIDS response. Epidemic update and health sector progress towards Universal Access. Progress Report 2011*. 23–27 (2011).

2. Armstrong, W., Calabrese, L. & Taege, A. HIV update 2005: Origins, issues, prospects, and complications. *Clev Clin J Med* **72**, 73–78 (2005).

3. Melekhin, V. V *et al.* Antiretroviral therapy initiation before, during, or after pregnancy in HIV-1-infected women: maternal virologic, immunologic, and clinical response. *PloS One* **4**, e6961 (2009).

4. Palella, F. Human immunodeficiency virus infection. *N Engl J Med* **338**, 853–860 (1998).

5. Panther, L. A. How HIV infection and its treatment affects the cardiovascular system: what is known, what is needed. *Am J Physiol Heart Circ Physiol* **283**, H1–H4 (2002).

6. Carr, A., Samaras, K., Chisholm, D. J. & Cooper, D. A. Pathogenesis of HIV-1-protease inhibitor-associated peripheral lipodystrophy, hyperlipidaemia, and insulin resistance. *Lancet* **351**, 1881–1883 (1998).

7. Carr, A. *et al.* A syndrome of peripheral lipodystrophy, hyperlipidaemia and insulin resistance in patients receiving HIV protease inhibitors. *AIDS* **12**, F51–F58 (1998).

8. Hui, D. Y. Effects of HIV protease inhibitor therapy on lipid metabolism. *Prog Lipid Res* **42**, 81–92 (2003).

9. Grinspoon, S. K. *et al.* State of the science conference: Initiative to decrease cardiovascular risk and increase quality of care for patients living with HIV/AIDS: executive summary. *Circulation* **118**, 198–210 (2008).

10. Gan, S. *et al.* Altered myocellular and abdominal fat partitioning predict disturbance in insulin action in HIV protease inhibitor-related Lipodystrophy. *Diabetes* **51**, 3163–3169 (2002).

11. Carr, A. *et al.* Diagnosis, prediction, and natural course of HIV-1 protease-inhibitor-associated lipodystrophy, hyperlipidaemia, and diabetes mellitus: a cohort study. *Lancet* **353**, 2093–2099 (1999).

12. Friis-Møller, N. *et al.* Class of antiretroviral drugs and the risk of myocardial infarction. *N Engl J Med* **356**, 1723–1735 (2007).

13. Mondy, K. E. *et al.* High prevalence of echocardiographic abnormalities among HIV-infected persons in the era of highly active antiretroviral therapy. *Clin Infec Dis* **52**, 378–386 (2011).

14. Becker, A. *et al.* Acute coronary syndromes in treatment- naive black South Africans with human immunodeficiency virus infection. *J Interven Cardiol* **23**, 70–77 (2010).

15. Lekakis, J. *et al.* HIV-positive patients treated with protease inhibitors have vascular changes resembling those observed in atherosclerotic cardiovascular disease. *Clin Science* **115**, 189–196 (2008).

16. Reyskens, K. & Essop, M. The maladaptive effects of HIV protease inhibitors (Lopinavir/Ritonavir) on the rat heart. *Int J Cardiol* **In press**, (2013).

17. Macho, A. *et al.* Mitochondrial dysfunctions in circulating T lymphocytes from human immunodeficiency virus-1 carriers. *Blood* **86**, 2481–2487 (1995).

18. Greenspan, H. C. & Aruoma, O. I. Oxidative stress and apoptosis in HIV infection: a role for plant-derived metabolites with synergistic antioxidant activity. *Immunol Today* **15**, 209–213 (1994).

19. Jiang, B. *et al.* HIV antiretroviral drug combination induces endothelial mitochondrial dysfunction and reactive oxygen species production, but not apoptosis. *Toxicol Appl Pharmacol* **224**, 60–71 (2007).

20. Matarrese, P. *et al.* Mitochondrial membrane hyperpolarization hijacks activated T lymphocytes toward the apoptotic-prone phenotype: homeostatic mechanisms of HIV protease inhibitors. *J Immunol* **170**, 6006–6015 (2003).

21. Riddle, T. M., Kuhel, D. G., Woollett, L. A., Fichtenbaum, C. J. & Hui, D. Y. HIV protease inhibitor induces fatty acid and sterol biosynthesis in liver and adipose tissues due to the accumulation of activated sterol regulatory element-binding proteins in the nucleus. *J Biol Chem* **276**, 37514–37519 (2001).

22. Eberlé, D., Hegarty, B., Bossard, P., Ferré, P. & Foufelle, F. SREBP transcription factors: master regulators of lipid homeostasis. *Biochimie* **86**, 839–48 (2004).

23. Vallett, S. M. *et al.* A direct role for sterol regulatory element binding protein in activation of 3-hydroxy-3-methylglutaryl coenzyme A reductase gene. *J Biol Chem* **271**, 12247–12253 (1996).

24. Schmidtke, G. *et al.* How an inhibitor of the HIV-I protease modulates proteasome activity. *J Biol Chem* **274**, 35734–35740 (1999).

25. Liang, J.-S. *et al.* HIV protease inhibitors protect apolipoprotein B from degradation by the proteasome: A potential mechanism for protease inhibitor-induced hyperlipidemia. *Nat Med* **7**, 1327–1331 (2001).

26. Punga, T., Bengoechea-Alonso, M. T. & Ericsson, J. Phosphorylation and ubiquitination of the transcription factor sterol regulatory element-binding protein-1 in response to DNA binding. *J Biol Chem* **281**, 25278–25286 (2006).

27. Hirano, Y., Yoshida, M., Shimizu, M. & Sato, R. Direct demonstration of rapid degradation of nuclear sterol regulatory element-binding proteins by the ubiquitin-proteasome pathway. *J Biol Chem* **276**, 36431–36437 (2001).

28. Willis, M. S. *et al.* Cardiac muscle ring finger-1 increases susceptibility to heart failure in vivo. *Circ Res* **105**, 80–8 (2009).

29. Willis, M. S. *et al.* Muscle ring finger 1, but not muscle ring finger 2, regulates cardiac hypertrophy in vivo. *Circ Res* **100**, 456–9 (2007).

30. Andersen, C. L., Jensen, J. L. & Ørntoft, T. F. Normalization of real-time quantitative reverse transcription-PCR data: a model-based variance estimation approach to identify genes suited for normalization, applied to bladder and colon cancer data sets. *Cancer Res* **64**, 5245–5250 (2004).

31. Vandesompele, J. *et al.* Accurate normalization of real-time quantitative RT-PCR data by geometric averaging of multiple internal control genes. *Genome Biol* **3**, research0034.I–research0034.II (2002).

32. Hecker, P. A. *et al.* Effects of glucose-6-phosphate dehydrogenase deficiency on the metabolic and cardiac responses to obesogenic or high-fructose diets. *Am J Physiol Endocrinol Metab* **303**, E959–E972 (2012).

33. Andrews, N. C. & Faller, D. V A rapid micropreparation technique for extraction of DNA-binding proteins from limiting numbers of mammalian cells. *Nucleic Acids Res* **19**, 2499 (1991).

34. Sato, A., Asano, T. & Ito, K. Ritonavir interacts with bortezomib to enhance protein ubiquitination and histone acetylation synergistically in renal cancer cells. *Urology* **79**, 966.e13–e21 (2012).

35. Mapanga, R. *et al.* Oleanolic Acid: A Novel Cardioprotective Agent that Blunts Hyperglycemia-induced Contractile Dysfunction. *PloS One* **7**, e47322 (2012).

36. Boudina, S. *et al.* Reduced mitochondrial oxidative capacity and increased mitochondrial uncoupling impair myocardial energetics in obesity. *Circulation* **112**, 2686–2695 (2005).

37. Levine, R., Wehr, N., Williams, J., Stadtman, E. & Shacter, E. Determination of carbonyl groups in oxidized proteins. *Methods Mol Biol* **99**, 15–24 (2000).

38. Aebi, H. Catalase in vitro. *Methods Enzymol* **105**, 121–126 (1984).

39. Rudich, A., Ben-Romano, R., Etzion, S. & Bashan, N. Cellular mechanisms of insulin resistance, lipodystrophy and atherosclerosis induced by HIV protease inhibitors. *Acta Physiol Scand* **183**, 75–88 (2005).

40. Walmsley, S. *et al.* Ritonavir versus nelfinavir for the initial treatment of HIV infection. *N Engl J Med* **346**, 2039–2046 (2002).

41. Carr, A. *et al.* Effects of boosted tipranavir and lopinavir on body composition, insulin sensitivity and adipocytokines in antiretroviral-naive adults. *AIDS* **22**, 2313–2321 (2008).

42. Ferrer, E. *et al.* Impact of switching from Lopinavir/Ritonavir to Atazanavir/Ritonavir on body fat redistribution in virologically suppressed HIV-infected adults. *Aids Res Hum Retrovir* **27**, 1061–1065 (2011).

43. Reyskens, K. *et al.* The maladaptive effects of HIV protease inhibitors (Lopinavir/Ritonavir) on the rat heart. *PloS One* **In press** (2013).

44. Louch, W., Stokke, M., Sjaastad, I., Christensen, G. & Sejersted, O. No rest for the weary: diastolic calcium homeostasis in the normal and failuing myocardium. *Physiology* **27**, 208–323 (2012).

45. VanSlyke, J. K., Deschenes, S. M. & Musil, L. S. Intracellular transport , assembly , and degradation of wild-type and disease-linked mutant gap junction proteins. *Mol Biol Cell* **11**, 1933–1946 (2000).

46. VanSlyke, J. K. & Musil, L. S. Dislocation and degradation from the ER are regulated by cytosolic stress. *J Cell Biol* **157**, 381–394 (2002).

47. Laing, J. G. & Beyer, E. C. The gap junction protein connexin 43 is degraded via the ubiquitin proteasome pathway. *J Biol Chem* **270**, 26399–403 (1995).

48. Laing, J. G., Tadros, P. N., Westphale, E. M. & Beyer, E. C. Degradation of connexin 43 gap junctions involves both the proteasome and the lysosome. *Exp Cell Res* **236**, 482–92 (1997).

49. Jeon, H. B. *et al.* A proteomics approach to identify the ubiquitinated proteins in mouse heart. *Biochem Biophys Res Commun* **357**, 731–6 (2007).

50. Huang, G. Y. *et al.* Alteration in connexin 43 gap junction gene dosage impairs conotruncal heart development. *Develop Biol* **198**, 32–44 (1998).

51. Nattel, S., Maguy, A., Le Bouter, S. & Yeh, Y. Arrythmogenic ion-channel remodeling in the heart: heart failure, myocardial infarction, and atrial fibrillation. *Physiol Rev* **87**, 425–456 (2007).

52. Nattel, S., Shiroshita-Takeshita, A., Brundel, B. & Rivard, L. Mechanism of atrial fibrillation: lessons from animal models. *Prog Cardiovasc Dis* **48**, 9–28 (2005).

53. Reaume, A. *et al.* Cardiac malformation in neonatal mice lacking connexin 43. *Science* **267**, 1831–1834 (1995).

54. Severs, N., Bruce, A., Dupont, E. & Rothery, S. Remodelling of gap junctions and connexin expression in diseased myocardium. *Cardiovasc Res* **80**, 9–19 (2008).

55. Ya, J. *et al.* Heart defects in connexin 43-deficient mice. *Circ Res* **82**, 360–366 (1998).

56. Chu, G. *et al.* Enhanced myocyte contractility and Ca2+ handling in a calcineurin transgenic model of heart failure. *Cardiovasc Res* **54**, 105–16 (2002).

57. Zarain-Herzberg, A., Fragoso-Medina, J. & Estrada-Avilés, R. Calcium-regulated transcriptional pathways in the normal and pathologic heart. *IUBMB life* **63**, 847–55 (2011).

58. Diedrichs, H. *et al.* Activation of the calcineurin/NFAT signalling cascade starts early in human hypertrophic myocardium. *J Int Med Res* **35**, 803–18 (2007).

59. Puigserver, P. Tissue-specific regulation of metabolic pathways through the transcriptional coactivator PGC1-alpha. *Intl J Obes* **29**, S5–S9 (2005).

60. Spiegelman, B. Transcriptional control of mitochondrial energy metabolism through the PGC1 coactivators. *Novartis Found Symp* **287**, 60–63 (2007).

61. Farhoud, M. *et al.* Impaired ubiquitin-proteasome-mediated PGC-1α protein turnover and induced mitochondrial biogenesis secondary to complex-I deficiency. *Proteomics* **12**, 1349–1362 (2012).

62. Trausch-Azar, J., Leone, T. C., Kelly, D. P. & Schwartz, A. L. Ubiquitin proteasome-dependent degradation of the transcriptional coactivator PGC-1α via the N-terminal pathway. *J Biol Chem* **285**, 40192–200 (2010).